Cardiff University

Thesis for the Degree of Doctor of Philosophy

Optimisation of a Vertical Axis Tidal Turbine and Testing of a Prototype in an Unblocked Environment

Luis Priegue Molinos

supervised by

Prof. Thorsten Stoesser and Prof. Alan Kwan

February 20, 2017

Contents

I Abstract **1**

II State Of The Art **3**

1 Overview **3**

1.1 World energy consumption 3

1.2 Renewable energy consumption 4

1.3 Wave and tidal energy 6

2 Energy policies **8**

2.1 Worldwide regulations and plans 8

2.2 European Union regulations and plans 9

2.3 United Kingdom regulations and plans 16

2.4 Tidal Energy regulations and plans 18

3 Marine and Off-Shore Energy Resources **20**

3.1 Overview 20

3.2 Tidal stream energy 21

3.3 Wave Energy 24

3.4 Tidal potential energy 26

3.5 Wind Energy 28

3.6 Other Marine Energy 30
3.6.1 Osmosis 30
3.6.2 Thermal energy 30
3.6.3 Marine biofuel 31

4 Marine renewable energy technology **31**

4.1 Tidal stream energy 31
4.1.1 Tidal Theory 31
4.1.2 Tidal turbine components 35
4.1.3 Turbine technologies 39
4.1.4 Horizontal Axis Tidal Turbines 39
4.1.5 Vertical Axis Tidal Turbines 49
4.1.6 Other Tidal Turbines designs 53
4.2 Wave energy 60
4.2.1 Shore devices 60
4.2.2 Off-shore devices 62
4.3 Tidal potential energy 65
4.4 Wind energy 68

5 Design Constraints **70**

5.1 Support structure 71
5.2 Material properties 74

5.2.1 Strength 74

5.2.2 Fouling 75

5.2.3 Corrosion 77

5.3 Cavitation 81

5.4 Environment-friendly 83

III Thesis Objectives **85**

IV Methodology and Facilities **87**

6 Tidal Stream Turbine Physics **88**

7 Experimental apparatus **95**

7.1 Hydraulics Laboratory 95

7.2 Mechanical system 99

7.3 Electrical system 101

7.4 Manufacturing and Construction 103

7.5 Instrument and Data Accuracy 106

V Effect of blade parameters and arrangement on the performance **109**

8 Flow speed **110**

9 Blade Shape **114**

10 Pitch Angle **120**

11 Solidity Ratio / Number of blades **124**

12 Angle of twist **131**

13 Spokes shape **133**

14 Winglets **136**

15 Obstacle influence **138**

16 Shaft size **142**

17 Inner blades **144**

18 Blockage **146**

VI Influence of blade roughness on the turbine performance **151**

19 Introduction **151**

20 Roughness and rotor characteristics **153**

21 Results and discussion **157**

VII Wake characteristics at maximum efficiency **163**

22 Introduction **163**

23 Experimental set up **165**

24 Results **168**

24.1 Flow velocity field 169

24.2 Water surface elevation 173

24.3 Comparison to HATT 175

VIII Field testing in a representative environment 179

25 Experimental testing **180**

25.1 Hydraulics Laboratory 180

25.2 Field testing 183

26 Results **187**

26.1 Hydraulics Laboratory 187

26.2 Field testing 191

26.3 Comparison between results 195

IX Discussion 197

X Conclusions 204

XI Acknowledgments 209

Appendices **236**

List of Figures

1 World energy consumption from 1800 to 2000 [1] 4

2 Global trends in the investment in renewable energy by geography. Source [3] 5

3 Electricity generation by main renewable sources since 2000. Source [4] 6

4 Renewable energy use in 2014. The hydro, wave & tidal sector includes hydroelectric power plants. Source [6] 7

5 Global trends in renewable energy investment by sector. Source [3] 7

6 Annual evolution of the electricity price per KWh (UK) [13] . . . 18

7 Worldwide tidal stream resource estimation based on the M2 tidal harmonic (acm) . Source [22] 22

8 European tidal stream resource estimation. Source [24] 23

9 United Kingdom tidal stream resource estimation. Left, The Crown Estate map [25]. Right, ABP-MER map [26]. 24

10 European wave resource estimation. Source [24] 25

11 UK wave resource estimation. Left, The Crown Estate map [25]. Right, ABP-MER map [26] 26

12 European tidal range estimation. Source [24] 27

13 Tidal range resource estimation. Left, The Crown Estate map [25]. Right, ABP-MER map [26] 28

14 Average wind speed values in Europe. Source [30] 29

15 Sketch diagram of the forces that the Moon exerts on the Earth. Dashed blue line, ocean representation 33

16 Influence of the tidal constituents in the world tide distribution. Source [41]. 35

17 Main Horizontal Axis Tidal Turbines in the market i). Photo references included in the text 41

18 Main Horizontal Axis Tidal Turbines in the market ii). Photo references included in the text 42

19 Main Horizontal Axis Tidal Turbines in the market iii). Photo references included in the text. 43

20 Main Horizontal Axis Tidal Turbines in the market. Photo references included in the text 44

21 Main Vertical Axis Tidal Turbines in the market. Photo references included in the text. 52

22 Transverse Horizontal Axis Tidal Turbines 53

23 Other typologies of Tidal Turbines 55

25 Left, Savounius sketch. Source [91]. Right, Savonius Keel and Wind Turbine Darrieus (SKWID) 56

26 On-shore wave converters 61

27 On-shore wave converters installed within a breakwater 62

28 Typology of wave energy converters 63

29 Wave power converters. Photo references included in the text . . 64

30 Tidal potential power ranges. 66

31 Structure for off-shore wind turbines. 69

32 Synergies between marine devices and wind turbines. Source [119] 70

33 Available support structure designs for off-shore wind turbines. From left to right: monopile, tripod, jacket, compliant, barge floater, tension leg platform and spar floater structure. Source [123] 72

34 Non-dimensional plot of scour depth data for monopile offshore wind farms. No scour protection. S= scour depth, D=diameter, h= water depth. Source [125] 73

35 Blade failure of Verdant Power Company. Source [129] 75

36 Biofouling examples. Left, barnacle attached to glass fiber composite sample after four months immersed, source [132]. Right Colonization by mussels on wind off-shore turbine structure, source [134] 76

37 Relative breakdown velocities for copper alloys in seawater. Source [140] 80

38 Comparison of the effect of a cathodic protection (left) and an exposed 90-10 copper-nickel alloy (right). Exposure time, 12 months. Source [140] 80

39 Blade tip cavitation created by a HATT at TSR=4. Source [143]. 83

40 Sketch and nomenclature of the upstream, centre of the turbine and downstream 89

41 Maximum theoretical power coefficient that a turbine is able to extract, corresponding to the function displayed in Equation 7. . 90

42 Sketch of the main velocities in a rotating system (a) and the angle of attack α as a function of the rotated angle θ at various tip speed ratios λ (b) 92

43 Perspective of the hydraulics flume at Cardiff University. Geometrical description of the facilities and the mechanical system. . 96

44 Correlation between Pump power and mean flow velocities. Source [159] 97

45 Bare channel testing of the velocity field for four different percentages of pump power. Modulus of the velocity vs. relative spanwise distance. Based on [160] 98

46 Bare channel testing of the turbulence four four different percentages of pump power. Modulus of the velocity vs. relative vertical depth. Based on [160] 98

47 Experimental set up in the laboratory flume 99

48 Data acquisition system at the Cardiff University laboratory . . . 100

49 Sketch of the laboratory experiment setup (left) and the electrical circuit (right) 101

50 Verification of torque constant given by manufacturer 103

51 Eppler 715. Blade shape for testing the turbine at different flow speeds 111

52 Flow speed tests, 3 blades. Left, Power Coefficient vs. λ. Right, Torque vs. λ. Down, Power vs. λ. 112

53 Hydrodynamical performance of an hydrofoil according to the Reynolds number. Source [178] 113

54 Blade shape tests. Rotor with discs, radius = 20 cm. U_0 = 1.15 m/s 116

55 Hydrofoil profiles used for blade shape testing 116

56 Blade shape tests. Spokes, radius = 15 cm. C_P vs. λ. 117

57 Lift coefficients versus AoA for different *Re*. Left, NACA 0018. Right, Eppler 715 - 100% thickness 118

58 Lift to drag ratio for different *Re*. Left, NACA 0018. Right, Eppler 715 119

59 Sketch of the pitch angle set up. GP= gravity point of the airfoil section (also named geometry centre), R= radius. 120

60 Pitch angle tests for NACA 0018 121

61 Pitch angle results for Eppler 715 -100% thickness 122

62 Pitch angle results. Left, Eppler 715 -70% thickness. Right, NACA 63412 122

63 Solidity tests for Eppler 715 - 100 % of thickness. 125

64 Number of blades tests. Rotor with discs as the blade/shaft connection, radius = 20 cm. 128

65 Number of blades tests three and four-bladed rotors. Eppler 715 - 100% 129

66 Sketch of the vortex shedding for λ = 2.14. Source [205]. 130

67 Left, sketch of the rotor design project on its 2D circumference development. Right, drawing of four blades with 0°, 15°, 30° and 45° of twist angle. 132

68 Angle of twist tests. Left, Power Coefficient vs. λ. Right, Torque vs. λ. 133

69 Left, rectangular stainless steel spokes. Centre and right, NACA 0012 sheel that covered the rectangular spokes. 134

70 Results corresponding to the tests of the two spokes shapes. . . . 135

71 Turbine set ups for winglets testing. Left, no winglets. Centre, Inwards winglets. Right, Outwards winglets. 137

72 Winglets testing power curves. 138

73 Illustration of materials and location of the cylinders for the obstacle influence testing . Flow coming from left to right, radius cylinder = 4 cm 139

74 Position of the cylinders and nomenclature for the obstacle influence testing. Incoming flow is from top to bottom, turbine is rotating in a counter-clockwise direction. The same colour circles down and upstream were tested together. 140

75 Results for testing the obstacle influence. Graphs corresponding to the figure 74 positioning. 141

76 Left, Mesh generated for the results interpolation . Right, Interpolation of the increase/decrease on the turbine performance due to presence of cylinders 142

77 Instantaneous power coefficient for one blade. Turbine rotating counter-clockwise. Source [173] 143

78 Aluminium cylinders used for the shaft size testing. Radii corresponding to 30, 50 and 70 mm 143

79 Results corresponding to the shaft size tests 144

80 Sketch of the four rotor set ups for the inner blades tests. Small red blade = 8 cm chord length, big red blade = 12 cm chord length 145

81 Results corresponding to the inner blades tests. $U_0 = 1.09m/s$. 145

82 Power curves corresponding to the blockage effect tests 149

83 Sketch of the ratio of the lift/drag coefficient ratio versus Reynolds number. Source [178] 152

84 Flow over hydrofoil at a high angle of attack: a) rough blade; b) smooth blade 153

85 Software output from Taylor Hobson's Talysurf 2. Spatial distribution of the blade surface elevations and statistical data 155

86 Turbine performance curves of rotors comprising blades of different materials and for three different flow rates. Three-bladed rotor, σ=0.19. 158

87 Turbine performance curves of rotors comprising blades of different materials and different chord length at U_0= 0.72 m/s. Three-bladed rotor. 159

88 Turbine performance curves of rotors comprising blades of different materials and different chord lengths at U_0= 1.15 m/s. Three-bladed rotor. 160

89 Turbine performance curves of two-, three- and four-bladed rotors comprising blades of different materials at two flow speeds. c=10 cm. 161

90 Comparison between results experiments carried out for this thesis, [226] and [227] 161

91 Sketch of the laboratory set up, main dimensions and reference points 165

92 Mesh of points for the flow velocities measurements 167

93 Wave probes disposition in the Hydraulics flume 168

94 Left: Mesh of points for the water surface measurements. Right: Picture of the wake surface downstream. 168

95 Left: Power coefficient curve. Right: Torque coefficient curve. Red dot, fixed point for wake measurements. Approach flow speed = 0.98 m/s 169

96 Visualization of the downstream stream-wise velocities 170

97 Left: Spanwise velocity distribution for z/d=0.5. Right: Vertical velocity distribution 171

98 Vorticity distribution, z/d = 0.5 171

99 Velocity deficit distribution, Z= half turbine height 172

100 Velocity deficit distribution, z/d = 0.5 173

101 Water surface interpolation 174

102 2D water surface elevation 175

103 Main curves of the water level distribution along the channel . . 176

104 Comparison of mean streamwise velocities between experimental studies of Horizontal Axis Turbines and the presented data. $I = 2\%$ in Tedds, $I \approx 12\%$ in Stallard, $I \approx 14\%$ in the case of study. . 176

105 Comparison of the water surface elevations between experimental studies for Horizontal Axis Turbines and the presented data. Bahaj et al. [1], U_0= 1.8 m/s, Bahaj et al. [2], U_0= 2.35 m/s (both data extracted from [241]), Exp, U_0= 1m/s 178

106 Lift coefficients versus AoA for different $Re = 10^5$ 181

107 Sketch of the laboratory setup, including the main dimensions of the NACA 4415 rotor. 182

108 Left: Top view of the White Water Rafting Centre. Top right: Upstream perspective. Top down: Downstream perspective. . . . 183

109 A CAD representation of the turbine tested in the White Water Rafting Centre, and the positioning of the devices for flow speed measurements. 184

110 Electromechanical circuit and data acquisition system. 185

111 Pitch angle tests for NACA 4415 blade shape. 187

112 Efficiency curves for the fully submerged rotor. Top: U_0= 0.72 m/s. Bottom: U_0= 1.09 m/s 188

113 Efficiency curves for the partially submerged rotor. Top: U_0= 0.72 m/s. Bottom: U_0= 1.09 m/s 189

114 Efficiency curves corrected using A_c for partially submerged rotors. Top: U_0= 0.72 m/s. Bottom: U_0= 1.09 m/s 190

115 Laboratory pictures for z/H=0. Left: no operation. Right: the Maximum efficiency point for U_0=1.09 m/s, with flow from left to right. 191

116 Field testing pictures. Top left: U_0=1.40 m/s, z/H ≈-60 %. Top right: U_0=1.28 m/s, z/H ≈-50 %. Bottom left: U_0=1.40 m/s, z/H ≈-10 %. Bottom right: U_0= 1.83 m/s, z/H>0%. 193

117 Field testing results. Left: Efficiency curves for different degrees of submergence and the flow meter used for flow velocities. Right: Efficiency curves for z/H>0. 194

118 Flow speed measurements. Left: velocimeter readings for streamwise velocity, U_0=1.35 m/s. Right: flow meter readings for total flow velocity. 194

119 Data extracted from the highest efficiency operational point reached during the fully immersed tests. Left: rotational speed. Right: torque. 195

120 Comparison between laboratory and field testing results. Field tests: U_0=1.83 m/s. Laboratory: U_0=1.09 m/s 196

121 Best and worse results for each experiment presented in this thesis 202

122 Example of the experimental set up used for part of the experiments. The set up is based on discs as the connection between blades and shaft. 236

123 Detailed drawing of the discs used for part of the experiments. . 237

124 Detailed drawing of a twisted bladed used for part of the experiments. Straight blades had the same distribution of holes and distances 238

125 Example of the experimental set up used for part of the experiments. The set up is based on spokes as the connection between blades and shaft. 239

126 Detailed drawing of the piece that connected spokes and shaft, set up that was used for part of the experiments. 240

127 Detailed drawing of the spokes used for part of the experiments. 241

128 Detailed drawing of the winglets used for part of the experiments 242

129 Drawings of the prototype tested at White Water Rafting Centre 243

List of Tables

1 Major policies and measures adopted by EU countries since 1975. Source [6]. MS = Multiple Sources 11

2 Major policies and measures adopted by the UK. Source [6]. MS = Multiple Sources 16

3 Major policies and measures adopted by EU countries on the tidal energy sector. Source [6]. MS = Multiple Sources 19

4 Sun-Earth energy transfers. Source [18]. 21

5 Examples of global power plant based on Ocean Thermal Energy Conversion. Source [34] 30

6 Summary of the Horizontal Axis Tidal Turbine Technologies . . . 46

7 Summary of the non-Horizontal Axis Tidal Turbines 58

8 Current tidal range constructions. Source [56] 66

9 Most significant tidal range projects currently under development. 67

10 Classification of the corrosion environments according to ISO 12944. Source [138]. 78

11 Laboratory equipment and accuracy according to their specifications sheet 106

12 Absolute and relative errors for maximum values of the variables involved in the main parameters at their peak of their performance curve 107

13 Absolute and relative errors for minimum values of the variables involved in the main parameters at their peak of their performance curve 108

14 Rotor parameters and main magnitudes for testing the turbine at different flow speeds 110

15 Research studies about vertical axis tidal turbines performance for different flow speeds and comparison to the results 114

16 Parameters and magnitudes for blade shape tests depending on the connection between blades and central shaft 115

17 Research studies about vertical axis tidal turbines performance for different flow speeds. 123

18 Research studies about vertical axis wind turbines performance for different pitch angles. 124

19 Summary of experimental testing for VATT which analysed solidity 127

20 Summary of numerical modelling for VATT which analysed solidity 128

21 Self-starting processes for different number of blades and pitch angle. X= success, - = no-success 131

22 Self-starting processes for different angles of twist. 133

23 Rotor most significant parameters for the tests of the blockage effect 149

24 Roughness statistics of Materials A, B and C 154

25 Relative roughness Reynolds numbers 155

26 Roughness statistics 156

27 Summary of the turbine's main characteristics. 186

28 Peak Cp and λ for each experiment 199

Nomenclature

α	Angle of attack [°]
$\bar{\omega}$	Vorticity in the streamwise direction [-]
β	Blockage ratio [%]
ϵ	Indirect error [-]
λ	Tip speed ratio (TSR) [-]
λ	Tip speed ratio in a blocked environment [-]
μ	Dynamic stress [kg/m s]
ν	Shear stress [Pa]
ω	Rotational speed [rad/s]
ϕ	Angle of twist of the blade [°]
ρ	Density [kg/m3]
σ	Rotor solidity [-]
θ	Angle of rotation [°]
a	Ratio between P_r and P_r [%]
A_c	Area of the turbine rotor submerged in water [m2]
A_f	Area of the flume cross-section [m2]
A_r	Area of the turbine rotor [m2]
c	Blade chord length [m]
C_D	Drag coefficient [-]

C_L Lift coefficient [-]

C_P Power coefficient [%]

C_T Torque coefficient [-]

$C_{P,max}$ Peak power coefficient [%]

Cp_b Power coefficient in a blocked environment [%]

Ct_b Torque coefficient in a blocked environment [%]

D Turbine diameter [m]

E Energy [J]

F_d Drag force [N]

F_d Lift force [N]

F_g Gravitational forces [N]

F_i Inertial forces [N]

F_l Lift force [N]

F_v Viscous forces [Nm]

Fr Fraude number [-]

g Gravitational acceleration [kg m/s2]

H Blade height or water height [m]

I Turbulence intensity [%]. Electrical Current [A]

K_G generator-specific constant [-]

k_s Relative roughness [-]

L Generic dimension unit [m]

m Mass [kg]

n_{crit}	Parameter for turbulence required by software Xfoil [-]
nb	Number of blades of the turbine [-]
P	Power [W]
P_0	Pressure [Pa]
P_1	Water power at the centre of the rotor [Pa]
P_2	Downstream power [Pa]
P_e	Electrical Power [m]
P_f	Incoming power in the flume cross-section [W]
P_r	Incoming power in the rotor area [W]
r	Turbine radius [m]
R_a	Roughness average height [μm]
R_{ku}	Roughness kurtosis [μm]
R_q	Roughness root mean square height [μm]
R_{sk}	Roughness skewness [μm]
R_t	Roughness maximum height [μm]
R_v	Roughness minimum height [μm]
Re	Reynolds number [m/s]
Re_*	Roughness Reynolds number [-]
Re_c	Reynolds number using the chord length of the blades as main dimension [-]
T	Torque [Nm]
u	Generic velocity [m/s]

U_*	Friction velocity [-]
U_0	Flow velocity at the center of the rotor [m/s]
U_1	Upstream flow velocity [m/s]
U_2	Downstrewam flow velocity [m/s]
U_m	Mean streamwise velocity [m/s]
V	Volume [m3]. Voltage [V]
V_m	Mean spanwise velocity [m/s]
W_m	Mean vertical velocity [m/s]
x	Distance from the centre of rotation of the turbine in the streamwise cross-section [m]
y	Distance from the centre of rotation of the turbine in the spanwise cross-section [m]
z	Distance from the bottom of the flume in the vertical direction [m]

Part I

Abstract

Vertical Axis Tidal Turbines (VATTs) have become the subject of increased interest in recent decades, but the development of this type of hydrokinetic turbine has faced several challenges that have not yet been overcome.

The influence of rotor parameters on turbine performance is one of these challenges. No axiom can be found in the literature about the effect of these parameters on the turbine behaviour, and sometimes research projects even show contradictory results. As a consequence, parameters that define turbine rotors may differ substantially from each other but have performed similarly in terms of efficiency.

In relation to this matter, experimental modelling has been carried out in the School of Engineering facility at Cardiff University. Using small-scale set-ups, experimental testing provided useful and reliable information that shed light into these design uncertainties. Blade roughness has been found to have a great impact on the turbine behaviour, and the influence of this parameter has been tested and analysed in depth in a subsequent chapter of the thesis.

Apart from the parametric analysis, a mechanical and an electrical system were utilised for the turbine set up. Thanks to these different systems of energy conversion, it was possible to compare the extracted power and to evaluate their inherent losses. Electricity was generated from the electrical approach, which was very useful in order to accurately evaluate the turbine efficiency.

Taking into account the results coming from physical testing, an optimised prototype of a VATT was designed and manufactured; estimated to be a 1:15 scale device. Not just the rotor but the whole super structure was built, in order to analyse both the efficiency and the performance of the rotor, as well as the

structural response of the entire device.

Performing experimental testing without removing the effect that a blocked channel provides to the turbine rotation is no trivial issue, and intermediate scale tests will become a fundamental step for recognition of the technology. Aiming to achieve a reliable source of information, the manufactured tidal turbine prototype has been tested in a water sports centre (White Water Rafting Centre, Cardiff).

There is a clear lack of information in the literature about testing tidal turbines on an intermediate scale, and the chance to test a tidal turbine is a very valuable opportunity. The experiments were accomplished in a very similar environment to a real tidal stream, but with the related advantages of complete control over the turbine deployment. Thus, these experiments are considered to provide very useful data for scientific knowledge and also the tidal stream energy sector.

Finally, the study of the hydrodynamic turbine wake in small scale was carried out. Not only velocity measurements were collected at the turbine operating point, but also water elevations upstream and downstream were measured by using depth gauges based on water conductivity. At the time of writing and to the best of the authors' knowledge, not many research articles have studied the wake characteristics of vertical axis tidal stream turbines, and none have used this equipment. The quality of the data is deemed to be excellent and the following process of the information described perfectly the near and far wake. This could be extremely useful for a future scale-up of the turbine, and the development of an array.

Part II

State Of The Art

1. Overview

1.1. World energy consumption

Humanity has always required sources of energy since developing new cultural, social, industrial and economical skills. The first resources of power understood and developed by our ancestors were: fire, the control of animal force and wind energy. These resources have been the main power means for many centuries and their use has become more efficient. For instance, wood was the main raw material turned into power due to access and ease of processing. Around the world, wood consumption values have remained constant throughout time, and is still used for household purposes and certain factories continue to utilise it [1].

The need of power supplies suffered a drastic change when the Industrial Revolution began in the 18th century. The advancements in industrial machinery and manufacturing processes required more powerful energy resources, hence coal began to gain importance exponentially. The invention of the steam engine in 1781 was a key factor on industrial development, also playing a vital role in the expansion of coal use [2].

When the internal combustion engine was developed at the end of the 19th century, steam engines and coal were steadily substituted by fossil fuels. Oil (beginning) and natural gas (later) became the most used materials for fuel and energy production. The amount of extracted fossil fuels has been increasing significantly, and at this moment in time, the world quantities of oil and gas utilisation are at its maximum. Other sources, including nuclear and hydroelectrical power, have started to yield significant amounts of power. However,

renewable energy technologies are still unable to challenge the large dependency on non-renewable energies. The distribution and values of the world's energy consumption, in terms of power resources, is shown in Figure 1. This diagram shows the evolution of energy sources used by mankind from 1800 to 2000. It's clear that energy consumption has been gradually increasing during this period of time [1].

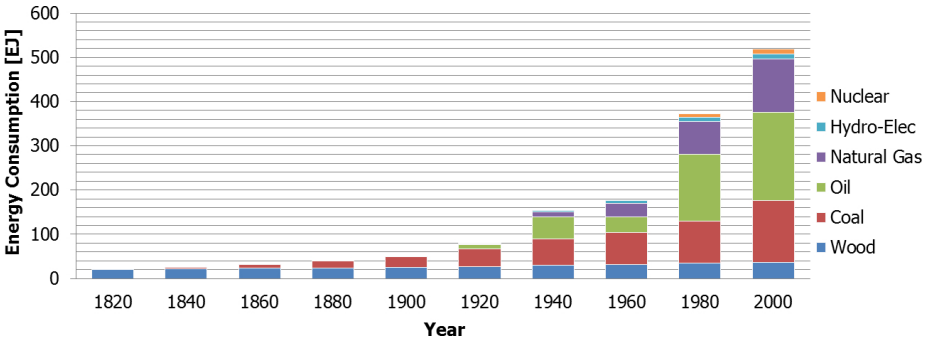

Figure 1: World energy consumption from 1800 to 2000 [1]

Since the last century, humanity has sorted its power necessity using fossil fuels. In the early 1900s, there were no studies about their environmental impact and almost no caution in avoiding contamination. The effects of pollution, from fuel combustions and the derived products created, were understood from 1960 onwards. This understanding was followed by a direct interest in the use of clean, environmentally-friendly and endless energy sources. This concept adopted the name 'renewable energy', becoming an important factor concerning science and the future of the planet. Within this wide concept it is possible to include different sources such as solar, wind, geothermal, biofuel, waste gas energy and the source which is the object of study in this thesis, marine renewable energy.

1.2. Renewable energy consumption

As fossil fuels are a finite resource, harmless energy sources and favourable energy policies became a target for nations worldwide. This has lead to in-

creased power generation from renewable sources in the last decade. Figure 2 displays the investment in renewable energies carried out by main regions of the world between 2005 and 2016. In general, the graph shows an upwards trend throughout this period of time, with almost a four-fold increase in 2016 when compared to capital invested in 2005.

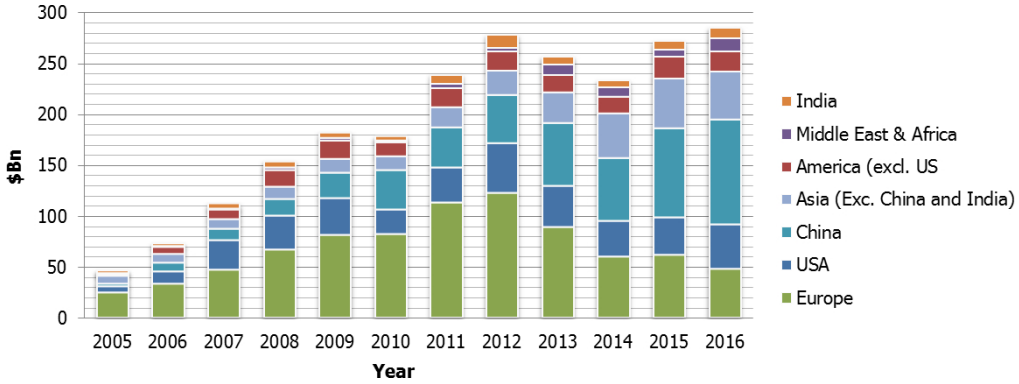

Figure 2: Global trends in the investment in renewable energy by geography. Source [3]

Although the growth in investment is remarkable, information gathered about funding in renewable energy by Europe has slowed in the last five years. The economical crisis that started in 2008 and the deceleration of the measures to incentive these technologies might have led to this recession. On the other hand, China has become the greatest economical contributor of renewable energy technologies. In addition to this, other developing countries including India, Brazil, South Africa, Chile and Mexico have increased their investment, to the point of reaching the top ten investing countries in 2015 [3].

As a result of this increase in global investment, the energy extracted via renewable energy has boosted. In the same period of time, the UK has generated about 600% more energy than fifteen years previously (Figure 3)

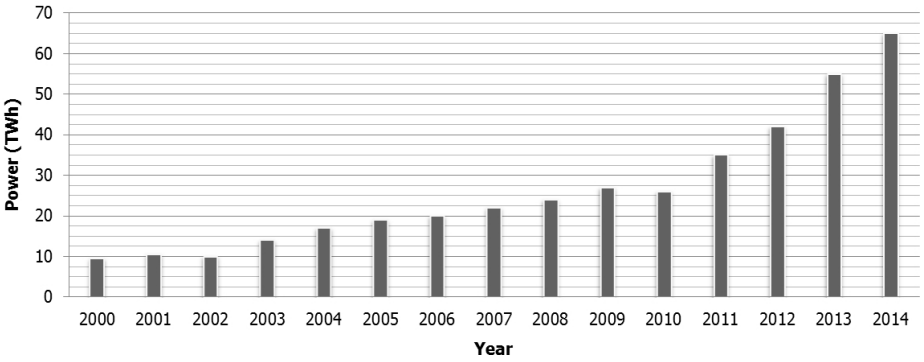

Figure 3: Electricity generation by main renewable sources since 2000. Source [4]

[5] highlighted the generic barriers that make development of renewable energies more difficult. The main restrictions consist of: economical issues related to costs, investment and competition between energy companies, administrative barriers due to a high number of authorities and their lack of methodologies, energy transport limitations as the current procedures are not efficient and, finally, social and environmental issues.

1.3. Wave and tidal energy

On the other hand, renewable energy and, more specifically, marine energy technologies are still at an early stage of development. As an example, wave and tidal constructions and devices provided just 9 MW to the UK's national grid in 2015 [4] ,which is the same amount of electricity extracted from marine renewable energies. Special attention must be paid to the fact that none of the renewable energy sources are clearly predominating, and different divisions of bioenergy sources supply a third of renewable energy consumed in 2014, in the UK (Figure 4).

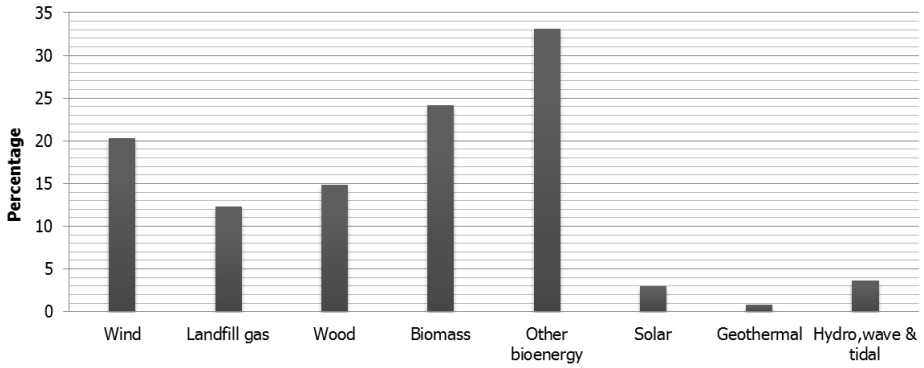

Figure 4: Renewable energy use in 2014. The hydro, wave & tidal sector includes hydroelectric power plants. Source [6]

However, the amount of investment in different renewable sectors, provided by the main countries of the world, does not match their use. Hence, the sector that received the largest financial support was Solar and Photovoltaic (PV) energy. Compared to the PV investment rates, marine, hydro and biofuel energy have obtained imperceptible amounts of capital in order to improve their harnessing. On the other hand, wind energy is the second most invested technology, with similar values to the PV quantities [3].

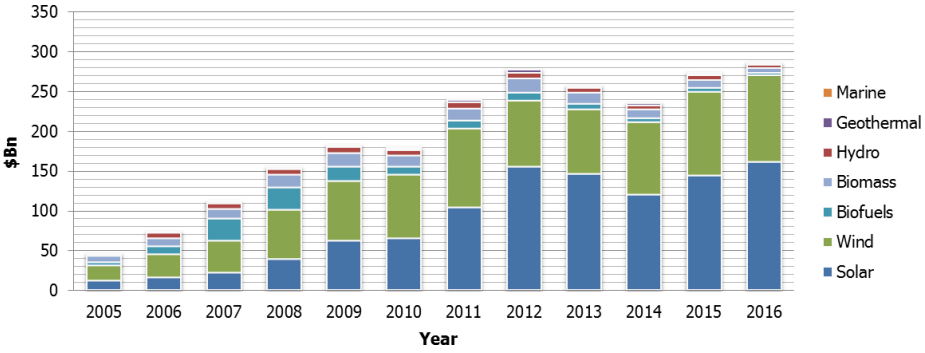

Figure 5: Global trends in renewable energy investment by sector. Source [3]

In spite of the low capital marine energy attracts from investors around the world, many public and private organisations are raising their level of contribution in marine renewable energy. For instance, West Wales and the Valleys

have received the most important degree of support from the EU. Research and development on marine renewable energy has been declared a priority in these areas, and funding close to €100 million has been consented [7].

As it is known, marine energy can also be split into different categories depending on their main source of action (offshore wind, wave and tidal energy). These technologies are still under development and this piece of work is focused specifically on the harnessing of tidal stream energy, using and optimising a novel vertical axis tidal turbine.

2. Energy policies

2.1. Worldwide regulations and plans

Many governments across the world had not taken into consideration the damaging effects global contamination has on Earth, until the last few decades. Therefore, energy consumption was not regulated and energy policies were rare in most nations.

The first step towards worldwide action against contamination could be considered to have happened in December 1997. The most industrialised countries have committed themselves to accept measures and constrictions in order to reduce the amount of polluting gas and greenhouse effects. This agreement was named as Kyoto Protocol and it is considered to be the first worldwide attempt to restrict the industrial contamination and soften the effect of the climate change around the world [8]. The main measure that these countries agreed consisted of a 5% reduction of the contaminating agents. This protocol catalysed the opening of new regulations controlling the quality of energy generation, as well as new policies to boost the power extraction through non-contaminating energy sources. Representatives from 192 countries took part in the conference, including most countries that form the G-20.

Annual International conferences about Climate Change are held to improve

action against pollution and to provide solutions to problems related to non-renewable energies. As an example, Copenhagen held the 15th Worldwide Conference in 2009, which was organised to set new objectives that would replace the Kyoto Protocol [9]. Although the same number of countries participated in the conferences, neither government obligations nor legal bindings were adopted, which was a common outcome from these conventions.

The next binding agreement was not achieved until November 2015. 196 countries came together at the conference and supported the Paris Agreement. The target of this agreement was to restrict the world's increase in temperature to a maximum of 2°C [10]. The conference was considered a success and the objectives of the agreement were expressed by an official certification, written for the International Organisation for Standardisation (ISO). Thus, ISO 20121 is based on the goals set in the Paris Agreement and will ensure the quality of sustainable measures collected in the conference. In order to fulfil the global restrictions accepted in the mentioned agreements, every region and continent provide regulations in relation to their levels of contamination and also economical, geographical and social situations.

2.2. European Union regulations and plans

In a European context, EU policy-makers established a combination of measures used to help and lead EU countries towards achieving specified goals. Within this context, EU country members set a legal binding package to ensure that the EU fulfils the energy and climate 2020 targets (also named objective 20-20-20). The three significant goals are: a 20% reduction in greenhouse gas pollution compared to levels in 1990, 20% of generated power must come from renewable energy and there must be a 20% improvement in energy efficiency. [5] suggests these targets are too ambitious and that some countries do not achieve the necessary growth rate for the use of renewable energies, required to meet the 2020 goals.

With the aim of keeping the same non-carbon trend, the 2030 Framework for energy and climate settled with new energetic targets and policy objectives for the years between 2020 and 2030. The objectives of these goals are to achieve a sustainable energy network and to meet its long-term contraction of greenhouse gas emissions. The main bullet points agreed in the 2030 Climate and Energy Framework are: at least a 40% reduction in CO_2 emissions, a minimum of 27% energy savings in comparison to the "business-as-usual" scenario and a minimum of 27% of renewable energy usage out of the whole energy consumption [11].

In case these targets are achieved, the EU commission has looked into more ambitious goals for 2050. In order to keep up the trend encouraged by previous regulations and policies, the EU has put effort into reducing emissions to 80% of levels in 1990, with milestones of reducing contaminating emissions to 40% by 2030 and 60% by 2040.

Apart from obligations contracted by EU country members, there are no regulations for the whole region, as every single country consists of inherited energetic, political and geographical circumstances. Therefore, the standards and procedures that countries must implement are decided by their governments, which implies that these measures can differ substantially.

Included in Table 1 are some of the key policies within in the renewable energy framework that EU countries have adopted since 1975. As it is displayed on the table, Nordic countries such as Denmark and Sweden were pioneers on the application of renewable energy policies, starting to develop strategies against power systems based on fossil fuels and favouring pioneering sectors in Europe, such as the wind turbine industry. In the last 40 years, up to 782 policies have been registered in the renewable energy policy framework database, that the International Energy Agency provides in [6].

Table 1: Major policies and measures adopted by EU countries since 1975. Source [6]. MS = Multiple Sources

TITLE	**COUNTRY**	**YEAR**	**POLICY TYPE**	**TARGET**
Energy Research and Development	Sweden	1975	RD&D	MS
Energy Research Programme	Denmark	1976	RD&D	MS
Regulation of alternative forms of energy	Greece	1985	Regulatory Instruments	-
Federal States Support for Renewable Energy	Germany	1985	Economic Instruments	MS
CO2 Tax on Fossil Fuels	Finland	1990	Economic Instruments	-
AMURE subsidies to support commercial and non commercial companies	Belgium	1990	Economic Instruments	MS
Measures to promote distributed generation and market liberalisation	Italy	1991	Strategic Planning	MS
Energy, Carbon Dioxide and Sulphur Taxation	Sweden	1991	Economic Instruments	MS
Declaration on	Croatia	1992	Strategic	

Environmental Protection			Planning	
Framework Law Concerning rational use of energy	Luxembourg	1993	Regulatory Instruments	MS
General Electricity Law 54/1997	Spain	1997	Regulatory Instruments	MS
The Electricity Certificate System	Sweden	2003	Economic Instruments	MS
Biofuels targets 2008-2013	Poland	2007	Strategic Planning	Bioenergy
A vehicle fleet independent of fossil fuel by 2030	Sweden	2009	Strategic Planning	Bioenergy
National Renewable Action Plan (NREAP)	Lithuania	2010	Strategic Planning	MS
National Renewable Energy Action Plan (NREAP)	Italy	2010	Strategic Planning	MS
National Renewable Energy Action Plan (NREAP)	Poland	2010	Strategic Planning	MS
National Renewable	Luxembourg	2010	Strategic	MS

Action Plan (NREAP)			Planning	
Energy Concept	Germany	2010	Regulatory Instruments	MS
National Renewable Energy Action Plan (NREAP)	Hungary	2011	Strategic Planning	
Energy from Renewable Sources Act (ERSA)	Bulgaria	2011	Economic Instruments	MS
Renewable Energy Feed-in Tariff	Ireland	2012	-	MS
Grand Schemes for Energy Efficiency	Cyprus	2012	-	MS
Danish Energy Agreement for 2012-2020	Denmark	2012	Economic Instruments	Bioenergy Wind
National Energy Strategy 2030	Italy	2013	Regulatory Instruments	MS
Biofuels targets 2013-2018	Poland	2013	Regulatory Instruments	Bioenergy
The Slovak Energy Efficiency and Renewable Energy Finance Facility	Slovakia	2014	Economic Instruments	MS
National Climate Change Plan	Czech Republic	2014	Policy	-

			Support	
Portugal Green Growth Commitment 2030	Portugal	2015	Strategic Planning	MS
Ground-mounted PV Auction Ordinance	Germany	2015	Economic Instruments	Solar
Energy Transition Act	France	2015	Strategic Planning	MS
Feed-in Tariffs for Electricity Produced from Renewable Energy Sources	Lithuania	2015	Economic Instruments	Wind Bioenergy Hydro
Slovenia Net-Metering System	Slovenia	2016	Regulatory Instruments	MS
Renewable Energy Law of Poland	Poland	2016	Regulatory Instruments	MS

Measures to encourage the use of renewable energy usually relate to economical advantages or tax deductions. Utilised most by EU country members are the following [6]:

- Feed-in Tariff. This method consists of an economic supplement that is given to companies or households that generate their own electricity through renewables. The supplement is always based on the cost of the renewable source extraction. These approaches are usually long-term contracts which ensure access to the electrical grid.
- Quota. This practice is based on the obligation to deliver a minimum percentage of biofuels into diesel distribution for road transport.
- Tenders. Small financial incentives for businesses and householders in the form of subsidies or tax deductions.

Apart from the group of policies and measures that facilitates the development of non-carbon energy generation, EU public institutions started to provide economical incentives to private initiatives. For example, the creation of Global Energy Efficiency and Renewable Energy Fund (GEEREF). This European capital investment from the European Investment Bank (EIB) is to encourage private funding in renewable energy projects. This organisation does not have projects solely in Europe, money has been invested in different sustainable projects and organisations in Africa, Asia and South America [12].

Along with support for research development (RD) of renewable energy projects, research to improve the efficiency of actual renewable energy systems and the invention of innovative renewable energy converters, has been encouraged throughout the last decades. The current EU program that invests in research and innovation for non-carbon projects is Horizon 2020. Research departments, high-tech institutes and also private companies could apply for funding through this plan.

Table 2: Major policies and measures adopted by the UK. Source [6]. MS = Multiple Sources

TITLE	YEAR	POLICY TYPE	TARGET
Non-Fossil Fuel Obligation	1990	-	MS
Climate Change Levy	2001	Economic Instruments	MS
Renewables Obligation (RO)	2002	Economic Instruments	MS
Renewable Transport Fuels Obligation	2008	Regulatory	Bioenergy
Feed-in Tariffs for renewable electricity for PV and non-PV technologies	2010	Economic Instruments	Wind Hydro Solar
Renewable Heat Incentive (RHI) for domestic and non-domestic generators	2011	Economic Instruments	MS
Green Deal	2013	Economic Instruments	Solar
Contract for Difference (CfD)	2014	Economic Instruments	Wind Hydro Solar Bioenergy

2.3. United Kingdom regulations and plans

The United Kingdom has been politically and financially proactive during the last decades, with a long list of policies and measures used to regulate the energy sector and encourage renewable energy. The Department of Energy and Climate Change (DECC) has formed a large amount of measures and actions, which is why the UK is one of the EU countries most likely to fulfil the obligations agreed in the Paris agreement and the 2030 Climate and Energy Framework. The main joint policies adopted in the past years are presented in Table 2.

The combined action of small scale measures presented in Table 2 hopes to accomplish and exceed the objectives accepted in previous agreements. According to the UK Renewable Energy Strategy [13], UK goals are slightly more ambitious and specific than those adopted from EU agreements. Hence, 30% of electricity created should be generated from renewable energy, outlining the importance of hydro, wave and tidal energy because of the UK's advantageous

geographical and environmental conditions. Moreover, 12% of heat created should come from renewable sources, and 10% of transport fuel consumption must be delivered by renewables.

The main bullet points of the Renewable Energy Strategy consist of: stronger economical support for renewables suited for a wide range of technology sectors, more efficient delivery that takes into account strategy systems, supply chains and grid connections, and a greater push on cutting-edge technologies and applied science, to add support to reducing the related costs of energy production.

Apart from being the first package of measures that introduced regulation on the tidal energy sector in the UK (Table 3), the initial legislation that encouraged the development of renewable resources in the UK is the regulation named Renewable Obligation of 2002. In this publication, the concept of the Renewable Obligation Certificate was announced, which means the target of achieving at least 3% of renewable energy production must be reached by any energy supplier. This percentage has increased to 10% in 2010 and 15 % in 2015. In case power suppliers can not meet their minimum of renewable energy production, companies are able to trade these certificates in order to fulfil these restrictions [14].

However, the development of some renewable energy technologies involves higher production costs for energy suppliers. This drawback might be sorted out with further research and development, able to reduce production and management costs and, therefore, be more competitive in the electricity market. Ideally, the financial advantages these policies provide to energy producers would not be required once technologies are fully optimised. So far, the energy price per KWh in the UK has experienced a similar upwards trend to the trend displayed by the number of renewable energy users and the number of measures in its favour (Figure 6).

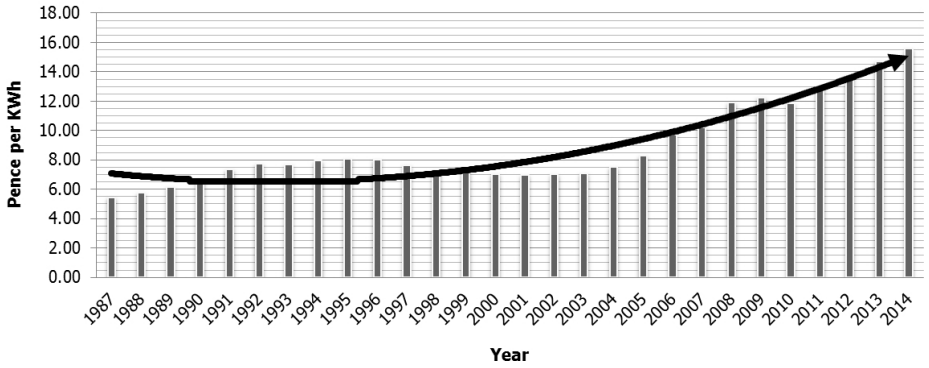

Figure 6: Annual evolution of the electricity price per KWh (UK) [13]

2.4. Tidal Energy regulations and plans

Not many standards have been stipulated in the EU about tidal energy generation, distribution or implementation. As this technology is yet to be fully developed, the main measures taken by different governments pursue financial and political support. According to [6], the listing of official regulations is not large, and just four countries (Italy, Belgium, Ireland and United Kingdom) legislated and normalised the inclusion of the tidal energy sector. These regulations are shown in Table 3.

The Irish Offshore Renewable Energy Development Plan [15], introduced initial steps for a market support scheme directed at wave and tidal energy. The essential points of this development plan are based on the analysis of market opportunities provided by wind and tidal energy sources situated on coasts, aiming to achieve a high economic impact whereby the marine environment remains undamaged.

The UK Renewable Energy Roadmap [16] is more specific about incentives given by the government encouraging the extraction of marine (wave and tidal) energy. Hence, around £20 million was invested in marine energy converters and in the commission of wave and tidal energy at The National Renewable Energy Centre. In addition to this initiative, The Crown Estate facilitated a

Table 3: Major policies and measures adopted by EU countries on the tidal energy sector. Source [6]. MS = Multiple Sources

TITLE	COUNTRY	YEAR
Renewables Obligation (RO)	United Kingdom	2002
Energy Act 2004	United Kingdom	2004
RES promotion Decree Implementing Directive	Italy	2004
Offshore Domanial Concessions for Wind and Ocean Energy Production	Belgium	2004
Renewable Energy Feed-In Tariff	Ireland	2005
Marine Research Development Fund	United Kingdom	2005
Energy Technologies Institute	United Kingdom	2007
"All inclusive" Feed-in Tariff for small renewable energy power plants	Italy	2008
Renewable energy provisions for the Green Certificates System	Italy	2008
Renewable Energy Strategy 2009	United Kingdom	2009
Low Carbon Industrial Strategy	United Kingdom	2009
Ireland Offshore Renewable Energy Development Plan	Ireland	2014
Contract for Difference	United Kingdom	2014

knowledge sharing system, used to speed up wave and tidal energy deployment and stimulating the supply chain through the institution, Marine Energy Parks. Besides this, marine regulations were specified in order to avoid conflicts between users of the sea, published in the Offshore Energy Strategic Environmental Assessment.

In 2014, the DECC published a law named Contract for Difference (CfD). This private policy is based on a contract between a renewable energy generator and the Low Carbon Contracts Company (LCCC), which is a public organisation [17]. A renewable generator is rewarded with the difference between the actual price that was necessary to generate the electricity and the average reference price for the electricity in the UK market. These measures aim to lower the effects that variable electricity prices could bring to supplier companies, at the same time as protecting energy consumers from paying unfair electricity rates.

A common approach for different governments in Europe is to support or-

ganisations, companies and regions in extracting non-carbon electricity with the use of small scale power systems. This policy is named Micro Generation-Feed in Tariffs and has been adopted by the UK in 2010 and by other countries such as Spain. The threshold between small and large scale power capacity is 5 MW in the UK, although it can differ between countries. The energy producer is enrolled with a particular electricity supplier license in relation to its capacity, and a similar reward to the one offered by the CfD is given to micro generation power systems.

3. Marine and Off-Shore Energy Resources

3.1. Overview

The Sun is the greatest energy source on Earth. Annually, the amount of solar radiation caught by the planet is around 945 EWh. This value is roughly six thousand times bigger than the world energy consumption per year. In other words, the Sun provides in 75 minutes the amount of power required by humanity for a whole year.

This gigantic amount of energy is mostly absorbed by continents and oceans. Hence, the estimated amount of energy absorbed by the oceans is around 570 EWh, which is approximately 60% of the energy emitted by the Sun towards the planet. Applying the same proportion, harnessing ideally marine energy would deliver in almost two hours the amount that humankind requires primarily [18].

The main process from which oceans absorb the solar energy is the transformation of the radiation into thermal energy or heat. As a consequence, thermal gradients in oceans are remarkable, with temperatures that vary from 0° (possible because of high values of salinity) to 30° . Waves and wind mix up the water heated by the Sun's energy, resulting in temperature gradients that are never constant. Temperature distribution depends on the geophysical location, but temperatures at one kilometre depth are reasonably uniform at about 4° C

[19].

As a consequence of solar radiation, many different sources of marine energy can be found on Earth, and more specifically, in the ocean. 96% of solar energy radiation is transferred via heat transmission, leading the list of Sun-Earth energy transfers (Figure 4). Although the percentage of solar radiation transformed into tidal and wave energy is almost insignificant, around 0.01%, these resources have a great potential, as current technologies are developing which can harness this energy efficiently. Identifying the resources location and quantification of the potential power of tidal, wave, wind and other marine energies are described in detail in this chapter.

Table 4: Sun-Earth energy transfers. Source [18].

Energy Transformations	**Power (TW)**
Thermal Gradients	40000
Saline gradients	1400
Ocean winds	20
Bio conversion	10
Marine currents	5
Tides	3
Waves	2.5

3.2. Tidal stream energy

The harnessing of tidal stream energy has become a topic of interest in the last century since the electrical industry is looking for new renewable energy resources. Firstly, resource assessments were carried out using visual measurements, able to provide rough estimations. The global distribution of marine measurement systems as ocean buoys and tidal gauges started to provide more accurate information, but numerical models in the last decades now predict, quite accurately, flow speed values for long sets of time data. However, tides are more predictable than currents, and tidal current simulations provide certain uncertainty [20]. In order to verify the results and measure the precision of the simulations, it is common practise incorporating the use of velocimeters as Acoustic Doppler Profiler (ADP) or Acoustic Doppler Velocimiter (ADV) for

field tests. A collection of the main tidal stream resource assessments that can be found on the literature has been published by [21]. Figure 7 shows a coarse simulation of the world's potential tidal stream energy. This solution has been provided by using a global tide finite element solution named fes99. Although the results can not be assumed as fully reliable and small scale studies must be always carried out, the map hints the locations where an array of tidal turbines could deployed in the near future [22].

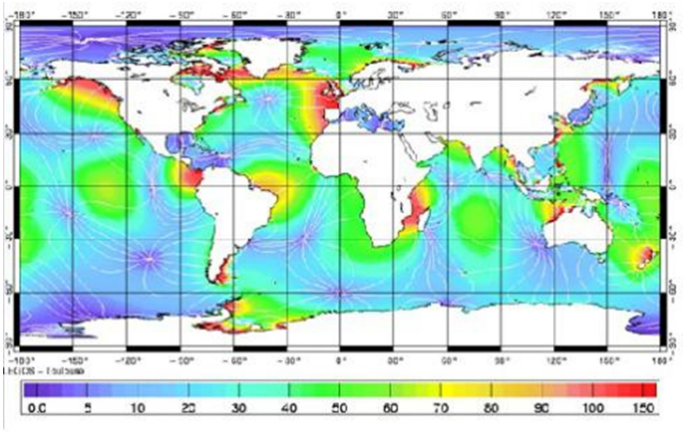

Figure 7: Worldwide tidal stream resource estimation based on the M2 tidal harmonic (acm) . Source [22]

European regions on the Atlantic coast can benefit from the attractive and fast tidal current velocities, coming from tidal periodical oscillation. On the other hand, the influence of oceanic currents in terms of potential energy is almost negligible, although other continents may profit from these streams. For instance, the Intergovernmental Panel on Climate Change (IPCC), suggests that oceanic currents could be a promising energy resource when technologies are capable of harnessing low velocity flows [23].

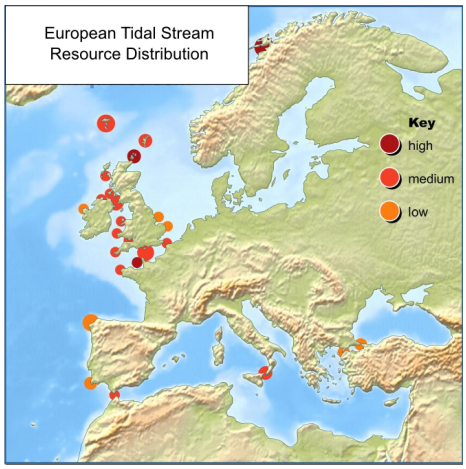

Figure 8: European tidal stream resource estimation. Source [24]

These tidal resources are perfectly localised. Across the world, high tidal stream velocities are available in coastal environments such as the East River (USA), Fundy Bay (Canada), Bass Strait (Australia) and Magallanes Strait (Chile) (Figure 7). Within the EU, several hydrokinetic hotspots are identified mainly in France and Great Britain, but also in Spain, Italy and Turkey. The cause of these hydrokinetic hotspots is due to the large continental shelf west of Europe, which eases the existence of large tidal ranges. The map from figure 8 introduces qualitatively these specific locations.

Specific to the UK, The Crown Estate [25] considers there to be potential for the deployment of tidal power converters capable of 95 TWh/year (32 GW). As it is shown in Figure 9 by two different maps estimating the tidal stream distribution, the resource potential is significant but it is distributed differently along the UK. As a consequence, powerful sources of hydrokinetic energy are available in specific locations. The Pentland Firth in north Scotland is one of the main hotspots for tidal energy. In addition to providing high stream velocities, a large number of islands that create accelerations of the flow due to a reduction of the flux area. Channel Islands, Severn Estuary, British Isles, Dover (South England), Islay and Orkney (location of the European Marine Energy Centre)

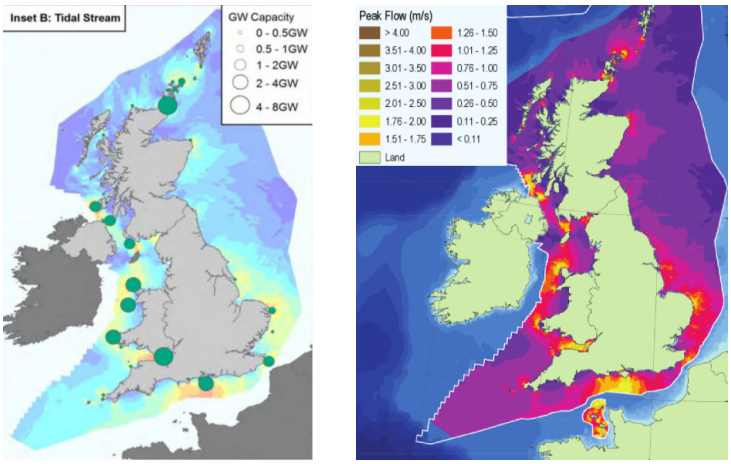

Figure 9: United Kingdom tidal stream resource estimation. Left, The Crown Estate map [25]. Right, ABP-MER map [26].

are also locations with great potential. The Welsh environment is particularly attractive, as Anglesey coast, Ramsey Sound, Pembrokeshire and the Severn Estuary provide large density flux on their shores.

3.3. Wave Energy

Wave energy is another consequence of solar radiation that is caught by Earth and transformed into another type of energy. In this case, ocean winds perform this energy transfer due to the combination of different temperature gradients between fluids and the influence of the Earth's rotation. The amount of energy transferred between air and water depends on wind velocity, period of time and the area affected by the oceanic wind. Although, potential energy values for a single train of waves cannot be calculated perfectly as these computations are dominated by variable criteria, a global estimation of the average energy density in the world oceans is considered to be within 5 and 10 KW per meter height [27].

The European Atlantic Coast is exposed to potent and energetic waves coming from the west. In general, countries such as Spain, France, Ireland, Norway

and the United Kingdom are fed by trains of waves with average energy densities around 40-50 KW/m. Some specific regions within these EU countries can reach up to 80-100 KW/m. Because of this high potential, efficient harnessing of wave energy has concentrated a great number of research projects. The main objective is to develop this technology towards its final stages, allowing the deployment of an array of wave energy converters. An estimation of wave range distribution in Europe is shown in figure 10.

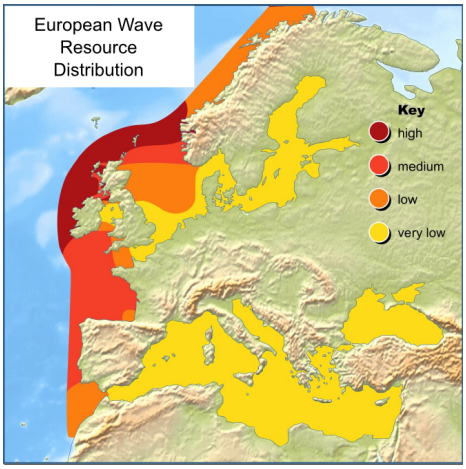

Figure 10: European wave resource estimation. Source [24]

Already, there are maps and reports which contain annual statistics of wave properties around the European coast, especially on the Atlantic shore. In addition to the visual reports and instrumental information gathered from the European buoy network, numerical simulations can predict accurately average energy values in any location of the ocean [28] [29]. Although, these numerical evaluations are subject to further work in order to increase the assessment quality for very specific locations.

The Crown Estate conducted as well a wave resource assessment using private and public organisms from Northern Ireland, Scotland, England and Wales [25]. Findings assert the potential wave resources in the United Kingdom would enable to provide an approximate energy of 70 TWh/year and 27 GW of power.

Wave resources, to an extent, are uniformly distributed on the north-west of Scotland, south-west of Wales and south-west of English coasts, with larger power densities when closer to the north (Figure 11). On the other hand, neither physical nor technical constraints from the deployment and management of wave energy converters, were taken into consideration when developing the map.

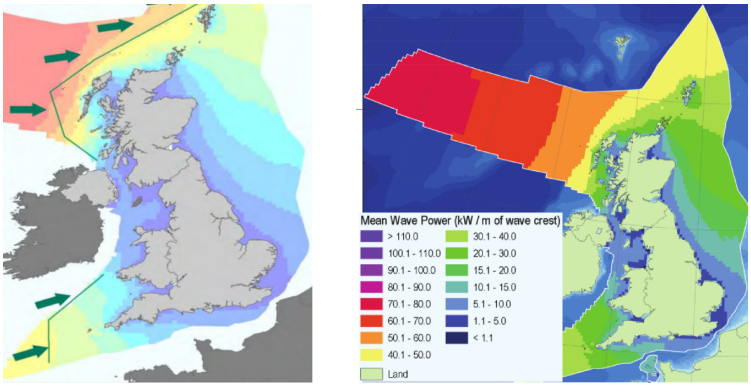

Figure 11: UK wave resource estimation. Left, The Crown Estate map [25]. Right, ABP-MER map [26]

3.4. Tidal potential energy

Energy generation via tidal potential energy can be achieved with the use of tidal power plants. This a concept which is similar to river hydro power stations, but completely isolating some areas of the shore. Although both constructions can be designed with sluices for navigation and fish ladders for certain species of fish, both are based on dam or breakwater structures which constrains the flow of water, altering the geographical and environmental conditions, both sides of the structure.

Within this marine renewable energy sector, France and the UK are the EU countries that enjoy the best environmental conditions in order to extract the ocean's potential energy with the use of tidal impoundments (Figure 12). Taking benefit of potential tidal energy requires large tidal ranges (difference between

lowest and highest water level height), as the equation that controls potential energy depends linearly on the water column height ($E_p = mgh$). These two countries have a very large continental shelf on their shores, which favours the existence of large tidal ranges. For instance, the maximum tidal range in the Severn Estuary, English Channel and the French north-west coast reaches up to 13 meters, listed as the second largest tidal range in the world.

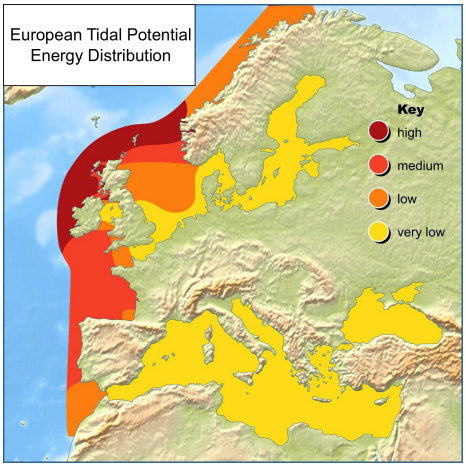

Figure 12: European tidal range estimation. Source [24]

In the UK, the potential energy from tidal potential energy, (including tidal barrage and tidal lagoon schemes) is around 120 TWh per year, and a corresponding power capacity of almost 60 GW [25]. In addition to the Severn Estuary case, which has been already mentioned, the other main location in the UK where tidal potential energy might provide a large source of electricity is the area between the east of the Isle of Man and the west coast of England, offering similar values in terms of potential power compared to the Severn Estuary. Finally, there are two potential energy spots on the east coast of England, coincident to two main river mouths that end into an estuary shape (Figure 13).

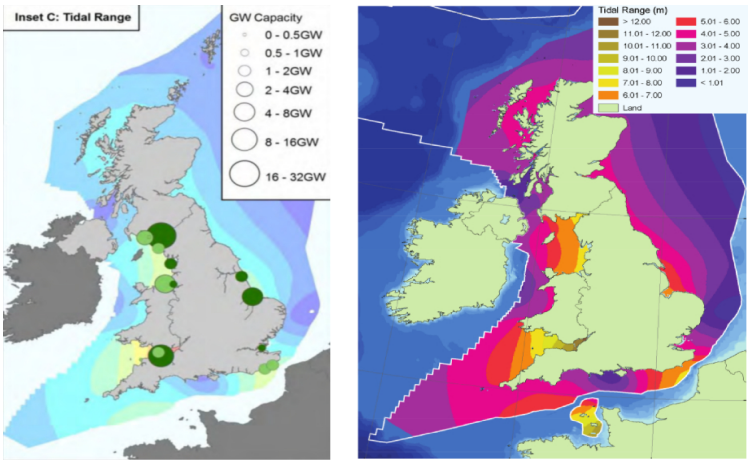

(a) The Crown Estate (b) Abp Mer

Figure 13: Tidal range resource estimation. Left, The Crown Estate map [25]. Right, ABP-MER map [26]

3.5. Wind Energy

Winds originated over the ocean are steadier than on mainland, as there are no geographical obstacles and the radiation and heat exchange between fluids is constant. Generally speaking, the further away from the coast, the steadier the winds are, but also the deeper the water level is [30]. Hence, power suppliers that use off-shore wind turbines are looking for novelties in the technology in order to deploy turbine arrays far from the coast, whilst not losing high performance from their structural and maintenance systems.

European winds are quite energetic 14, and those countries whose coasts are adjoined to the North Sea (Germany, Denmark, the Netherlends, etc.) are naturally supplied with capable wind speeds for off-shore wind turbine deployment. To a lesser extent, more punctual locations in the United Kingdom, north-west of France and the north-west of Spain are provided with high average wind speeds.

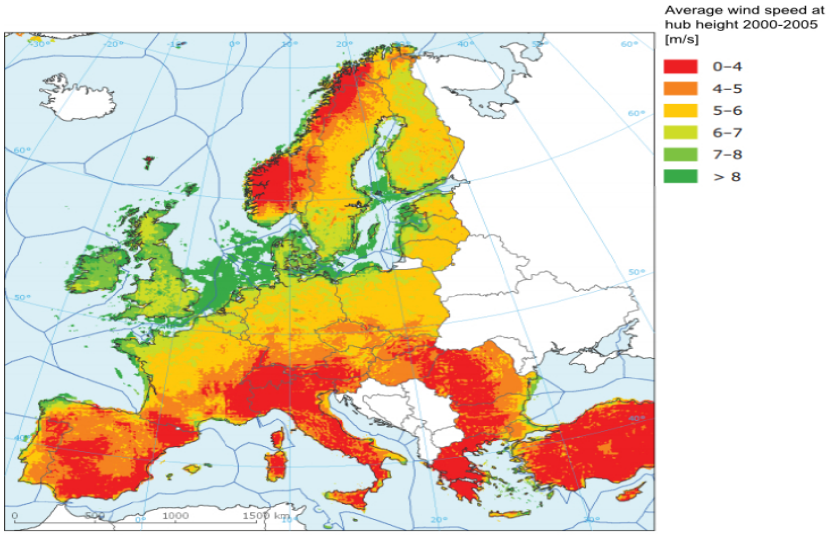

Figure 14: Average wind speed values in Europe. Source [30]

However, the harnessing of wind energy must not be analysed simply in terms of density energy values, the continental shelf area in coastal regions is also a significant parameter. Whereas the North Sea features wide regions with low water depths, the Atlantic Ocean is less suited for the deployment and foundation of off-shore wind turbines. Currently, civil engineering companies are unable to offer engineering solutions to wind turbines installed in water deeper than 40 m. This is an issue for regions such as the north of Spain and west France, where these depths can be reached just 5 km off-shore. This fact seems to encourage the evolution of floating structure technologies by countries in south-west Europe. The UK's location presents intermediate conditions in terms of water depth. Thus, high wind speeds are available on and off-shore, and water depths are not as deep as in Portugal, Spain and France, but the scenario is not as ideal as the environment of the North Sea.

3.6. Other Marine Energy

3.6.1. Osmosis

The concept of osmotic power (also named blue energy) resides in the energy available due to heat generated by chemical reactions that take place when two water bodies with different salt concentrations are merged. Two main procedures are used to obtain energy from this exothermic reaction, pressure retarded osmosis (PRO) and reverse electro-dialysis (RED). Both methods consist of osmosis with anion and cation exchange membranes [31], but PRE offers a higher potential for power generation as the saline brines used with this technique display higher power densities [32]. The process leads to the creation of a waste product called brackish water. This water, which is the consequence of a natural chemical reaction, is the product that is harnessed. The first osmotic energy power plant in the world has been installed in Tofte (Norway) which has a capacity of 10 kW, and has been operating successfully since 2009 [33].

3.6.2. Thermal energy

Ocean Thermal Energy Conversion (OTEC) is a technique that takes advantage of the temperature gradient between warm and cold water bodies. Thus, warm water bodies located in tropical oceans and cold water bodies placed at the bottom of oceans which come from the North and South Pole are used for this purpose. The difference between hot and cold temperatures in water bodies can be greater than 20° [34]. Table 5 displays some of the power plants that use OTEC technology, and its development throughout the last century.

Table 5: Examples of global power plant based on Ocean Thermal Energy Conversion. Source [34]

Name	**Country**	**Year**	**Power capacity**
Matanzas	Cuba	1930	22KWe
Abidjan	Ivory Coast	1954	-
Nauru	Japan	1970	100 KW
Keahole Point	Hawaii	1993	210KW
Tamil Nadu	India	2000	1MW

The finance that these power plants require is its main drawback, as investment could be ten times more than a traditional energetic system. Also, the efficiency of OTEC plants is quite low when compared to other energy extraction systems, and their location demands very specific conditions in terms of depth, oceanic current and distance from the coast. As a conclusion, island nations might be attracted by the idea of developing this technology in the near future [35].

3.6.3. Marine biofuel

Coasts benefit from their advantageous marine environment and micro-algae can be farmed in order to create biofuel. This marine biofuel is specially interesting in coastal areas that are more exposed to solar radiation, i.e. Spain and Portugal. Facilities designed for other particular objectives could be readjusted for micro-algae cultivation. For instance, an old natural kaolinite deposit is an area of interest for the mentioned farming purposes [36]. Another example is the project En-algae, in which researchers are developing a new biofuel based on algae [37].

Developments in harvesting and processing micro-algae are expected to further improve the cost-efficiency ratio. [38] shows in their review that Biodiesel, Bio-oil, Biosyngas and Biohydrogen can be derived from different micro-algal processes.

4. Marine renewable energy technology

4.1. Tidal stream energy

4.1.1. Tidal Theory

Tides are oscillatory movements on the water level of oceans due to the gravitational forces from the Moon and Sun exerted on Earth. The tide's periodic behaviour and difference of water level depends on the relative position of these

three elements, Earth, Moon and Sun. The exact influence of these components also depends on factors such as geographical location, meteorology, ocean depth and seabed shape.

Two clear processes are involved in the physics of tides: the rotation of the Moon and Earth as a whole, and the relative positions of the three system solar components. Firstly, tides are affected by the centrifuge force created when the Moon and the Earth rotate over each other in space. As the Earth's mass is about 100 times bigger than the Moon's mass, the movement of the Moon is more ostensible. However, the relative rotational axis between the Earth and Moon is not located exactly at the middle point of distance between the two bodies. Due to the superior mass of the Earth, the axis of rotation is closer to the Earth than to the Moon (the axis is even geometrically located within the Earth sphere). Figure 15 sketches the phenomena. The mutual rotation around this axis produces a centrifuge force which is stronger on water bodies located on the furthest side of the Earth, with regards to the Moon. Therefore, on this further side the water would have a stronger attraction, creating high tides. A centrifuge force is also created in oceans that are closer to the Moon, but is a weaker force. This force is, obviously, smaller because the distance between the water surface to the common rotational axis (located within the boundaries of the Earth's sphere) is smaller as well. The second process is linked to the gravitational effect that the Moon exerts on the Earth. Therefore, the water bodies that are closer to the Moon will be affected more by the Moon's attraction (high tide), whereas the further away from the Moon, the lower the influence of the moon will be [39].

In summary, there is a small centrifuge force and a strong gravitational force that act on the closer oceans to the Moon, and a strong centrifuge force and a weak gravitational force for further water bodies. If a strictly mathematical analysis was carried out, the existing water alterations on every side of the Earth would be equal, but in practise there are factors such as rotational axis

inclination and the ocean's topography that distort the magnitude of alterations.

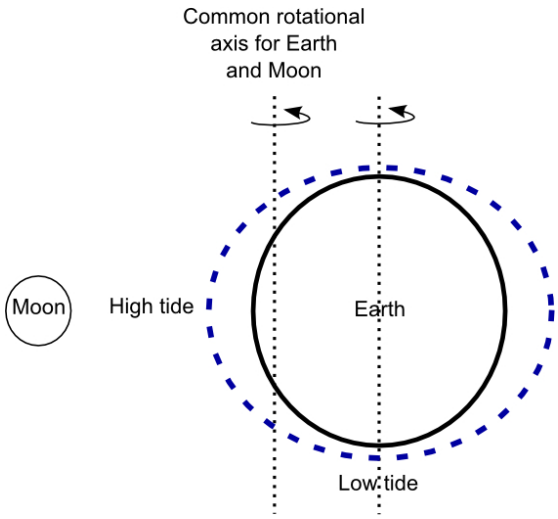

Figure 15: Sketch diagram of the forces that the Moon exerts on the Earth. Dashed blue line, ocean representation

On the same basis, the Sun causes increases and decreases in ocean water levels. Nevertheless, the gravitational force is proportional to the mass but it is in inverse proportion to the squared distance between bodies. Therefore, although the Sun's mass is 27,000,000% greater than the Moon, the distance between bodies is also 400,000% larger. This fact brings as a conclusion that the effect of the Moon on the tides doubles the influence of the Sun.

According to the physics herein explained, at full and new moon times (when the Sun, Earth and Moon are aligned), forces are coincidently at their maximum, causing spring tides (the greatest difference between low and high tide). On the other hand, when the angle between the Sun, Earth and Moon is 90%, gravitational and centrifuge forces are counteracted. This phenomenon is called neap tides, which means the amplitude of tides is at its minimum.

As explained previously, the study of astronomic tides can be addressed from the scope of Newton's laws of motion. However, this approach can be derived

into the harmonic analysis of tidal periodical components. This analysis is based on the physical and mathematical identification of periodical or oscillating components that form tides. The theory confirms that water level variations can be described and identified as a function of harmonic contributions added by different force components. The study of the Earth-Moon-Sun's relative positioning remains the main aspect taken into consideration when implementing and adding up harmonic components. The analysis of wave propagations is a complex study, as every ocean has different environmental, meteorological and geographical conditions. Tidal gauges can show graphically water elevation versus time and, as a consequence, characterise the tide components at that particular point and subsequently predict the water elevation.

Each tidal component has its own amplitude, phase and period, and although many components of the oscillations have been identified, usually the periodical components that can identify the tidal oscillation are just four. Thus, the main harmonic components or tidal constituents associated to the Moon's influence are named M2 and O1, where the main components linked to the Sun's influence are S2 and K1. M2 is a semidiurnal component equal to half a lunar day (12 hours and 25 minutes) and S2 is also semidiurnal, equalling half a solar/earth day (12 hours). O1 and K1 are diurnal components, and both are exactly double the time of their semidiurnal companion. Because of the 50 minute difference between lunar and solar oscillation components, high and low tide times are also shifted, periodically, 50 minutes every day [40].

Figure 16 shows the global distribution of the different types of tides. It can be seen that semidiurnal tides are the most common tidal type (almost the entire European coast is dominated by this type of tide), and diurnal tides exist only in punctual locations but are predominant on the Antarctic shore. Depending on the influence that tides exert on shores, estuary tides can be also classified regarding their hydrodynamical effect. Therefore, macrotidal estuaries are known to greatly affect shores because of the tidal motion (tidal ranges

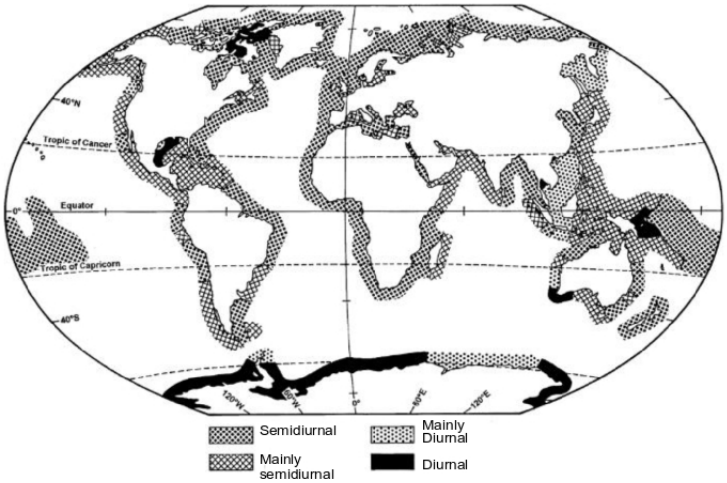

Figure 16: Influence of the tidal constituents in the world tide distribution. Source [41].

larger than 4m), mesotidal estuaries are influenced by the tides, but they do not completely control the water motion (tidal ranges between 2m and 4m), and microtidal estuaries are characterised by small tides which are not able to modify the marine condition in the estuary (tidal range smaller than 2m) [42].

4.1.2. Tidal turbine components

Tidal stream turbines, which utilise high flow currents, can be considered similar to under water wind turbines. The main divergences reside in harsher environmental conditions and higher densities that are achieved in water. Although many specific devices will not display all these parts, the main components of a tidal stream turbine are briefly described.

1. Support structure. This part of the turbine ensures the stability and resilience of the entire tidal turbine structure, in addition to bearing the torque curves and fatigue loads [43]. Five main strategies are commonly used for the turbine's support.

    - Monopile. This type of structure is based on a column or pile that penetrates the seabed by up to 25m in soft seabed conditions. Usually

the design consists of a hollow-steel pile with a large diameter. In the specific case of a rocky seabed, pre-drilling is required, elevating the costs. Also, the economical cost of drilling the seabed increases exponentially the greater the depth is.

- Jacket. In this structural decision, a structural base with protuberances in its corners is anchored to the bottom using steel piles. The steel piles penetrate slightly less than monopile cases, around 15m into the seabed for soft conditions. This type of structure has been used for many years in the oil industry, therefore there is more theoretical and practical information for future uses.
- Gravity base. A gravity structure that holds the tidal device in position and resists translation and rotation by its own weight. Usually concrete is the main material, although sand, water or steel can be used to fill the base and add weight to the structure. The main advantages are the following: easy construction, transportation and deployment, where the difficulties in deploying a gravity structure for large depths and the possible scour that could be produced are the drawbacks of this structural component.
- Floating structure. A floating structure allows the structure to move in relation to the oscillation of the sea. This technical solution maximises the tidal stream resource, as the higher speeds are located closer to the surface. Moreover, this structure allows the deployment of tidal turbines in deeper places compared to other solutions. On the other hand, ideal mooring lines have not yet been found, and both rigid and flexible mooring lines are looking for a compromise between bearing very high load curves (tight mooring), or large device displacements (loose mooring).
- Hydrofoil lift downforce. This component takes advantage of the lift force that a hydrofoil generates when the flow of water goes through its surface. Thus, several hydrofoils leads this lift force downwards,

which holds the device in position.

2. Rotor. This turbine component converts water kinetic energy into mechanical energy. The rotor consists simply of blades (which transform the energy flux into hydrodynamical lift/drag force) and the connection between blades and shaft. The number of blades might differ between designs, and projects with two-bladed rotors and twelve-bladed rotors have displayed good performances. However, the predominant rotor lay up includes three blades for a horizontal tidal turbine. Blades are usually made of composites, which could be carbon-fibre reinforced plastic (CFRP) or glass-fibre plastic (GRP). Some rotors may have mechanisms to control the orientation of the blade in two directions, which are commonly called pitch and yaw [44].

    - Pitch. Pitch control is referred to the angle of attack from the blade. Varying the pitch angle allows an increase and decrease in the ratio of lift/drag force, ratio that drives the rotational speed of the rotor. It is commonly used to slow down the rotor speed when the incoming flow speed is larger than the accepted maximum flow speed.
    - Yaw. Yaw control is described as the angle between flow direction and blade positioning. Misalignments on this angle might result in lower efficiency values and higher irregular loads. As tides are not fully bi- directional, these mechanisms would tweak the position of the blades into the optimised place.

3. Drive Train. This component consists of the entire electro-mechanic system that converts the mechanical energy into electricity. Within this wide description, basic components including the gearbox, generator, safety breaks and shafts are included. These components are commonly connected by the use of mechanical couplings.

    - Gearbox. The gearbox converts slow rotational speeds coming from the rotor shaft into the very high rotational speeds that the generators require. Rotations per minute can be estimated to be within

the range of 10-40 for full scale devices, although this speed would always depend on the rotor size. Despite the fact that main gearboxes in the market are made for decreasing the rotational speed, planetary gearboxes allow the increase of speed, reducing the torque that reaches the generator shaft. These high torque values might be an issue, and more resilient gearboxes are usually specifically made for these uses. A gearbox causes losses on power extraction, losses that are usually within the range of 95-97% for one-stage gearboxes [45].

- Generator. The generator is responsible for transforming mechanical energy, coming from the rotor which is modified by the gearbox, into electricity. Brushed DC motors and induction generators are possible, but permanent magnet generators are the most common option for this component. A current technological challenge consists of decreasing the rotational speed rate for generators, in order to decrease the gearbox ratio as much as possible. Ideally, very slow generators would not require gearboxes (direct drive), although the larger the turbine dimensions are, the lower the generator's rotational speed rate must be. A research work developed a specific generator for tidal turbine conditions, but dimensions of the generator are larger than common generators [46]
- Couplings. Mechanical (or even magnetic) couplings are used to connect two different shafts so that rotational speed and torque is transmitted from one shaft to the other. In addition to its joint function, shafts are unlikely to be completely aligned, and couplings enable slight tolerances in terms of axis misalignments.
- Safety Break. This part protects the rotor from any possible damage when high stream velocities are reached. If the approach flow speed is higher than the turbine's limitations, the break comes into operation, not releasing the shaft motion until the flow speed has decreased.

4. Nacelle. The nacelle is a common part of HATT designs and is responsible for holding the drive train in position. This part usually lies on the support structure with the use of special bearings and sealing strategies. The issues related to the components of the mechanical-electrical system that is held by the nacelle are studied in depth by academia and industry, as maintenance problems related to these components include the nacelle giving rise to the highest costs on turbine operation and management [47]. Other turbine technologies might not need the use of this component, but they will face similar replacement and repair operations for other components.

4.1.3. Turbine technologies

This chapter presents the main power converters that have been built or projected for the extraction of electrical energy from tidal currents. Devices and designs that claim more than 200 KW of power capacity and significant designs which provide novelty to the research topic are described in depth. The most common pattern observed in most powerful rotors that reached full scale sizes is based on three-bladed horizontal axis tidal turbines, but other designs differ from this convention and deliver reasonable efficiencies and power capacities.

4.1.4. Horizontal Axis Tidal Turbines

In a few words, horizontal axis tidal turbines generate energy from water streams in a similar way as horizontal wind turbines extract power from air streams. The water flowing through the rotor creates hydrodynamical forces that turns the blades, causing the rotor to spin over its axis, generating mechanical energy. This technology has taken advantage of available knowledge taken from wind turbines, which in some aspects can be applied to marine environments. The great quantity of information that has been refined throughout research and development projects during the last decades, and the high efficiency values that this typology is able to achieve are the main motivations that

led tidal turbine engineers to this design. At this moment only HATTs seem to be the most advanced design, technologically and financially, for full scale tidal stream converters with power capacities over 500 kW [48].

The company named Alstom have proposed a horizontal axis turbine consisting of three blades which are able to change their pitch angle. A three-foot gravity base holds the 24m long nacelle and 18m diameter rotor. In order to provide stability to the whole structure, the device's total weight is 150Tn. A full scale prototype was tested in Orkney, Scotland, at the European Marine Energy Centre facilities (EMEC). The device performed robustly, as the design was able to operate independently in an environment 40m below water. The large scale device delivered 1MW of power, and their ultimate device named "Innovative Oceade" is claimed to reach up to 1.4 MW [49].

The Alstom's device and the projects named Andritz Hydro Hammerfest, Atlantis and Voith share similar characteristics. The three devices have displayed steady performances, all of them featuring three-bladed rotors with gravity base born by three feet as well. The Atlantis tidal stream turbine's current speed has been rated at 65m/s for 1MW, the Andritz Hydro Hammerfest 1 MW device has also been deployed at the EMEC in full scale and the company Voith have operated their devices in Europe and in Korea. On the other hand, blade shapes and rotor sizes differ between designs. Thus, the Atlantis project provides the largest rotor diameter (18m), whereas Andritz Hydro Hammerfest and Voith are 16m and 13m [50], [51]. Pictures of the full scale devices are enclosed in figure 17.

In 2015, the company Tidal Delta Stream deployed in Pembrokeshire, Wales, an analogous power device (three blades and gravity base). The main discrepancy in comparison to other projects derives from the ambitious target of having three identical rotors using just one gravity base. The design company deployed the whole structure with just one rotor rated at 0.4MW, and further work is being carried out in order to install two more rotors [52].

(a) Alstom [49]

(b) Sea Gen [56]

(c) Andritz Andro Hammerfest [50]

(d) Tidal Delta Stream [52]

Figure 17: Main Horizontal Axis Tidal Turbines in the market i). Photo references included in the text

The Sea Gen turbine is a tidal turbine design that consists of a monopile structure that bears two two-bladed rotors. Its design is substantially different compared to previous power converters. The first main stage of this project was carried out in 2003, when a 300 kW device was the world's first tidal stream turbine in operation and on a full scale (named Seaflow at that time). The development of the technology has been widely described throughout the last decade [55] and derived on a bigger turbine, with a 16m diameter and a power take off system that enables to extract up to 1.2 MW. In other words, this device which is able to work 18 to 20 hours a day, is able to provide electricity for approximately 1000 houses. The full scale device has operated in a natural environment, with the structural pile seen above the water's surface. At the time of the writing, the project is at its final stage, aiming to upgrade the design to reach up to 2 MW [56].

The Sabella project is also based on a three-foot gravity base, but their rotor shows six fixed blades without any mechanism to modify the pitch angle. With a 10m diameter and 1MW of power generation, the Sabella prototype was tested

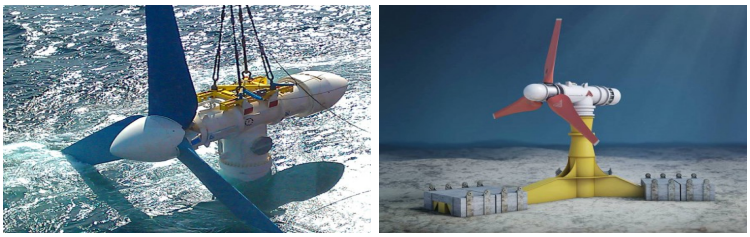

(a) Voith [51]

(b) Atlantis [53]

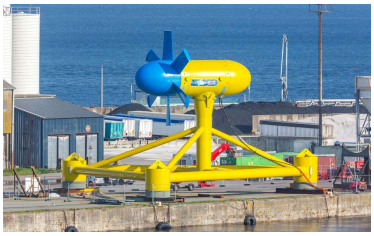

(c) Sabella [57]

(d) Open Hydro [54]

Figure 18: Main Horizontal Axis Tidal Turbines in the market ii). Photo references included in the text

at full scale in Fromveur Strait, France in 2015. The design team is currently working on the development of a 2.5MW device [57].

The technology corresponding to the turbine designed by Verdant Power slightly resembles some of the previous rotor compositions. The three-bladed rotor includes a system to change the yaw angle of the whole nacelle, and the structure is sustained by a vertical pile support. The rotor diameter is 5m long, although further improvements are expected enabling an increase in the capacity of power generation up to 2.25 MW [58]. This turbine and the others previously mentioned are included in figure 18.

Hydra Tidal showed a distant structural approach, as a floating structure was chosen. This buoyant structure enables to install four rotors, rotors that consist of two pitchable blades. The full scale prototype was tested in Lofoten, Norway in 2010, although the technology is still under development due to fatigue problems [59].

A floating structure is also the structural decision chosen by Scotrenewables.

(a) Clean Current [63]

(b) Nautricity [62]

(c) Magallanes [60]

(d) Scotsrenewable [61]

Figure 19: Main Horizontal Axis Tidal Turbines in the market iii). Photo references included in the text.

Their buoyant structure is 33m long and bears two rotors consisted of two blades. The device delivered 250 KW for a rated current velocity of 3m/s, but a 2 MW power converter is currently under development [61].

The Nautricity project registered a pioneering device consisting of a three-bladed rotor interlinked with a four-bladed rotor. Their Cormat device has not been tested in full scale and the prototype requires further development to achieve the intended 0.5 MW power capacity [62].

The Open Hydro project presents a novel design. A double piling structure holds in position and distributes loads and stresses, whereas the number of blades may differ from 10 to 18 blades depending on the turbine scale. The 23m diameter rotor is lowered into the sea using two hydraulic winches, and their 7th prototype generation design is able to produce up to 1MW. The generators magnets are embedded within the blades whereas the winding is located in the rotor case [64], which is a different approach for the power generation in comparison to the usual electromechanical systems used in tidal turbines.

Clean Current's tidal stream device presents a ducted horizontal axis rotor. The prototype was tested at the Race Rocks in Canada and, as with the Open Hydro turbine, the generator's magnets are set inside the blade. Although the company who designed it claimed to achieve an increase on the power output close to 40% when compared to non-diffuser turbines, the project exited in 2015 [64].

The Hydro Green Energy tidal turbine introduces a diffuser, aiming to drive and accelerate the flow towards the direction of the turbine. The three-bladed rotor was tested in a downstream position at a hydroelectric power station. An environmental study that analysed the fish survival rate was published, reporting 99.6% of fish survived [65].

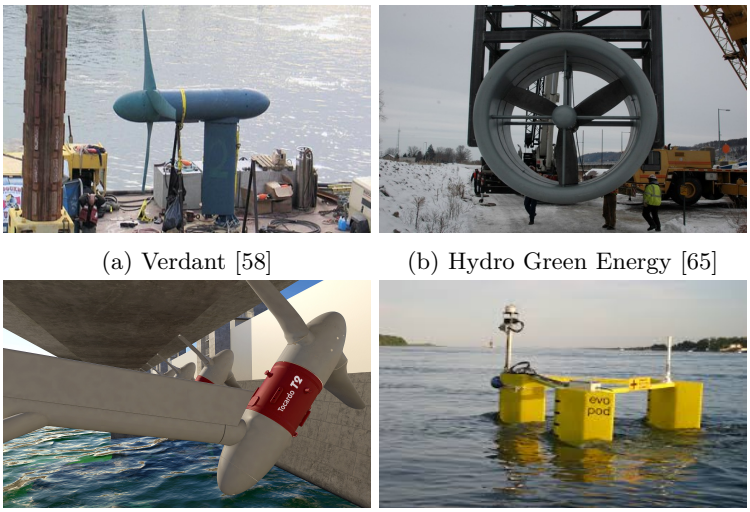

(a) Verdant [58] (b) Hydro Green Energy [65]

(c) Tocardo [66] (d) Evopod [67]

Figure 20: Main Horizontal Axis Tidal Turbines in the market. Photo references included in the text

Tocardo's design idea is based on a floating platform which can hold several 9 m two-bladed turbines. The technology has been verified although the limitations of size are under research. The power take-off is gear-less, which is unusual as the rotational speed of the device is rated at 45 rpm [66]. A picture of the this device and other tidal turbines can be seen in figure 19.

A large number of tidal stream devices have been projected and tested with low power capacity, less than 0.1MW. Some of these projects either did not continue their research or they are still under development. All the recognised designs found in literature and their main characteristics are included in Table 6.

Table 6: Summary of the Horizontal Axis Tidal Turbine Technologies

Project Name	**Main properties**	**Size**	**Power**	**Research Stage and Significant Information**
Alstom	3 Pitchable Blades Gravity Base - 3 Feet	Diameter - 18m Weight - 150 Tn Nacelle - 24m	1MW	Full scale tested Testing fully independence Tests at Orkney, Scotland (EMEC) Tested for 40m water depth
Sea Gen	2 Blades 2 Rotors Monopile structure	Diameter - 16m	1.2MW	Full scale tested 2 MW Under Development Pile seen above water surface
Andritz Hydro Hammerfest	3 Blades Gravity Base - 3 Feet	Total height - 30 m	1MW	Full scale tested Tests at Orkney, Scotland (EMEC)
Atlantis	3 Blades Gravity Base - 3 Feet	Diameter - 18m Weight - 1300 Tn Total height- 22.5m	1MW	Full scale tested 1.5 MW Under Development Rated Current speed - 2.65 m/s
Voith	3 Blades Gravity Base - 3 Feet	Diameter - 13m Weight 200 Tn Pile length - 23m	1MW	Full scale tested 1:3 scale prototype tested in Korea.
Hydra Tidal	2 Pitchable Blades 4 Rotors Floating structure	Diameter - 23m	1.5MW	Full scale tested Technology under development Problems due to fatigue Wooden blades Tested in Lofoten, Norway (2010)
Sabella	6 Fixed Blades Gravity Base - 3 Feet	Diameter - 10m	1MW	Full scale tested 2.5 MW Under Development Deployed in Fromveur Strait, France (2015)
Open Hydro	10 to 18 Blades Double Piling	16m Diameter	1MW	7th Prototype Generation Lowered into the sea using

				two hydraulic winches
Rotech Tidal Turbine	5 Blades Venturi Diffuser Gravity Base	Diameter - 15m Weight - 600Kg	1MW	1.5MW Under development
Nautricity	1 Rotor - 3 Blades 1 Rotor - 4 Blades	Diameter - 9m	500KW	Full scale under development Water depths from 8 to 500m
Tidal Delta Stream	3 Blades Gravity Base - 3 Feet	Diameter -15m Total height - 20m	400KW	1.2 MW Under Development Deployed at Ramsey Sound, Wales (2015)
Scotrenewables Energy	2 Blades Floating structure	Total length - 33m Total weight - 500Tn	250KW	2 MW Under Development Rated current velocity - 3m/s
Clean Current	3 Blades Diffuser	Diameter - 7m	247 KW	Intermediate scale - 1.5 m Rotor Towering boat Rated current velocity - 3m/s Central yawing
Tocardo	2 Fixed Blades Floating platform	Diameter - Up to 9m	200KW	Technology verified Size limits under research Gearless Rated Current Velocity – 45 rpm
Magallanes	3 Fixed Blades 2 Rotors Floating structure	Length - 40m Weight - 750 Tn	75KW	1:10 Scale Model Full Scale Under development Aiming at 2MW
Hydro Green Energy	3 Blades Diffuser	Diameter - 3m	100KW	Commercial prototype Downstream hydroelectric plant 99.6 Fish survival
Schottel	3 Blades Variable structure	Diameter - 4m	50KW	Adaptable to different structures Tested at Strangford Lough, Northern Ireland
Sea Urchin	12 Blades Diffuser	Diameter - 1.1m Length - 1.2m	2KW	1/10 Tested 1 MW Under development

				Minimum current velocity 1.5 m/s
Verdant Power	3 Blades Vertical pile support	Diameter - 5m	-	2.25 MW Under development Gearbox Yawing system
Triton	2 Blades 3 Rotor Buoyant + Anchorage	Diamater - 1.5m	-	1/10 Scale Tested Full Scale Under development Tested in the river Thames (UK)
Free flow power	7 Blades Diffuser	Diameter - 1.8m	40KW	10 MW array under development Minimum current velocity - 2.2 m/s Rated rotational speed - 32rpm
Evopod	Horizontal axis 4 Blades Floating structure	-	35KW	1/40 and 1/4 Tested Full scale under development Catenary mooring system

4.1.5. Vertical Axis Tidal Turbines

This typology of tidal turbines has also been researched in depth in order to harness wind energy. Then, the tidal stream energy sector has been taking advantage of knowledge gathered throughout past research studies. The number of marine power converters that use this particular design is less than the amount of horizontal axis turbines that has been projected so far, which is one of the main reasons that led to the publication of this thesis. In addition to this matter, the projects involved in the design of vertical axis turbines have not yet been able to develop any full scale devices, having tested just prototypes with low power capacities. Table 7 shows the different turbine projects that have been collected from the literature. This type of rotor gives rise to advantages and drawbacks when compared to horizontal axis tidal turbines [68], [69].

Main advantages:

- Omni-directionality. The vertical axis tidal turbine can rotate independently of the direction of flow. This fact is probably the greatest interest of this design, because it implies that there is no need for a mechanism that changes the yaw angle of the blades. Another consequence of this feature is the ability of the rotor to spin in reverse, which means that the turbine can operate in ebb and flood tides.

- Constant blade section. The HATT described in the previous section does not display uniform blade cross-sections, whereas some of these rotor designs can be built with a constant blade section. Hence, the simpler the blade manufacturing becomes, the greater the decrease in construction costs.

- Structural flexibility. The vertical shaft gives room to a wide range of structural compositions. As a result, some devices perform with power take-off above the rotor or even above the water surface.

Main Disadvantages:

- Self-start processes. The physics behind the turbine's rotation becomes more difficult, since parameters like the angle of attack (AoA) are not constant any more. In addition to this, rotors wrongly dimensioned may not start on their own. It has been found that parameters such as flow speed, number of blades, blade thickness and solidity can be key factors associated with the turbine's starting torque, which controls the start of the turbine's rotation [71]. This issue is analysed in depth in the following section where the influence of the rotor parameters is scientifically analysed and quantified.

- Low efficiencies. Although they provide reasonable efficiency values, horizontal axis seem to provide a superior performance. As a ball-park figure, horizontal axis can provide between 30 to 40% efficiency, whereas an approximate efficiency value for vertical axis tidal turbines would remain at 25 to 35%. The reasoning behind this figures is anew explained in the section where the parameters that lead the turbine rotation are studied in depth.

- Vibration and fatigue. As the turbine's rotation is not driven by constant forces, the torque and rotational speed curves are not uniform. As a consequence, vibrations on the support structure can be derived, which affect the durability of the device and increase the number of maintenance operations.

Similarly to the characterisation of the current HATT technologies, a wide description of existent or paused tidal turbine projects based on VATT designs is included in this section.

The Kobold project is considered one of the most successful research projects in the VATT area. A three-straight-bladed rotor was tested using a floating

structure to hold the turbine in position. Blades were 6 m high and had a chord length of 0.4 m, creating a 6 m diameter rotor. The 80 KW was tested in Messina Strait, Italy, displaying a self-start initial rotation and an average rotational speed close to 12 rpm (revolution per minute). Several pieces of work provided by very useful information for future research [72] [73].

The device conceived by New Energy Corporation is recognised as the turbine with the highest power capacity. The turbine claims to achieve a power extraction of 250KW for several commercial schemes, all of them including a gearbox and a safety break on their power take-off system when it is not in operation. The largest commercial device consists of four straight blades, which are included in a 7 m diameter arrangement. The technical solution chosen for the connection between blade-shaft was accomplished by two spokes per blade [74].

The company Tidal Energy Pty designed a four-straight-bladed rotor, although in this case the connection blade-shaft consisted of two solid discs adjusted on top and bottom of the blade. A Venturi diffuser is added to accelerate the flow and the system is sustained by a gravity base [75].

The main characteristic of the Gorlov turbine resides in their twisted blades. This concept has been studied deeply throughout the last decades and, as it is explained in detail in the following section, twisted blades provide higher rotational speeds, favours the self-start of the rotor and gives rise to steadier torque curves [76]. Therefore, the Gorlov Helical Turbine group (GKC Technology) continued the research developed by A. Gorlov and the current objective is to deploy an array of turbines in Korea which would extract up to 100MW [77].

Current Power tested in Uppsala, Finland a 5KW device which consisted of a three-twisted-bladed rotor. The full scale device is expected to have slow rotational speeds, close to 10 rotations per minute [78]. A similar project in terms of scale named Encurrent drew up a rotor with four straight blades. 7.6

m diameter and 7.6 m height are the predicted dimensions for the expected final product, having tested a 25 KW device in natural conditions so far [79]. These devices are depicted in figure 21.

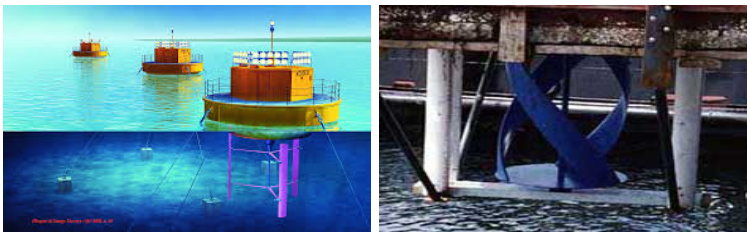

(a) Kobold [73]

(b) GCK technology [77]

(c) EnCurrent [79]

(d) Neptune [81]

Figure 21: Main Vertical Axis Tidal Turbines in the market. Photo references included in the text.

The research Neptune Proteus was one of the first vertical axis turbine designs that appeared on the scientific scene, although research based on this idea has been paused [80]. The full scale prototype was measured to weight up to 150Tn and to have a maximum length of 20m for the Venturi diffuser. Unfortunately, this technology did not take off and went in 2013 into administration [81].

The Blue Energy marine turbine consists of four or three-bladed rotors. Their fixed blades are connected by spokes to the rotor, and the rotor is placed within a concrete marine caisson, which anchors the unit to the seabed. The duct or diffuser directs the flow stream in the direction of the rotor and also supports the power take-off system. This Canadian design was tested in 1981 for at 20 KW, and the research group claims that a five-fold increase on efficiency was achieved [64].

4.1.6. Other Tidal Turbines designs

Apart from the two main turbine approaches characterised by the alignment of the turbine axis, many other concepts of energy extraction have been engineered in order to harness tidal stream energy.

Transverse Horizontal Axis Tidal Turbines (THATT) is an approach that incorporates concepts from both horizontal and vertical axis turbines. The rotational axis is horizontal, but in this case the rotor is placed perpendicular to the direction of flow. However, the rotor has been adopted from VATT technology, and the usual design of this relies on twisted blades. The main advantage of this concept resides on the possibility of creating tidal fences, i,e. broad turbine systems which can be extended along the sea bed for kilometres. These power converters might not be as efficient as other technologies but due to their considerable lengths, their power capacity can be superior to other tidal turbine designs.

Two main projects have taken the lead in research of this new concept. The Kepler project is studying the properties of a three-twisted-bladed rotor for very large lengths. The company claims to be attempting to design a 5.2MW device for a flow speed of 2.5m/s [82].

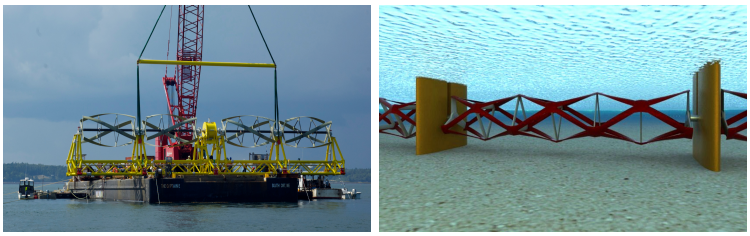

(a) TidGen [83] (b) Kepler [82]

Figure 22: Transverse Horizontal Axis Tidal Turbines

The other primary project for transverse horizontal axis turbines is TidGen. The main rotor parameters are kept (three twisted blades), but the device can reach up to 600KW of power capacity which has already been tested in Cobscook

Bay, USA. A larger device is planned to be built in 2020 [83]. Pictures can be seen in figure 22.

In addition to previous tidal turbine approaches which take advantage of hydrodynamic forces generated by hydrofoils, other concepts that involve completely different physics have been designed to transform kinetic energy into electricity.

The Flumill project is based on the Archimedes Screw concept. This design consists of a screw (helical pattern) that rotates within a hollow cylinder which is placed on an inclined plane. For the common and old use of this concept (pump water from lower positions to higher), this inclination can elevate the fluid located underneath the rotational axis. However, in this case water goes through the screw and presses the blades of the turbine, which forces the turbine to rotate. It is considered very environmentally and fish friendly, with low maintenance costs and cavitation issues. The power capacity is proportional to the screw diameter, and the largest diameter that has been tested was 2m and a length of 8m. A 1:4 scale prototype with a power capacity of 0.3 MW was tested at the EMEC, and further work expects to develop a 2.2 MW device in order to deploy it in Norway [84].

The Minesto project has engineered an underwater kite. The water stream creates a lift force on the kite which pushes it. The kite follows an eight-shaped trajectory by the use of a rudder, which can reach a velocity ten times faster than the approach flow speed. Due to the high speed of the kite, the power take-off is gearless, as the rated nominal speed of the generator is achieved. A 850KW device has been tested, with a corresponding wingspan of 14m and a total weight of 7Tn. The developer's target consists of deploying an array of 10 MW kites in Holyhead Deep [85].

The Atlantis AN is a shallow water device which has been successfully tested in San Remo, Australia. The turbine uses a very large number of hydrofoils

(a) Flumill [84]

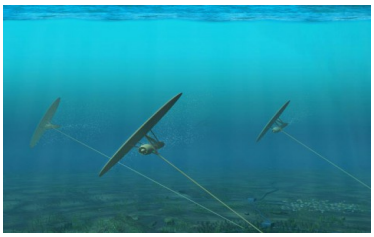

(b) Minesto [85]

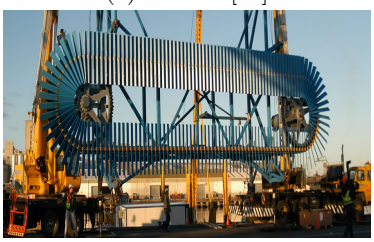

(c) Atlantis AN [86]

(d) Pulse Tidal [87]

Figure 23: Other typologies of Tidal Turbines

(around 100 blades) connected to a chain that is perpendicular to the flow. These hydrofoils capture momentum from the flow driving a chain that is perpendicular to the flow. The greatest device weighed 30Tn in order to generate 150 kW, and the next generation of turbines is currently under development [86].

The project Pulse Tidal is based on a system that uses hydrofoils or 'sea-wings' which move horizontal blades up and down in order to harness the tidal stream power. The Crown Estate has awarded Pulse Tidal with an Agreement for Lease at the Marine Energy Park in Devon (UK), which allows the company to deploy a 1.2MW tidal device [87]. These devices are depicted in figure 23.

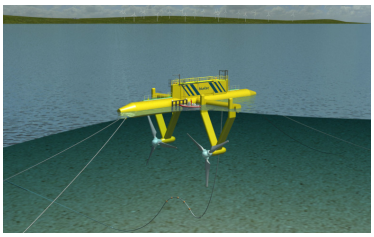

(a) Blue Tec [92]

(b) Sea Snail [93]

Apart from devices based on lift/drag forces created because of pressure distributions over the blade's profile, the Savonius turbine is based on forces created using the flow's momentum to push a solid component. The basic design of a Savonius turbine consists of two half cylinders with concave sides facing the incoming flow (Figure 25). Several research studies have analysed the parameters that characterise the performance of a Savonius rotor, in order to optimise its design and maximise its efficiency [88].

This type of vertical axis turbine has not been yet assessed for large scale devices because of its low efficiency (lower than 20 %) and low rotational speeds (they rotate slower than the upcoming flow). However, this type of rotor attracted the interest of researchers because of the chance of combining it with either a vertical axis tidal turbine [89] or a vertical axis wind turbine [90] as depicted in figure 25. Also, small river streams and weirs can benefit from this steady structure [89].

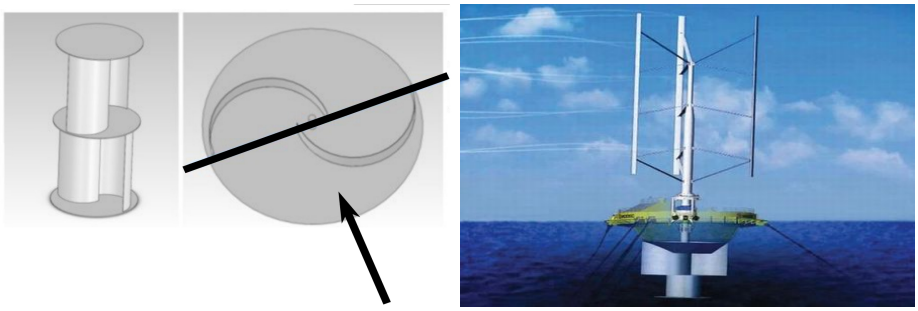

Figure 25: Left, Savounius sketch. Source [91]. Right, Savonius Keel and Wind Turbine Darrieus (SKWID)

Besides all the different available technologies planned to harness tidal stream energy on a large scale, certain projects have focused their efforts on designing structural supports for tidal turbines. Thus, BlueTec have engineered a floating structure which can be used for horizontal and vertical tidal turbines [92]. This floating base which is 24m wide and 40m long would require a minimum water depth of 8m in order to guarantee a valid structural performance. Another creative innovation is presented in [93]. The 30 Tn support base named Sea-Snail is

based on hydrofoils which generate a force downwards anchoring the structure to the bottom of the ocean.

Table 7: Summary of the non-Horizontal Axis Tidal Turbines

Project Name	**Main properties**	**Size**	**Power**	**Reserach Stage and Significant Information**
TidGen	Transverse Horizontal Axis 3 Twisted Blades	-	600KW	Aiming at full scale for 2020
Kepler	Transverse Horizontal Axis 3 Twisted Blades	-	-	Under development 5.2 MW potential for v=2.5 m/s Aiming at very large lengths (kms)
New Energy Corporation	Vertical Axis 4 blades	Diameter - 7.4m	250 KW	Several Commercial Designs Gearbox and Safety brake
Tidal Energy Pty	Vertical Axis 4 Blades Venturi Diffuser Discs as connection Blade-shaft Gravity Base	Diameter - 1.5m	15 KW	1/10 Scale Tested Commercialization stage
GKC Technology	Vertical Axis 3 Twisted Blades Top spokes as connection Blade- shaft	-	-	Aiming at 100MW array in Korea Gorlov concept has been researched throughout the last decades
Current Power	Vertical Axis 3 Blades Spokes as connection blade - shaft	-	5KW	Full Scale Under development Rated rotational speed - 10 rpm Tested at Uppsala University (Finland)
EnCurrent	Vertical axis 4 blades	Diameter -7.6m Height - 7.6m	25KW	-
Kobold	Vertical axis 3 Blades Floating structure	Diameter - 5m Height - 6m Chord length - 0.4m	80KW	Tested in Messina, Italy Rotational speed around12 rpm Self-Starting
Neptune	Vertical axis	Total diffuser length - 20m	-	Research has been slowed down

Proteus	Venturi Diffuser	Weight - 150Tn		
Flumill	Archimedes Screw concept Gravity Base or Predrilled Piles	Total length - 8m Diameter screw - 2m	300KW	1/4 Scale 2.2MW under development Buoyancy of the main rotor component
Minesto	Underwater Kite	Wingspan - 14m Total weight - 7 Tn	850KW	Three-kite array 10 MW in Holyhead Deep Need of a rudder Current velocity range - 1.2-2.5 m
Atlantis AN Series	Hydrofoils connect to a chain Around 100 Hydrofoils Monopile structure	Total weight - 30Tn	150KW	Next Generation Under development
BlueTec	Floating structure for Horizontal and Vertical Turbines	Floating base - 24 x 40 m		Minimum Water Depth - 8m

4.2. Wave energy

Wave energy converters can be classified according to their deployment position. Thus, either the wave energy device is set on-shore or off-shore. Nowadays, on-shore devices use the oscillation water column principle (OWC) to generate power, whereas off-shore devices accept a wide range of concepts or technical solutions to create energy. The engineering solutions for off-shore devices usually consist of taking advantage from disrupting the wave's motion and/or adapting to it, although the OWC concept is also taken into account for some prototypes.

Many devices have already been tested but none of them have been proved as a flawless solution, and the scientific field has not found the best physical concept in order to optimise energy extraction. Therefore, many concepts have been tested, which lead to building devices that differ substantially among them.

4.2.1. Shore devices

As mentioned, the majority of shore wave converters moored or attached to the coast takes advantage of the oscillation water column principle (OWC). This concept is based on driving the water pushed by the wave inside a network of chambers filled with air. The water flows into a chamber, moving the air that was filling the space, then, the air displacement moves a turbine (usually a Wells turbine) that is attached to a generator. Soon after that, the water from the wave flows out, allowing the chamber to be filled with air again and the process is repeated in a wave period basis.

Several of these shoreline fixed devices have been already built. The Limpet system (Scotland) and Pico (Portugal) were built as isolated systems, but in Mutriku (Spain) and in Sakata (Japan) were built as part of a breakwater cross-section. On the other hand, a Tapchan system (Tapered Channel in a Waver Power Plant) in Norway uses an overtopping solution. This technology is currently in its research and development stage and once its optimisation is

reached and their operation is fully guaranteed, these devices could be included in future coastal constructions and also adapted into existing defence structures.

(a) Limpet [94]

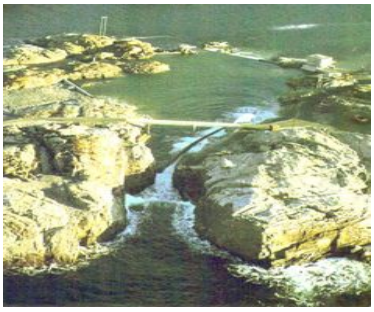

(b) Tapchan [95]

(c) Pico [96]

Figure 26: On-shore wave converters

The OWC system called Limpet is a wave converter that has been used to competently extract wave energy since 2000. This system had a maximum production rate of 500kW, although it has been reduced to 250kW. The Limpet wave energy device has been operating on the edge of an exposed cliff on the Island of Islay (UK). The design of this wave converter is optimal for wave energy intensities between 15 and 25kW/m. The wave power plants in Pico and Tapchan also follow this method with great results in terms of performance and efficiency.

The Limpet wave power plant scheme, which was patented and supported by Wavegen company in cooperation with Queen Belfast University, has been used for the Mutriku wave converter in the Basque Country. Thus, the use of

the OWC concept has been proved to work efficiently from a commercial point of view as well as its successful adaptation to other harbour structures.

(a) Mutriku [97] (b) Sakata [98]

Figure 27: On-shore wave converters installed within a breakwater

The Mutriku wave energy station was erected on the outer part of a 100 m rubblemound breakwater. This 296 KW power station is able to generate up to 600 GWh of electricity per annum since 2011. The rubblemound breakwater where the power plant was built is located in the Bay of Biscay in the Basque Country (Spain) [99].

Despite these successful projects [100] [101], the installation and operation of these power plants is not simple and these facilities have been hardly taken into account for marine energy developers and coastal breakwater designers. A picture of the described wave converter can be seen in figure 27.

4.2.2. Off-shore devices

As previously mentioned, power converters for wave energy are still under development and the optimal concept has yet to be agreed. Hence, off-shore device typologies admits different classifications depending on the technique and/or engineering concept adopted to produce energy from waves. Figure 28 visualises the three main classifications for off-shore wave power converters.

Interceptors. Wave energy converters which receive and physically stop the motion of the wave are classified as interceptors devices. A wide range of

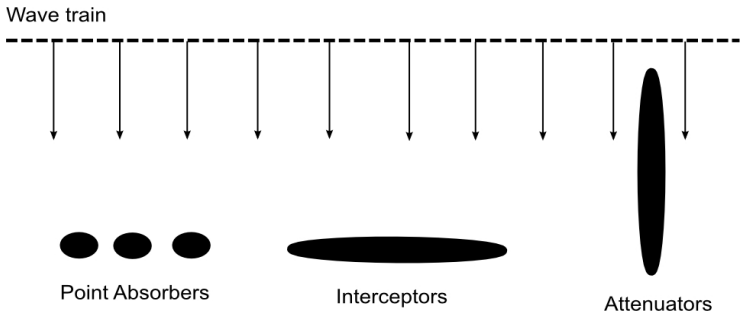

Figure 28: Typology of wave energy converters

power generators are included within this concept, therefore this classification could be split into floating devices such as Wave Dragon or submerged devices such as Oyster 800, for instance.

Wavedragon is a slack-moored wave converter which uses an overtopping method. A ramp elevates the water that comes in from the wave. Kinetic energy from the elevated water above the sea level is driven into turbines coupled with generators. The last tested prototype has a power rate of 7 MW and is able to generate up to 12 GW/year on an annual basis and weighs 23 Tn [102]. On the other hand, the Oyster technology has a buoyant structure, with a hinged flap attached to the seabed. The optimum water depth for this power converter stays between 10 and 15 metres [103].

Attenuators. Devices classified as attenuators are based on generating power in the moment the wave moves past it. Their common structure for this type of wave converter is a floating system. If the device is not an articulated structure and they are considered as isolated energy structures, the device is classified as a point absorber.

The Pelamis power converter is the main device included within this category. Three Pelamis devices were deployed in 2008 by Ocean Power Delivery at 5km from the Portuguese shore. This ambitious project was aimed at 2.25MW of capacity, but its operation stopped due to maintenance problems and contin-

(a) Wave Dragon [102]

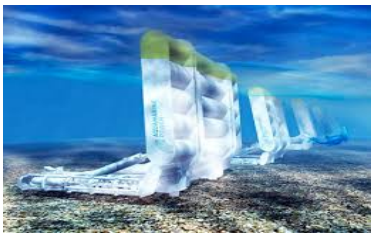

(b) Oyster [103]

(c) Pelamis [104]

(d) Power Buoy [105]

(e) Searev [106]

Figure 29: Wave power converters. Photo references included in the text

ues in its development stage [104].

Point absorbers. As explained previously, these devices are not extended in any direction of the water surface, therefore their cross-section area and total height play a fundamental role. The list of devices within the point absorber classification is large, and technologies such as Rig Drive, AquaGen Technologies, Wave Energy, Aquaboy, Archimedes Waveswing, Searev and Power Buoy are some of the main examples on the list. Some of these technologies are based on the Oscillation Water Column principle, similar to the wave power generators located on-shore.

As an example, Power Buoy is one of the leading projects for this device

typology. Tested in 2002 in New Jersey (USA), this buoy moves vertically due to the wave's thrust, and the floating movement acts on a hydraulic circuit which, coupled to a generator, is able to generate up to 50 kW. This device is designed for waves with heights between 1 and 6m. Buoys lock their position for waves higher than their design wave height in order to avoid damaging the device [105]. The power converter Searev is also included within this category. Many research studies were carried out throughout the last twenty years and important progress was achieved for the prototype [106] at a moderate project cost. Figure 29 shows pictures of the devices previously described.

4.3. Tidal potential energy

This type of technology consists of taking advantage through tidal power plants of water potential energy, i.e. the existing energy when there is a difference on the water level for two water bodies. There are not many operational cases at this moment in time, but in the engineering world this technical solution has become a matter of study in the last decades. Several ambitious and cutting-edge projects, still in an early stage of implementation, have been running since 1960 for countries with large tidal ranges such as Canada, China or Russia (Table 8).

The huge level of productivity that this technology has reached due to its optimisation throughout the last decades are one of the main advantages. Nevertheless, a wide and detailed analysis of the impacts on the marine environment and coastal ecosystems is required when installing these constructions. Recent designs aim to minimise any environmental hazard when building these constructions.

An example of this technology can be found in Brittany (France). With an output capacity of 240 MW, the power station named La Rance has been working since 1966 and, taking advantage from the greater than 8m tidal range average, is able to generate up to 540 GWh per annum. This power plant has

Table 8: Current tidal range constructions. Source [56]

Name	**Country**	**MW**	**Year**
Kislobusk	Russia	0.4	1968
San Jose	Argentina	-	1972
Jiangxia	China	3.2	1980
Annapolis Royale	Canada	20	1984

a rectilinear shape, which means this technology can somehow be compared to the extraction system that operates in river dams.

La Rance's renewable power plant has been the greatest power plant in terms of productivity until 2011, when the construction of a power plant in Sihwa Lake (Korea) surpassed its output capacity [107]. This tidal barrage readjusted a seawall that was built by the South Korean government. The resulting design included 10 turbines with 25.4MW of power capacity in its 12.5km barrage. Examples of tidal power plants can be seen in figure 30.

In addition to the dam-like approach, many designs have analysed hydrodynamics, energy efficiency and productivity of tidal lagoons. If tidal power stations work similarly to river dams (a barrage on the river that is adapted to the physical shape of a valley to constrict the water), these circle-shape lagoons isolate large water bodies with barely any interaction with the coast [56].

(a) La Rance [108] (b) Annapolis [109]

Figure 30: Tidal potential power ranges.

Currently, one of the greatest tidal lagoon plans in the world is at Swansea Bay [110]. The power station is to be placed in the Severn (UK), one of the

largest tidal range spots in the world, with an average tidal range close to 9m. This project, which has been approved in 2013, includes several secondary facilities in addition to its 240 MW generation system. Thus, recreational centres and sea promenades are also included in their design. A 10 km long circular seawall (with a cross-section that resembles the typical sections of rubblemound breakwaters) will form an artificial lagoon where two-ebb generation turbines will be able to extract up to 400 GWh on an annual basis.

In addition to the Tidal Lagoon, the Severn barrage has been projected for the last decades. This design would act like the La Rance tidal structure, holding the water in relation to the tides in order to cause a difference in the water head downstream and upstream. The original project included a 17 km barrage which connect both side of the Estuary, allowing its utilisation as a road infrastructure [111]. These and other tidal range projects which are expected to be built in the near future are included in table9. For instance, China has granted support for a 300 MW tidal lagoon project that will be built near the mouth of the Yalu River. When completed, the 300 MW facility will be the largest in the world .

Table 9: Most significant tidal range projects currently under development.

Name	**Country**	**Length**	**TWh/year**
The Bay of Fundy	Canada	8	12
Severn Estuary	UK	17	13
Khanbhat Gulf	India	25	16
Solvay Firth	UK	30	10

Another concept has been developed to extract energy from potential tidal energy. Dynamic tidal power (DTP) is a novel method of tidal power generation. It is based on a t-shaped open barrier, which is formed by a sea-well perpendicular to the coast and then a 90° barrier at the far end. This technology has not yet been tested, although previous work ensures it is promising and efficient [112].

Even though this type of renewable energy resource does not use water as energy input, wind energy that is extracted off-shore can be included in this classification because the technology overlaps with some aspects of the marine energy devices. At the beginning, a direct application of on-shore wind turbine technology to extract energy from off-shore winds was carried out, because wind turbine devices have been widely tested and optimised. However, this extrapolation brings clear limitations, and the adaptation and marinisation of the device demands new engineering solutions.

Following this idea, first off-shore wind turbines were based on knowledge about foundations gathered from wind energy devices. Although the required techniques to adapt this support structures to the harsh marine conditions are quite known in the coastal and civil engineering world, the marinisation of the structure has to address limitations in terms of construction materials and building costs. Horizontal Axis Wind Turbines with off-shore monopile structures are working successfully at the moment. For instance, a monopile wind turbine array has been projected for the North Sea, where 150 wind turbines will be installed in water depths that reach up to 37 metres [113].

Looking for solutions to the limitations that this type of water construction requires, new prototypes based on gravity bases were designed and constructed. A gravity base is a massive support base where the turbine structure rests. Its high weight overcomes any force that could lead into a unbalance, slipping or overturning force. Finally, this technology requires a gravel base on the sea bed in order to ensure a flat surface where the gravity base is placed and also a correct distribution of the loads. The "Gravitas" gravity base has been already deployed and installed, and a set of specifications for their design, manufacturing and installation has been published as well [114].

Floating structures for wind turbines are upcoming design solutions for the

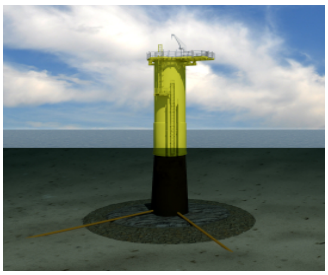

(a) Monopile. Ramboll [115]

(b) Gravity Base. Arup [116]

(c) Floating base. Sway [117]

Figure 31: Structure for off-shore wind turbines.

support structure. In Europe, as the continental shelf is quite small, large water depths are reached not far from the coast, which troubles any foundation works and increases the final costs. Several projects like Sway (Norway), Hywind (Scotland), or Winfloat (Portugal) have already worked in this type of floating base [118]. Pictures of the three types of structures for off-shore wind turbines are presented in figure 31.

The interaction between the corresponding technology from wave and tidal power converters and the on- and off-shore wind energy knowledge had a great influence in both fields. The research carried out by different organisations in both fields prompted direct synergies, and this combined effort has been quantified in [119]. Figure 32 shows that the greatest synergies occurred in the operation and management sector and also in the power take-off systems, areas were both methodologies share similar characteristics.

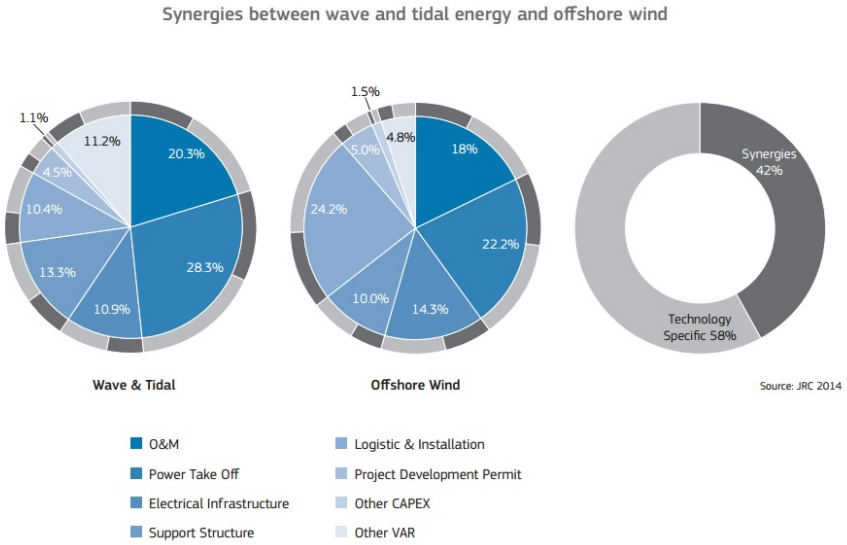

Figure 32: Synergies between marine devices and wind turbines. Source [119]

5. Design Constraints

The technologies to harness the marine energy have not yet been fully developed. Although research and development have shed some light into some of the main difficulties, even the most advanced tidal stream device is still facing technical limitations and environmental restrictions. With the goal of reviewing these obstacles and barriers on the tidal technology, this chapter has focused on highlighting which are the engineering improvements that are currently required.

In order to improve the quality of the technology and guide new constructions, several sets of specifications were published , thanks to the funding given by the Scottish Government and the Department for Business, Enterprise and Regulatory Reform, which carried out by acknowledged experts [120]. The standards and guides that refer to tidal energy converters are the following:

- Assessment of Performance of Tidal Energy Conversion Systems

- Assessment of Tidal Energy Resource
- Guidelines for Health and Safety in the Marine Energy Industry
- Guidelines for Marine Energy Certification Schemes
- Guidelines for Design Basis of Marine Energy Conversion Systems
- Guidelines for Reliability, Maintainability and Survivability of Marine Energy Conversion Systems
- Guidelines for Grid Connection of Marine Energy Conversion Systems
- Guidelines for Project Development in the Marine Energy Industry
- Guidelines for Manufacturing, Assembly and Testing of Marine Energy Conversion Systems

In addition to this, companies as Alstom or Voith [121] followed the standards provided by Germanischer Lloyd (GL) Renewables Certification, which aims to deliver certain degree of confidence in the safety and integrity of tidal turbine projects. The international certification body and classification society Det Norske Veritas (DNV) merged with GL in 2013 and, together with the UK's Energy Technologies Institute (ETI) agreed some official industry standards for marine renewable devices. These set of specifications are able to guide the design process and ensure the quality of future tidal devices [122].

5.1. Support structure

As previously discussed, research about tidal turbines has been inspired by wind turbine knowledge, and more specifically by knowledge from off-shore wind turbines. Even though the fluid characteristics and turbine performance are quite different (higher density, lower speeds, components that generate corrosion, etc), technology, design, physics and structure can be compared between

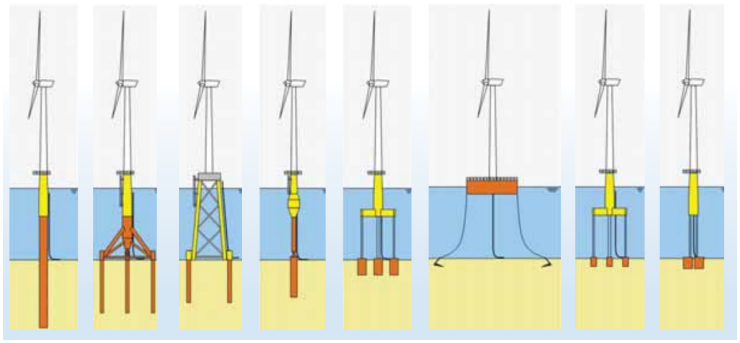

Figure 33: Available support structure designs for off-shore wind turbines. From left to right: monopile, tripod, jacket, compliant, barge floater, tension leg platform and spar floater structure. Source [123]

both models. The foundation concepts achieved from wind turbine super- structures have been also applied for the ocean devices.

Following this idea, piling has been and still is the main option for tidal turbine designers. Some successful projects, which are in an advance stage of development, have this feature as their main support structure. Although monopile, tripod-pile and jacket have been already tested with positive achievements for tidal turbines, any piling foundation display some disadvantages that are not easy to be avoided.

Firstly, high construction costs can delimit the available area of deployment. Submarine drills and tunnelling machines that work from vessels are the two common ways of drilling for pile building, and both have issues for water depths larger than 30-50m. There are no submarine drills in the market that can handle high pressures caused by large depths, and costs for tunnelling machines increase exponentially when the distance between seabed and surface is too large. These disadvantages prompt the existence of a new engineering solution that solves these limitations, offering a larger area of possible locations for the installation of tidal turbine s[124].

Scour related to the installation of structures into the seabed is an issue that has been widely studied. At first, this instability on the structure was perceived

by off-shore oil structures and, more currently, by off-shore wind turbines. [125] studied and dimensioned the scour of several monopile off-shore wind turbines. The data collection enabled to represent the findings quantitatively through the figure 34. The deepest scour noticed in this study was 1.77 times the pile diameter, for a maximum approach flow speed of a 1.5 m/s.

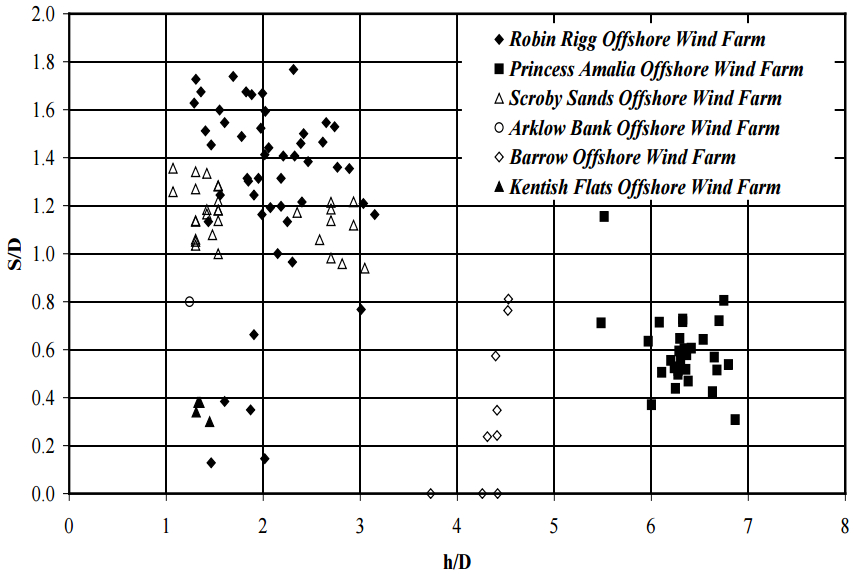

Figure 34: Non-dimensional plot of scour depth data for monopile offshore wind farms. No scour protection. S= scour depth, D=diameter, h= water depth. Source [125]

[126] analysed the effect of scour protections that were installed at some wind turbine sites in order to add structural stability. Some solutions showed changes on the hydrodynamics near the pile, and this modification of the flow generated secondary scour on the bottom of the area of protection area. Extreme cases presented a deeper scour in protected cases than in exposed structures.

In order to protect the pile base, a layer of gravel on the seabed around the pile is a common measure, either before the installation of the foundation or after. However, it is essential that scour has not started to develop. A layer of rocks can be added on top of the gravel layer as a protection layer if the environmental conditions allow it. The stability effect of these protection

cross-sections has been already assessed by [126].

5.2. Material properties

5.2.1. Strength

In general, knowledge and experience gained from on-shore wind turbine blades was applied to the tidal turbine technology. Thus, the initial approach to design the first blades was based on composite as the main material. Nevertheless, the marine environment features more aggressive conditions (chemical and biological seawater components, irregular torque curves, high turbulence intensities, wave–flow current interaction, etc.) and the higher forces and bending moments bring as a consequence structural failures to the tidal energy turbine.

[127] registered that the loads that tidal turbine blades must bear, differ substantially in comparison with blades from wind turbines. This research work concluded that the differences on the loads are mainly due to load fluctuations and cavitation. It is inferred as well that carbon/epoxy, glass/epoxy and glass-reinforced composites are the main materials used currently by tidal turbines designers.

Large bending moments along the main blade dimension is one of the main restrictions in order to maximise the size of the turbine and its power capacity. [128] found out, using their hydrodynamic model, that large bending moments under normal and intense operating conditions were predicted to produce substantial strains in glass fibre reinforced polymer (GFRP). The influence of this stress distribution is crucial, as the increase on the bending moment leads into material failure. [44] tested turbine blades made of several types of GFRPs for different fatigue cases in air and ocean environments, and concluded that tidal blades age dramatically faster, reducing the resistance of the blades to fatigue.

Figure 35: Blade failure of Verdant Power Company. Source [129]

The selection of the blade shape is based on the optimisation of the following parameters: high performance in terms of efficiency, low mechanical stresses, avoidance of turbine stall and cavitation. [129] emphasised that a simple efficiency analysis based on lift and drag ratios might no deliver the best structural solution.

OpenHydro carried out tests on their prototype in 2010 and the outcome provided a proof of the technological challenges that tidal devices must face. After testing the turbine performance and bring the device back to the shore, the support structure was in good condition but severely affected by biofouling and corrosion [130] and, most importantly, all the 12 turbine blades failed and were missing. The Verdant HATT also experienced failure on their rotor blades (Figure 35). [131] suggested that blade fatigue is a key factor for the blade design, as tidal blades would need to bear up to 10.000.000 cycles over 20 years of life time.

5.2.2. Fouling

Research studies and turbine field testing show the maintenance issues that marine power converters have to endure in these harsh conditions, and specifi-

cally in the form of blade fouling. Pieces of research as [132] [133] suggest that biofouling might reduce the turbine performance considerably.

[135] studied this phenomenon together with corrosion, which is analysed more in depth in the following section. In this study, samples of stainless steel, structural steel, standard steel, aluminium, glass and carbon fibre composites were submerged into the ocean for periods of time that varied between three and ten months. These materials are widely use for the support structure, nacelle, blades or foundation. The environmental conditions where the samples were deployed consisted of flow velocities up to almost 3 m/s and water depths between 55 and 75 m.

Figure 36: Biofouling examples. Left, barnacle attached to glass fiber composite sample after four months immersed, source [132]. Right Colonization by mussels on wind off-shore turbine structure, source [134]

The results extracted from [135] confirmed that glass fibre composite and carbon composite, which are commonly used for the rotor components, displayed low levels of surface fouling after 10 months of deployment. However, the general trend seems to be that biological fouling is more common on edges and in bulges, as they showed more biological fouling when compared to smooth zones. Nevertheless, the thickness and density of the marine growth has also a strong impact on the structural hydrodynamic loads of offshore wind turbines [136]. Common steel, structural steel and stainless steel were also deployed in the marine environment. Both materials showed similar high percentages of rust on the surface. However, when an anodic protection was attached to both

materials, structural steel experienced and considerable reduction on the level of oxidization.

[137] carried out experimental tests on cylinders covered by biofouling to specify its hydrodynamic impact. The tests showed that marine fouling can increase up to 70 % the drag coefficient. This coefficient has been proven to be an essential factor on the turbine performance and this increase on the roughness would imply a reduction on the turbine efficiency.

5.2.3. Corrosion

Corrosion is an attack on metal elements led by chemical reactions that have an effect on the material properties (chemical changes on non-metal elements are not considered corrosion cases). When these changes are caused by physical actions, the phenomenon is named erosion, although both circumstances are complementary in some cases.

A metal element tends naturally and spontaneously to interact with the environment, in order to lose electrons (positive valence) and reach more stable states. If the environment where the metal is located does also tend to gain electrons (negative valence), an electron current is established. Finally, if the metal losses electrons implies that the metal (or anode) is oxidizing, which is the most usual nomenclature for this electrochemical phenomenon. So that electrochemical corrosion occurs, anode and cathode (chemical element with negative valence), require a catalyst, i.e. an environment which allows the electrons transfer. This catalyst is named electrolyte.

Depending on the environment where the material is immersed and the likelihood of an oxidation process to occur, the material can be classified as active, passive or immune. The ISO 12944 is a set of specifications which classifies five types of corrosion, considering their level of material aggression (Table 10).

Hence, the marine environment is agreed to be the most aggressive in terms

Table 10: Classification of the corrosion environments according to ISO 12944. Source [138].

Nomenclature	**Description**
C1	Heated buildings/neutral atmosphere
C2	Rural areas, low pollution
C3	Urban and industrial atmospheres Moderate sulphur dioxide levels Production areas with high humidity
C4	Industrial and coastal Chemical processing plants
C5I	Industrial areas with high humidity and aggressive atmospheres
C5M	Marine, offshore, estuaries, coastal areas with high salinity

of corrosion for materials based on metals. The best scenario in order to favour the chemical oxidation is provided by coastal and ocean environments with dry-wet conditions. If common metal oxidation occurs with the presence of oxygen and water, areas splashed by water periodically provide both oxidising agents in large quantities. Besides, seasalt and other particles contained in the ocean also act as catalysts.

Corrosion can deteriorate the strength, shape or efficiency of the material, and therefore compromise the turbine operation because of its influence on structural and rotor parts. Ideally, metallic components are specially treated before the turbine deployment on the corrosive environment, in order to maximise the operational life-time of the device. When materials are immersed into corrosive environments and also immersed in presence of erosive agents, synergies between both effects are produced and damage on the material surfaces might occurred quickly and in a non-linear proportion. This effect is named erosion-corrosion, and even though this phenomenon has not yet been fully described scientifically, new research work provided important advances in order to understand the involved processes.

In order to protect a material which is based on metal elements, several measures or treatments have already been applied to the tidal energy technolo-

gies. [127] analysed the long-term performance of different composites based on carbon/epoxy through accelerated-ageing techniques. Their numerical modelling has measured an important contraction of the composite strengths after saturation in water, whilst longer periods of time with the material submerged leads into small modifications on its properties.

The treatments or measures that have been usually adopted to avoid material corrosion in submerged environments are the following:

- Material selection

  The first concept consists of optimising the material selection, in order to avoid or reduce as much as possible the electrochemical reaction. The utilization of composite for the blade manufacturing would enhance the protection properties of the blade to face corrosion, as their resistance to corrosion is considerably high [139]. Moreover, the durability of metals in comparison with composite material is significantly inferior to metals in terms of erosion.

  The limitations on the flow velocity that runs through pipes made of alloys and metals depending on the corrosion rates can be observed in Figure 37 obtained from [140]. Thus, copper-nickel alloys outperform aluminium and copper for high flow velocities.

  The properties of the elements added to the alloy is a key factor. Stainless steel is usually used because of its inherent resistance to corrosion. This type of steel is made of chromium and nickel and whereas chromium is the element that adds most of the protection against corrosion, nickel adds atomic stability to the stainless steel. Plus, stainless steel can content up to a maximum of 0.05% carbon in ocean environments [141].

- Cathodic Protection

  This is a technique that enables to drive the corrosion of the material that wants to be protected to another specific material. In order to do

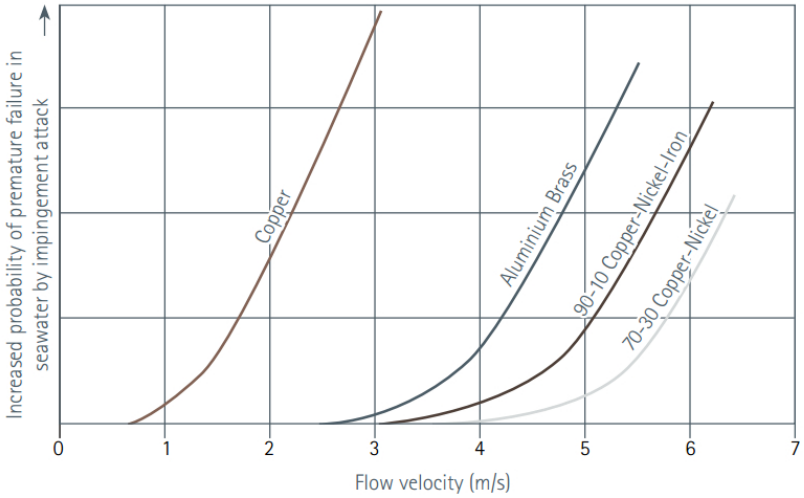

Figure 37: Relative breakdown velocities for copper alloys in seawater. Source [140]

so, a metal that is more prone to be corroded called sacrificial metal is connected to the material that needs to be protected. Hence, the sacrificial metal will act as an anode and will oxidise instead of the protected metal.

Figure 38: Comparison of the effect of a cathodic protection (left) and an exposed 90-10 copper-nickel alloy (right). Exposure time, 12 months. Source [140]

In addition to delay the material oxidisation, this type of protection enable to improve the biofouling resistance of the material. Figure 38 shows qualitatively the level of protection that this solution offers to the materials.

- Isolation

  The main method to isolate the materials from corrosive agents consists of adding anti-corrosion coatings on the surface. Thus, the coating acts as a barrier and does not allow the contact between chemical components and the protected material. The perfect coating characteristics have not yet been perfectly defined and the definition of the paint properties via physical tests is only accepted for specific cases. Hence, these tests are an indicator of the rightness of a specific coating, and does not ensure the resilience for the entire life-span [141].

  The research study carried out by [132] analysed three types of coatings on glass and carbon fibre composite: high copper, low copper and an inert coating. The three of them developed very low signs of fouling on both flat surfaces or edges, although the inert coating performed slightly worse than the other two. Coatings must also take into account bio-fouling processes, in order to avoid and disrupt the growth of marine biofouling.

5.3. Cavitation

Cavitation is a physical phenomenon defined as the generation of pressure voids within a fluid due to the translation or rotation of a solid body. When the local pressure is lower than free-stream pressure, the liquid particles tend to stick to the edges of the trajectory that the solid in motion. The particles inertia varies to the square of the flow velocity, and the higher the inertia, the higher is the pressure needed to force the particle to follow the trajectory of a surface. In order to cause the cavitation effect, three main conditions are required; high flow speed, low pressures and sudden changes on the body motion. Therefore, tidal turbines are likely subjects to suffer cavitation issues.

The cavitation phenomenon erodes material surfaces. In the specific case of a tidal turbine, these low pressure points can damage the upper side of the blade borders. This is because the distribution of lower pressures are on this side of

the blade, whereas the high pressure area that generates lift forces is located on the lower surface [142]. The most representative characteristics of cavitation is the appearance of small bubbles, which dimensions have been specified and quantified in [143]. As a result, cavitation bubble have an average diameter of 0.635 cm and last around 3 ms.

Analyses of this phenomenon have been carried out for Horizontal Axis Tidal Turbines [144] and [145]. Physical tests were undertaken by [145], concluding that cavitation occurred when the rotational speed of the rotor reached up to seven times the approach flow speed. [143] studied experimentally the cavitation generated by their HATT for different operating conditions and recorded the results with a high frequency camera. The influence of parameters such as surface of the blade profile, rotational speed, upstream flow speed and level of shaft immersion were analysed. Two cavitation types were observed in this research, the main one related to the continuous tip vortex cavitation (Figure 39), and its evolution into a blurry cavitation when rotor speed was increased. Also, the higher the rotational speed of the turbine, the more blurry the visual cavitation was. Cavitation was registered and measured for rotational speeds three times faster than the flow speed. However, the flow speed for these tests was 4 m/s, value that is achieved occasionally in very energetic tidal streams, in both laboratory and natural environments.

Hence, HATT set ups can achieve these substantially high rotational speed values, specially for small scale devices. However, VATTs are, in general, far from reaching these values and the hypothesis that VATTs will not face cavitation issues could be accepted. Nevertheless, it is a factor that must be taken into consideration for any tidal turbine which performs at high rotational speeds. Physical and mathematical approaches are included in the subsequent thesis chapter.

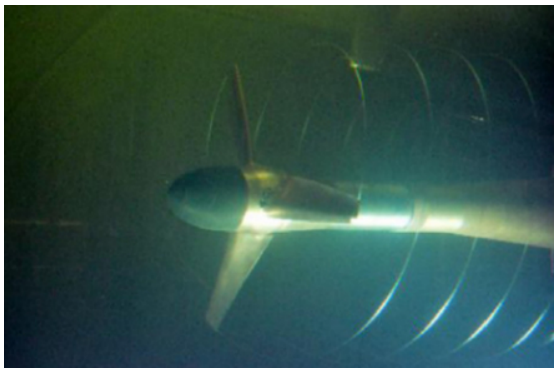

Figure 39: Blade tip cavitation created by a HATT at TSR=4. Source [143].

5.4. Environment-friendly

Although harnessing tidal energy will be beneficial in order to reduce the non-renewable energy supply, it does not mean that the extraction of this kind of energy is already environment-friendly. The processes related to the manufacturing, operation and maintenance of tidal devices must be studied to ensure that no harm is been produced on the environment. Environmental implications related to tidal stream turbines deployed on estuaries have not been analysed beforehand, and a few analysis have been carried out after the device deployment. In [21] have summarised the Environmental Impact Assessments or EIA (which aim to make sure that environmental thresholds are not exceeded) and Life Cycle Assessments or LCA (which are used to measure the effect of industrial products on the marine environment) that have been undertaken in the scientific field.

Not many existent EIAs about tidal energy technologies are available due to the reduced amount of devices that have been deployed. In general, the EIAs have mainly studied the interaction between tidal energy devices and marine animals, the increase on the acoustic levels and its effect on the life conditions of certain marine species, as well as variations on the estuary hydrodynamics and sediment transport.

[146] and [147] imply that the the risk of harm or kill marine species due to the operation of tidal turbines is low. [147] tested, in an intermediate scale (turbine diameter ≈2 m), the fish mortality due to a VATT operation. According to this study, a straight-bladed and a twisted-bladed rotor offered survivability rates above 99% for an approach flow speed of 2.5 m/s and at their maximum rotational speed.

Noise impact stands as a significant issue related to the rotation of tidal stream turbine devices. [135] ensure in their work that high noise levels could have an disruptive effect on marine species, and specially on marine mammals. In order to quantify the noise variations due to a turbine operation, [143] recorded noise measurements of their HATT for incoming flows corresponding to 2, 3 and 4 m/s . However, the research work indicated that the acoustic levels of a typical HATT were comparable to the level of background noise while the turbine was not bearing cavitation (normal operation).

To the author's best knowledge, the only Life Cycle Assessment carried out about a full scale device is the Sea Gen study [148]. The research work studied the life cycle energy use and CO_2 emissions related to the manufacturing, construction, installation and operation of the Seagen turbines. The research study concluded that the energy and carbon intensities that tidal turbine require are just above the wind turbine levels. Therefore, this fact means that the energy intensity is low when compared to photovoltaic energy converters and very low when compared to emissions associated to fossil fuels.

Part III

Thesis Objectives

As the State of the Art describes in depth, marine renewable energy has a great potential and, more specifically, harnessing tidal energy by means of hydrokinetic turbines. In spite of the large number of designs and prototypes that have been tested throughout the last decades, the perfect tidal turbine has not been found yet. Within the tidal turbine typologies, Vertical Axis Tidal Turbines offer several advantages that could mechanically and operationally outperform other designs. Hence, the targets of this thesis strived to increase the knowledge of the scientific community on this topic in order to benefit from the aforementioned advantages. Thus, the analysis of the physics and hydrodynamics related to the operation of this type of turbine has been widely studied.

The main goals of this work aimed to obtain an optimised design for a VATT, therefore the goals involved in this work are mainly related to increasing the theoretical and practical knowledge of this new technology. At the same time, improving and enhancing the turbine performance and its efficiency were also studied. The main objectives of the research project are as follows:

- To add and improve crucial knowledge about the physics relating to the operation of VATTs and the rotor performance depending on the main parameters that characterise its conduct.
- To assess the influence of different degrees of blade surface roughness on the performance of VATTs, providing a method to classify blades for hydrokinetic turbines according to their roughness.
- To provide data sets of wake velocities and water elevations, in order to quantify the hydrodynamic changes in the water channel introduced by the turbine.

- To demonstrate the technical feasibility of a vertical axis tidal turbine by designing, manufacturing and testing a VATT prototype of intermediate scale.
- To show the accuracy of using a water sports centre as a reliable facility for testing not just the tidal turbine rotor but also the power take-off equipment.
- To take advantage of the experience gained from the design, construction and operation of a shore-line device, in order to develop larger scale devices for deeper water and harsher conditions.
- To provide the means for assessing and validating the overall device, including the geometry and the performance of the rotor design, gravity base and support structure.

Part IV

Methodology and Facilities

This part of the thesis reports and analyses the findings of an experimental study investigating the influence of the parameters that characterise the performance of a vertical axis tidal turbine. Many factors exert an influence on the turbine conduct. In order to establish the best design for the rotor of a VATT, it was necessary to examine all these parameters separately. Besides these analyses, the correlation among factors is very significant to determine the optimal design of the turbine. A long list of tests were run in the facilities at Cardiff University in order to understand and gain knowledge about the following topics.

- Performance for different flow speeds and/or Reynolds numbers
- Influence on the efficiency depending on the blade shape and its pitch angle.
- Influence of the blade chord length of the blade and its proportion to the diameter (Solidity).
- Influence of the number of blades of the rotor.
- Influence of the angle of twist of the blades.
- Effect on the efficiency due to the winglets.
- Influence of the diameter of the shaft.
- Increase of the performance due to the shape of the spokes.
- Analysis of the effect that secondary columns place upstream and downstream the turbine provide to the rotor performance.
- Effect that blades placed at different distances to the shaft cause to the performance.

- Influence of the proportion flume area/rotor area (Blockage)

6. Tidal Stream Turbine Physics

Flow stream energy corresponds to the kinetic energy of the moving water. The kinetic energy E is proportional to half of the mass m and to the squared velocity U_0. (Equation 1). If mass is expressed as a product of density (ρ) and volume (V) (Equation 2), the kinetic energy can also be determined as Equation 3 shows.

$$E = \frac{1}{2} m U_0^2 \quad (1) \qquad m = \rho V \quad (2) \qquad E = \frac{1}{2} \rho V U_0^2 \quad (3)$$

Power of a flow stream (P) is based on the kinetic energy generated per unit time (Equation 4), which is a scalar magnitude, such as energy. Depending on the mathematical approach that is introduced on the expression, power can be defined as well as Equation 5 shows.

$$P = \frac{dE}{dt} \quad (4) \qquad P = \frac{\rho A_r U_0^3}{2} \quad (5)$$

Equation 5 displays the total amount of energy that is possible to extract from a flow stream, and it will be the reference value in order to analyse the turbine efficiency. In order to express the maximum power extraction that a turbine is able to generate from a fluid, the Betz limit has been found by [149]. This limit is explained briefly in the following paragraphs and is based on the comparison between the mass conservation law and the energy conservation law.

If P_0 is the power extracted at the rotor location, and assuming that the difference in the upstream and the downstream power is equal to the power ex-

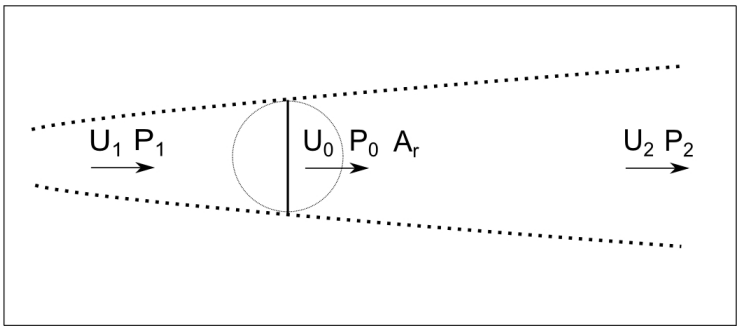

Figure 40: Sketch and nomenclature of the upstream, centre of the turbine and downstream

tracted by the rotor, the mathematical power that the rotor achieves is displayed in Equation 6.

$$P_0 = P_1 - P_2 = \frac{1}{2}\rho A_r (U_1 - U_2)(U_1^2 - U_2^2) \tag{6}$$

Taking advantage of the assumption that the velocity at the rotor is the average between the upstream and downstream velocity (U_1, U_2), the power coefficient remains as Equation 7 presents. a is a variable introduced to simplify the expression, being the ratio between upstream and downstream velocity ($a = \frac{U_2}{U_1}$). According to this expression, the maximum of the function is reached when $a = 1/3$, which means that the maximum efficiency is 16/27 of the incoming power, being this value the Betz limit.

$$C_p = \frac{P_r}{P_f} = \frac{\frac{1}{4}\rho A U_0^3 (1 - a^2)(1 + a)}{\frac{1}{2}\rho A U_0^3} = \frac{(1 - a^2)(1 + a)}{2} \tag{7}$$

Pieces of work undermine the Betz limit, considering that ducts, diffusers or shrouds are able to increase the rate. Certain research studies claimed to exceed this limit in the laboratory [151] [173] [153], through numerical simulations [154] and in a natural environment [80] [155]. However, once a duct accelerates the flow, U_0 is accelerated as well, and either this increase on the flow speed or at least a new cross-section related to the area of the diffuser must be taken into

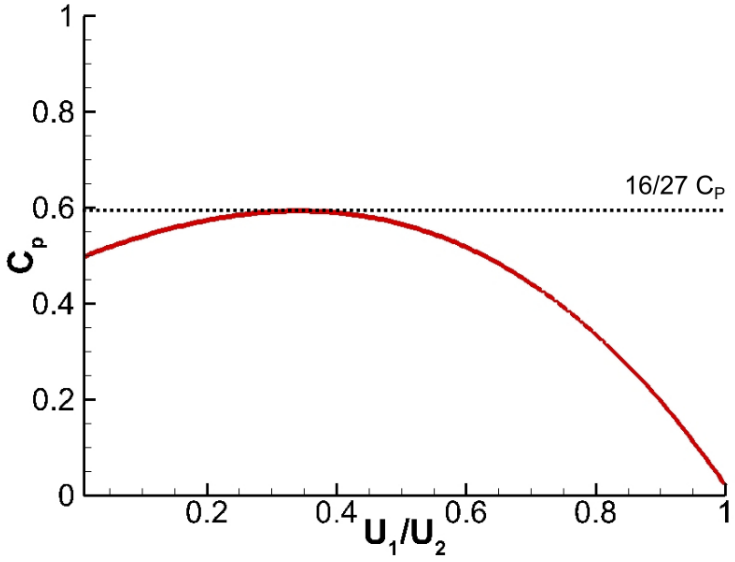

Figure 41: Maximum theoretical power coefficient that a turbine is able to extract, corresponding to the function displayed in Equation 7.

account for the power calculations [156].

The power that an energy extraction system generates can also be analysed in terms of mechanical magnitudes. Thus, following first Newton's law, power is proportional to the force that is acting and the velocity of this force (Equation 8). Many parameters quantify the turbine performance or its efficiency, but every mechanical approach is based on the most significant magnitudes to measure the performance of a hydrokinetic turbine; rotational speed (ω) and torque (T). In relation to the rotational speed (ω) , it is more usual to present it in terms of tip speed ratio or TSR (λ)). This parameter relates the turbine velocity and its radius (r) to the approach flow speed (U_0), displaying how fast the turbine rotates compared to the flow velocity (Equation 9).

$$P_0 = \frac{dE}{dt} = F\frac{dx}{dt} = FU_{(lineal)} = T\omega_{(rotational)} \tag{8}$$

The turbine efficiency, also named power coefficient (C_p) was then calculated

for each ω as Equation 10 shows, where ρ is the density of the water,A_r is the projected area of the turbine cross-section and U_0 is the average approach flow velocity. The turbine efficiency is usually plotted as a function of λ, in order to describe and quantify the rotor performance in relation to the rotational speed.

Ultimately, a dimensionless parameter named torque coefficient (C_T) is able to provide useful information about the turbine behaviour (Equation 11). For instance, a common method to control the generation of electrical power is the maximum power-point tracking control (MPPT), which is closely based on the torque coefficient [176].

$$\lambda = \frac{\omega D}{2u} \qquad (9) \qquad C_P = \frac{T\omega}{\frac{1}{2}A_r {U_0}^3 \rho} \quad (10) \qquad C_T = \frac{T}{\frac{1}{2}\rho A_r {U_0}^2 r} \quad (11)$$

Another important velocity in the operation of a vertical axis turbine is the relative speed, w, which is the vector sum of the rotational speed, $v = \omega D/2$ and approach flow U_0, as sketched in figure 42. The relative speed varies during one revolution in the rotation of a vertical axis turbine, i.e. angles of rotation between $\theta = 0$ and $\theta = 360$ where w is a function of λ as Equation 12 presents.

$$w = v\sqrt{2\lambda \cos\theta + \lambda^2 + 1} \qquad (12)$$

During operation of the turbine the angle of attack α (or AoA) changes constantly, and so does the lift-to-drag ratio. At large α values, the flow separates from the hydrofoil, known as stall, which leads into a sudden large increase in the drag force, d, and to zero or even negative in the lift force (l). Figure 42 graphs α as a function of angle of rotation θ for three different λ between +45° and -45°. Although the figure shows the more representative values (as the highest lift/drag ratio are achieved), hydrodynamic forces appear for the whole rotation and must be taken into account as well. The dashed line signifies high

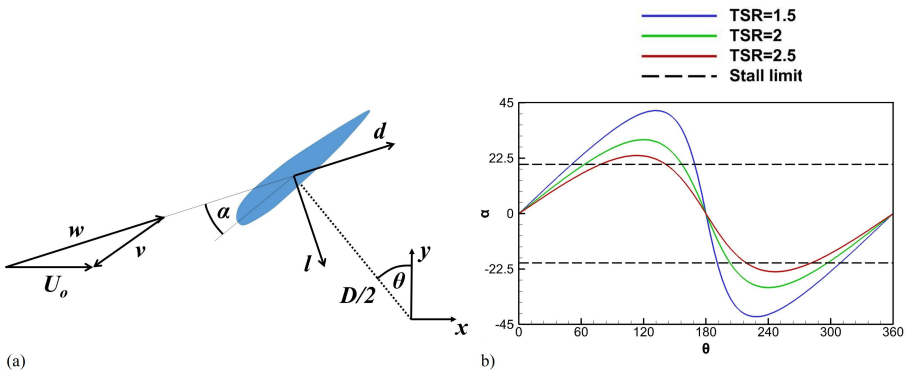

Figure 42: Sketch of the main velocities in a rotating system (a) and the angle of attack α as a function of the rotated angle θ at various tip speed ratios λ (b)

angles of attack at which stall is expected to occur and stall particularly important at low λ, as it occurs over substantial periods of time during the turbine rotation. These dashed lines that show the dynamic stall are not constant, and they are dependent on the hydrofoil chosen.

The dimensionless Reynolds number (Re) is a parameter that displays the rate between inertial forces and viscous forces that lies in a fluid in motion. Inertial forces F_i are described by Newton's laws as mass times acceleration (Equation 13), whereas viscous forces have been explained as the proportion between shear stress (ν) and velocity gradient, which is proportional to the dynamic viscosity (μ) (Equation 14).

$$F_i = ma \qquad (13) \qquad\qquad F_v = \tau = \mu \frac{dU}{dL} \qquad (14)$$

If the ratio between inertial forces and viscous forces in a certain flow area (L^2) is calculated, the resultant value is named as the Reynolds number (Equation 15), which is commonly used to know the predominant forces in a fluid. This parameter has a great significance on the flow characterisation, as fluid properties vary drastically depending on its value. Hence, low Reynolds num-

bers would be predominantly viscous and difficult to be moved, whereas high enough Reynolds numbers belong to high kinetic fluids, where viscous forces do not have a great importance. Flows performing at low Reynolds numbers are classified as laminar flows, whilst high Reynolds values are considered to provide turbulent flows.

$$Re = \frac{F_i}{F_v} = \frac{\rho L^2 U^2}{\mu \frac{U}{L} L^2} = \frac{\rho U L}{\mu} \tag{15}$$

In order to achieve an accurate Reynolds number, this parameter requires a main dimension in order to establish the comparison between forces. Aiming to look at the predominant forces within a water stream, the main dimension is usually the smallest dimension, which usually is the water depth (d) (Equation 16). However, the analysis of the local flow regime that has an effect on the rotor blades might be more interesting for tidal turbines. Therefore, the chord length can be considered to be the main dimension, and the Reynolds number changes his name into Reynolds chord number (Re_c) (Equation 17). For the Reynolds chord number, c is the blade chord length and w is the relative velocity of the blade.

$$Re = \frac{\rho U d}{\mu} \tag{16}$$

$$Re_c = \frac{\rho w c}{\mu} \tag{17}$$

The Froude number (Fr) has also a great relevance on the flow characterisation. Whether the Reynolds number describes the proportionality between inertial and viscous forces, the Froude number establishes a relationship between inertial forces and the effect of gravity (F_g). According to the Newton's laws, the attraction force that any body receives from the Earth is equal to its body mass times gravity (g). Thus, this number has been proven to be a reference to understand whether the flow inertia prevails instead of the gravity action or if

it is the contrary case. This number is mathematically expressed by Equation 18 and 19.

$$\frac{F_i}{F_g} = \frac{\rho L^2 U^2}{\rho L^3 g} = \frac{U^2}{Lg} \qquad (18) \qquad\qquad Fr = \sqrt{\frac{F_i}{F_g}} = \frac{U}{\sqrt{Lg}} \qquad (19)$$

Then, flows can be characterised according to their Froude number and water bodies can be classified as supercritical or subcritical. A supercritical flow would provide Froude numbers greater than one, which implies that gravitational wave forces will be able to develop as they are more energetic than the kinetic forces. On the other hand, a flow is subcritical when $Fr < 1$, which means that gravity forces will not resist the flow momentum and hence they will be dissipated by the flow inertia.

In order to use the laboratory flume for experimental tests, general modelling rules must be followed. These rules are based on scaling laws that permit to adjust physical models for future scale down or up. Hence, three main similarity rules must be used; geometrical, kinematic and dynamic similarity. Geometrical similarity law implies that dimensional proportion or geometrical ratio (ϵ) must be assumed for the model and its scaled version D_M and D_S, whereas kinematic similarity evidences the need of providing similar velocity ratios for model and version. In the tidal turbine case, velocities must keep the similarity in both directions (XY planes) and also keep the circular motion (geometrical similarity). Therefore, the only solution to apply the modelling rule consists of keeping the angular velocity for both the model (ω_M) and the scaled version (ω_S) as Equation 20 shows.

$$\epsilon = \frac{Model}{Scale} = \frac{D_M}{D_S}; \omega_M = \omega_S \qquad (20)$$

The dynamic similarity is not as straightforward as the geometrical and

kinematic rules. In this case, proportions between different forces must be the same for the model and for the scaled version. Thus, the identification of the predominant forces must be obtained, in order to scale the model according to the governing forces. The Froude number is used for experiments where gravity has a great significance in the fluid physics as, for instance, wave effects in coastal engineering. In the tidal turbine case, inertial and viscous forces are the main source of thrust for the rotor blades and its distribution around the blades surfaces. Therefore, scaling rules follow mainly the Reynolds number criteria. Occasionally , Froude number must be taken into account for flows that present wavy surfaces which could have an influence on the turbine operation [157]. Pieces of research consider that geometrical scale up cannot be adopted without looking into the blade profile hydrodynamics, as large blade profiles can lead into detrimental lift and drag ratios [158].

7. Experimental apparatus

7.1. Hydraulics Laboratory

The experimental testing was carried out at the Hydraulics laboratory in the School of Engineering at Cardiff University. This flume 1.2 m wide and 17 m long can provide constant flow speeds up to 1.3 m/s for a water depth of 0.5 m. The side walls and the bottom of the flume are made of glass, allowing for visual monitoring of the turbine tests. The outlet of the channel pump incorporates a flow straightener in order to provide a uniform flow. A metallic cage is set downstream of the flume to gather any possible debris and finally the water goes into a pipe which cycles the water back to the the pump inlet. The experimental rig was not located in the centre of the channel and all the experiments were carried out closer to the inflow. The position of the experimental set up was 8 meter far from the incoming flow in the streamwise direction. This distance was chosen as a compromise between obtaining a uniform flow and leaving enough distance downstream the turbine for further wake analysis (Figure 44)

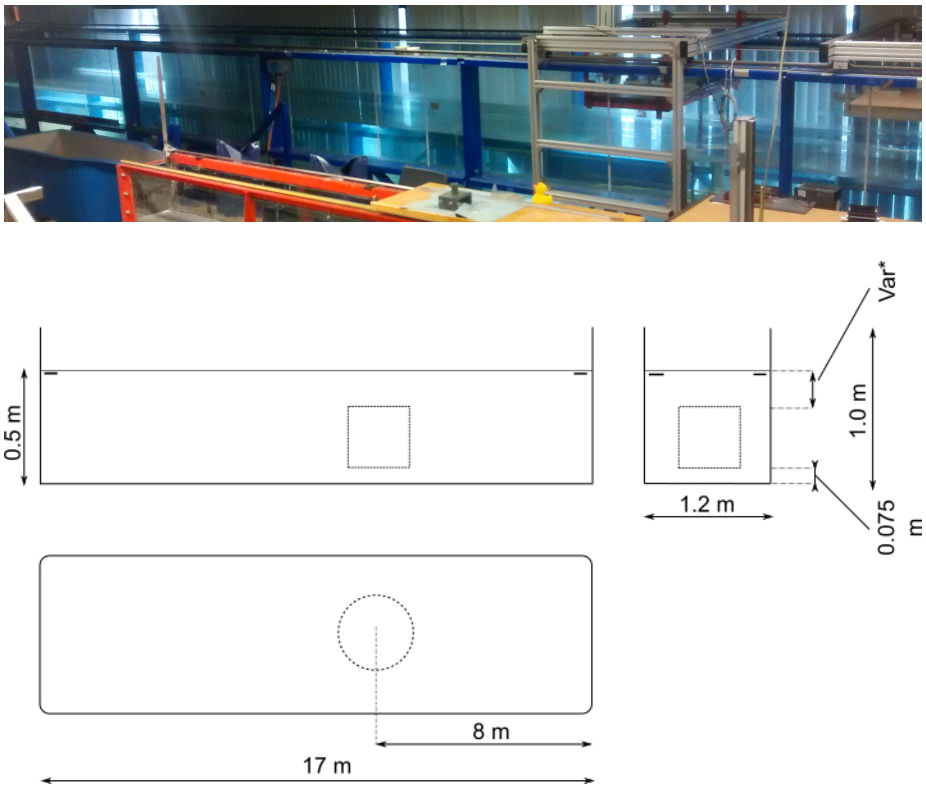

Figure 43: Perspective of the hydraulics flume at Cardiff University. Geometrical description of the facilities and the mechanical system.

The correlation between pump power and flow velocities has been widely evaluated and verified in previous works at the University [159]. According to the flume calibration, the relationship between pump power values and and flow velocities has been obtained and hence it can be displayed as a parabolic curve which is a function of the power pump. Previous tests showed that the water profile became unsteady and wavy for water depths lower than 0.5 m or flow velocities faster than 1.3 m

The results obtained from small scale experiments are greatly influenced by the accuracy of the upstream velocity. Thus, unstable or non-constant flows might lead to errors in the data, which would add uncertainty to the experiments

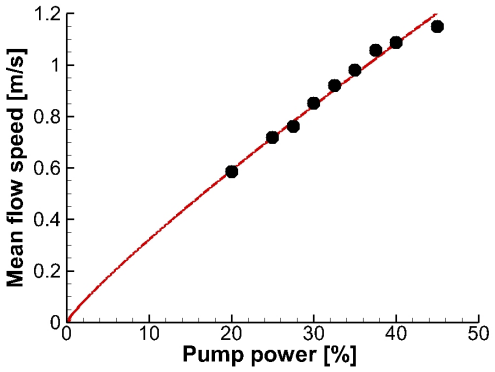

Figure 44: Correlation between Pump power and mean flow velocities. Source [159]

outcome. The following data has been extracted from the work carried out by [160], who used the same facilities in his thesis. In this piece of research, the flow regime was characterised for the precise position were the turbine set up for the present thesis was located. ADV measurements were used in order to calculate the flow velocities in the cross-section 8 m far away from the inlet of the flume. These measurement made possible to measure and define the streamwise, spanwise velocities and also the turbulence of the flow. Figures 45 and 46 show the modulus of the velocity for four different pump power, i.e., 25%, 30%, 35% and 40%.

The procedure followed by [160] consisted of averaging the total velocities in the cross-section area where the turbine would be tested. Once the velocity field in the cross-section was hydrodynamically defined, the upstream velocity values within the range -0.25$<y/B<$0.25 were considered to calculate the absolute main velocity (U_0), being y the spanwise distance from the centre of the flume and B width of the flume . This velocity was estimated to be a precise value for the calculation of the main parameters that characterise the turbine performance. Turbulence plays a significant role on the turbine behaviour and both hydrodynamical and structural studies are profoundly affected by this parameter. Turbulence intensity (I) , defined as the ratio between mean velocity

and standard deviation, was also worked for the four sets of tests as a result of the aforementioned flow measurements (Figure 45 and 46).

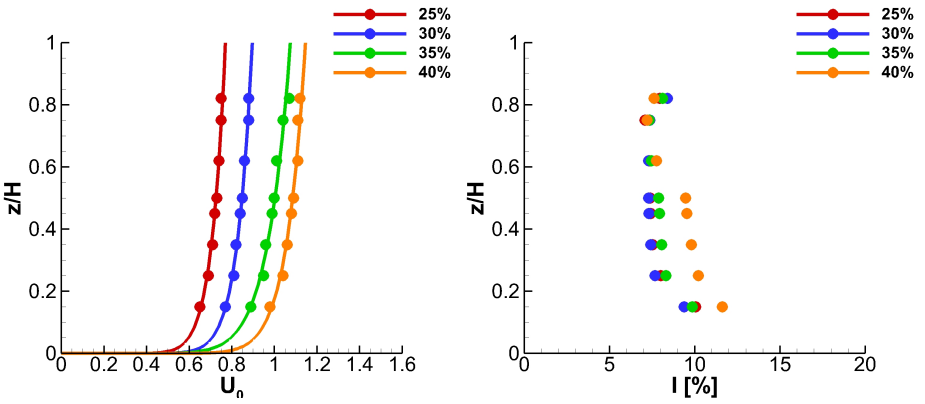

Figure 45: Bare channel testing of the velocity field for four different percentages of pump power. Modulus of the velocity vs. relative spanwise distance. Based on [160]

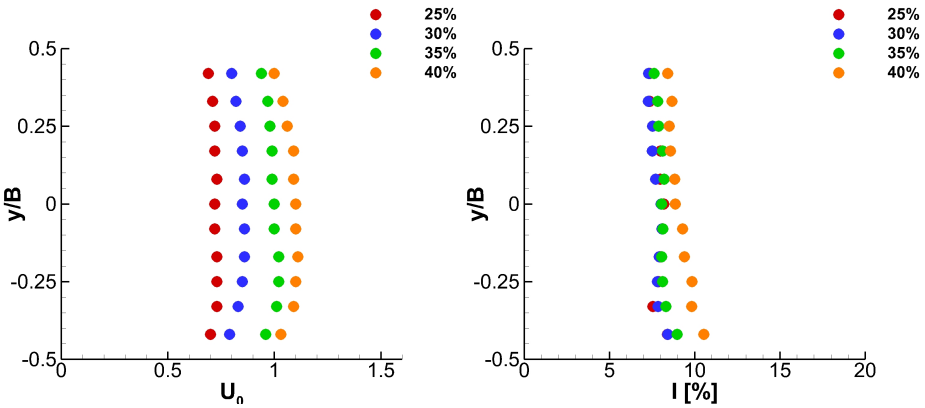

Figure 46: Bare channel testing of the turbulence four four different percentages of pump power. Modulus of the velocity vs. relative vertical depth. Based on [160]

These facilities are excellent to develop these specific tests but VATTs should be tested in an unblocked environment when possible. As commented in previous parts of this thesis, if the cross-section area of the flume is not large enough when compared to the cross-section area occupied by the rotor, the flume is partially blocked and the effect of this blockage has a great influence on the outcome. The range of blockage ratios (i.e. percentage of the flume cross-section which is occupied by the turbine) varies from 11% (turbine radius = 13

cm, height = 30 cm) to 22% (turbine radius = 25 cm, height = 30 cm).

7.2. Mechanical system

The physical magnitudes required to describe, define and analyse the rotor performance have been measured following a mechanical approach instead of an electrical system. Thus, sensors and technical equipment have been installed in order to track perfectly the rotational speed and the torque transferred to the shaft at any position and time. The experimental set up consisted of a mechanical brake which adds resistance to the turbine motion, a contactless torque transducer which measures the extracted torque and a rotary encoder in order to measure the rotational speed (Figure 47). The whole structure is supported by bearings which are placed on a stable structure above the water and on the channel bed.

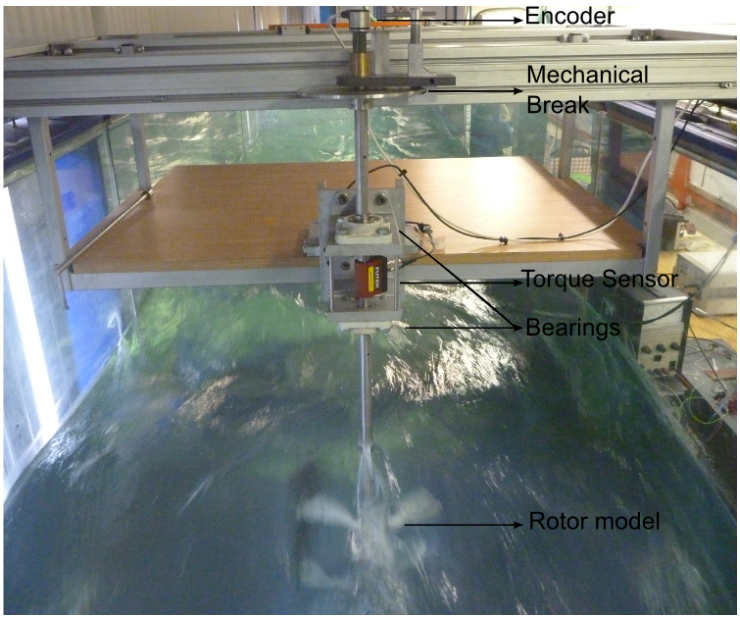

Figure 47: Experimental set up in the laboratory flume

The torque transducer (Futek TSR600 [161]) is a contactless technology based on strain gauge concepts. This stainless-steel rotary torque sensor pro-

vided output values between ±5V, but required an external power supply in order to provide between 11 to 26 V, which is the voltage required by the sensor to work. The device admitted torque values up to 5 Nm, which delimited the maximum scale of the model. Its analogue signal was led into a data logger (LabJack U6 [162]), which allowed to transfer unsteady voltage curves into data that their software can transform into readable and measurable data.

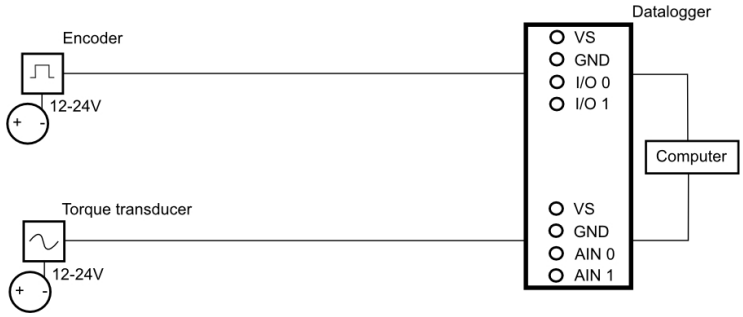

Figure 48: Data acquisition system at the Cardiff University laboratory

So as to measure the rotational speed, a shaft rotary encoder was placed on top of the shaft (Hengstler - RS 332 [163]). Its digital signal and its 2048 pulses per rotation were transmitted to the data logger and directed to a desktop, providing data with a frequency of 200 Hz and allowing tracking the position of the turbine at any moment of the rotation, and therefore knowing the rotational speed. Figure 48 depicts a diagram that sketches the data acquisition system.

The data logger transformed the data from these two pieces of equipment into binary information. To utilise the data received from the computer, subroutines had to be implemented in the software that the data logger company provides (DataFactory [164]). The subroutines are needed in order to guide the software to undertake data synchronisation and conversion, channels specification, frequency and data visualisation.

7.3. Electrical system

In addition to the mechanical system already described, some of the experiments introduced in the present study were undertaken using an electrical approach. Not just only to compare both data acquisition systems, but also to obtain reliable data that could be used for future scaling up. The structure of this set up consisted of a frame with a bearing on the bottom of the flume, a vertical shaft and a permanent magnet generator, which is connected to a horizontal metal bar. This horizontal bar is attached, in turn, to the flume, providing the necessary rigidity to the structure. The set up inside the flume is sketched in the figure 49. The rotor was held in place by two roller bearings, one mounted on the bottom of the flume and the second on the cross-beam above the flume. DVE Technology's 200 W permanent magnet generator [165] was attached to the end of the shaft and above the water surface.

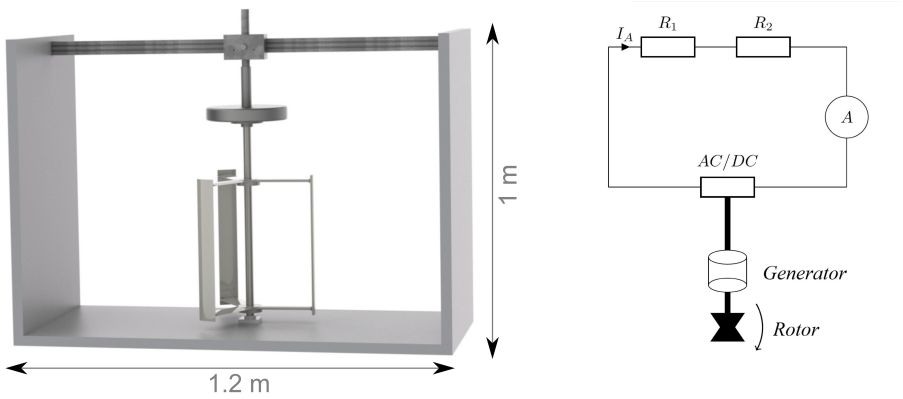

Figure 49: Sketch of the laboratory experiment setup (left) and the electrical circuit (right)

The electrical circuit, which is depicted on the right hand side of the figure 49, consisted of a rectifier (AC/DC) that changes the current from AC to DC, a load bank comprising two variable resistors set in series (R_1 and R_2) rated at 20 Ω each and an amperemeter (A). This amperemeter enabled to measure the electrical current I_A was during tests. Additionally, a tachometer was used to determine the rotational speed of the rotor. With the measured quantities the

electrical power (P_e) of the generator is computed as:

$$P_e = \omega T_e \tag{21}$$

where T_e is the electrical torque obtained from:

$$T_e = K_G I_A \tag{22}$$

where K_G is a generator-specific constant that relates voltage to rotational speed, which was provided by the generator manufacturer and confirmed in our facilities (Figure 50).

In order to extract the efficiency curves for the various turbine setups, the values of the resistors R were varied, altering the voltage V flowing through the circuit and, as a result, the current I. Those magnitudes are related by means of Ohm's Law (12).

$$V = IR \tag{23}$$

Thus, for this type of circuit, it can be said that the lower the resistance, the higher must be the current. This factor causes a drop in the voltage values and, consequently, slows down the turbine's rotation. Once the resistance value is too low - exceeding the generation capacity of the brushless generator - the turbine stops revolving [166]. The method is completely accurate from an electrical point of view, although the range of error is slightly larger than other mechanical approaches. The accuracy of the amperemeter is included within the range $\pm 2\%$ per 1A [167], and the accuracy of the tachometer is is around $\pm 1.5\%$ [168], in contrast to torque transducers, which are able to provide an approximate accuracy of $\pm 0.01\%$ in the torque readings [161]. The data sample rate for both current and rotational speed measurements are averaged after 1 minute.

The amperemeter is able to provide an average value, but pulses read by the tachometer must be registered and saved manually.

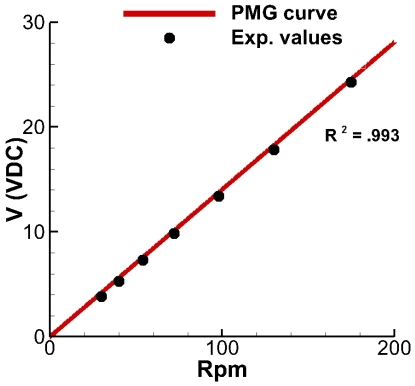

Figure 50: Verification of torque constant given by manufacturer

Turbine characteristics curves, i.e. turbine efficiency as a function of its rotational speed, were obtained by varying the electrical load on the generator using two resistors, which allowed controlling the rotational speed of the turbine. The turbine operated between little load and turbine-stall by varying $R1 + R2$ between 40 Ω (close to free-wheeling) and ≈5 Ω (which is approximately where turbine-stall occurred). For every increment of the resistance, average rotational speed, ω, and electrical current were measured over a 60 s interval. A similar technique to decrease the rotational speed of the generator has been used in other studies as [46].

7.4. Manufacturing and Construction

The small scale models used for experimental tests were formed by a few key components. Some of these components needed a long procedure to be manufactured, but their construction did not required innovative manufacturing methodologies.

- Blades. Two main methodologies were used in order to produce the blades. One of these methodologies consisted of machining and shaping a block of material into the desired outline, while the other method was based on the utilisation of a 3D printer which generated the entire blade. At this stage, no special measures were taken in order to save up material in the blade cross-sections, therefore blades were designed as solid bodies.

  The process to machine the blades for the small scale tests started with its design in Solidworks. Hence, a file containing the point of the 2D blade profile was imported. Once the X and Y points of the hydrofoil were obtained, the profile either was extruded with the required height for straight blades, or was swept along a helix curve with the required height and angle of twist for twisted blades. The Solidworks file was converted into IGES format and sent to the Mechanical Workshop at Cardiff University. The milling machine from the Mechanical Workshop shaped the rectangular chunk of material into the blade profile. So that the machining was successful, two blocks at the end of the chunk were perfectly clamped to the sides of the mill, using an additional volume of material to ensure that the block stayed in position and therefore, ensuring the quality of the machining. Two main materials were used, polyethylene plastic (Nylon) and polyvinyl chloride (PVC), which delivered similar density and strength values, and also provided smoother surfaces to the blade (surface roughness are defined in the following chapter).

  The manufacturing process for the blades that consisted of a 3D printer also started with its design in Solidworks, and the design procedure for the drawing was exactly as the other procedure. However, the 3D printer from the School of Engineering requires a file with STL format to understand the data and carry out the blade generation. This device builds the components layer by layer and, in contrast to the milling machine, the printer cannot clamp or attach any material. Thus, the required had to be statically stable for any stage of the printing. If that is not the case

and the model moves whilst it is being generated, the printing would be ruined. This fact implied the inclusion of a rectangular base on the design to ensure the stability of the blade, and then cutting the base with a saw. The blades were made from polyamide thermoplastic or thermosoftening plastic, which is mouldable above a certain temperature and solidifies when cooling down.

- Blades/shaft connection. Two main concepts have been tested for this mechanical connection, the use of two spokes per blade that connect every blade individually to the shaft, and two discs that connect top and bottom of the blades as a solid to the shaft. For the spokes manufacturing, the machining mill and the 3D printer were used for different spoke designs and the same materials as for blade manufacturing were handled, whilst discs were easily shaped from a PVC sheet with 4 mm of thickness.

- Shaft. A cylindrical bar made of stainless steel was purchased. With a radius of 10 mm and a height of 1000 mm, a height reduction was needed to fit the shaft into the laboratory flume. In addition to this reduction, small arrangements for mechanical couplings for components such as rotor, torque transducer, mechanical brake and encoder.

The other turbine components from the small scale turbine list such as bearings, couplings and mechanical brake did not require any manufacturing process.

Engineering drawings of the whole experimental set up and the different turbine designs that were tested are attached in the Appendix. Specifically, the two turbine devices based on discs as connection between shaft and blades and spokes as the main connection are depicted and dimensioned from figure 123 to figure 127.

Experimental tests are subordinated to the accuracy of the measurements. Hence, the study of the possible measuring error and to enclose it within a known range is a recognize good practise in research. In relation to the nature of the measuring errors, these errors can be classified as random or systematic errors. Definition and explanation of random (or accidental) errors cannot be provided theoretically, as many uncontrollable factors can be involved. To quantify and delimit random errors, probability distribution must be extracted from a large number of samples. Opposed to random errors, systematic errors can be quantified, and their effect can be delimited if the error analysis is accurate. Sources of systematic errors are: equipment, researcher, precision of the manufactured geometries and environmental factors.

Table 11: Laboratory equipment and accuracy according to their specifications sheet

Magnitude	**Instrument**	**Maximum or Nominal Output**	**Percentage**
Torque	Torque sensor	5N	0.05%
Rotational Speed	Encoder	2048 pulses/rev	0.06%
Flow Velocity	ADV	1.15 m/s	0.50%
Area	Measuring Equipment	0.12 m2 H=0.3, D=0.4	0.15%
Density	Salinity	999 m3/kg	0.09%

In order to evaluate the effect of systematic errors on a magnitude that is a function of several variables, differential calculus is required. As an example, the indirect error corresponding to a magnitude ϵ, which is a function of the x, y, z variables ($\epsilon = \epsilon(x, y, z)$) would be analysed as Equation 24 shows.

$$\epsilon = \frac{\partial \epsilon}{\partial x} dx + \frac{\partial \epsilon}{\partial y} dy + \frac{\partial \epsilon}{\partial z} dz \tag{24}$$

If differentiations are interpreted as errors in the measurements for any variable, the error distribution for the power coefficient function remains as Equation 25 displays.

$$C_P = |\frac{\partial C_P}{\partial T}|dT + |\frac{\partial C_P}{\partial \omega}|d\omega + |\frac{\partial C_P}{\partial \rho}|d\rho + |\frac{\partial C_P}{\partial A_r}|dA_r + |\frac{\partial C_P}{\partial U_0}|dU_0 \qquad (25)$$

In order to avoid the illogical and non-representative situation that ΔC_P is zero, absolute values are taken when this method is applied to experimental testing and equipment measurements. As seen previously, the approach flow speed is the variable which delivers more uncertainty to the the turbine power calculation, as this speed is cubed in the equation. The other variables just provide linear increments to the error propagation (Equation 26).

$$C_P = |k_1|dT + |k_2|d\omega + |k_3\rho|d\rho + |k_4|dA_r + |3k_5|dU_0 \qquad (26)$$

According to the specifications of error ranges provided by the equipment companies, instrumentation has been proved to be quite accurate, and these errors due to equipment precision are included in Table 11. Assuming that a root mean square propagation of possible errors for linear products of different variables, estimated errors for the maximum and minimum values for all variables included in the C_P, ω and C_T are given in table 12 and 13.

Table 12: Absolute and relative errors for maximum values of the variables involved in the main parameters at their peak of their performance curve

Maximum values at peak performance			
Value	**Equipment tolerance (%)**	**Deviation**	
4.589 Nm	0.100%	4.594 Nm	
15.98 rad/s	0.060%	15.99 rad/s	
1.150 m/s	0.500%	1.144 m/s	
0.120 m2	0.100%	0.119 m2	
999.000 kg/m3	0.100%	998.001 kg/m3	
	Measured Value	**Absolute Error**	**Relative Error**
Cp	40.22%	1.85%	4.59%
λ	4.17	0.56%	0.13%
Ct	0.37	1.25%	3.39%

Error ranges for torque, rotational speed measurements and approach flow velocity are obtained from their technical documentation, and devices achieved quality certifications and were calibrated by the equipment companies. Regarding the tolerance values for the area, visual measurements for lengths and distances from measuring stuff (rulers and similar instrumentation), they were estimated to contain an error of approximately 0.1 mm. In order to estimate the density, a value of 999 Kg/m3 was used for an average temperature of approximately 15 °, and an uniform distribution of the density values was assumed, considering that the corresponding values to 10 and 20° C are the limit values (999.7% and 998.2 % kg/m3 in turn), values that are not far form the right density distribution [169].

Table 13: Absolute and relative errors for minimum values of the variables involved in the main parameters at their peak of their performance curve

Minimum values at peak performance			
Value	**Equipment tolerance (%)**	**Deviation**	
2.2 Nm	0.100%	2.21 Nm	
8 rad/s	0.060%	8.02 rad/s	
0.72 m/s	0.500%	0.697 m/s	
0.12 m2	0.100%	0.119 m2	
999 kg/m3	0.100%	998.001 kg/m3	
	Measured Value	**Absolute Error**	**Relative Error**
Cp	39.33%	1.87%	4.76%
λ	3.33	0.56%	0.17%
Ct	0.23	1.27%	5.59%

In addition to delimit the instrumental errors corresponding the the instrumentation or the magnitude measurements, indirect parameters are also linked to the divergence in results between research studies within the scientific community. Thus, parameters as Reynolds number, blade roughness, flow turbulence, channel blockage, aspect ratio (proportion between turbine height and turbine diameter) or friction in the laboratory set up will also add uncertainty to the results. The influence of parameters involved on the rotor design will be also analysed in the following chapter.

Part V

Effect of blade parameters and arrangement on the performance

The emergence of the perfect turbine appears elusive so far. Due to the complex intertwining of these parameters, experimental testing of VATTs cannot provide a full explanation as to why certain turbine design parameters work better than others. Therefore, absolute conclusions about the perfect values for these parameters have not yet been reached, giving rise to differing articles of research based on experimental testing. The hydrodynamics related to a VATT operation are not simple enough to be measured in experimental research, as the angle of attack changes constantly and the vortex shed by the blades interacts with the other parts of the rotor throughout the rotation. Thus, research that uses numerical codes based on Large Eddy Simulation [170] [171] and Reynolds-Averaged Navier-Stokes [172] [173] provide important details of the complex flow physics through vertical axis or cross-flow tidal turbines. The design of a VATT might benefit from many years of research into the optimisation of the Darrieus- type vertical axis wind turbines, e.g. [70] [174] [175]. However, the significant differences between wind and water in terms of approach flow speed and fluid properties mean that this knowledge cannot be applied directly.

Experimental tests and analyses of the different parameters that play a role on the turbine operation have been undertaken. With the target of enhancing the knowledge of the scientific community, a comparison between results obtained from the experiments presented here, and other research studies found in the literature has been elaborated.

8. Flow speed

The first series of tests were focused on understanding the effect of the flow speed on turbine performance. Although power curves for certain types of rotors can be found in the literature, geometrical and environmental conditions and also the accuracy of the facilities might alter results between different physical tests. The exponential increase of the extracted power with regards to the flow velocity is known, but the evolution of the efficiency trends according to the approach flow velocity has not yet been fully defined for every single rotor. In these experiments, the Reynolds number corresponding to the tests was varied just by modifying the upstream flow speed, whilst the other parameters were kept constant. A wider analysis of the Reynolds number will be introduced in the Solidity section, when chord length will be modified whilst keeping U_0 constant (U_0 will be also referred as v) .

Rotor parameters for the flow speed tests are presented in Table 14. The Eppler 715 (Figure 51) shape was used for the blade manufacture, about which the hydrodynamic properties are described in the section of the thesis that analyses the impact of the blade shapes on the blade performance. The positive 7.5° pitch angle was chosen due to the results that can be viewed in the Pitch Angle section of the thesis, where this angle was proven to be the optimum value.

Table 14: Rotor parameters and main magnitudes for testing the turbine at different flow speeds

Parameter	**Value**	**Parameter**	**Value**
Height	30cm	Chord length	12cm
Radius	20cm	Pitch angle	7.5°
Blade shape	Eppler 715 – 100% thickness	Angle of twist	0°
		Connection blade/shaft	Discs

Third order polynomial curves were used to plot the efficiency graphs. These curves did not match perfectly with the results but they provided a stable solution for all the gathered data. More precise approaches for the efficiency

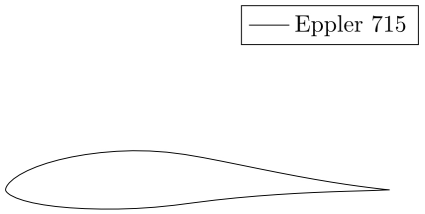

Figure 51: Eppler 715. Blade shape for testing the turbine at different flow speeds

functions exist, such as the splines calculated in [176]. Nonetheless, the data acquired in the afore-mentioned study are much more detailed than the data acquired from these experimental tests.

The experiments show that the efficiency of the turbine increases quickly up to a certain velocity. Once this specific flow speed is reached, efficiency curves become quite similar, despite changing the incoming flow velocity. Figure 52 shows that the peaks on the efficiency curves do not vary for all the tests from 0.85 to 1.15 m/s, but the performance of the turbine drops drastically for the lowest value (0.72 m/s). 36.5% is the maximum efficiency achieved in these tests, a value that was reached for a flow speed of 1.15 m/s and delivering a tip speed ratio of 1.82. This decrease in performance at low speeds has been also found in the literature. Thus, articles of research that run their experiments at similar Reynolds numbers also found this turning point on the trend of the turbine performance, although the flow speed boundary is very difficult to obtain with precision.

Some research studies are able to depict the entire curve from λ values close to zero [177], but their experimental set-up differs to the one used in this research, as the motion of the turbine is guided by a servo-motor. Torque values are then measured for prescribed rotational speeds, which do not describe the intrinsic behaviour of the turbine, as dynamic stall is avoided mechanically.

A plausible explanation would be related to the influence of viscous effects. At the lowest Reynolds number (Re= 3.6$\cdot$ 10^5, Re_c= 1.19 $\cdot$ 10^5), the increase of

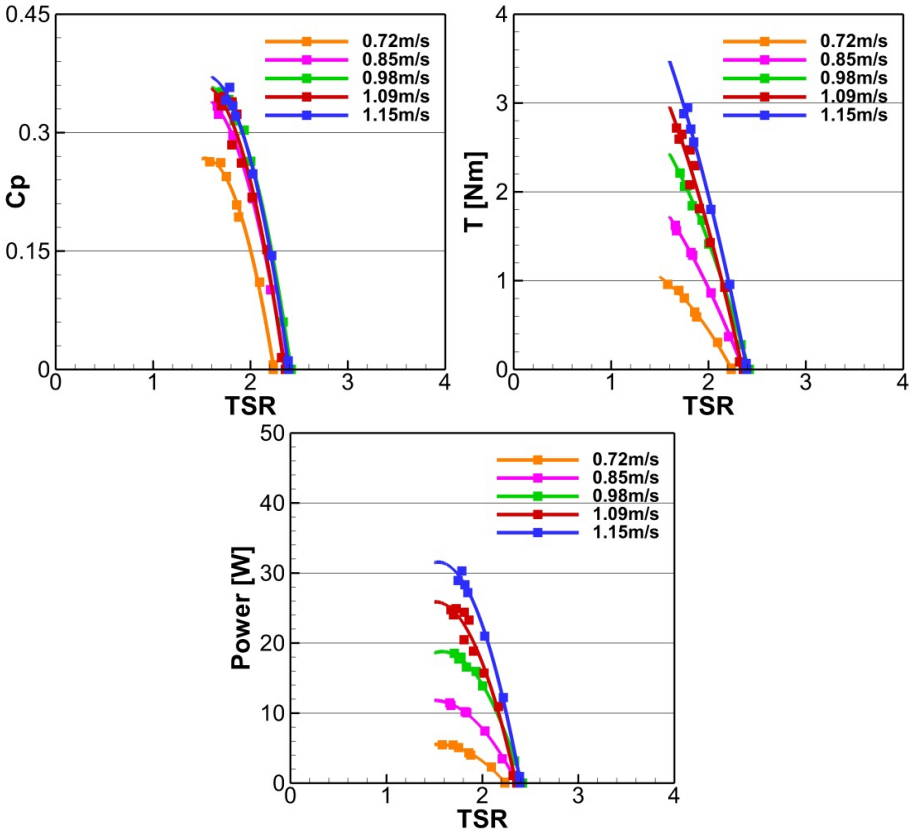

Figure 52: Flow speed tests, 3 blades. Left, Power Coefficient vs. λ. Right, Torque vs. λ. Down, Power vs. λ.

the hydrofoil performance is constant to some extent. Once a certain Reynolds number is reached, the extra drag added by the smooth flow separation becomes more relevant in the blade hydrodynamics, a fact that could lead to a substantial drop on the total drag. [178] analysed in depth the behaviour for the aerofoils at low Reynolds numbers, and the influence of the Reynolds number in the increase of the separation resistance of the turbulent boundary layer is depicted in Fig. 53.

Results from other work found in the literature are displayed by the Table 15. These experimental tests show that the maximum efficiencies tend to be achieved after an approach speed within the range of 1 and 1.2 m/s. Some

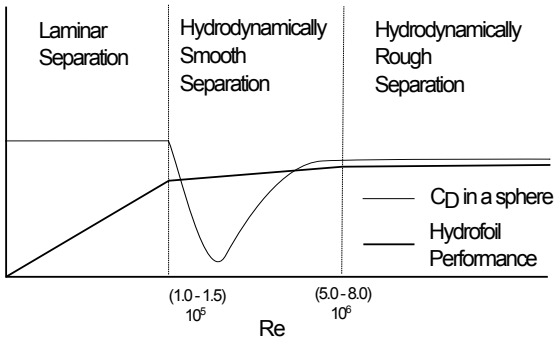

Figure 53: Hydrodynamical performance of an hydrofoil according to the Reynolds number. Source [178]

studies detected that low Reynolds values do not favour the appearance of high lift-to-drag ratios. As a result, power coefficients are not as high as they could be under higher Reynolds number conditions [71] [177]. However, the velocity limit found in these experiments seems to be within the range of Reynolds numbers where the turbine hydrodynamic forces are completely developed.

It will be observed in the next sections that the influence of other rotor parameters such as the number of blades, blade shape or the angle of twist do not have an effect on the flow velocity limit where power curves become analogous. However, experimental tests depend on parameters such as Reynolds number, blockage, blade roughness and/or flow turbulence; factors that modify the outcome. This large number of uncertainties dictates that direct comparisons between different experimental research are unlikely to be accurate, and therefore they can complicate a statement of definite conclusions.

The results extracted from the literature share these findings to some extent. Bearing in mind the difficulties and inaccuracies of comparing outcomes between different physical experiments, the flow speed threshold from which peak efficiencies start to stagnate can be included within the range [0.8-1.0] m/s. The Reynolds number analysis does not seem to be an accurate approach, as no common trend can be observed and every test series provides a different individual trend. On the other hand, the graph that compares peak efficiencies to

Table 15: Research studies about vertical axis tidal turbines performance for different flow speeds and comparison to the results

Research Author	**Flow speed [m/s]**	**Cp/Cpmax**	**TSR**	Re_c	Re
Shiono et al. [71]	0.6	0.50	1	6.90E+004	-
	0.8	0.98	1.3	1.20E+005	-
	1	0.96	1.25	1.44E+005	-
	1.2	1.00	1.25	1.73E+005	-
	1.4	0.90	1.2	1.93E+005	-
Bachant et al. [177]	0.3	0.67	1.8	7.56E+004	7.32E+005
	0.5	0.86	1.8	1.26E+005	1.22E+006
	0.7	0.92	1.8	1.76E+005	1.71E+006
	0.9	0.95	1.8	2.27E+005	2.20E+006
	1.1	1.00	1.8	2.77E+005	2.68E+006
B. Yang et al. [179]	0.5	0.83	0.8	3.60E+004	-
	0.75	0.89	0.9	6.41E+004	-
	1	0.95	0.95	8.10E+004	-
	1.25	0.98	0.95	1.10E+005	-
	1.5	1.00	0.95	1.32E+005	-
Kyozuka et al. [180]	0.5	0.79	2.25	9.00E+004	6.00E+005
	0.6	0.81	2.2	1.06E+005	7.20E+005
	0.7	0.86	2.15	1.20E+005	8.40E+005
	0.8	0.88	2.1	1.34E+005	9.60E+005
	0.9	0.93	2.05	1.48E+005	1.08E+006
	1	1.00	1.95	1.56E+005	1.20E+006
Present study	0.72	0.73	1.65	1.19E+005	3.60E+005
	0.85	0.93	1.78	1.51E+005	4.25E+005
	0.98	0.96	1.8	1.76E+005	4.90E+005
	1.09	0.98	1.8	1.96E+005	5.45E+005
	1.15	1.00	1.83	2.07E+005	5.75E+005

the Reynolds chord number does depict a similar result to the flow speed analysis, and the range $[(1.2\text{-}1.6)\cdot 10^5]$ seems to delimit accurately this performance limitation.

9. Blade Shape

The shape of the blade is one of the most important parameters for a VATT rotor. Not only can the shape enhance the turbine performance, but can also improve magnitudes such as rotational speed and torque, delaying the dynamic stall or increasing the blade strength. The blade profile is a complex feature, of which different parameters play an important role. Chord length, thickness

and pitch angle intertwine their influence, meaning that the optimal shape for a vertical axis turbine has not yet been defined.

Table 16: Parameters and magnitudes for blade shape tests depending on the connection between blades and central shaft

Parameter	**Value**	**Parameter**	**Value**
Height	30cm	Height	30cm
Radius	20cm	Radius	15cm
Connection Blade/shaft	Discs	Connection Blade/shaft	Spokes
Number of blades	3	Number of blades	3
Chord length	10 cm	Chord length	10 cm
Angle of twist	0°	Angle of twist	0°

Similarly to research carried out about HATTs, knowledge transfer from wind to water is not straightforward. For instance, most straight-bladed wind turbines feature symmetric NACA aerofoils, achieving fairly good results [181] [182] [183]. However, it has been shown that asymmetric or cambered hydrofoils can outperform the results delivered by symmetric hydrofoils for some VATT designs [179]. Hydrofoils must possess essential properties if they are adopted into the blade design; specifically, they must display a sufficiently high lift-to-drag ratio throughout the entire turbine rotation ([179], [184]). [185] compared wind and tidal blade shapes and concluded that a minority of profiles for both technologies are thin, as blade resistance is still a significant concern. Therefore, this fact implies that some thin profiles that deliver high lift-to-drag ratios at low Reynolds numbers cannot be adopted until materials gain in strength and resilience. [186] also hints that asymmetrical blade shapes employed in wind turbines can outperform symmetrical ones.

A very important parameter is the pitch angle. Articles of research have already suggested that the blade shape should not be tested without taking into account the influence of the pitch angle for both tidal and wind turbines ([180], [181]). These research studies concluded that testing the hydrofoil only at a certain pitch angle is not the correct methodology, as the optimum angle of pitch

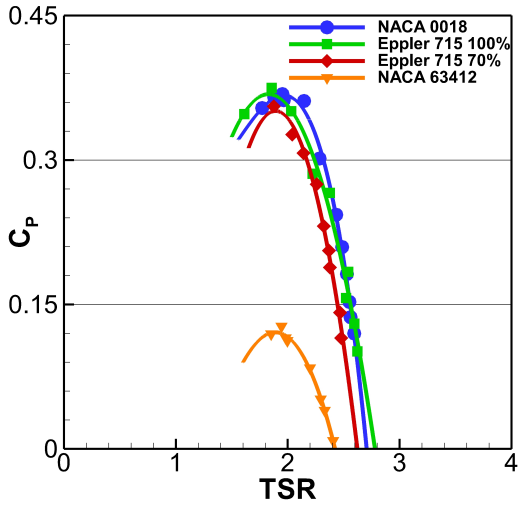

Figure 54: Blade shape tests. Rotor with discs, radius = 20 cm. U_0 = 1.15 m/s

might vary from one hydrofoil to the other. Therefore, efficiency and turbine properties in consonance to the blade shape can only be compared when the optimum pitch angle is set. [187] tested the hydro-dynamical force distribution for some NACA cambered and non-cambered shapes. From this work, the optimum pitch angle was considered to be the angle which adopts the closest curvature to the turbine trajectory. These experimental tests performed by [187] displayed encouraging blade efficiencies in cambered NACA foils.

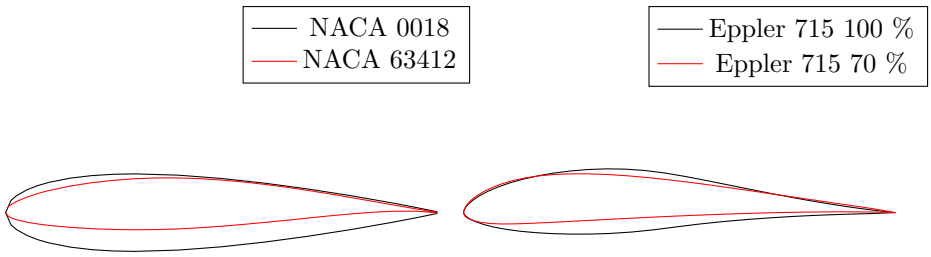

Figure 55: Hydrofoil profiles used for blade shape testing

Taking into consideration the significance of the hydrofoil angle of pitch, the blade shapes that are presented here were tested at the optimum pitch angle, i.e., the angle that delivered the highest peak on the power coefficient curve. These optimum angles are explained in depth in the Pitch Angle section of this thesis.

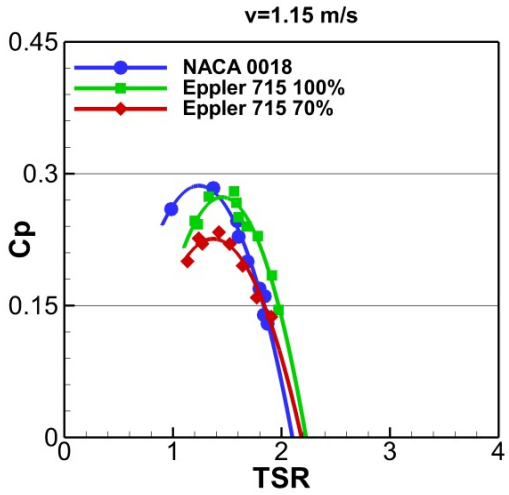

Figure 56: Blade shape tests. Spokes, radius = 15 cm. C_P vs. λ.

Several blade shapes were analysed in our flume (Figure 55), with the aim of finding the blade that provides the cross-flow turbine with the best power extraction. NACA 0018, NACA 63412 and Eppler 715 with a thickness percentage of 100% and 70% were tested for two different type of vertical axis turbine, the details of which are listed in the table 16. Results were very similar for both type of turbines, which shows the consistency of the methodology and the data acquisition system. Tests carried out for the largest rotor (discs connecting shaft and blades) showed that NACA 0018 at +2.5° and Eppler 715 -100% thickness at +7.5° performed similarly, whereas Eppler 715 with 70% thickness performed slightly worse. Finally NACA 63412 did not achieve good results in terms of power extraction (Figure 54). Similar tests were undertaken with a smaller radius and spokes instead of end-discs as a connection between blade and shaft. In these tests NACA 0018 and Eppler 715 - 100% yielded very similar values

and Eppler 715 70% performed about 6% less of the absolute efficiency of the other two blades (Figure 56).

The lift-to-drag ratio along different angles of attack is proven to be one of the main parameters in the evaluation of the efficiency of a hydrofoil. The software Xfoil [188] simulates the aerodynamics involved when an aerofoil is placed in a straight flow for different Reynolds numbers, enabling the provision of lift-to-drag curves. NACA 0018 and Eppler 715 - 100% graphs correspond to a fully inviscid model and a turbulence energy of a dirty wind tunnel ($n_{crit} = 5$, from [189]) have been extracted). The level of disturbance in this model might not be as turbulent as in a tidal stream, and therefore there is some uncertainty about these values; although this value was chosen as the software performs with more instability at higher turbulence [190], [191].

The distribution of the lift coefficients along the different angles of attack and at Reynolds numbers between $Re = 5 \cdot 10^4$ and $Re = 2 \cdot 10^5$ for NACA 0018 and Eppler 715 - 100 % is plotted in figure 57. According to these figures, lift coefficients and, therefore, lift forces increase their values as long as the Reynolds number also increases. The NACA 0018 case showed even clearer than the Eppler 715 plot that, the larger the Reynolds number, the larger the angle of attack provides high lift coefficients.

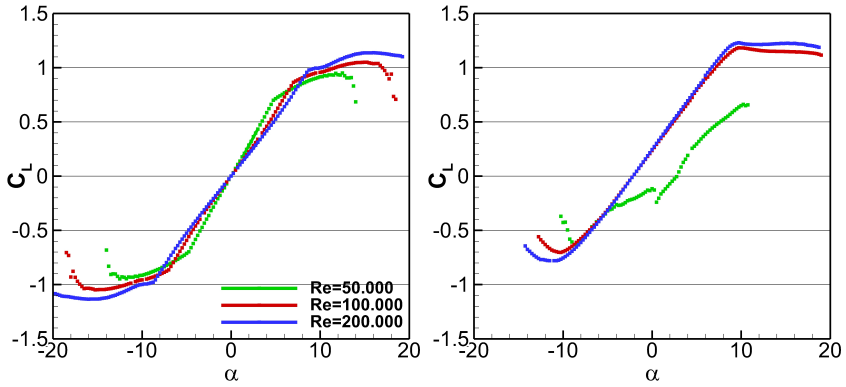

Figure 57: Lift coefficients versus AoA for different *Re*. Left, NACA 0018. Right, Eppler 715 - 100% thickness

Significant information can be extracted from the analysis of the ratio lift coefficient versus drag coefficient according to the angle of attack (Figure 58). The angle of attack where the Eppler 715 shape delivers the highest peak on the curve for Reynolds is equal to $5 \cdot 10^4$ is 12.25° , and for NACA 0018 is 6.25° but, whereas the angle of attack with the largest ratio decreases the larger the Reynolds number is for the Eppler shape ($Re = 2 \cdot 10^5$, α=8.25°), the optimum angle of attack for the NACA 0018 increases the larger the Reynolds number (8.75°). Although other parameters and hydrodynamic forces are involved in the turbine rotation, optimum pitch angle and angle of attack where the largest C_L/C_D are achieved could be related and play a significant role on the VATT blade optimisation.

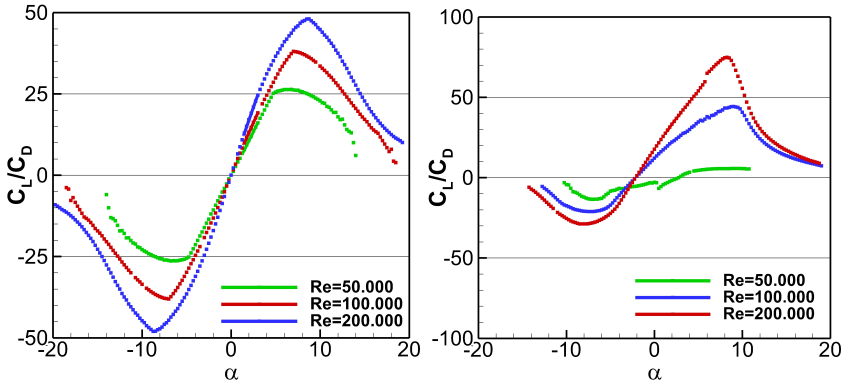

Figure 58: Lift to drag ratio for different *Re*. Left, NACA 0018. Right, Eppler 715

Innovative concepts have been tested and patented in order to improve the performance of the blades. Flexible hydrofoils with self-adjustable cambering [192], oscillating hydrofoils [193], or a flap on the trailing edge in order to avoid dynamic stall as much as possible [194] have been tried with successful results even for wind turbines [195], although these technologies are still in an early stage of development. In general, these new concepts add new mechanical systems to the turbine structure, which have not yet been optimised and, therefore, reduce the lifetime of the structure due to fatigue and maintenance problems.

A system to control the pitch angle would enable the addition of electrical

and mechanical stability to wind and tidal turbines for flow speeds higher than rated values [174]. On the other hand, VATTs must face higher viscosities and flow densities than wind turbines. This implies that a system to control the pitch angle might weaken the resilience of the turbine design.

10. Pitch Angle

As mentioned previously, the angle of pitch is a significant variable to take into account. In order to analyse and compare the performance of different blade shapes, the optimum angle of pitch must be found.

The angle of attack is a different concept for cross-flow turbines than for HATTs. As this type of turbine rotates about its vertical axis, the turbine operation does not depend on the direction of the water flow. Also, the angle of attack changes constantly over the rotation, whilst this angle is quasi-constant for HATTs. Figure 73 depicts how the angle of pitch for positive and negative values was defined at our facilities. Some pieces of work prefer to set the reference or mounting point in the centre of the line that joins the trailing and the leading edge of the hydrofoil but, in these tests, the angle was set with the gravity point / geometry centre of every hydrofoil as a reference. With regards to the fact that positive pitch angles could feature better than negative angles, the influence of the pitch angle and the curvature of the blades were evaluated.

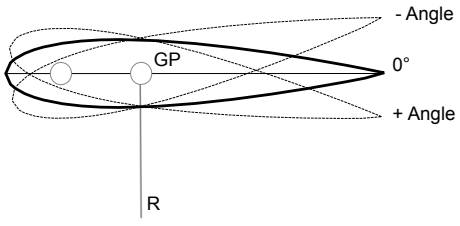

Figure 59: Sketch of the pitch angle set up. GP= gravity point of the airfoil section (also named geometry centre), R= radius.

The sensitivity of the turbine performance due to the changes on the pitch angle is observed in the outcomes that every experiment for testing blade shapes

provided. The best angles for any blade are within a range no larger than ±2.5°. Outside this range, the performance of the cross-flow turbine is low and the rotor might not even be able to spin.

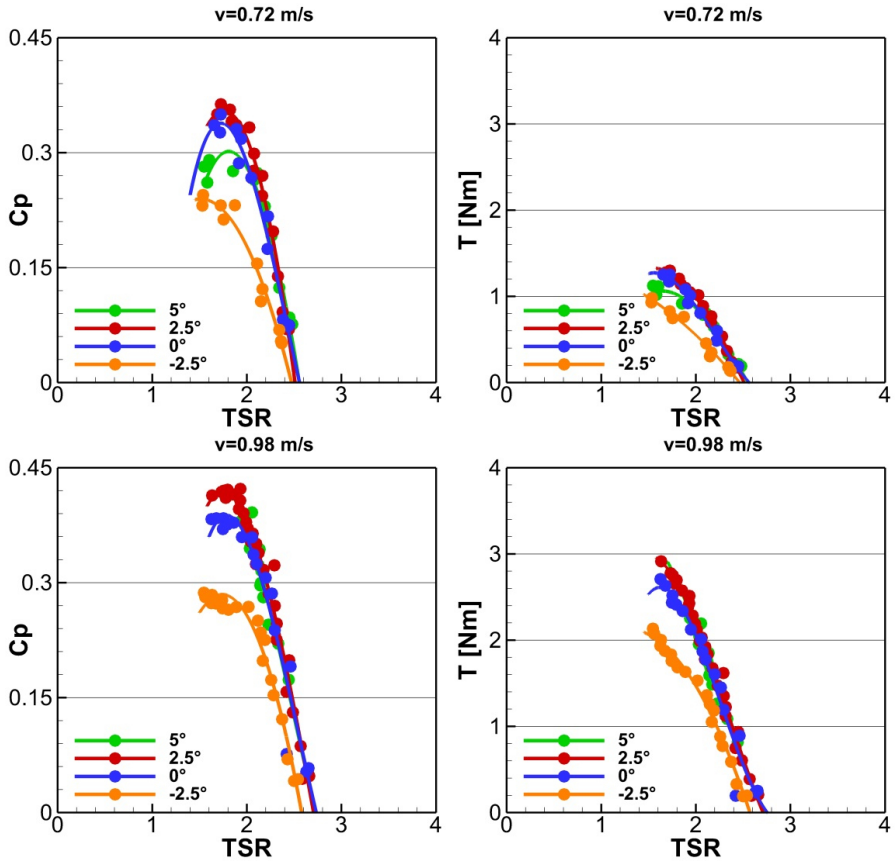

Figure 60: Pitch angle tests for NACA 0018

The NACA 0018 shape displayed an optimum pitch angle for +2.5° . Experiments for two different flow speeds corroborated this value, which is also confirmed by the torque curves (Figure 60). For these tests, the operational range of the turbine is between -2.5° and +5.0° , much closer to 0° than the Eppler shapes. This fact might be related to the inherent properties of the hydrofoil that were described in the previous chapter.

As expected, the results showed the significance of finding out the optimal

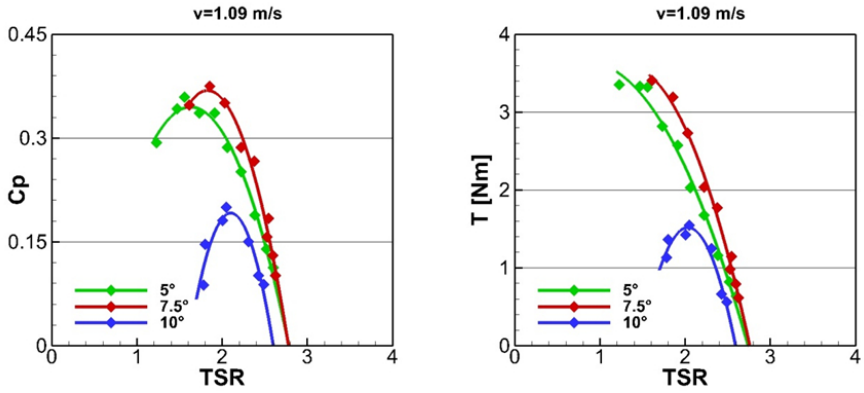

Figure 61: Pitch angle results for Eppler 715 -100% thickness

value for the pitch angle according to the blade shape. Thus, sensitivity of the pitch angle in the turbine performance is easily appreciated from the results corresponding to the Eppler 715 - 100% of thickness shape (figure 61). The position of the blade accepts a range of just five degrees and the performance of the cross-flow turbine decreases substantially outside this range. For the Eppler shape, the pitch angle value of +7.5° offered the best operation in terms of efficiency, although +5.0° displayed very similar power coefficients. These pitch angle tests were performed for an approach flow speed of 0.72 m/s as well, confirming the findings showed by the figure 61.

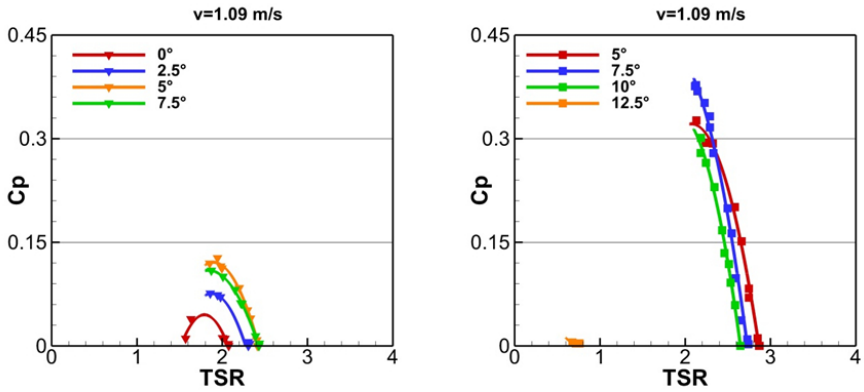

Figure 62: Pitch angle results. Left, Eppler 715 -70% thickness. Right, NACA 63412

Besides the experiments corresponding to Eppler 715 - 100% shape, Eppler 715 - 70% thickness and NACA 63412 were also tested. For both Eppler shapes, the pitch angle value of +7.5° offered the best operation in terms of efficiency, although the +5.0° experiment from the latter shape did not display such a great performance as the Eppler 715 - 100 %.The NACA 63412 profile displayed poor performances at an optimum pitch angle of +5° , a fact that could be related to the sharp trailing edge of this shape. For these tests, both efficiency and range of valid angles are reduced in comparison with NACA 0018 and both Eppler 715.

Table 17: Research studies about vertical axis tidal turbines performance for different flow speeds.

Research Author	**Blade shape**	**Pitch angle** [○]	**Flow speed** [**m/s**]	Re_c	Cp/Cp_{max}
Kyozuka et al. [180]	NACA 0018	0	1	9.05E+004	0.83
		5		8.21E+004	1.00
		10		7.79E+004	0.89
		-5		1.14E+005	0.33
		-10		1.26E+004	0.02
Zhao et al. [196]	NACA 0018	-3	1	2.31E+005	0.44
		0		2.16E+005	0.82
		3		1.99E+005	0.95
		5		1.98E+005	1.00
	NACA 0018	5		1.98E+005	0.89
		6		1.80E+005	0.95
		7		1.82E+005	1.00
		8		1.81E+005	0.98
Kirke [68]	NACA 0020	5	0.91	4.02E+004	0.64
		10		4.69E+004	1.00
Present study	NACA 0018	-2.5	0.98	1.76E+005	0.67
		0		1.81E+005	0.90
		2.5		1.86E+005	1.00
		5		1.91E+005	0.95

The influence of the angle of pitch has been analysed in some research studies. Table 17 shows pieces of work that tested experimentally different pitch angles for the NACA 0018 shape or similar for VATTs. The range of optimum values is between 5° and 10° , slightly higher than the optimum value found in our tests. Plenty of parameters such as Reynolds number, blockage effect, blade manufacturing, laboratory equipment and/or turbulence can play a significant

role toward these discrepancies.

Similar research studies were carried out to analyse the angle of the blade pitch for vertical axis wind turbines. Table 18 shows some of these studies for NACA 0015 and NACA 0021. Positive pitch angles also showed the best results in terms of efficiency. However, the range of optimum values is closer to zero than for tidal turbines, perhaps due to their higher Reynolds values. Once again, vertical wind turbines and vertical tidal turbines share physics and concepts, but results cannot be extrapolated without a deep analysis, both experimentally and numerically.

Table 18: Research studies about vertical axis wind turbines performance for different pitch angles.

Research Author	**Blade shape**	**Pitch angle** [○]	**Flow speed** [**m/s**]	Re_c	Cp/Cp_{max}
Fiedler et al. [181]	NACA 0015	7.80	10	4.92E+05	1.00
		3.90	10	4.92E+05	0.88
		0.00	10	4.92E+05	0.74
		-3.90	10	4.92E+05	0.44
		-7.80	10	4.92E+05	0.00
	NACA 0021	7.80	10	4.67E+05	1.00
		3.90	10	4.67E+05	0.86
		0.00	10	4.67E+05	0.81
		-3.90	10	4.67E+05	0.67
		-7.80	10	4.67E+05	0.42
Klimas et al. [197]	NACA 0015	7.00	45.8	6.95E+05	0.67
		4.00	45.8	6.65E+05	0.94
		2.00	45.8	6.65E+05	1.00
		0.50	45.8	6.65E+05	0.94
		-1.00	45.8	7.50E+05	0.92
		-3.00	45.8	6.95E+05	0.64

11. Solidity Ratio / Number of blades

One of the significant characteristics of a cross-flow turbine is its solidity. Solidity (σ) can be defined as the percentage of the area within the turbine's rotational path that is occupied by the blades at one time (Equation 27, nb = number of blades). Several studies in the literature have analysed this factor,

from both experimental and numerical modelling. From this, its optimization is considered to be difficult, owing to the importance of other parameters such as blade shape, pitch angle, blockage of the channel and the most important for the analysis this parameter, number of blades. As solidity is directly related to the number of blades of the turbine, the research study must approach the effect of this parameter taking into account both elements. Thus, results and data post-processing of these two intertwined parameters are shown in the same section.

$$\sigma = \frac{nb \cdot c}{2\pi r} \tag{27}$$

Tests were performed considering rotors that comprised three blades with varying chord length, i.e. 8, 10 and 12 cm, which yielded turbine solidities of σ= 0.19, 0.24 and 0.29, respectively. Solidity tests were run using the Eppler 715 - 100% hydrofoil but with the three different chord lengths. Taking into account previous pitch angle results, each experiment was carried out with three blades set at a pitch angle of +7.5° .

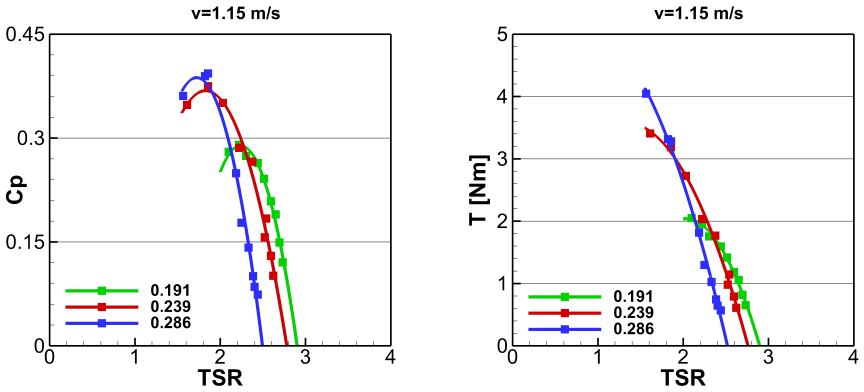

Figure 63: Solidity tests for Eppler 715 - 100 % of thickness.

Figure 63 shows that the rotors with low solidities reach higher rotational speeds, even though this positive effect does not imply the achievement of higher efficiencies. On the contrary, the highest efficiency was achieved by the greatest

solidity, 28.6%. Thus, 12 cm of chord length displayed a maximum efficiency of 38.8%, and also the greatest torque values.

The results for the rotor performance in relation to solidity agreed with the literature. The higher the solidity, the greater the torque values are, according to [71]. The results also reflect that the smaller solidity values, the larger is the rotational speed.[198] suggests that low solidities for wind turbines will provide a lower likelihood of it starting rotating on its own, but will perform at a higher λ, whilst a rotor with high solidity features better starting torque characteristics.

A summary of experimental and numerical research studies gathered from the literature is displayed in table 19. As parameters vary greatly between research works in terms of blade shapes, non-identical laboratory conditions and so on, the optimum solidity value for experimental studies varies between 8% and 26%, which are values slightly smaller than the optimum solidity obtained from the experiments presented here. On the other hand, studies based on numerical modelling provided a wider range of optimum solidities, the best solidity value being between 8% and 45 % (Table 20).

Although high solidities provided high efficiency values, an analysis of hydrodynamical variations due to the flow curvature must be taken into consideration. When the parameter chord to radius is low, the influence of the flow curvature is not reflected on the performance, but an increase on the value can enlarge this effect. Hence, in the case of high solidity, the relative speed (w) could change along the chord of the blade, leading to a detriment on the lift and drag curves. This effect has been studied in both wind and tidal turbines, although tidal turbines accept higher chord to length ratios without a noticeable reduction in the performance [202] [203].

The same experimental procedure as in previous tests was followed, to analyse the influence that the number of blades has on a VATT rotor. The optimum pitch angle for the Eppler 715 - 100% profile tested previously was adopted,

Table 19: Summary of experimental testing for VATT which analysed solidity

Research Author	**Blade shape**	**Solidity**	**Flow speed m/s**	Re_c	Cp/Cp_{max}
Shiono et al. [71]	NACA 633-018	6.28	1.00	6.28E+004	0.88
		9.42	1.00	1.18E+005	1.00
		12.57	1.00	1.91E+005	0.98
		15.71	1.00	2.91E+005	0.88
Shiono et al. [76]	NACA 63018	53.7	1	1.61E+005	0.54
		44.6	1	1.48E+005	0.67
		36.6	1	1.44E+005	0.92
		26.9	1	1.09E+005	0.96
		22.4	1	1.05E+005	0.98
		17.9	1	9.52E+004	1.00
		13.4	1	7.98E+004	0.75
		10.8	1	7.14E+004	0.54
Dai et al. [199]	NACA 0025	17.29	1.22	-	1.00
		14.09		-	0.83
		11.49		-	0.60
		9.36		-	0.47
	NACA 0025	21.20	1.22	-	1.00
		17.28		-	0.77
		14.08		-	0.70
		11.48		-	0.57
	NACA 0025	26.03	1.22	-	1.00
		21.22		-	0.83
		17.29		-	0.65
		14.10		-	0.09
Present study	Eppler 715	0.18	1.15	2.07E+005	0.7
	-100% thickness	0.23	1.15	2.21E+005	0.96
		0.28	1.15	1.93E+005	1.00

which means a positive pitch angle of $+7.5°$. As a result, two-, three- and four-bladed rotors were tested for U_0=1.09 m/s .

The efficiency values differ substantially between the three different rotors (Figure 64). The two-bladed rotor achieved an efficiency of 42%, although no self-starting modes were observed. For three-and four-bladed rotors, the maximum efficiencies obtained from the tests were 37.5% and 32% respectively, but during some of these experiments the rotors did start rotating without any additional mechanical thrust. The torque curves have also been influenced by the different number of blades; the tests showed higher torque values for the set-up that had fewer blades. On the other hand, a high number of blades provided

Table 20: Summary of numerical modelling for VATT which analysed solidity

Research Author	**Blade shape**	**Solidity ()**	**Flow speed m/s**	Re_c	Cp/Cp_{max}
Hwang [174]	NACA 0018	7.6	2	3.36E+005	1.00
		9.5	2	4.60E+005	0.90
		11.5	2	6.24E+005	0.79
		13.4	2	8.12E+005	0.69
Antheaume [200]	NACA 0012	9.55	3	1.26E+006	0.86
		12.74	3	1.92E+006	0.93
		15.92	3	2.70E+006	1.00
Khan [201]	NACA 63018	15	-	-	0.33
		25	-	-	0.56
		35	-	-	0.78
		45	-	-	1.00

an additional supply of inertial forces and more stable torque curves during the rotation. These facts are consistent with the findings from the literature. For instance, [71] tested their straight-bladed turbines with rotors featuring one, two and three blades showing similar efficiency, rotational speed and torque distribution trends.

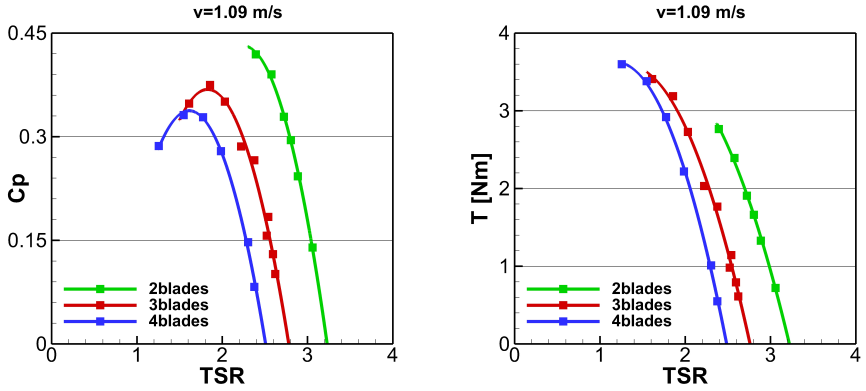

Figure 64: Number of blades tests. Rotor with discs as the blade/shaft connection, radius = 20 cm.

As a rotor with two blades was unable to start the rotation without any mechanical help, more tests were undertaken for three and four-bladed rotors. Although the rotor with three blades provided a higher efficiency, the symmetry over two axes and the higher inertial forces that a four-bladed rotor offers are

also interesting features from a rotor-design point of view.

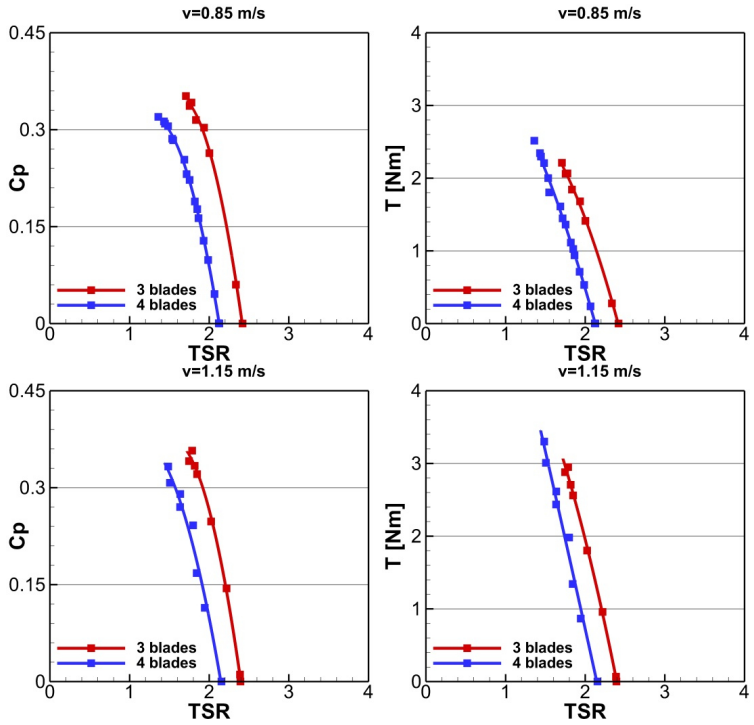

Figure 65: Number of blades tests three and four-bladed rotors. Eppler 715 - 100%

The graphs do not show any significant difference on the shape and/or length of the power curves (figure 65). This fact allows the conclusion that, from a practical point of view, a three-bladed rotor gives better efficiencies than a four-bladed turbine all along the power curve. Tension and vibration tests would be needed to evaluate the structural performance of the rotor depending on the number of the blades.

A plausible explanation to the influence that the number of blades has on the turbine performance could be related to the absence or presence of blades that generate negative forces when they are in counter-flow positions. According to this assumption, fewer blades would slow down the turbine rotation and create less vortex shedding that would interact negatively with the rest of blades, as figure 66 depicts [204] [205]. Also, a larger benefit from the created forces in

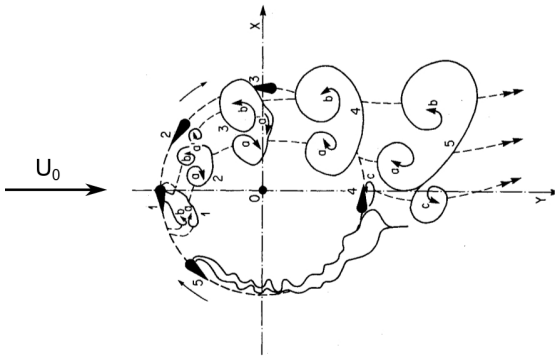

Figure 66: Sketch of the vortex shedding for $\lambda = 2.14$. Source [205].

the upstream position could be achieved, as fewer blades would be located in negative sectors during the turbine rotation. Blade shape also plays a role on the turbine self-start. Research studies carried out into studying this assumption for vertical axis wind turbines showed that cambered aerofoils might lead to a better performance in terms of initiating the turbine rotation [206], [207].

In addition to the tests that analysed the performance of the rotors depending on the number of blades in their design, the number of cases in which the turbine displayed a self-starting behaviour was also counted, for different pitch angles and different flow speeds. The initial position was not arranged, favouring the randomness of the test conditions. This is an important fact, as other research work experimented with the significance of the initial position and the existence of critical ranges of angles to cause the turbine self-start [208].

Summing up all the results, the total amount of positive events for this hydrofoil was very similar between the rotors that have three and those with four blades, although they featured a different number of successful events depending on the pitch angle (Table 21). It is noticeable that there is a slight divergence between the most efficient pitch angle ($+7.5°$) and the angle with the best self-starting results ($+5.0°$). However, this could be related to the fact that the initial acceleration is greater when the pitch angle decreases for vertical wind turbines [139].

		Pitch angle		
nb	**Uo**	5.0°	7.5°	10.0°
2 blades	0.72 m/s	-	-	-
	0.98 m/s	-	-	-
	1.14 m/s	-	-	-
3 blades	0.72 m/s	-	-	-
	0.98 m/s	X	X	-
	1.14 m/s	-	X	-
4 blades	0.72 m/s	X	-	-
	0.98 m/s	X	X	-
	1.14 m/s	X	-	-

Table 21: Self-starting processes for different number of blades and pitch angle. X= success, - = no-success

12. Angle of twist

Cross-flow or vertical axis tidal turbines are based on straight-bladed rotors, but when the rotors exhibit an angle of twist in their blades, it can also be called a Gorlov turbine, due to its inventor [209]. This exclusive design aims to improve the turbine behaviour in terms of self-starting and also a more uniform torque curve.

The angle of twist (ϕ) gives a higher likelihood of having a part of the blade in the optimum position to enable the turbine to start rotating without any additional mechanical supply. In order to quantify the effect of the angle of twist on the turbine rotation, blade wrap (ψ) is defined as the percentage of the turbine on its three-dimensional trajectory that is occupied when projected in a 2D plane (Equation 28). The main difference between solidity and blade wrap resides in the angle of twist. Whereas solidity measures the ratio between lengths on a plane, blade wrap projects on the same plane all the length occupied by the whole blade volume. In fact, if the turbine consisted of straight blades, blade wrap would be coincident to solidity, but when an angle of twist is provided to the blades, the blade wrap increases substantially. This parameter is more commonly used for water head turbines [210], in which blade wrap percentages are close to the unit.

$$\psi = \frac{nb}{2\pi r}(c + Htg^{-1}\phi) \tag{28}$$

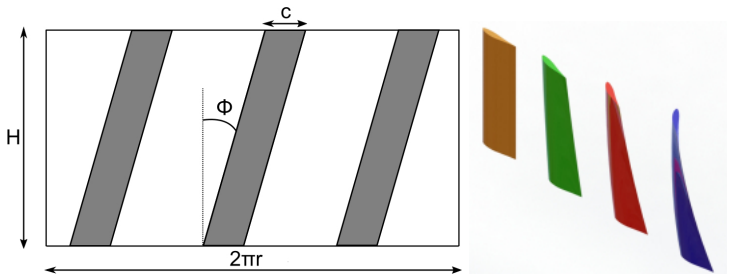

Figure 67: Left, sketch of the rotor design project on its 2D circumference development. Right, drawing of four blades with 0°, 15°, 30° and 45° of twist angle.

These experiments were carried out with three-bladed rotors, which were manufactured using an Eppler 715 shape - 100% of thickness. The height of the rotor was 0.3 m and the diameter 0.4 m, with discs as a main connection between blades and shaft. The main parameters and a 3D CAD drawing of the twisted blades are depicted in Figure 67.

The results obtained from the angle of twist tests are presented in figure 68. Straight-bladed rotors (ϕ=0°) provided the highest power coefficient values, reaching up to 36 % of efficiency for a tip speed ratio of 1.9, although very similar results were obtained by the turbine set up corresponding to ϕ=15° . The decrease on the efficiency becomes a more pronounced trend for ϕ=30° and ϕ=45°. The greatest angle of twist showed the lowest peak power coefficient (26.5%), in spite of shifting the performance curve to the right, which implies reaching higher rotational speeds.

In relation to the results obtained from the tests, a compromise between efficiency, rated rotational speed, maximum torque accepted by the rotor strength and self-starting processes must be taken into account in order to design the rotor of a VATT. However, (and in consistency with the literature [76]) the output shows that, although introducing twist to the rotor's blades leads to lower efficiencies when compared with a straight-bladed rotor, this angle of twist pro-

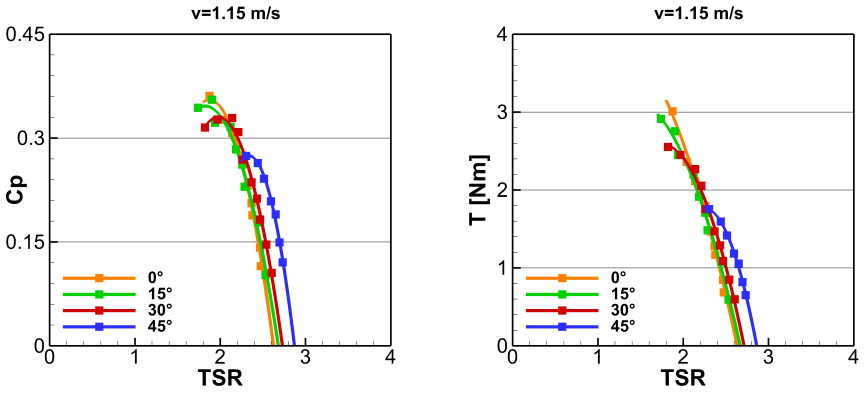

Figure 68: Angle of twist tests. Left, Power Coefficient vs. λ. Right, Torque vs. λ.

vides improvements in significant properties such as higher rotational speeds, lower torque values or better self-starting characteristics.

The study of the turbine self-starting behaviour was undertaken with similarity to the tests carried out for the analysis of the number of blades of the rotor. Thus, the initial position of the blades was not arranged beforehand, aiming to replicate more realistic environmental conditions. Table 22 presents the testing cases which delivered self-starting processes. A clear trend is spotted, as the larger the rotors' angle of twist is (or larger blade wrap), the higher is the likelihood of the rotor starting the rotation on its own.

	Angle of twist/ /Blade wrap			
Uo	0°//24%	15°//32%	30°//40%	45°//48%
0.72 m/s	-	-	X	X
0.98 m/s	X	X	X	X
1.15 m/s	X	-	X	X

Table 22: Self-starting processes for different angles of twist.

13. Spokes shape

The physical part that connects the blades and shaft has been proven to be one of the most important components of the turbine. Its influence on the

losses that might apply or the hydro-dynamical changes that may have occurred due to their presence are significant consequences related to the overall object. Moreover, spokes might add a mechanical limitation to the rotor design, as these connections are usually parts with low thickness and little material, which must transmit and bear the forces given by the rotor. The connection between blades and shaft could be achieved by adding a disc to the blade's top and bottom, but this alternative would require a very large amount of material to manufacture full-scale devices. Therefore, spokes seemed to be the most reasonable option, and many of the technologies observed in the literature used this approach.

Figure 69: Left, rectangular stainless steel spokes. Centre and right, NACA 0012 sheel that covered the rectangular spokes.

In the tests presented in this thesis, stainless steel and 6mm-thickness rectangular cross-section spokes were firstly adopted to the blade shape and the shaft connector (Figure 69). Afterwards, a shell with a hydrodynamic shape was designed in order to introduce the rectangular spokes inside the shell. Thus, the previously used spokes were covered by a shell based on the NACA 0012. Ideally, drag forces would be minimised, as this shape delivers a much lower drag coefficient (C_d) compared to rectangular shapes. Also, the lower the percentage of thickness of the hydrofoil, the lower drag would be produced [211]. The spokes used to carry out these tests are described in detail in the Appendix (figure 125).

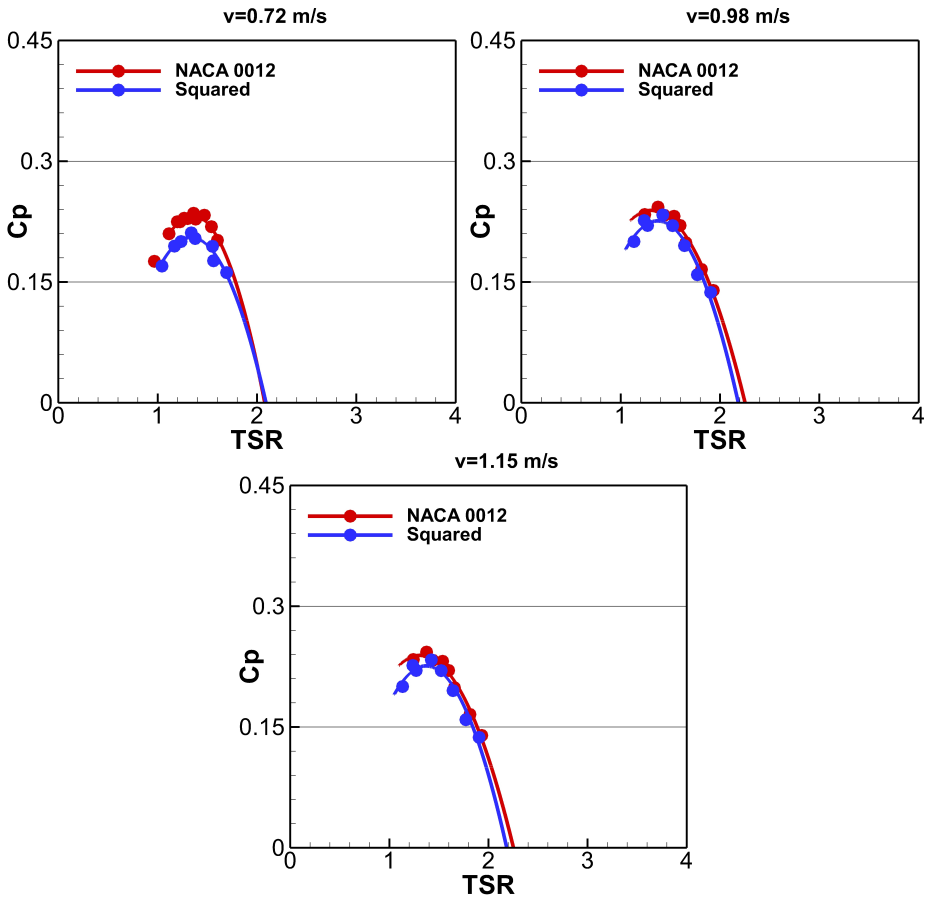

Figure 70: Results corresponding to the tests of the two spokes shapes.

Tests were undertaken with three NACA 0018 blades. A chord length of 10 cm and a turbine radius of 15 cm provided 32% of solidity, higher than most of the tests run with discs (r=20 cm). The improvement on the efficiency curves has been detected, as the figure 70 reflects on the outcome corresponding to U_0= 0.72, 0.98 and 1.15 m/s. The largest effect is observed for the lowest Reynolds number, as an increase of 3% on the absolute efficiency has been measured. The increase on the power coefficient is lower for the other two Reynolds numbers, just enhancing by 1.5% the efficiency that the turbine delivered with rectangular spokes.

According to the information gathered from the literature, a larger improvement was expected. [212]analysed the influence of three different shapes: a flat, a rounded and a hydrofoil shape for the spokes. The hydrofoil outperformed the flat spoke by a larger efficiency margin (15%), although its rounded shape did perform similarly to the rectangular spoke tested here. Similar results were achieved by [213], where NACA 0012 delivered smaller losses than rounded spokes. [214] tested experimentally and numerically the influence on the turbine efficiency due to spokes with NACA 0012, NACA 0015 and NACA 4415 shapes, and both methods agreed that the thinnest shape (NACA 0012) provided the best results in terms of power coefficient and drag minimisation.

These findings seem to ensure that a hydrofoil shape must always be adopted for the VATT design, although the rectangular thin shape used in this thesis might not prompt the appearance of drag forces as the theory suggests. If rectangular spokes have to be used for non-hydrodynamic reasons, spoke thickness should be as low as possible to not increase detrimental drag forces.

Another possibility could be related to the small size of the shell. Thus, the shape of the NACA 0012 shell could be very similar to a flat shape, as the geometry is quite small (shell width = 60 mm) and therefore, the shape would not be able to deliver its supposed hydro-dynamical response.

14. Winglets

As mentioned in previous sections of this thesis, knowledge from aerospace and wind engineering has been adapted somewhat to tidal technologies. Inspired by aerospace devices that are currently in operation, a novel aspect of this work consisted of testing and analysing the effect on the performance that a winglet at the end of the blades could yield.

A winglet is a common component in aircraft. It is attached to the end of the wings in order to decrease the resistance against the flow. The use of winglets

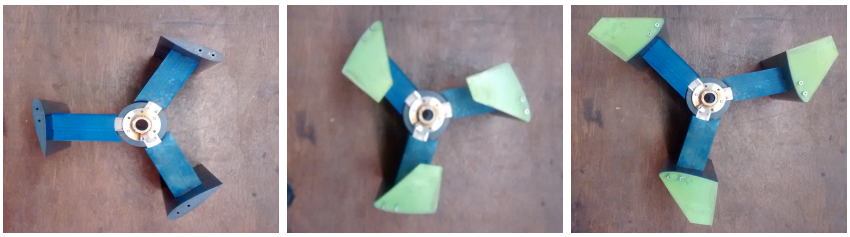

Figure 71: Turbine set ups for winglets testing. Left, no winglets. Centre, Inwards winglets. Right, Outwards winglets.

attempts to interrupt the secondary flow currents that create a vortex at the tip of the blade and, therefore, cause an induced drag. They are successfully used in aerospace engineering, as an increase on ratio lift-drag forces by around 9% and a reduction on the induced drag close to 20 % and have been proven [215], but they have not been analysed in depth for tidal turbines. Research tested the idea of distorting secondary flows and three-dimensional effects in the span-wise direction. Thus, a flat-plate on the blade top and bottom was used, which lead to an increase on the efficiency around a relative 10% [213] .

Taking into account the physical phenomena involved on the hydrodynamics of the turbine rotation, the influence of a 3D winglet in the performance of a cross-flow turbine was analysed. The winglet has the same width as the blade chord length, and its length is 6 cm, which is 40% of the rotor radius (Figure 71). Engineering drawings are shown in the Appendix (Figure 128).

The improvement on the efficiency performance is significantly displayed on the efficiency and rotational speed (Figure 72). The turbine efficiency goes from 26% to 33%, which is an increase of 21% in relative values. Besides this, the winglet contributes to increasing the turbine rotational speed. λ varies from 1.4 without any winglet to 1.55 at peak efficiencies, which is 7% faster than without the winglet. The winglet placed deliberately outwards was also tested, with no detrimental effect in terms of the efficiency measured; there was even a slight improvement noticed on the performance curve. In contrast to the possible increase on the induced drag due to the winglet shape, its beneficial effect in

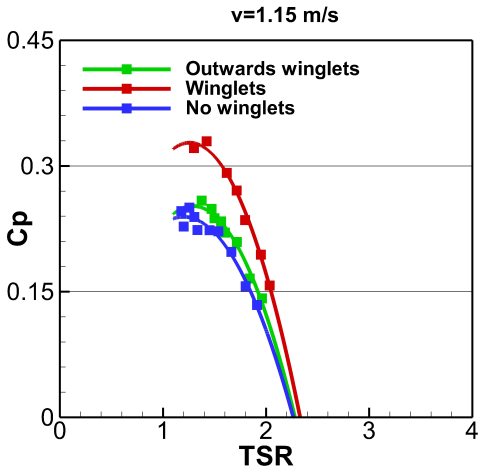

Figure 72: Winglets testing power curves.

avoiding vortex generation at the blade tip seems to have a greater impact on the power coefficient. In spite of this, [213] speculates that 3D effects can be almost neglected when the aspect ratio is large enough ($H/D > 3.5$), a fact that is partially supported by [216]. This research tested a wide range of aspect ratios for wind turbines and found that for the larger the ratio, the larger the efficiency. These high values can be achieved by some devices, but probably a high aspect ratio could lead into structural and manufacturing problems for a full scale de- vice. On the other hand, [217] suggests in their experimental testing for tidal turbines that the optimum aspect ratio value that provides higher rotational speeds and better efficiencies is 1; a statement that does not agree with other articles within the literature.

15. Obstacle influence

The influence of placing secondary cylinders upstream and downstream in areas near the turbine was also tested in the facilities at Cardiff University. Two main goals are targeted with the placement of these cylinders: Firstly, because obstacles would change the hydrodynamics of the flow stream, it is needed

to look for an optimum position where the cylinder deviates and accelerates the flow to the zones where it could supply an increase of the performance. Secondly, the possibility of providing additional support to the turbine structure if necessary. Thinking about full-scale devices, these cylinders could simulate piles or columns which could help avoiding displacements and vibrations.

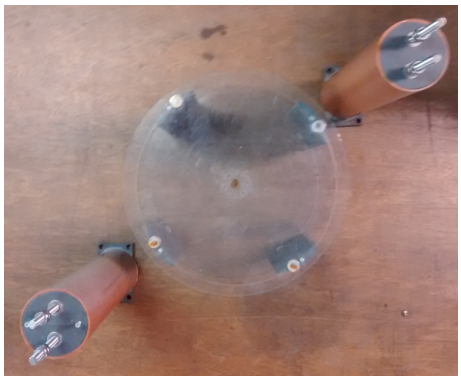

Figure 73: Illustration of materials and location of the cylinders for the obstacle influence testing . Flow coming from left to right, radius cylinder = 4 cm

Firstly, the turbine was tested without any secondary cylinders, the characteristics of which are the same as the spokes shape tests with the NACA 0012 shell. Having these values as a reference, the increase or decrease on the efficiency with secondary cylinders added was measured. Up to 14 different set-ups were tested, measuring the influence of these cylinders horizontally and then vertically. Figure 74 depicts an example of the cylinders set-up; cylinders which are made of plastic hollow pipes and are filled with water. These cylinders were placed symmetrically in downstream positions as well, in order to simulate real environmental conditions (assuming that flow would be bi-directional).

Initially, the influence of the cylindrical obstacles was approached horizontally. Three main trends can be observed from the graphs (Figure 75). For NW positions, the further away from the centre are the more efficient the power curves. The best position was the one named 3-NW, which delivered better results than tests without obstacles. On the other hand, the closer to the cen-

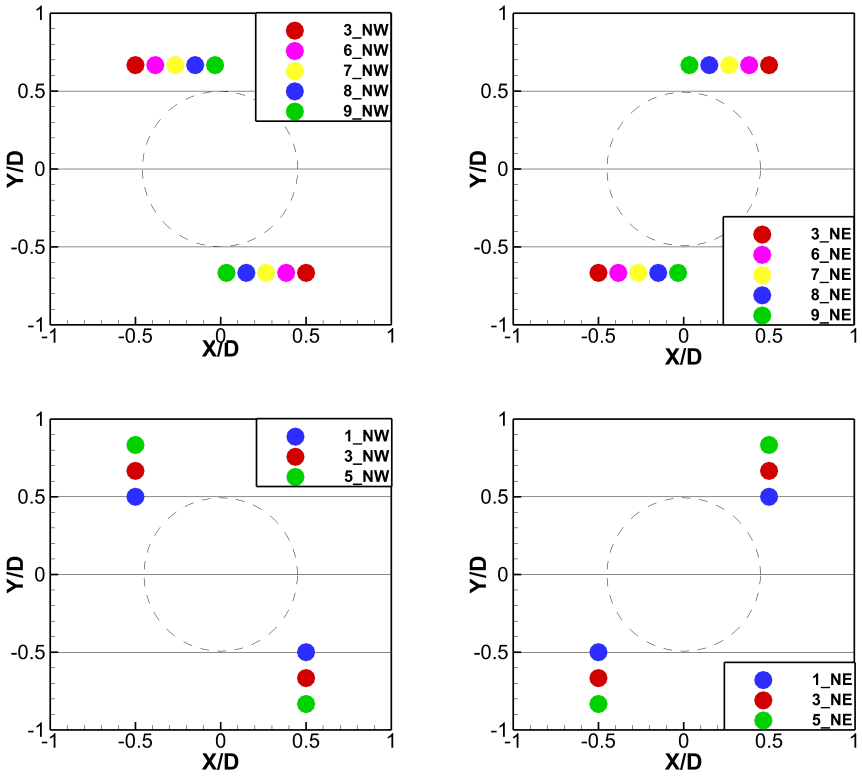

Figure 74: Position of the cylinders and nomenclature for the obstacle influence testing. Incoming flow is from top to bottom, turbine is rotating in a counter-clockwise direction. The same colour circles down and upstream were tested together.

tre of the turbine (8-NW,9-NW,9-NE,8-NE), the worse the outcome in terms of efficiency and rotational speed. Finally, the NE area did not alter much the turbine operation, although we can see that the closer to the 3-NE position, the higher were the efficiencies.

According to the results, 3-NW and 3-NE tests performed the best, and that is the reason why vertical tests were undertaken from that position. The NW sector showed encouraging results, as the closer to the turbine, the higher the efficiency. The 1-NW position (x/D=y/D = 0.5 when considering the centre of the turbine as coordinates axis) provided up to 8% more of absolute efficiency; and the further away vertically, the lower the influence on the performance.

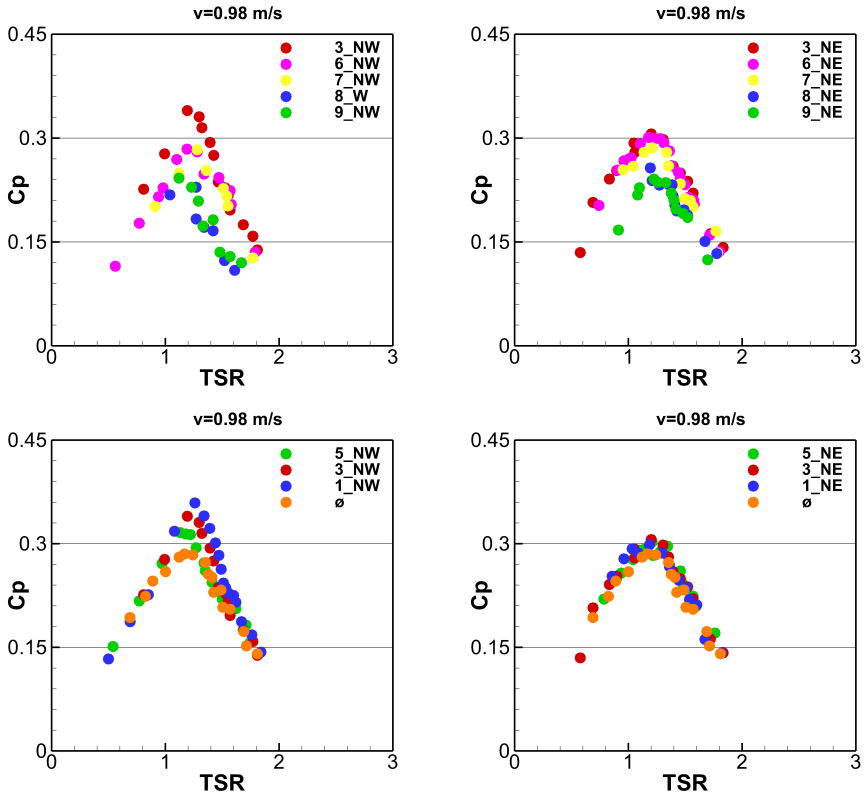

Figure 75: Results for testing the obstacle influence. Graphs corresponding to the figure 74 positioning.

However, the three tested cases outperformed the experiments without any obstacles. For the NE cases, results were almost coincident, which implies that its influence on the flow hydrodynamics do not have a great effect on the rotor performance.

An interpolation of the results in order to depict the optimum locations for secondary columns was successfully undertaken. Hence, the peak efficiencies and their corresponding locations were interpolated to a mesh (figure 76). The results show the areas where a vertical cylinder would increase the efficiency (figure 76, dark blue) and where the effect of cylinders would generate losses on the performance (white areas). These are very promising results, although

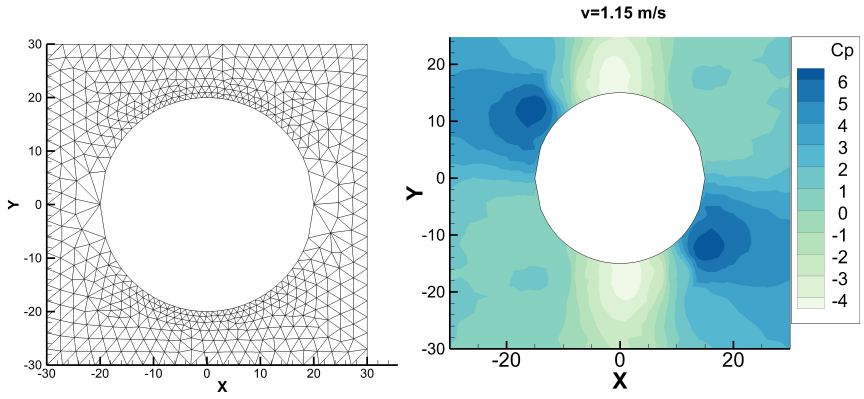

Figure 76: Left, Mesh generated for the results interpolation . Right, Interpolation of the increase/decrease on the turbine performance due to presence of cylinders

the use of secondary columns is not as easy as it could be for full-scale devices. For instance, a non-fully bi-directional flow would change the optimum position of the cylinders, and favourable positions which increase the power extraction would turn into disadvantageous conditions.

In order to understand the physics behind this increase of the efficiency, Figure 77 shows the distribution of instantaneous power generated by one blade over an entire rotation [173]. This figure shows that the largest efficiencies are obtained when the blade is located at an angle of 90° . This might be the reason why the less favourable locations for the secondary columns did not perform well, as they slowed down the flow in the most important areas in terms of power generation. On the other hand, the optimum positions for the columns might accelerate the flow in these areas where the maximum individual efficiencies are obtained.

16. Shaft size

Aiming to optimise every component of the turbine, the size of the shaft was taken into consideration for physical tests. Three cylinders made of aluminium with radii 30, 50 and 70 cm were manufactured to analyse the influence of the

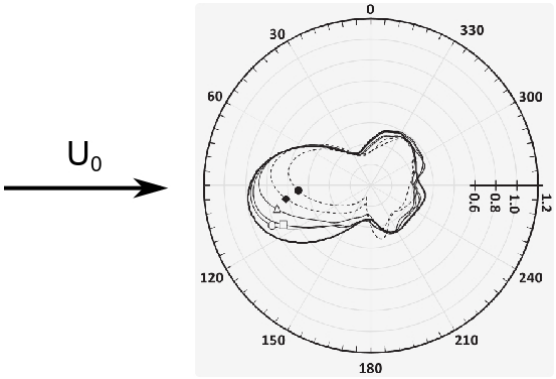

Figure 77: Instantaneous power coefficient for one blade. Turbine rotating counter-clockwise. Source [173]

shaft diameter on the turbine performance (Figure 78). These three components were adapted to fit the stainless steel shaft that belongs to the main turbine design (r=10cm)

Figure 78: Aluminium cylinders used for the shaft size testing. Radii corresponding to 30, 50 and 70 mm

Tests were undertaken using NACA 0018 with 2.5° of pitch angle, 20cm-radius discs connecting blades and shaft. This solution allowed the use of the aluminium shaft, whilst the spokes design did not permit the installation of these cylinders around the shaft.

No improvement can be observed from the graphs (Figure 79). The two smallest radii perform similarly, but the rotor set up with a shaft radius of 50 cm provided worse efficiency values and the largest radius, 70 cm, performed the worst of the four tests. No big changes were noticed from the torque curve

graphs either.

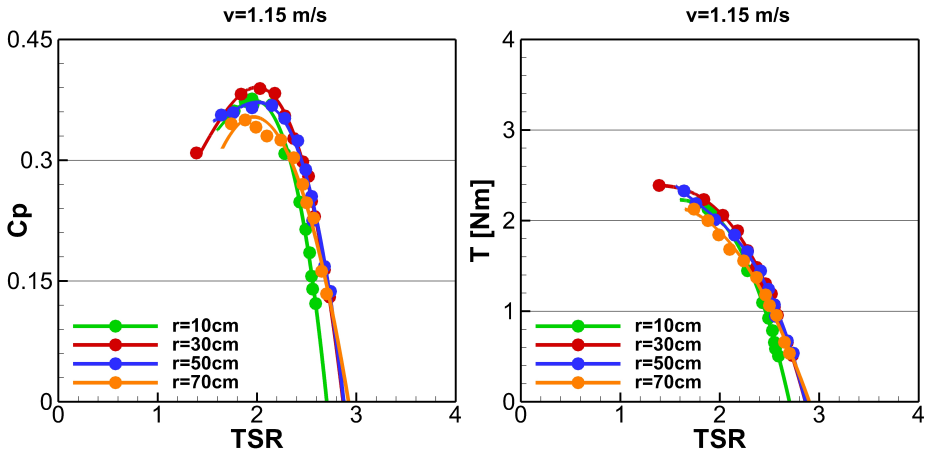

Figure 79: Results corresponding to the shaft size tests

The experimental data does not show a physical explanation for the drop on the efficiency, although a large size of the shaft could affect the hydrodynamics around its rotation. Nevertheless, knowing the limitations on the shaft size is very significant from a design point of view. Although a more detailed range of values for different shaft size/rotor diameter ratios can be obtained in future experimental work, and numerical simulations might shed some light over this topic, a preliminary range of shaft sizes can already be suggested. According to the results obtained here, the shaft radius must be smaller than 15% of the turbine in order not to detrimentally alter the characteristic power curves of the turbine.

17. Inner blades

To create the necessary starting torque in order to start the turbine operation, an original concept has been tested. With the target of adding more blades, which could help the turbine to rotate at the first revolutions, a rotor with blades at two different radii was built. Apart from the usual 20 cm-radius discs, inner blades located in a 10 cm-radius were placed in the same turbine

design.

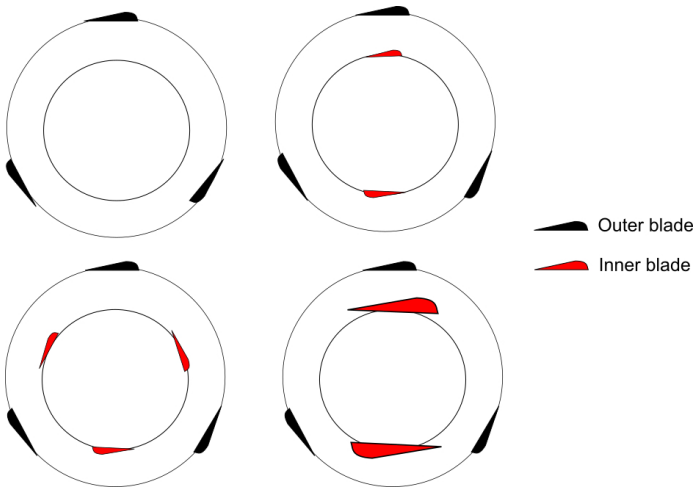

Figure 80: Sketch of the four rotor set ups for the inner blades tests. Small red blade = 8 cm chord length, big red blade = 12 cm chord length

Three main configurations were tested, in addition to the main case without any blades in inner positions. Thus, an outer three-bladed rotor with an inner three-bladed rotor, and a three-bladed rotor with an inner two-bladed rotor with two different chord lengths were tested. Figure 80 shows a drawing with these three tested configurations. All the outer blades were based on the Eppler 715 - 70% at 7.5° of pitch angle and 10 cm of chord length, whilst inner blades consisted of Eppler 715 - 100% thickness and 8 cm or 12 cm of chord length.

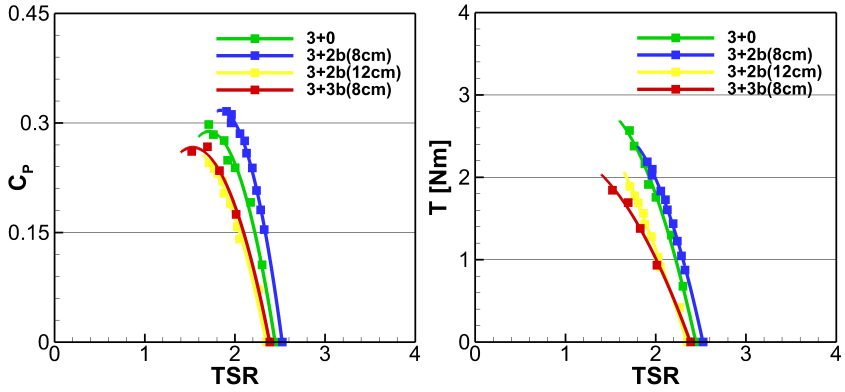

Figure 81: Results corresponding to the inner blades tests. $U_0 = 1.09m/s$

Unfortunately, the inner blades did not help the turbine to self-start and the turbine did not gain neither a better self-starting process nor any improvement on the turbine efficiency. Figure 81 displays the contraction of the power curves, which was larger for the more inner blades the turbine presented. Thus, the lowest efficiency was obtained for the six-bladed turbine, which was expected to add at least a beneficial effect on the turbine self-starting, but none of the rotors here presented was able to start rotating on its own.

18. Blockage

The laboratory flume at Cardiff University is 1.2 m wide and was used with 0.5 m of water depth. This effect from the blockage leads into an increase in the flow on the sides of the turbine. The rotor acts as an obstacle, deviating and accelerating the water to the sides. This acceleration does not appear when the turbine is spinning in a real environment as the natural channel is usually wide enough to negate its impact. In order to quantify the increase on the turbine efficiency due to this artificial effect, the concept of blockage ratio is needed. The blockage ratio is the rotor's cross-section (A_r) divided by the flume's cross-section (A_f). As a general rule, the greater the blockage ratio, the larger will be the distortion of the results, although blockage ratios near to one (flume close to be blocked) do not outperform lower blockage ratios [218].

Several studies have addressed the effect of blockage on hydrokinetic turbine performance. A research work about horizontal tidal turbines carried out a mathematical approach that explains the blockage influence as a function of different flow velocities upstream, downstream and velocity through the turbine [145]. The downstream velocities are negatively affected by the energy extraction produced by the turbine, which is transformed into torque generation. [219] undertook a series of studies to analyse the theoretical influence of a constrained flow due to the turbine rotation. Initial equations are coinciding, however this work continues developing the mathematical expression, adding new concepts to

the formulae such as the number of turbines set in the channel. [220] presents a theoretical model to predict power efficiencies which takes into consideration the free-surface phenomena. Hence, this piece of work includes in their equations the drop on the water surface that appears in down-stream positions. After accepting several assumptions and equating hydraulics laws, a quadratic equation leads into a mathematical solution for the blockage correction. The main problem of this empirical answer is its dependence on four factors. Whereas Froude number and blockage ratio are trivial, the other two parameters depend on the velocity distribution far downstream from the turbine position, which is not easy to specify and tends to demand certain subjectivity. Further approaches regarding the blockage effect of a turbine array over a channel cross-section has been analysed by [221]. Their theoretical analysis differentiates between local flow effects related to a single turbine and global flow effects that are linked to the whole flow that is disturbed by the turbines acting as an obstacle.

One of the most common formulations in quantifying the increase on the turbine performance because of the effect of blockage is displayed in Equations 29, 30, 31. Their accuracy has been proved to be fairly good to some extent, and such articles as [145] or [177] use them to correct their efficiency curves. However, these coefficients depend on upstream and downstream flow measurements, which require special equipment to measure these velocities. Besides this fact, these correction factors also depend on the flow speed that goes through the turbine rotation, a magnitude that is difficult to be obtained by experimental testing based on vertical axis turbines.

$$Cp_b = Cp(\frac{U_r}{U_1})^3 \quad (29) \qquad Ct_b = Ct(\frac{U_r}{U_1})^2 \quad (30) \qquad \lambda_b = \lambda(\frac{U_r}{U_1}) \quad (31)$$

Another expression that intends to quantify the influence of the turbine efficiency is extracted by works such as [222], which is a derivation of the for-

mulation created by [219] for small blockage values. This expression, obtained after several assumptions and simplifications, evaluates the turbine power coefficients according only to its blockage ratio (β). According to this expression (Equation 33), C_p increases drastically for $\beta \approx 1$, therefore another approach of the function must be take into account when $\beta \approx 1$.

$$\beta = \frac{A_r}{A_f} \qquad (32) \qquad\qquad Cp_B = Cp(1-\beta)^2 \qquad (33)$$

With the target of recognizing the artificial increase on the rotor performance at these facilities, a series of tests were carried out at the laboratory. Thus, three rotors that differed on the diameter length were tested for a NACA 0018 blade, 30cm height and a positive pitch angle of 2.5°. Radii values were 12, 20 and 23cm and approach flow speed corresponded to 0.98 m/s.

Results depicted in figure 82 showed a clear trend on the turbine performance. Not only does the peak efficiency increase according to the blockage ratio, but the whole curve is shifted to the right because of their higher rotational speeds. Thus, the efficiency varies from 28% for the rotor that provides the lowest blockage ratio, to 50% for the rotor with the largest diameter (46cm), and therefore the highest blockage ratio.

Nevertheless, these results must be analysed carefully. Whereas the outcome is completely accurate and the curves are perfectly defined regardless of the influence of the blocked flow, imprecisions in terms of maintaining the geometrical scale led into inaccuracies in significant parameters that should have been kept constant. The main feature that introduces uncertainty to the outcome is the use of the same blades for the three tests. As blade dimensions were not scaled up or down in relation to the size of the turbine, parameters such as solidity or aspect ratio were not kept constant. Hence, chord length was kept as 10 cm for the three tests, introducing variations on the solidity values that, as seen

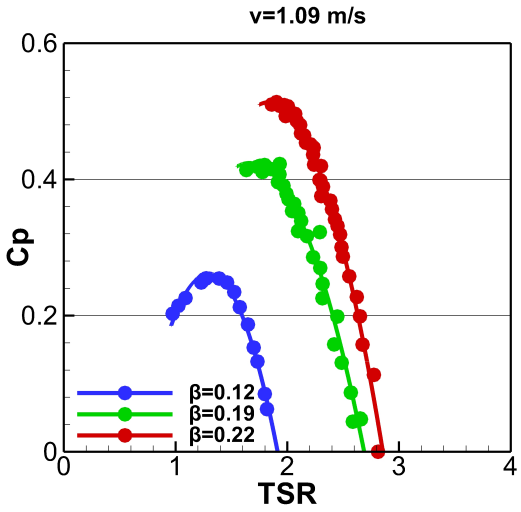

Figure 82: Power curves corresponding to the blockage effect tests

previously, provided very different characteristics to the efficiency and torque curves. Then, as blade height has not been changed either, the aspect ratio (known as the ratio between rotor height and diameter) has not been considered. Although it has not been studied in depth for VATTs, some research work shows that depending on this ratio, rotational speed and torque can vary and, therefore, efficiency can be also affected. The exact values of these parameters are presented in Table 23.

Table 23: Rotor most significant parameters for the tests of the blockage effect

Radius	**Blockage**	**Solidity**	**Aspect Ratio**	**Cp**	**Corrected Cp**
23 cm	0.22	0.21	0.65	50 %	30 %
20cm	0.19	0.24	0.75	42 %	27 %
12cm	0.12	0.40	1.25	28 %	22 %

If the correction factor displayed in Equation 33 is applied to the results, a 40 % relative drop on the efficiency is calculated for the biggest rotor. Both corrected efficiencies for the two largest rotors are quite similar to the smallest set up. The 12 cm-radius rotor delivers a blockage ratio near 10%, which is considered to be the limit where blockage effect can be negated for wind turbines

[223]. On the other hand, the solidity value for the smallest turbine is fairly high($\sigma = 0.4$), which means that the efficiency values could have de-creased as this solidity could be outside the optimum range of values. Also, flow curvature could have affected the turbine operation, performing different relative velocities along the blade profile which are detrimental to the generation of hydrodynamical forces.

Part VI

Influence of blade roughness on the turbine performance

19. Introduction

This part of thesis reports the findings of a study of the influence of blade roughness on the performance of a VATT. Due to their design, vertical axis turbines undergo periods of stall, i.e. flow separation from the blade, over each revolution. It is hypothesised that roughening turbine blades delays flow separation (in analogy to bluff body flows) and hence reduces turbine stall with the goal of increasing turbine performance. Laboratory experiments were undertaken with rotors comprising of smooth and rough blades. Three different values of surface roughness were tested, with the results showing a significant reduction in performance when using rougher blades at high approach flow speeds. The combined effect of both the blade roughness and the rotor solidity and both the blade roughness and the number of rotor blades were also analysed to determine their influence on the performance of vertical axis turbines.

As discussed previously, one important aspect in the design of VATTs is the choice of blade shape and its lift-to-drag-ratio. Generally, for any lift-driven turbine, the greater this ratio, the better the performance of the turbine. Acknowledging this, the influence of surface roughness on the lift-to-drag ratio of an aerofoil was analysed as an additional factor by some researchers [224], [225] who concluded that smooth-surface blades cause greater lift and less drag compared with rough-surface blades. Nevertheless, the results must be used carefully because these studies did not consider the influence of rotation.

Roughness for vertical axis wind turbines was analysed in [226]. In this work, experiments with low Reynold numbers showed better results for rougher

rotors, whereas once a critical Reynolds number was reached, smooth-bladed rotors outperformed rough-bladed designs. Similar results were achieved by [227], in this case for a horizontal axis tidal turbine. Experimental testing was carried out in this piece of work, performing smooth-bladed rotors better than rough-bladed for high Reynolds numbers.

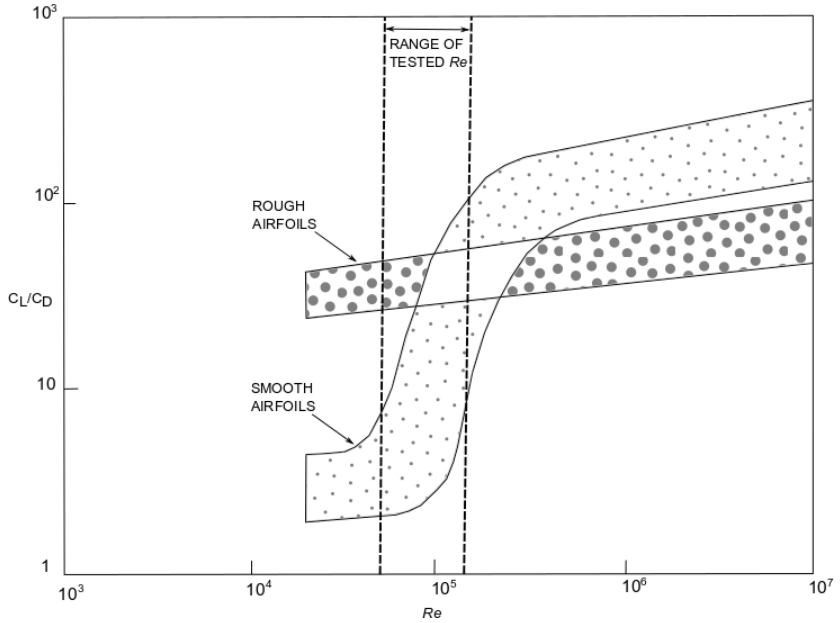

Figure 83: Sketch of the ratio of the lift/drag coefficient ratio versus Reynolds number. Source [178]

[226] explains the results as a matter of balance between skin friction and form drag. For low Reynolds numbers, the increase on "form drag" could have a larger effect than drag from skin friction. Once a certain Reynolds number is reached, the extra drag added by rough surfaces becomes more relevant in the blade hydrodynamics, which would lead into a substantial drop on the total drag. [178] analysed in depth the behaviour for the aerofoils for low Reynolds numbers and the influence of the Reynolds number in the increase of the separation resistance of the turbulent boundary layer is depicted in figure 83

On the other hand, [228] confirmed that, at high Reynolds numbers, a

rougher surface of an obstacle favours the attachment of the fluid to the surface and, therefore, reduces the size of the shed vortex. Also, [204] and [229] show that the interaction between vortex and blade over its rotation. The effect of this interaction could be diminished if the successive generation of flow separation is reduced by roughening the blades. This scenario is sketched in figure 84.

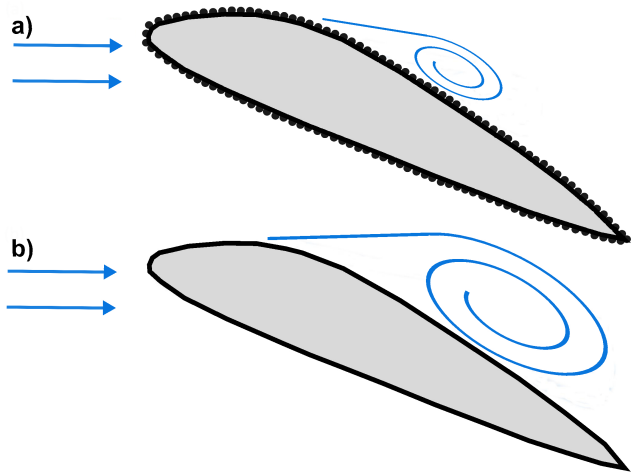

Figure 84: Flow over hydrofoil at a high angle of attack: a) rough blade; b) smooth blade

20. Roughness and rotor characteristics

In this study of the roughness, blades were made from two different materials, polyethylen plastic (Material A) and polyamide thermoplastic (Material C). The blades of Material A where trimmed and shaped from a chunk of material in a mechanical workshop at Cardiff University. The blades of Material C were manufactured by a rapid prototyping procedure known as laser sintering and they came out rather rough due to the manufacturing process. After testing the blades made of Material C, they were sanded and painted in order to reduce their surface roughness which yielded an intermediate roughness and this material is denoted Material B.

Quantity	Variable	A	B	C
Average height	R_a [μm]	0.9	5.5	19.3
Minimum height	R_v [μm]	4.8	25.7	78.1
Maximum height	R_t [μm]	11.7	46.0	138.5
Average maximum height	R_z [μm]	8.4	36.9	133.1
Root mean square height	R_q [μm]	1.2	7.4	24.0
Kurtosis	R_{ku} [μm]	4.5	4.9	2.9
Skewness	R_{sk} [μm]	-0.5	-1.75	-0.2

Table 24: Roughness statistics of Materials A, B and C

The blade roughness was measured with a surface profiler measured at half way point in the chord direction, direction where lift and drag forces are generated . The instrument (Talysurf Series 2 - Taylor Hobson, [230]) consists of a contact-less gauge with namometric precision. The measurement data were analysed by the instrument's accompanying software to obtain the roughness statistics of each surface. An example of surface roughness data and software output for Material A is presented in Fig. 85. This sample shows the corresponding surface profile for the smoothest material, and the software is also able to provide on its own the main features of the surface. The outputs of the roughness measurements and analysis of the three blades are summarized in Table 24.

In order to characterize the blades' hydrodynamic performance it is necessary to convert absolute roughness heights of the blade into the relative (or sandpaper) roughness k_s, with the goal of classifying the roughness following Nikuradse [231]. As Bons acknowledges [232], conversion from absolute roughness values to a sandpaper roughness roughness is not trivial. Bons [232] provides an excellent literature review of how absolute roughness is converted into a k_s value. For the three materials used in this study, converted k_s values are provided in Table 25. They are obtained as an average of 17 proposed conversions which are given in Table 26.

A hydrodynamic appreciation of blade roughness is obtained from the rough-

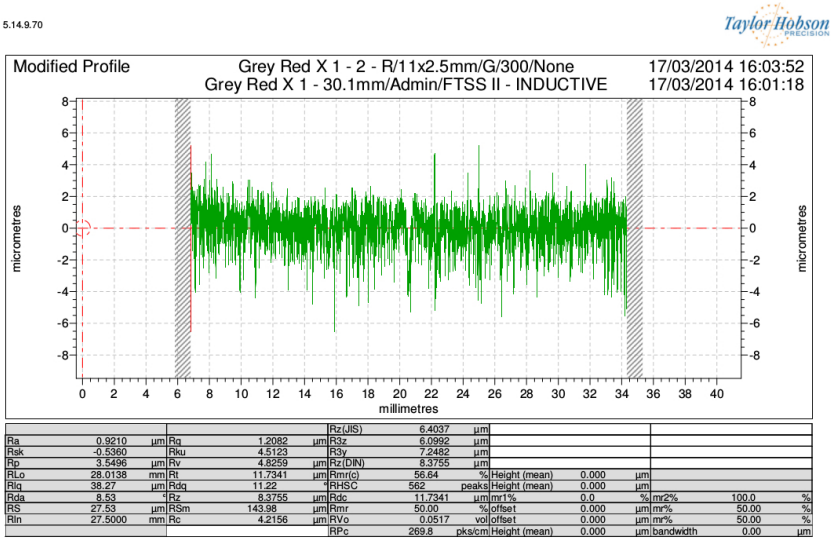

Figure 85: Software output from Taylor Hobson's Talysurf 2. Spatial distribution of the blade surface elevations and statistical data

Table 25: Relative roughness Reynolds numbers

Material	k_s	Re_*(0.72 m/s)	Re_*(0.98 m/s)	Re_*(1.15 m/s)
A	6.6	1.1	1.5	1.7
B	36.4	6.3	8.2	9.2
C	125.3	21.8	28.2	31.6

ness Reynolds number (Re_*), which is calculated as Equation 34 displays, where the friction velocity, u_* is estimated conservatively to be 10% of the relative velocity w, which is computed from equation 12 for the onset of stall, i.e. $\theta = 60^o$ and for $\lambda = 2.0$ which, on average, corresponds to peak power extraction. In this study, three different approach flow speeds were considered, i.e. U_0=0.72, 0.98, 1.15 m/s and, therefore, the blades of the different materials were subjected to a range of roughness Reynolds numbers. Minimum and maximum values of Re_* for each material and for each of the three approach flow velocities are provided in Table 25. The blades made of Material A are hydrodynamically smooth (i.e. $Re_* < 3$), and the ones made from Materials B and C are considered to be in the transitional range (i.e. $3 < Re_* < 100$). Blades made of Material C however

Author	Formulae	Mat A	Mat B	Mat C
Speidel - 1962	Rz/5	1.68	7.38	26.61
Forster - 1967	Rz/2.56	3.27	14.42	51.98
Forster - 1967	2Ra	1.84	11.08	38.64
Forster - 1967	7Ra	6.44	38.78	135.24
Koch and Smith - 1976	6Ra	5.52	33.24	115.92
Bammert and Sandstede - 1976	$2.2Ra^{0.88}$	2.04	9.92	29.79
Schaffler - 1980	8.9Ra	8.19	49.31	171.95
Barlow and Kim - 1997	16Ra	14.72	88.64	309.12
Hoffs et al. - 1996	Rz	8.38	36.92	133.06
Guo et al. - 1998	Rz	8.38	36.92	133.06
Bogard et al. - 1998	4Ra	3.68	22.16	77.28
Boyle et al. - 2001	2.1Rq	2.54	15.46	50.34
Boyle and Senyitko - 2003	4.8Rq	5.81	35.33	115.06
Bunker - 2003	10Ra	9.20	55.40	193.20
Shabbir and Turner - 2004	8.9Ra	8.19	49.31	171.95
Zhang and Ligrani - 2004	1.9Ra	15.92	70.15	252.81
Hummel et al. - 2005	5.2Ra	4.78	28.81	100.46
Average		**6.6**	**36.4**	**125.3**

Table 26: Roughness statistics

are appreciably rougher than blades made of Materials A and B.

$$Re_* = \frac{k_s u_*}{\nu} \tag{34}$$

The turbine itself was 0.30 m in height, had a radius of 0.2 m and had an aspect ratio (height divided by diameter) of 0.75. A disc of 4 mm in thickness connected the blades to the shaft. The blades were shaped according to the Eppler 715 - 100% thickness and the set of experiments involved tests with three chord lengths and three flow speeds. Therefore, up to nine different Reynolds chord numbers were put to test, from $5.8{\cdot}10^4$ to $1.{*}{\cdot}10^5$. Froude number had values from 0.35 to 0.52, showing that the tests were undertaken under subcritical flow conditions. The influence of blade roughness was examined for three approach flow velocities, U_0=0.72, 0.98, 1.15 m/s, and for different turbine solidities, $\sigma = nb{\cdot}c/(\pi D)$, achieved by using blades of different chord lengths (c=8,

10, 12 cm). Finally the significance of the number of blades on the performance was also tested (nb=2, 3 or 4).

21. Results and discussion

The first set of tests used rotors comprising three blades of 8 cm chord length (σ=0.19) and made of materials A, B and C, respectively. Their performance was evaluated for three approach flow velocities, i.e. U_0= 0.72, 0.98 and 1.15 m/s, respectively. The turbine characteristics curves which are presented in Figure 86 show that at the lowest flow speed the effect of roughness is fairly small, as all three curves appear to collapse. Nevertheless, the low Reynolds number causes might prompt the fact that the turbine performance is quite poor (C_p<20%). At high flow speed the turbines with blades made of materials A and B behave similarly, reaching peak efficiencies of C_p=30%, and both clearly outperform the turbine with the rough blades. The latter only reaches $C_p \approx$20%, which is approximately 30% less than turbines featuring smoother blades. It seems clear that the value of Re_* becomes more relevant for high flow speeds.

Further tests were performed considering rotors that comprise three blades with varying chord length, i.e. 8, 10 and 12 cm, which yielded turbine solidities of σ = 0.19, 0.24 and 0.29, respectively, with the goal of studying the combined effect of blade roughness and turbine solidity. Figures 87 and 88 present turbine characteristics curves for the low approach and high approach flow speed and for blades made of Materials B and C. As before, the influence of blade roughness is negligibly small for the lowest approach flow velocity, and the testing reflects the significant effect of solidity. The turbine with the smallest blades performs worst with $C_{p,\max} \approx$ 18%, whereas turbines with larger blades and higher solidity achieve $C_{p,\max} \approx$ 24-26%. The rotor with c=10 cm blades performs best for this low flow speed.

Blade roughness affects turbine performance negatively, as can be seen by

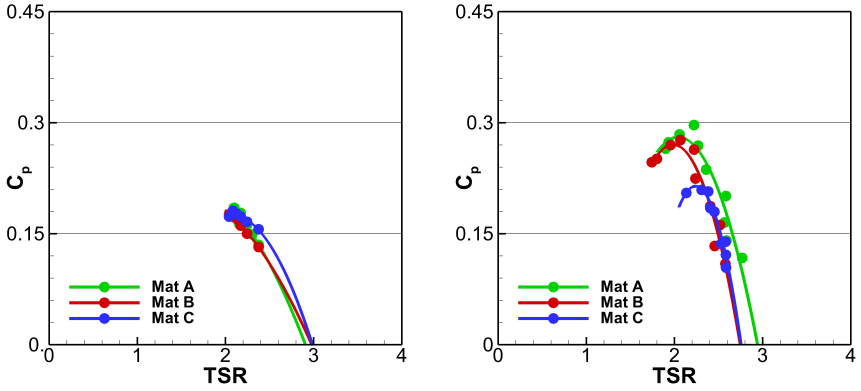

(a) $U_0 = 0.72$ m/s (b) $U_0 = 0.98$ m/s

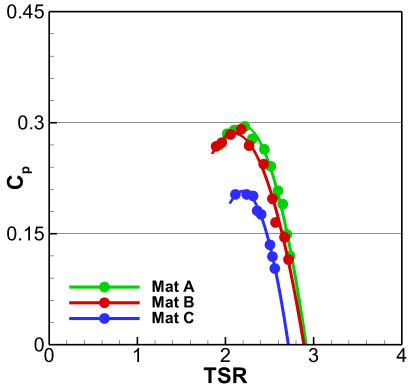

(c) $U_0 = 1.15$ m/s

Figure 86: Turbine performance curves of rotors comprising blades of different materials and for three different flow rates. Three-bladed rotor, σ=0.19.

comparing $C_{p,\max}$ values of the two rotors. The rotor with the highest solidity (c=12 cm) performs best for 1.15 m/s, and the performance gain due to using smoother blades is approximately 10% of the relative efficiency. The low solidity rotor spins faster (i.e. it operates at higher λ) and thus the difference in performance between smooth bladed rotors and rough bladed rotors is more substantial; rotors with smooth blades perform approx. 30% better than rotors with rough blades.

Turbine rotors with two, three and four blade configurations (c=10 cm and σ=0.16, σ=0.24, σ=0.32), were tested with the aim of establishing the ad-

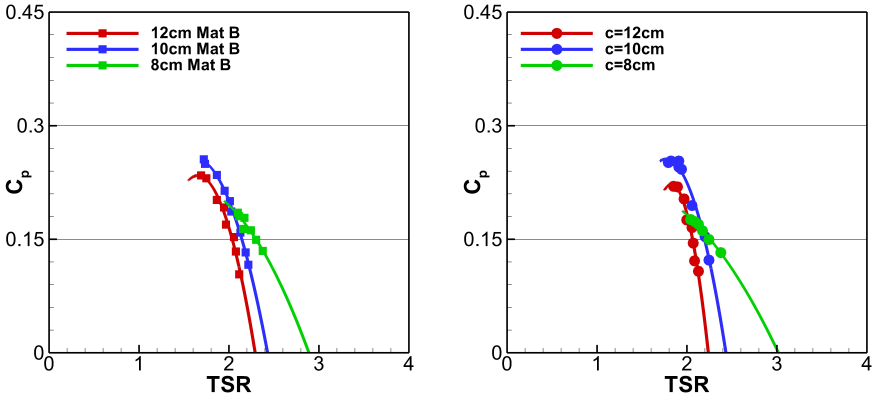

(a) Material B (b) Material C

Figure 87: Turbine performance curves of rotors comprising blades of different materials and different chord length at U_0= 0.72 m/s. Three-bladed rotor.

ditional influence of number of blades on turbine performance. These three different setups each have their own advantages and drawbacks as seen in the previous chapter. As Figure 89 shows, four-bladed turbines perform worse than three-bladed turbines, which perform worse than two-bladed turbines. As before, the turbines with smoother blades (Material B) perform better than the ones featuring rougher blades (Material C), most notably at higher speeds, and there the gain in performance is approximately 27% for two-bladed rotors, 33% for three-bladed rotors and 36% for the four-bladed rotor, i.e. the more blades the more influential is blade roughness. Although the results are linked to the influence of the number of blades, this is not completely precise. In this case, the effect of roughness in the turbine performance is influenced by a combination between number of blades, solidity and Reynolds number. Thus, results must be analysed carefully, as rotors with different number of blades but same solidity values have not been tested.

The observations and findings made with the help of Figures 86 to 88 suggest that the increase in friction drag due to surface roughness cannot be compensated by delay in flow separation (onset of stall) as was hypothesised above.

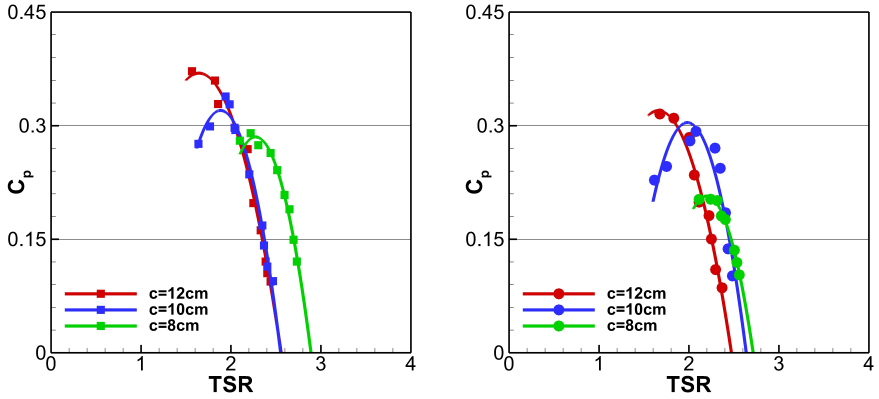

(a) Material B (b) Material C

Figure 88: Turbine performance curves of rotors comprising blades of different materials and different chord lengths at U_0= 1.15 m/s. Three-bladed rotor.

Even though the results obtained from the experiments have been plotted with the approach flow speed as main variable, an analysis of power curves versus Reynolds numbers was carried out. This study might explain more precisely the impact of effect of blade roughness. Figure 90 shows that roughness has barely no influence for low Reynolds numbers, whereas at high Reynolds numbers there is a drop in the performance for rough-bladed rotors. These results are consequent with the physics [178]. Experiments undertaken for vertical axis wind turbine [226] and horizontal axis tidal turbine [227] follow the behaviour of the lift to drag ratio described in figure 83.

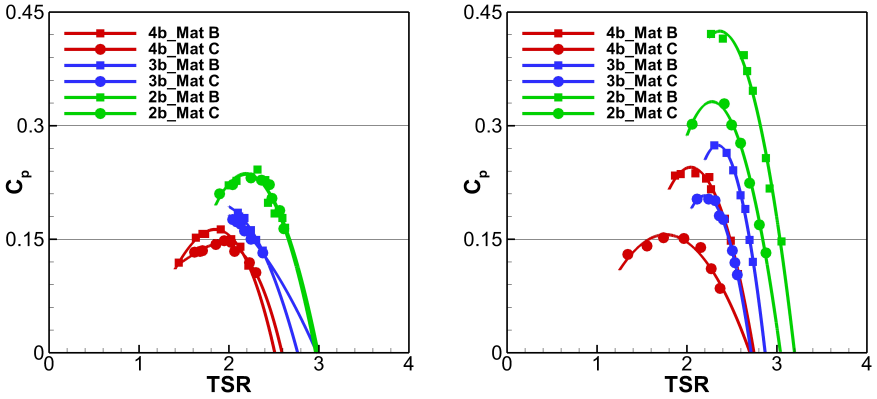

(a) $U_0 = 0.72$ m/s (b) $U_0 = 1.15$ m/s

Figure 89: Turbine performance curves of two-, three- and four-bladed rotors comprising blades of different materials at two flow speeds. c=10 cm.

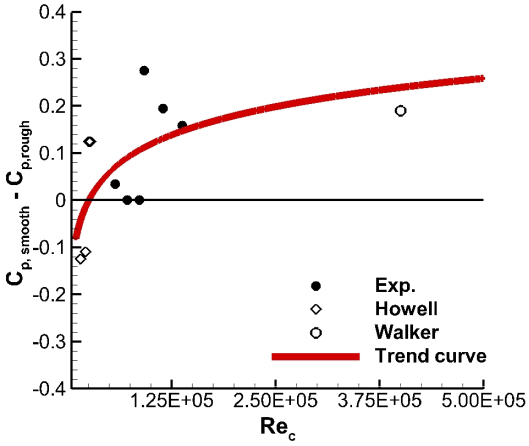

Figure 90: Comparison between results experiments carried out for this thesis, [226] and [227]

A parametric analysis of the results show that the critical Reynolds chord number number from which rough blades start performing worse than smooth blades is within the range $[8 \cdot 10^4 - 9 \cdot 10^4]$, quite close to $7 \cdot 10^4$, value considered in [178]. Besides, roughness Reynolds number using sandpaper roughness (k_s) was found as a good approach in order to enlighten the phenomena. Hence, around $Re_* > 25$ appeared to be the critical value where smooth-bladed rotor

provided a more efficient extraction of the kinetic power.

Part VII

Wake characteristics at maximum efficiency

22. Introduction

This chapter of the thesis is focused on providing new data sets of wake velocities and water elevations for a cross-flow tidal turbine. In addition to these measurements undertaken at the Hydraulics lab in Cardiff University, a complete comparison with the data found in the literature for horizontal axis tidal turbines has been evaluated, with the aim of shedding some light to the complex hydrodynamics that are involved in the physics around a vertical axis hydrokinetic turbine.

The interaction between the coastal environment and tidal power converters must also be taken into account in order to precisely calculate the dimensions of the turbine structure. In this study [233], the wave-current interaction with horizontal axis turbines has been analysed for horizontal axis tidal turbines, and this has been confirmed to have a significant effect on the performance, depending on different factors like flow velocity, wave intensity or distance between the top of the rotor and the water surface.

As the main tidal devices are based on horizontal axis rotors, research that has addressed the study of the wake of tidal stream turbines focused mainly on these specific rotors. Several articles of research that have studied wake characteristics with computational models can be found in the literature. These works [218] and [234] have analysed the performance of these devices in a blocked channel and the resulting flow velocities field, running numerical simulations which use RANS as its turbulence model. Comparable studies have been performed using LES, taken using the disc actuator theory [235] or a complete rotor

composition [236].

Experimental research has also been carried out in order to measure the flow velocity field. [237] and [238] studied the wake characteristics for different horizontal axis rotors using an Acoustic Doppler Velocimeter (ADV), and [239] was capable of analysing the wake interactions between tidal turbines set in the same streamwise cross-section. This instrument enabled the measurement of the three velocity components in downstream positions and also evaluated the influence of the turbulence intensity. Another item of equipment named the Laser Doppler Velocimeter (LDV) has been used by [240], providing good visual data thanks to the utilization of a radial measurement mesh.

Not many research works quantified the variations in the water level for tidal turbines. [234] provided water surface data on their simulations which agree to some extent with the experimental results from [241]. In this study, the difference of water levels upstream and downstream of the turbine location has been measured in the streamwise centreline using a drop depth gauge. In addition to the previous data about wake velocities and water depth, [242] quantifies the influence that the turbine degree of submergence has on the performance. These findings are valuable in terms of calculating the dimensions of a full-scale turbine according to environmental and geometrical site conditions.

The measurements of wake characteristics that are presented in this research work should be evaluated according to the level of constriction that an obstacle (a turbine in this case) produces in the flume. The acceleration on the flow that an obstacle creates in a constrained channel has been analysed, not only for a tidal turbine but also for different kind of obstacles [243]. Thus, this section of the thesis includes the calculations of the drop on the water surface that arises in downstream positions because of the effect of the flume blockage previously analysed.

23. Experimental set up

Experimental research was undertaken in the Hydraulics laboratory in order to understand the hydrodynamics associated to the wake of a vertical axis hydrokinetic turbine. Flow velocities were measured up to 10 D of distance downstream using a Velocimeter, the water surface was monitored using wave probes, and a comparison between wakes originating from a horizontal axis turbine (from other research studies) and the wake derived from the vertical axis turbine here described was elaborated. The experiments were carried out at an operational point very close to the maximum efficiency that the turbine is able to provide in these precise facilities.

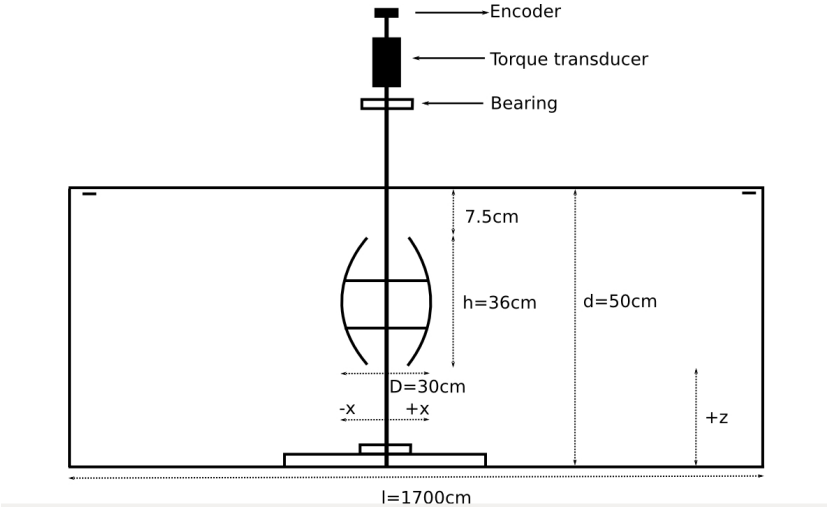

Figure 91: Sketch of the laboratory set up, main dimensions and reference points

The laboratory system is the same as for the rotor parameters experiments and consisted of a mechanical brake which adds resistance to the turbine motion, a contactless torque transducer which measures the extracted torque, and a rotary encoder in order to measure the rotational speed. Figure 91 shows the main dimensions that are required to define the rotor's position according to our coordinate axes.

Flow velocities were measured for a mean flow speed of 0.98 m/s. This velocity gives a Reynolds number of $5 \cdot 10^5$ when water depth is the main magnitude, whereas it is $\approx 1 \cdot 10^5$ when chord length is considered as the main dimension. The Reynolds number plays a key role as some studies detected that low Reynolds values do not favour the appearance of high lift-to-drag ratios. As a result, power coefficients are not as high as they could be in faster waters as seen in the preceding sections. However, this velocity seems to be within the range of Reynolds numbers where the turbine hydrodynamic forces are completely developed. The instrument used for flow speed measurements was an Accoustic Doppler Velocimeter, using a sampling frequency of 25 Hz and a sampling time of 30s period for every point. Figure 92depicts the mesh of points where the velocity was measured.

Flow velocities were measured for a mean flow speed of 0.98 m/s. This velocity gives a Reynolds number of $5 \cdot 10^5$ when water depth is the main magnitude, whereas $\approx 1 \cdot 10^5$ when chord length is considered as the main dimension. The Reynolds number plays a key role as some studies detected that low Reynolds values do not favour the appearance of high lift-to-drag ratios. As a result, power coefficients are not as high as they could be in faster waters as seen in the preceding sections. However, this velocity seems to be within the range of Reynolds numbers were the turbine hydrodynamic forces are completely developed. The instrument used for flow speed measurements was an Accoustic Doppler Velocimeter, using a sampling frequency of 25 Hz and a sampling time of 30 s period for every point. 92 depicts the mesh of points where the velocity was measured.

Water elevations were extracted for the same flow speed. In every location of the flume, the Froude number stood always below 0.75, which means that the flow has not reached supercritical values. This fact implies that inertia forces prevail when compared to the gravitational forces, and no hydraulic jump occurs. Two wave probes were utilised in order to measure water elevations (figure 93).

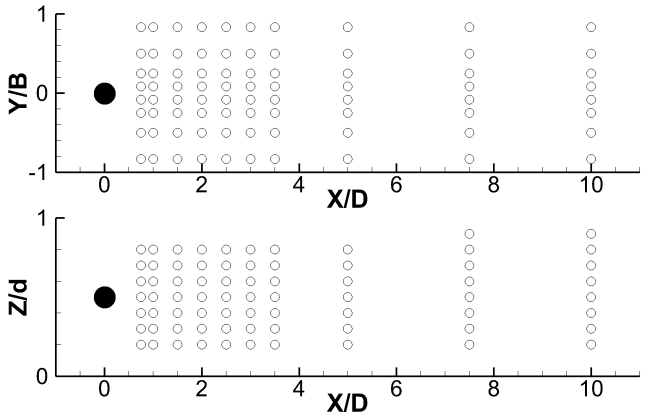

Figure 92: Mesh of points for the flow velocities measurements

Experiments were run with a sample frequency of 20 Hz and every position was recorded for a 30 s period. Probes were calibrated every day, as the increased rate of the water conductivity changes 2% per 1° approximately. Two probes enabled the extraction of around double the amount of data that was extracted on the water velocities tests for the same amount of time. The water level measurements were more focused on the near-wake, with the aim of recording as accurately as possible the step originated on the wake. Therefore, the density of measurement points was weighted from near to far-wake, as shown in figure 94.

Tests were based on a three-bladed rotor; aiming to have a balance between high performance, even load curves and turbine self-starting, with blades featuring a twist angle of 30° . The blade shape used was NACA 4415 at an optimum pitch angle of +5° . This set up has been tested previously and in other research, presenting good blade efficiency values [187]. Solidity is a parameter with a significant influence on the turbine performance. This parameter can be understood as the ratio between the length of the rotation circumference which is occupied by blades. Thus, the turbine's solidity is 0.29, trying to follow on from previous studies using these facilities and also moving within the range of most efficient values that different studies featured in their research work.

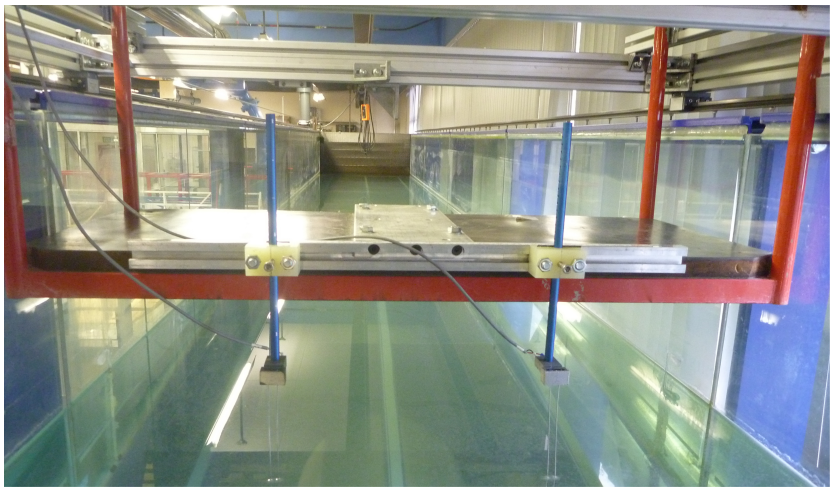

Figure 93: Wave probes disposition in the Hydraulics flume

Power curves according to the pitch angle and the performance of this rotor area are defined in greater depth in the following section, as this blade shape was chosen for the intermediate tests.

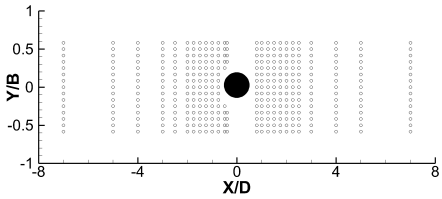

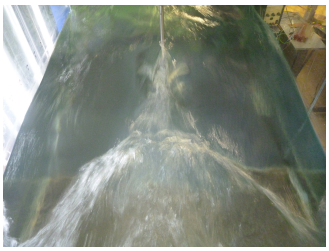

Figure 94: Left: Mesh of points for the water surface measurements. Right: Picture of the wake surface downstream.

24. Results

Adopting an approach flow speed of 0.98 m/s, the rotor previously described was tested in order to record in detail the flow velocity field and the elevations of the water surface. In order to obtain quality data that represents the hydro-

dynamics linked to the turbine operation in authentic conditions, the rotor was spinning close to the maximum efficiency, i.e., near the peak of the efficiency curve from figure 95, λ=1.91, C_p=38 %. The precise maximum efficiency was difficult to be kept in operation for a long period of time, therefore the selection of the operational point was not a straight-forward issue. The combination of a set up that added some irregular friction to the turbine rotation and the high levels of turbulence intensity provided a non-steady turbine motion. However, the experiments were carried out just 1% away from the peak efficiency value. Therefore, a safety factor was somehow applied, a practice that is also common for full-scale turbines.

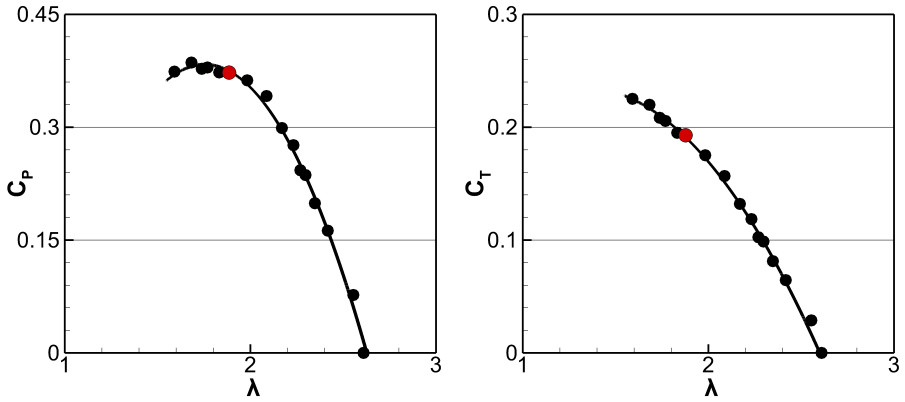

Figure 95: Left: Power coefficient curve. Right: Torque coefficient curve. Red dot, fixed point for wake measurements. Approach flow speed = 0.98 m/s

24.1. Flow velocity field

The mesh of points where flow velocities have been measured was fine and acceptable enough as to provide a reliable interpolation of the velocities in the three dimensions of the space. The Inverse-Distance Weighting interpolation (IDW) was chosen, selecting eight as the number of power parameter points.

Plots for the mean streamwise velocity (U_m) at z/d = 0.25, 0.5, 0.75 are displayed in Figure 96. The influence of the turbine as an obstacle can be

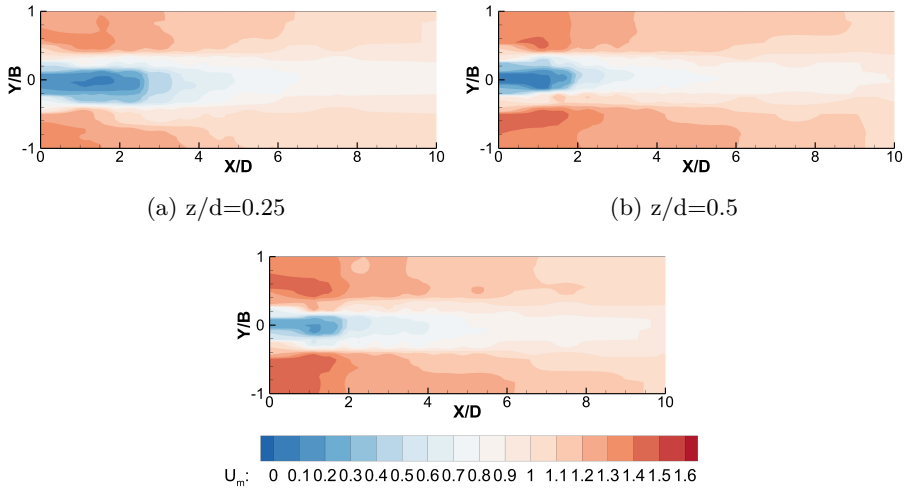

(a) z/d=0.25

(b) z/d=0.5

(c) z/d=0.75

Figure 96: Visualization of the downstream stream-wise velocities

observed, with an increase on the velocities on the flume sides (y/B < -0.4, y/B > 0.4) and a loss on the flow speed values near the centreline of the flume. The velocity values for z/d = 0.25 differ substantially compared to the velocity field at half the height of the turbine than the same comparison taking into account the velocities for z/d = 0.75. This divergence could be due to the presence of the water surface near the top of the turbine blades. The counter clockwise rotation of the turbine does not seem to have a great impact on this component of the velocity, as just a slight asymmetry on the flow acceleration that is generated on the sides was recorded.

Opposed to the data gathered from the mean streamwise velocities, mean spanwise velocity (V_m) and mean vertical velocity (W_m) expose better the effect of the turbine rotation (figure 97). The distribution of the spanwise velocities follows almost identical patterns, delivering positive velocities for y/B < 0 and

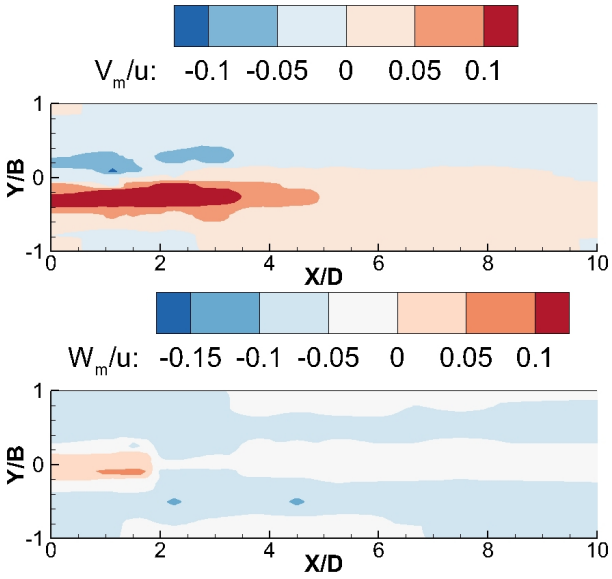

Figure 97: Left: Spanwise velocity distribution for z/d=0.5. Right: Vertical velocity distribution

negative velocities for y/B>0. The counter clockwise rotation produces higher velocity values in the y-direction in y/B $<$ 0 than in y/B>0 , but this quantitative divergence does not impede the evaluation that the contour V_m/u = 0 is quite coincident with the plane corresponding to y/B = 0.

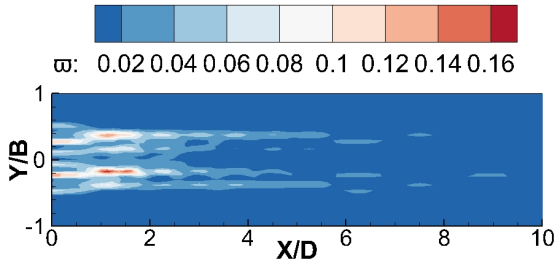

Figure 98: Vorticity distribution, z/d = 0.5

The vertical velocity W_m exhibited two distinct sectors depending on the y/B value and the distance on the y-direction. Thus, positive vertical velocities can be recognised on the wake in the region -0.4 $<$ y/B $<$ 0.4 between 1.5 D and 2 D, whereas negative vertical velocities are generated in the outer regions

between the channel sides and the turbine range of action.

The impact that the turbine rotation creates on the hydrodynamics can be examined in terms of vorticity. Vorticity in the streamwise direction ($\bar{\omega}$) is displayed in Fig. 98, showing clearly that the highest vorticity values are located at y/B = ±0.4, where the limits of the turbine extension are located. In the near wake, the trail of the turbine rotation is perfectly defined. Nevertheless, from x/D = 6 onwards, the vorticity influence is almost non-existent. Vorticity was calculated as Equation 35 displays.

$$\bar{\omega} = \frac{\partial U_m}{\partial y} - \frac{\partial V_m}{\partial x} \tag{35}$$

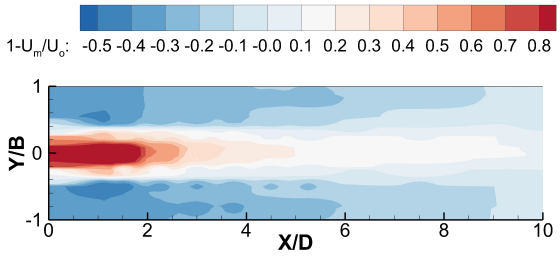

Figure 99: Velocity deficit distribution, Z= half turbine height

The velocity deficit is recognised as the ratio between flow velocity (U_m) and approach flow speed (U_o) compared to 1 and is presented in Fig. 99. This parameter is similar to the streamwise velocity plot as the upstream flow speed is close to 1 m/s. The velocity deficit distribution graph shows that the hydrodynamics are clearly dependent on the turbine geometry and the channel dimensions. Hence, the acceleration of the flow on the turbine sides reaches values up to 50% of the approach flow speed. The velocity deficit graph shows that, 10 diameters away from the turbine on streamwise direction, the recovery of the upstream velocity conditions was not completed. Conversely, velocities close to 0 are observed on the centreline for 1.5 and 2D, values that have certain similarity to other studies that analyse the wake for horizontal axis turbines.

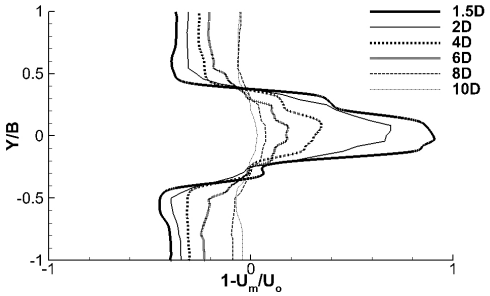

Figure 100: Velocity deficit distribution, z/d = 0.5

A better approach to appreciate the evolution of the velocity deficit is the analysis of the velocities in spanwise cross-sections (Fig. 100). The recovery of the velocity is not fully achieved, as the velocity deficit is not a constant zero at x/D = 10, but the range of velocity deficit values delivered by the measurements for x/D = 10 is within the range ±0.05. There is no evidence in the results to assume that the shape of the curves changes significantly due to the counter clockwise rotation.

24.2. Water surface elevation

A similar methodology to the one carried out for the flow field was adopted for the interpolation of the water surface data, though the number of power parameters points used in this case was four, as every point of the mesh was included in a 2D plane (XY).

The three-dimensional image of the water surface is depicted in Figure 101. A clear difference between water elevation values upstream and downstream is noticed. No remarkable pattern is observed for upstream position, apart from being quiet constantly above the initial water depth. The downstream region is very descriptive, as a step on the wake is perfectly depicted within the range 0.5 < x/D < 2. This V-shape step separates the lowest elevations that the turbine creates from the higher points of the water surface.

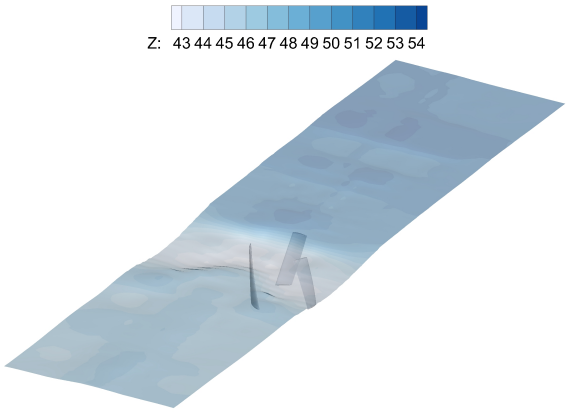

Figure 101: Water surface interpolation

Further away from the turbine action (x/D > 2), the water levels acquire a more uniform distribution in the y-direction. The step generated close on the wake downstream close to the turbine is dissipated, and the highest water levels in any cross-section along the channel are found in the centre of the channel (y/B ≈ 0).

Figure 102 shows in detail the interpretations already described. The lowest values of the water elevations are formed around y/B ≈ 0 and a is the closest distance to the turbine in the x-direction, 0.5 D.

The figure also presents certain periodicity on the water elevation for the upstream sector. In order to dismiss the possibility of obtaining this periodic behaviour due to the turbine operation, the water surface was measured with no rotor installed. The comparison between centreline is included in figure 103. As the water surface curve without any rotor exhibits a wavy shape, with similar wobbles upstream to the curve y/B=0 with a rotor, the assumption of wave generation due to the turbine rotation was dismissed. Thus, the sinuous discrepancies between the water elevations without a rotor and a constant water height of 50 cm are must be bounded to certain frequency that is intrinsic to

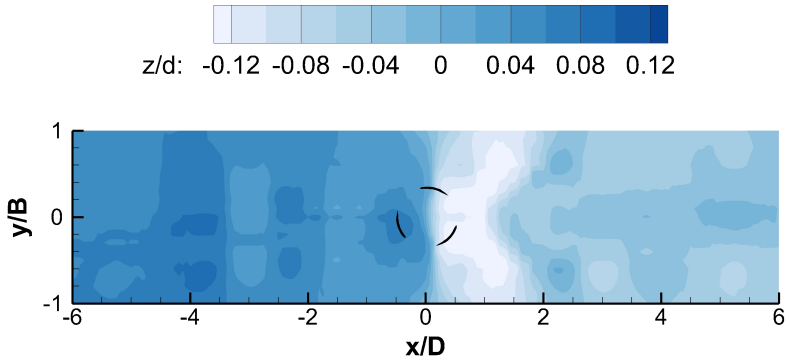

Figure 102: 2D water surface elevation

flume conditions and pump system characteristics.

24.3. Comparison to HATT

With the aim of contrasting our data and examining the differences between wakes from Horizontal Axis Tidal Turbines and Vertical Axis Tidal Turbines, a comparison between studies based on laboratory experiments was elaborated.

Experimental research carried out by [238] showed a flow acceleration on the sides for a similar y/B value, but this increase is just around 20% of the incoming flow. This difference between velocity fields could be explained as a matter of rotor geometry, as horizontal axis rotors comprise less area than vertical axis turbines that feature the same radius. On the other hand, both sets of experiments present similar blockage ratios (β = 18 % in this study, β = 16 % in [238])), therefore the difference between results should not be fully interpreted as an effect of the channel blockage. The turbulence intensity (I) (mean flow velocity over standard deviation) could be a parameter with

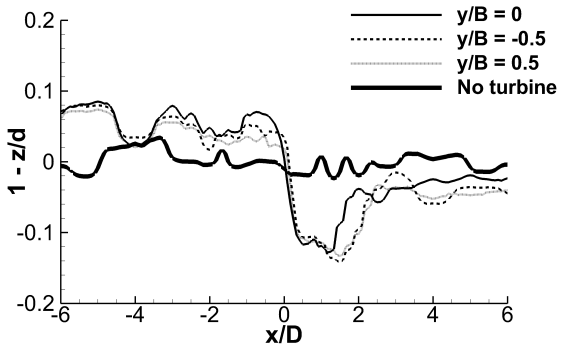

Figure 103: Main curves of the water level distribution along the channel

an influence on the velocity field, and [244] and [245] demonstrated that this parameter has a great impact on the wake evolution. Thus, the compared tests were run for an approximate I = 2% , much lower than the value delivered in the Hydraulics lab, 14%.

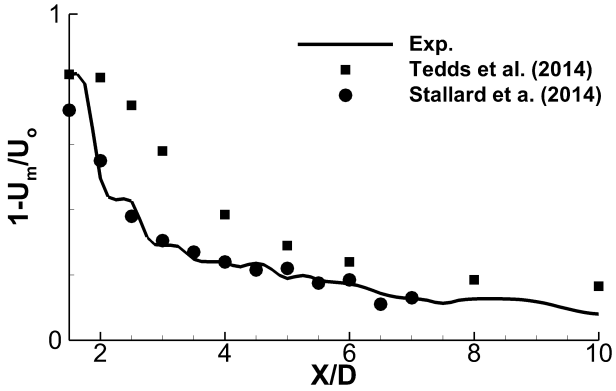

Figure 104: Comparison of mean streamwise velocities between experimental studies of Horizontal Axis Turbines and the presented data. $I = 2\%$ in Tedds, $I \approx 12\%$ in Stallard, $I \approx 14\%$ in the case of study.

Other studies of research that present domains wide enough to dissipate any blockage effect ([239] with experimental testing, [234] based on numerical simulations) do not display those strong accelerations on the turbine sides. ($\beta = 6\%$,

β= 3% , in turn). Figure 104 shows a comparison between velocity deficit curves from the two mentioned experimental studies and the results herein presented. Although similar trends are formed, the deficit near the turbine displayed higher values in the case of the vertical axis tidal turbine than for the other horizontal axis turbines cases. Further away from the rotor, a pronounced decrease on the streamwise velocity arises, and the velocity experiences a recovery that follows a logarithmic curve. When x/D=10, the velocity has reached up to 92% of the approach velocity on the x-direction.

In terms of water surface measurements, [241] presented information of the water levels that their horizontal axis turbine created. The data was measured in the centreline of the flume and for two flow speeds that are much faster than the case of study, 1.8 and 2.35 m/s. Although differences between tests are significant (β = 12%, larger turbine dimensions, and another distance from the top of the blades to the water surface), a similar trend can be noticed. According to the figure 105, higher Reynolds numbers would extend the effect of the turbine rotation on the decrease of the water levels. On the other hand, in spite of performing with a flow speed almost 50% slower compared the 1.8 m/s tests from [241], the lowest normalised value of the water level is almost identical (1-z/d $\approx$ -0.13).

In the upstream region, [241]'s tests showed a quasi-instantaneous recovery, as the results for x/D=1 are already near or even lower than the initial water depth. This fact does not coincide with the measurements from this study, because the initial values of the water surface are not reached even after x/D=6.

In their numerical model based on LES, where a single horizontal axis turbine and different arrays of turbines was simulated, the tests in [246] delivered a similar behaviour on the water surface to the conduct observed in the vertical axis tests. Therefore, the small rise before the turbine rotation and the significant decrease on the water levels downstream from the turbine rotation are also in evidence. In addition to this aspect, the initial water depth was not reached

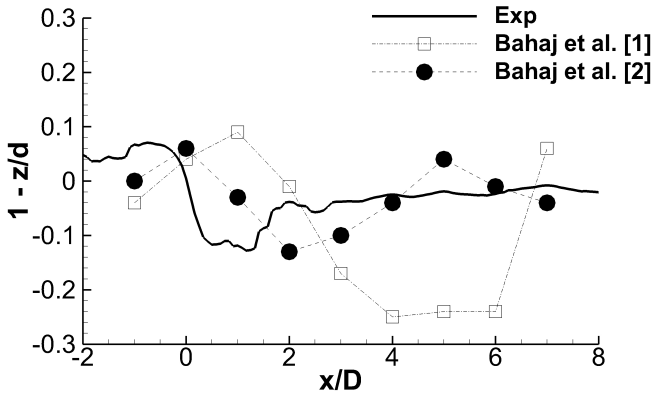

Figure 105: Comparison of the water surface elevations between experimental studies for Horizontal Axis Turbines and the presented data. Bahaj et al. [1], U_0= 1.8 m/s, Bahaj et al. [2], U_0= 2.35 m/s (both data extracted from [241]), Exp, U_0= 1m/s

for the furthest positions of their simulations (x/D=-10 D and x/D=10).

Part VIII

Field testing in a representative environment

Hydrokinetic turbines remain at an early stage of their development, and the main reasons consist of financial constraints and the difficulty of their construction and operation.Thus, arranging the testing of the physical modelling in a naturalistic environment is no simple matter. Aiming to find a reliable source of information, and to find verification of the knowledge gathered from the literature and from previous experiments, an optimized design of a vertical axis tidal turbine was tested in a quasi-natural environment. The whole turbine structure was then manufactured, then tested at a water sports centre, simulating various different scenarios. These facilities provided the chance to test a tidal turbine under very turbulent flows. This was similar to a real environment, but offering the additional advantage of better control over the turbine deployment and monitoring. As a result, it was possible to test the performance of the turbine at different flow speeds and at various degrees of submergence.

Experimental tests of tidal turbines in real world conditions are not commonly displayed in scientific publications, but some studies can be found in the literature. These studies demonstrate the usefulness of such real world data. Projects such as [247], [68], [202] and [180] tested a vertical axis tidal turbine in a natural environment, presenting a wide number of results, which characterize perfectly the performance and behaviour of the turbine. [247] tested a cross-flow turbine with twisted blades. It employed a platform which was piled into the seabed, holding the 3.6 m height rotor in place. The research team in [68] tested their rotors using a towing boat to replicate the effect of a moving flow. They quantified the effect on a diffuser introduced by variations in the pitch angle and on the rotor solidity. [202] tested a Darrieus turbine set 5 m high in the Strait

of Messina, using a floating base and leaving the power take-off system above the water surface. [180] took advantage of a bridge pier to ensure the position of their Darrieus turbine, and tested the efficiency of different blade shapes and pitch angles.

In general, results in an unblocked environment usually appear more scattered, due to the randomness of the environmental conditions. But the information gathered in intermediate scale testing is essential for the final design of a full scale hydrokinetic turbine. The studies introduced here suggest that the efficiency of vertical axis turbines varies between 16% and 39%. Although the range of values is wide, these efficiency rates are fairly high compared to, for instance, Savonius turbines [248].

With the objective of analysing the performance of a rotor design for a vertical tidal turbine, a large series of tests was carried out - first in the facilities at Cardiff University and then in a relevant unblocked environment. Although experiments in the laboratory provided useful knowledge regarding the rotors' performance in fully and partially submerged conditions, the influence of a very turbulent flow and higher flow speeds cannot be ascertained through laboratory testing alone. Thus, we built a whole, scaled-up turbine system, choosing a water sports centre as the venue for testing the prototype.

25. Experimental testing

25.1. Hydraulics Laboratory

As explained earlier in the present work, the laboratory setup is composed of a home-made mechanical brake (to add resistance against the turbine rotation); a frictionless torque transducer, which measures the extracted torque; and a rotary encoder, whose purpose is to measure rotational speed. The whole structure is supported by bearings which are placed on a solid structure above the water and on the flume bed (Fig. 47).

The cross-flow turbine used in these experiments is a three-bladed rotor, with blades featuring a helical twist of 30°. Research findings have confirmed that the fewer blades the higher the efficiency, but a two-bladed rotor is not capable of starting the rotation on its own. Although introducing twist to the rotor's blades leads to lower efficiencies when compared with a straight-bladed rotor, this blade twist provides improvements in terms of such significant properties as a higher rotational speed, more constant torque curve or a better self-starting characteristic.

Previous works concluded that hydrofoils must possess several essential properties if they are adopted for the blade design and, at least, they must display a sufficiently high lift-to-drag ratio. Also, the blade shape should not be tested without taking into account the influence of the pitch angle. In this research project, the blade shape NACA 4415 was selected. Similarly cambered NACA foils have been tested in previous studies. For instance, [187] tested the hydrodynamical force distribution for some NACA cambered and non-cambered shapes, having displayed encouraging blade efficiencies in cambered NACA foils. Analysing the lift and drag coefficients for a fixed Reynolds number obtained from [190], larger ratios of C_L/C_D are found for the NACA 4415, encouraging the adoption of this profile for future testing (Figure 106).

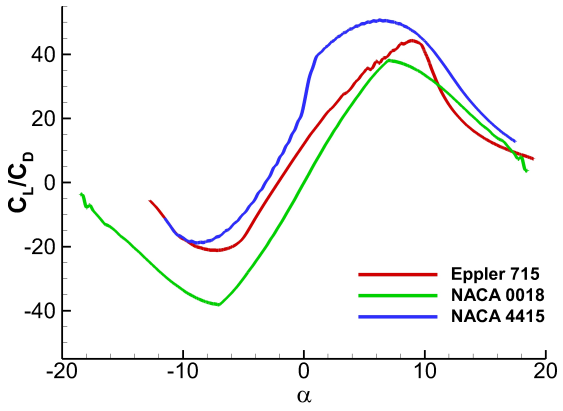

Figure 106: Lift coefficients versus AoA for different $Re = 10^5$

The turbine aspect ratio, i.e. the ratio between the turbine height and turbine diameter, is 1.2. This value tries to strike a good compromise between a high rotational speed and a low blockage ratio. Blockage ratio (β) can be expressed as the ratio between the respective areas of the turbine cross-section (A_r) and the flume cross-section area (A_f). The blockage ratio is 0.18 in this study and, despite this being only a low value, a slight increase on the efficiency due to the blockage effect must not be ignored.

The rotor blades have been tested in the laboratory for various Reynolds numbers and for different degrees of submergence. Altering the distance between the top of the rotor (z) and the water level reference (d = 500 cm), a reliable description of the turbine performance with regards to the degree of the rotor submergence was achieved. The dimensions and main parameters of the laboratory setup can be seen in Fig. 107.

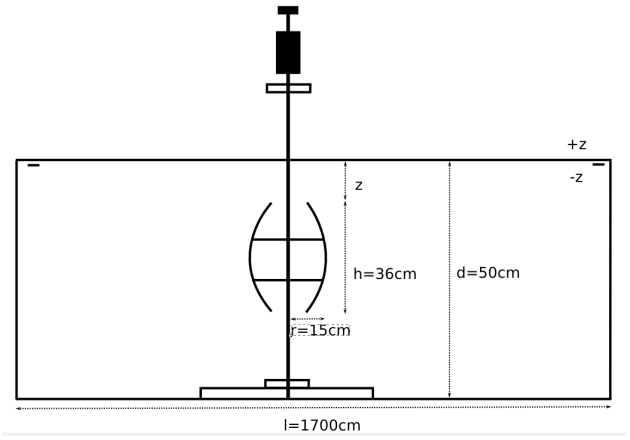

Figure 107: Sketch of the laboratory setup, including the main dimensions of the NACA 4415 rotor.

After the long rack of tests carried out for the present thesis and its corresponding analysing and data post-process, a final and optimized design for our cross-flow turbine based on the rotor just described was accomplished. Although the experiments have showed us the knowledge that our project needed for the initial design: the structural behaviour of the turbine, the influence of a natural environment and how the prototype faces other important issues cannot be found out just with tests in a laboratory.

The White Water Rafting Centre is a water facility located in the International Sports Village, Cardiff, UK. This centre provides a water channel with an approximate width of 10 meters - enough to rule out the existence of any blockage capable of affecting the turbine performance (figure 108).

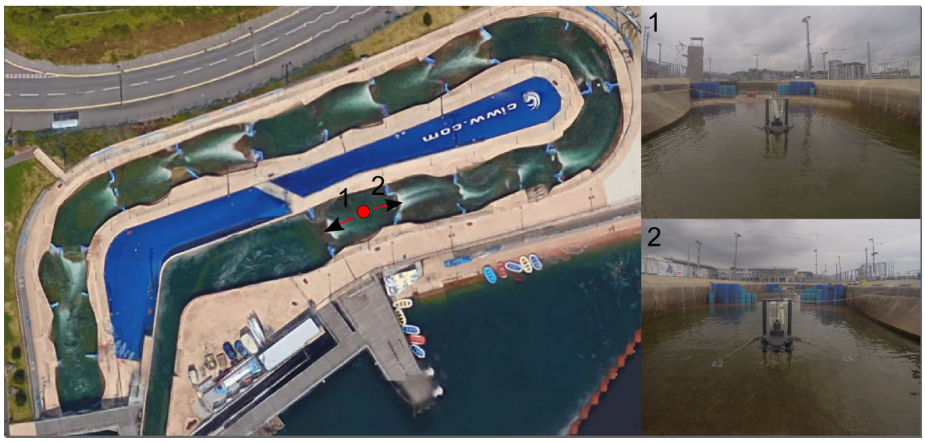

Figure 108: Left: Top view of the White Water Rafting Centre. Top right: Upstream perspective. Top down: Downstream perspective.

The sufficiency of the water's depth was an issue that had to be taken into consideration. In order to achieve the required water depth in the artificial channel, the up and downstream cross-sections were modified. Any change in the cross-section obstacles would display an impact on the channel's hydrodynamics, affecting not just the water height but also the flow speed and position of the recirculation zones.

The flow discharge was capable of being varied from 4 m3/s to 10 m3/s. Consequently, the flow speed could also be easily modified, allowing testing of the turbine performance at different velocities. The flow speed measurements were initially carried out using a flow meter (Valeport Model 002). Pulses were generated with the rotation of the impeller head, and average values for every 10 second period were recorded. As shown in Fig. 4, the turbine rotation could exert a substantial impact on the flow speed measurements - a fact that gave rise to the running of the last channel set up using a velocimeter (Nortek Vectrino) and without the turbine in position. Collecting velocity measurements throughout the three-dimensional space, with a specific frequency of 20 Hz and without the turbine operation, the device allowed us to use the same methodology as that in the laboratory, and to prevent turbine interference exerting an impact on the incoming flow speed.

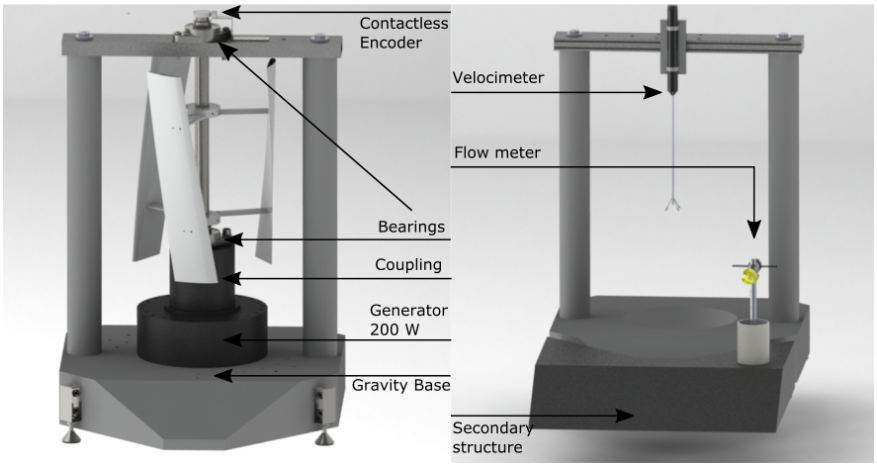

Figure 109: A CAD representation of the turbine tested in the White Water Rafting Centre, and the positioning of the devices for flow speed measurements.

In order to analyse the magnitudes of the power produced, and to achieve precise control over this power, a generator able to transform mechanical energy into electricity and an electrical system was attached to the turbine. Following this idea, a permanent magnet generator (PMG) with a maximum output power

of 200 W was connected to the shaft. Since this generator outputs AC current, the electricity from the PMG is driven into an inverter, changing the current to DC. Once current has been modified by the inverter, it reaches a load bank comprising two variable resistors in series, rated at Ω each. After the resistors, a multimeter (Fluke 123) is placed (A) - for measuring the current and then to measure voltage (V) from the electrical circuit (Figure 110).

So as to measure the rotational speed, a contactless magnetic encoder was placed on top of the shaft (a RLS rotary magnetic encoder LM13). Its analogue signal was transformed by a Labjack U6 and redirected to a laptop, providing data with a frequency of 200 Hz and allowing tracking of the position and rotational speed of the turbine at any moment of the rotation.

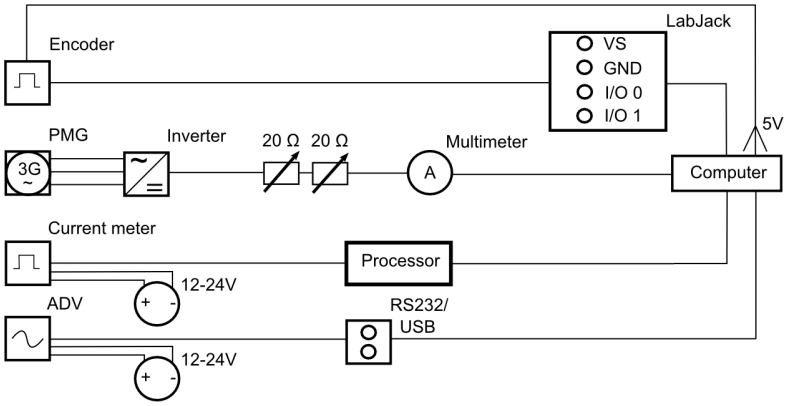

Figure 110: Electromechanical circuit and data acquisition system.

As mentioned previously, the manufactured prototype was based on the design tested at the Hydraulics laboratory. The main components of the design are described in the following points.

1. Support Base. A concrete base was chosen to bear the loads coming from the turbine, adding stability to the structure and protecting the generator with a waterproof case. This support base has an irregular octagonal 3D shape. And, although more material - and therefore resistance - was created in the intended

flow direction, the regularity of the shape provides significant structural support, independently of the resultant forces. The chosen type of concrete is made of light aggregate with steel fibres, aiming for a combination of low weight (so as to deploy the turbine without the need of a crane) and high resistance from the fibres.

2. Rotor. The parameters used in the experimental laboratory testing have been used to scale the rotor up. Hence, NACA 4415 with 30 ° and 5° angle of pitch, blade height of 56 cm, a solidity and aspect ratio maintained at the level of previous experiments: 28% and 1.2 respectively. Chunks of polyamide were shaped at the University's mechanical workshop, resulting in a weight of approximately 1 kg per blade.

3. Generator. A permanent magnet generator (PMG) with a nominal power output of 200 W was attached to the bottom of the turbine. As no gearbox was installed, the mechanical power from the rotor was driven through a coupling directly to the generator, whose optimum rotational speed is 200 rpm. It is possible to achieve such velocities for this turbine size. But, for larger scales, it will be necessary to investigate the utilization of gearboxes or specific generators capable of working with low velocities. All the characteristics of the turbine design are shown in table 27 and drawings that define the device in depth are included in the Appendix (Figure 129).

Table 27: Summary of the turbine's main characteristics.

Gravity Base		**Rotor**		**Generator**	
Max. Dimensions	750x1500x 900 mm	Blade Shape	NACA 4415	Description	Permanent Magnet Generator (PMG)
		Blade Height	560 mm		
Weight	260 Kg	Twist Angle	30°	Output Rate	200 rpm
Density Concrete	1910 kg/m3	Solidity	28.9 %	Max. Efficiency	87 %
Water/Cement	0.59	Weight	3.1 Kg	Starting Torque	0.03 Nm
Steel fibers	0.05 %	Material	Polyamide (Nylon)	Diameter	246 mm
				Height	300 mm
		Diameter	400 mm	Weight	11 Kg

26. Results

26.1. Hydraulics Laboratory

Pitch angle test were carried out applying the same methodology as in the previous section. As a result, power curves for three different angles of pitch were obtained. The NACA 4415 shape displayed an optimum pitch angle for $+5°$ for flow speeds of 1.09 m/s. This value was also confirmed by the torque curves (figure 111). For these tests, the operational range of the turbine was enclosed between $+2.5°$ and $+7.5°$, value enclosed between. These tests were undertaken using discs as a connection between blades and shaft, providing a radius of 20 cm and a height of 30 cm ($\beta = 0.12$).

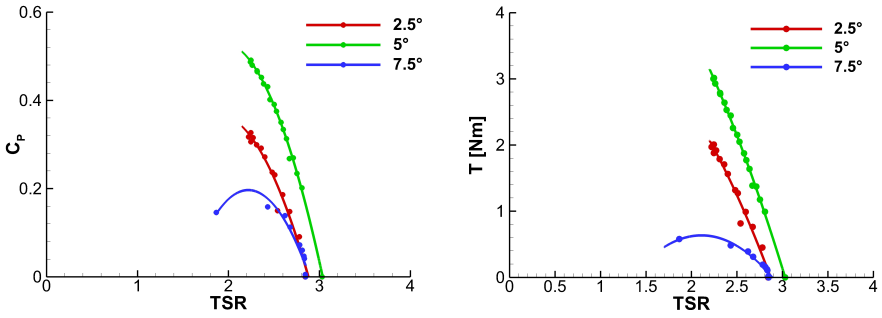

Figure 111: Pitch angle tests for NACA 4415 blade shape.

The influence of the turbine's level of submergence was tested in detail in the laboratory flume, at two different flow speeds: 0.72 m/s and 1.09 m/s. Both experiments display the parametric performance of this particular rotor for fully submerged conditions - which knowledge assists us in quantifying the potential power and torque distribution for future turbine upscaling. However, as Fig. 112 show, there is a substantial contrast between the tests' results in terms of the efficiency they describe. Taking as a reference $z/H = -21\%$ for both curves, the efficiency curve for 0.72 m/s drops not just in terms of efficiency; also the whole curve is shifted, due to the lower values of λ. There are research articles in the literature [177] [178] suggesting that with low Reynolds numbers the lift-

to-drag ratio does not reach optimum values. Hence, the performance of some rotors within the cross-flow turbines range could vary depending on the existing Reynolds number. These low efficiency values agree with other experimental tests, such as [71] or the present study, in which tests the cross-flow rotors did not reach peak efficiencies and quasi-constant efficiency curves up to Reynolds numbers based on the chord length close to $7 \cdot 10^4$ and $9 \cdot 10^4$.

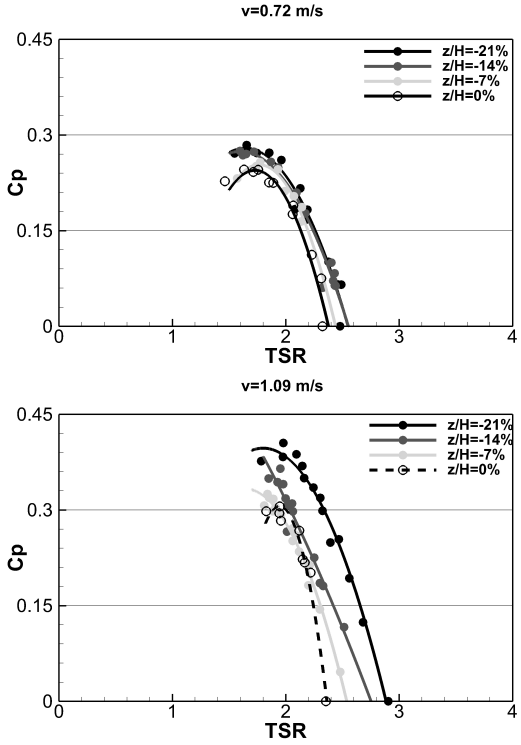

Figure 112: Efficiency curves for the fully submerged rotor. Top: U_0= 0.72 m/s. Bottom: U_0= 1.09 m/s

The behaviour of the turbines for different levels of submergence is distinct. The curves for $z/H = -21\%$ are similar for the lowest flow speed, therefore it can be assumed that the turbine performance starts to drop at $z/H = -7\%$. However, with a flow velocity of 1.09 m/s, the performance already drops substantially at $z/H = -14\%$. These results imply that an overlay distance

between the top of the rotor and water surface must be increased according to the Reynolds number. This has proven to be a technical constraint to take into consideration.

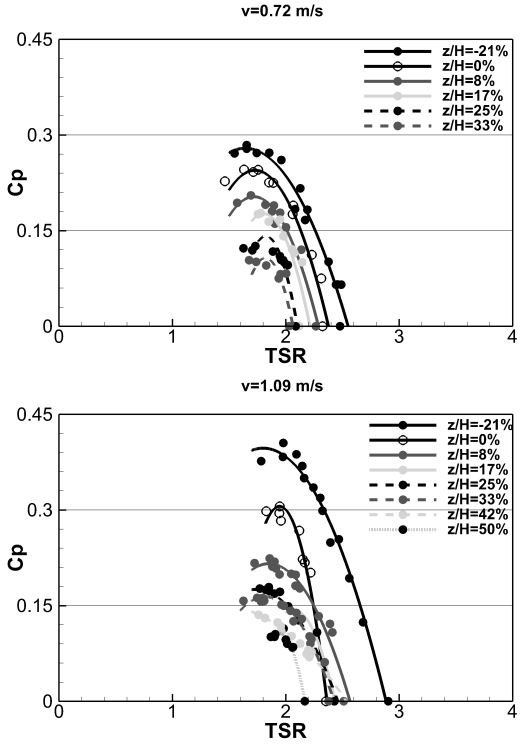

Figure 113: Efficiency curves for the partially submerged rotor. Top: U_0= 0.72 m/s. Bottom: U_0= 1.09 m/s

The rotor also exhibits different operational behaviour when the turbine is partially submerged. Tests for U_0=0.72 m/s indicated that the turbine can operate with up to 33% of the blade height covered by water (z/H = 33%) whereas, when the tests were undertaken with a flow speed of 1.09 m/s, the turbine was able to rotate at up to $z/H = 50\%$ (figure 113).

Certainly, the torque distribution becomes more uneven. But both mean and peak values remain quite low compared to those for a fully submerged device. These results could imply that, whilst the turbine is partially submerged, the

turbine could keep generating some power without reaching the extreme torque values sufficient to damage the structure.

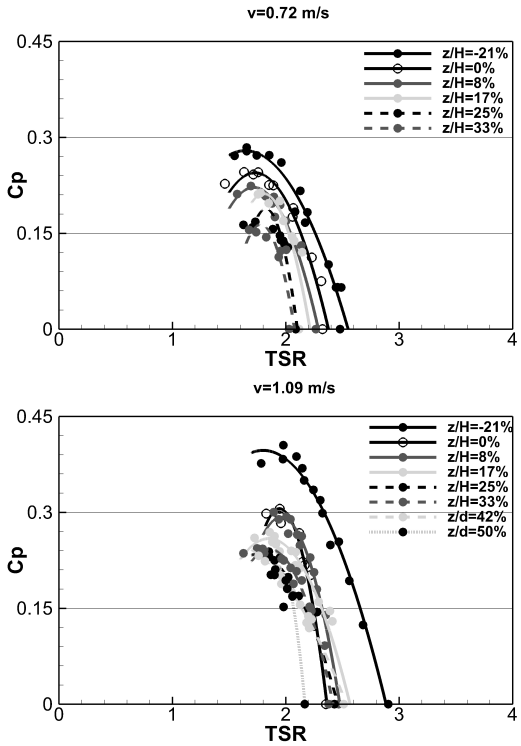

Figure 114: Efficiency curves corrected using A_c for partially submerged rotors. Top: U_0= 0.72 m/s. Bottom: U_0= 1.09 m/s

A corrected efficiency curve is plotted in Fig. 114. It has been considered that A_r is no longer constant in partially submerged turbines, because not the whole of the blade height is immersed. Hence, A_r has been rectified as A_c following (Equation 36).

$$A_c = D \cdot |H - z| = A_r \cdot \frac{|H - z|}{H} \tag{36}$$

The resultant efficiency curves are closer to the $z/H = 0$ curves, but still far from replicating the peak efficiencies. It is remarkable that, in the range

$20\% > z/H > 0\%$ and for the highest speed, the turbine started spinning faster than it had in more immersed scenarios. This positive behaviour was then diminished; after this moment, the turbine setup could not achieve similar peak efficiencies. A possible explanation for this phenomenon could reside in the water depth difference between the upstream and the downstream positions. A lower water depth downstream could perhaps favour faster spinning while low torque values are being generated, because the most beneficial force distribution on the turbine rotation is created in the upstream blade positions [170] [173]. Meanwhile, when torque is produced, those parts of the blades that are not adding any force in the downstream positions could become detrimental to the performance. The differences in the water level can be observed in figure 115. A remarkable decrease can be observed in the water depth downstream and also an increase in the upstream region.

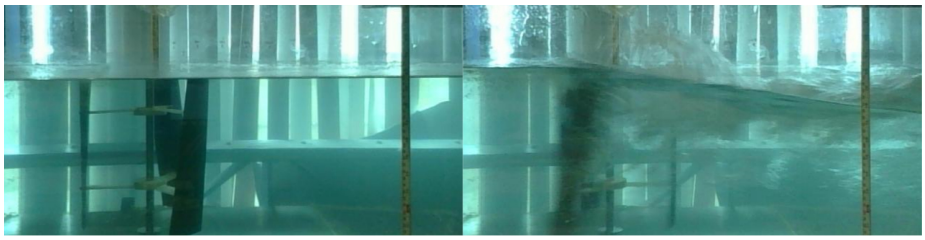

Figure 115: Laboratory pictures for z/H=0. Left: no operation. Right: the Maximum efficiency point for U_0=1.09 m/s, with flow from left to right.

26.2. Field testing

Continuing the turbine prototype development, various tests were undertaken at the White Water Centre with a scaled up rotor and a whole structure holding the device in position. Three tests were completed with the turbine partially submerged, and two tests with a z/H value at least smaller than 0 (water depth values were not measured). Every experiment was based on flow speed measurements carried out using the flow meter, except for the last one - in which the velocimeter was employed. Flow discharges varied from 4 m3/s

to 8 m3/s, and the configuration of the cross-sections up and downstream were transformed in order to change the flow velocity and the water depth.

The first rack of tests was run with a certain degree of uncertainty. Despite the fact that previous calculations testified to the strength of the structure, the real impact of the forces, displacements and vibrations were not found out until the tests were conducted. In terms of self-starting, the turbine started spinning for every single test when the water stream had reached about 1/3 of the blade height (z/H = -66 %). This behaviour supports the identification of this design as one that ensures the self-starting of the rotation - a topic that has been addressed in different research studies [76], [249].

The partially submerged tests displayed curve patterns similar to those observed in the laboratory tests. In these study cases, the turbine was able to spin at z/H values close to 40%, and these low submergence values - which were not performed in previous tests - were likely achieved here because of higher upstream flow speeds. Depending on the area that is chosen for the calculations, the power curves can change drastically. However, an approximation of the effective rotor areas was taken realistically, based on site pictures (figure 116).

The power coefficient curves were consistent, showing similar drops in the efficiency, and verifying the findings from those previous experiments undertaken in the laboratory. The peak values of the efficiency were fairly high, reaching up to 30.5% of the efficiency shown in a TSR close to 1.75. As for the laboratory tests, third order polynomial curves where used for plotting the efficiency curves, not accurately matching the results but instead adding a stable approach to the data. Nonetheless, the data acquired in the above mentioned study are much more detailed than the data acquired from field testing here.

The two tests agreed with the free-spinning value of the tip speed ratio: close to 2.5. It is more difficult to conclude a value for the λ that corresponds to the

C_p curve peak, because this is where the data oscillates the most. However, it can be identified this value as being within the range 1.65-1.85 (figure 117).

Figure 116: Field testing pictures. Top left: U_0=1.40 m/s, z/H ≈-60 %. Top right: U_0=1.28 m/s, z/H ≈-50 %. Bottom left: U_0=1.40 m/s, z/H ≈-10 %. Bottom right: U_0= 1.83 m/s, z/H>0%.

Significant information can be also extracted from the fully submerged efficiency curves, because these curves are very similar. However, as the optimum power rate of the attached generator is 200 rpm, the power extraction system achieved higher efficiencies for U_0=1.83 m/s, because the rotational speed values were closer to the optimum rate. Therefore it can be assumed that efficiency values for U_0=1.35 m/s could be even greater.

Flow speed measurements can be observed in Fig. 118. he first four experiments were based on the readings from the flow meter. Although this instrument provided accurate information in terms of average values, its low frequency did not permit a deep analysis of the flow velocities. Hence, a velocimeter was installed for one of the tests, in order to measure the three velocity components and its fluctuations over time. [250] considers that the turbulence intensity (I), has a substantial influence on the fatigue loads that a tidal turbine has

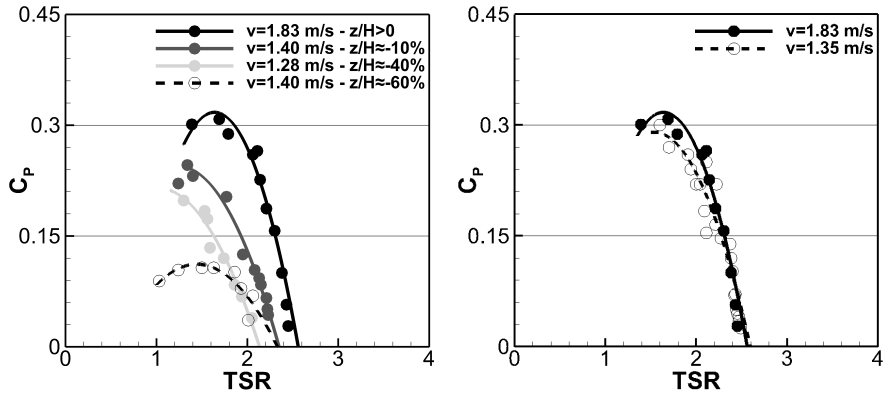

Figure 117: Field testing results. Left: Efficiency curves for different degrees of submergence and the flow meter used for flow velocities. Right: Efficiency curves for z/H>0.

to endure. For our field testing site, I=27% for the mean streamwise velocity. Despite being a fairly high value, [251] describes other natural locations - which showed similar turbulence ratios - and also indicates that the turbulence intensity could be specific to the site characteristics.

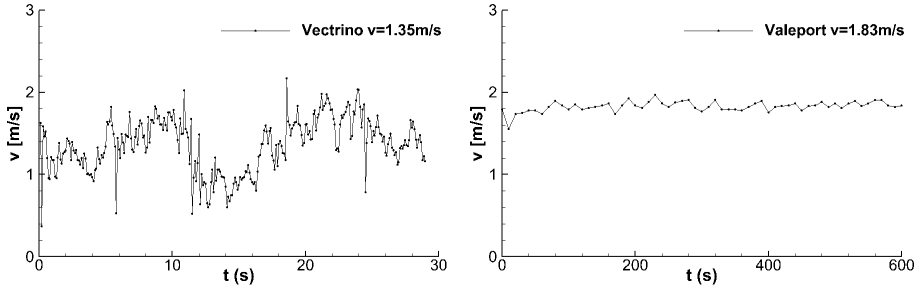

Figure 118: Flow speed measurements. Left: velocimeter readings for streamwise velocity, U_0=1.35 m/s. Right: flow meter readings for total flow velocity.

The impact of the turbulence on the flow can be observed in the rotational speed and torque data. Figure 119 hows the great oscillations in both sets of data. The higher the flow speed, the higher the standard deviation for both parameters. Especially significant is the data deviation on the torque values for the highest speed. Although no turbulence data exist from those tests, it can be assumed that the appearance of significant spikes in the torque curve is

attributable to enduringly high turbulence flows. These characteristics must be taken into account, because irregular torque curves could lead to the emergence of structural problems due to vibrations [69].

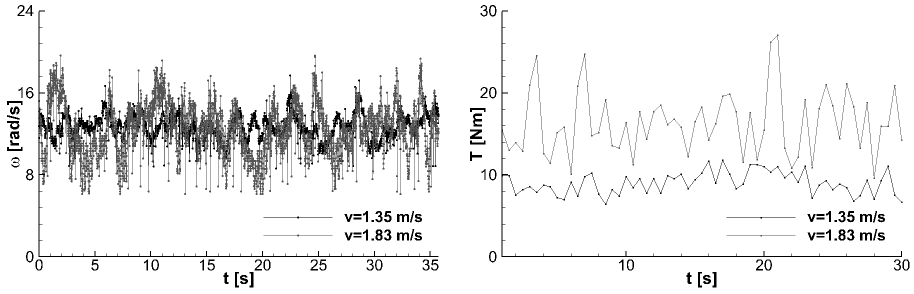

Figure 119: Data extracted from the highest efficiency operational point reached during the fully immersed tests. Left: rotational speed. Right: torque.

26.3. Comparison between results

The main power coefficient curves from the two racks of tests are shown in Figure 120. A drop on the efficiency and in the λ is clearly visible when the turbine was operated in the water centre. Several possible disadvantages can be said to lead to such a decrease in performance. The influence of the flow blockage in the laboratory could be seen as playing a role, as β=0.18.

In addition to the blockage impact, the electrical approach added further losses to the power intake. Thus, the generator cannot convert the entirety of the mechanical power that it is receiving from the rotor rotation. The generator used for the power extraction is stated as having an 87% maximum efficiency rate, and the optimum rate of 200 rpm has never been reached for the peak power coefficient values. Also, the inverter we used claims to have an 97% efficiency rate. The fact that it has not been possible to determine the actual degree of submergence of the blades for the field testing must be highlighted. Hence, the exact value of z/H was not obtained. And pictures and data cannot conclude whether more immersed blades would improve the efficiency curves produced by the turbine at the unblocked facilities.

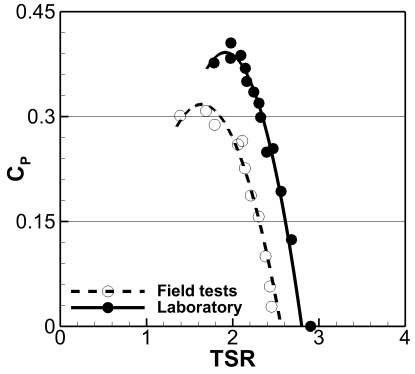

Figure 120: Comparison between laboratory and field testing results. Field tests: U_0=1.83 m/s. Laboratory: U_0=1.09 m/s

Finally, the accuracy of the equipment used for the flow measurements was not ideal. A possible acceleration or deceleration of the flow could have occurred due to the influence on the hydrodynamics of any of the parts in the turbine structure. For instance, the shape of the support base could have increased the flow in the area close to the impeller. And it must be acknowledged that efficiency curves are very sensitive to the approaching flow speed, as Cp and λ are directly dependent on this value.

Part IX

Discussion

The analysis of the performance and behaviour of VATTs has been challenging the scientific community for the last decades. Many factors exert a great influence on the experiments outcome, which means the research on this field usually involves certain degree of uncertainty. Some of the topics here studied, tested and analysed were previously explored, but the pieces of work found in the literature hardly ever agreed in their conclusions. One of the main aspects that characterises the experimental testing is the laboratory flume. Practically none of the laboratories in the research centre share the same geometric and hydrodynamic properties, therefore the initial and boundary conditions differ between studies. The geometrical and structural conditions of the flume are critical parameters for the tests development. Hence, not only width, length and height are key factors for the development of the tests, but also development, but power pump models, flume surfaces and even temperature and salinity play a substantial role. In addition to this, the hydrodynamical conditions of a particular flume are again very hard to be emulated. Velocity fields, Reynolds and Froude number, together with the flow turbulence are unique to each laboratory. Finally, and as it has been proved in the present work, the materials of the experimental set up of the turbine might be defined and identified as well due to their significance. Thus, the roughness of the materials used for the blade manufacturing must be measured and also be consistent for all the experiments. Additionally to these circumstances, the blockage of the flume due to the presence of a moving obstacle such a vertical turbine becomes as one of the factors with the greatest impact on the outcome of the tests. I personally find this lengthy description to be necessary in order to understand the reason why research studies with similar characteristics differ in their results. Furthermore, these considerations also show the restrictions related to small-scale testing and

state how important intermediate-scale tests are for a complete understanding of this technology.

Having said that, this substantial test regime and its post-process provided enough information to evaluate some essential parameters for VATT's performance and also found out very interesting engineering solutions in terms of efficiency optimisation. Moreover, direct comparison between different set ups was possible, giving very valuable data for future turbine manufacturers. Table 28 displays the most and least efficient set ups for each analysed parameter, together with the peak of the performance curve and its corresponding tip speed ratio.

The main part for, not just a tidal turbine but any turbine, is the shape of the blade. Up to five different blade shapes were tested in the facilities at Cardiff University in order to analyse in our facilities its influence on the turbine performance and also to compare to other pieces of research. The optimum pitch angle for the five shapes had to be tested firstly, as it was proven that a mere analysis of the blade shapes without finding the most efficient pitch angle would not allow an accurate evaluation of the performance delivered by the shape. The commonly-tested NACA shapes outperformed the Eppler shapes, although the gaining margin in terms of energy extraction was minor. The best shape was found to be the NACA 4415 for a pitch angle of 5° whereas NACA 63412 clearly performed worse than the other four blades. It is significant the fact that each optimum pitch angle blade was always found for positive pitch angles (tip of the blade outwards) and within a short range [+2.5°,+7.5°]. On the other hand, turbines with negative pitch angles never provided better results than positive angles, which is consequent with the literature and the physics. As lift and drag forces are clearly dependent on the Reynolds number and the fact that the range of flow stream velocities in a estuary can be enclosed within the values slower than 4.0 m/s, further research might focus on a more in depth analysis of the blade shape according to the characteristic Reynolds number of

Table 28: Peak Cp and λ for each experiment

Parameter	**Turbine Performance**	**TSR**	**Cp**	**Value**
Flow speed	Best	1.9	0.36	1.15 m/s
	Worse	1.6	0.26	0.72 m/s
Blade shape	Best	2	0.365	NACA 4415
	Worse	1.95	0.12	NACA 63412
Pitch Angle	Best	1.88	0.37	+2.5°
	Worse	1.5	0.245	-2.5°
Solidity	Best	1.82	0.39	29 %
	Worse	2.35	0.29	19 %
Number of blades	Best	2.8	0.415	2 blades
	Worse	1.65	0.325	4 blades
Angle of twist	Best	1.85	0.36	0°
	Worse	2.35	0.27	45°
Spokes shape	Best	1.55	0.24	NACA 0012
	Worse	1.5	0.21	Squared
Winglets	Best	1.6	0.335	3D winglets
	Worse	1.35	0.265	No winglets
Cylindrical Obstacles	Best	1.4	0.36	Obstacle in 3_NW
	Worse	1.2	0.24	Obstacle in 9_NE
Shaft size	Best	2.1	0.39	r=10cm
	Worse	1.92	0.345	r=70cm
Inner blades	Best	1.95	0.32	3 outer + 0 inner
	Worse	1.6	0.75	3 outer + 3 inner
Blockage	Best	2.05	0.425	β =0.22
	Worse	1.4	0.26	β =0.12
Roughness	Best	2.25	0.3	k_s=6.6
	Worse	2.3	0.4	k_s=125.3

the environment.

The influence of rotor solidity on the performance of the turbine is not easy to be studied without taking into consideration the number of blades of the turbine set up. Although they are clearly intertwined, the results suggest that they should not be treated as just one parameter. Looking at the outcome of the experiments that tested the influence of the number of blades, two-bladed turbines with a low solidity value (16 %) provided the most efficient and fastest turbine. However, when pinning the number of blades of the turbine to three, the best set up in terms of power coefficient was performed by the highest

solidity rotor (28%). On top of that, the three-bladed turbine design with the lowest solidity (18%) was the least efficient of the set ups. As a conclusion, the analysis of both parameters must be analysed both individually and jointly. Looking into the most efficient rotor with ability of self-starting, a three-bladed turbine with a solidity of 28 % must be considered as the best rotor design. The two-bladed turbine would provide higher efficiencies indeed, but the self-starting tests showed that this design would need an extra device to thrust initially the rotor and therefore start rotating. Turbines with three and four blades displayed good responses in terms of self-starting.

The experiments carried out in order to study the effect of adding twist on the turbine blades provided very interesting results. Certainly this is one of the most important parameters because an the optimum value is very difficult to be obtained. This is because different angles deliver different pros and cons that should be considered by prototype designers. The straighter the blade is, the more efficient the design will be. However, the more twisted the blades are, the more beneficial for the set up in terms of self-starting and torque curves. To design, create and manufacture the prototype for the intermediate-scale tests, a balance between efficiency and favourable self-starting characteristics was adopted, choosing 30° as the angle of twist. Another relevant conclusion that can be extracted from the experiments is the need of using hydrodynamically smooth spokes, otherwise the struts will add drag to the turbine rotaiton and therefore they will slow down the device. Thus, NACA 0012 was adopted to build the spokes for the turbine design.

Apart from these experiments where a certain parameter was analysed in detail in order to find the optimum value, other kind of experiments were carried out with the objective of studying innovative ideas and concepts to improve the efficiency of the design. The study of the influence that winglets could exert on the turbine efficiency can be included within these category. These tests and the corresponding results provided one of the most relevant findings of this research.

Thus, it has been found that Winglets can enhance the efficiency of the turbine, and a particular design has been proved to improve the device. In addition to this, the fact that the radius of the shaft must not overcome certain threshold must be also taken into consideration for future VATT designs. According to the tests, the ratio shaft radius / turbine radius must be smaller than 0.15 so that the losses can be minimised. Probably a large radius would slow down the flow at the downstream sector, which would imply a reduction on the lift and drag forces generated by the hydrofoil.

The presence of obstacles on the flow which modify the hydrodynamics with the aim of accelerating the flow where more beneficial for the turbine rotation is, yielded very promising results. Having thought of engineering ideas to enhance the structural support of the turbine, a possible increase of the turbine efficiency was also analysed. The interpolation of the results provided a map of best and worse locations. Ideally, this kind of test should be tested for larger scales to corroborate that this increase on the efficiency is not caused by any small scale effect.

Finally, the study of the role that the material roughness brings on the turbine performance was tested and analysed. In general, high blade roughness affects negatively the capacity of extracting power of the turbine. Thus, the roughest blades ($k_s \approx 125$) provided the worse results in both efficiency and rotational speed. On the hand, the smoothest blades ($k_s \approx 5$ and 25) performed quite similarly. Therefore, these findings will encourage engineers and manufacturers to design VATT with low relative roughness values.

This extensive series of tests showed a large number of improvements and delivered values or specific ranges where the power coefficients can reach their maximum. In figure 121 is displayed the difference between the most and least efficient set ups for all the tests carried out for the creation of this thesis (the data to create this graph comes from figure 28. Clearly, the optimisation process was successful and a positive improvements for the turbine performance was found.

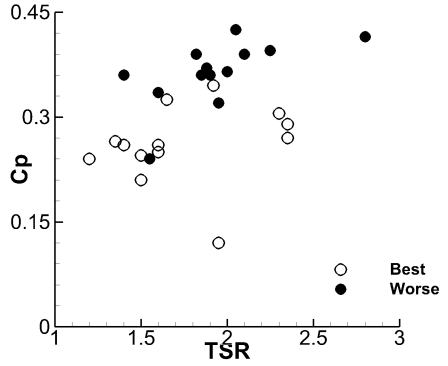

Figure 121: Best and worse results for each experiment presented in this thesis

The last two chapters of the thesis provide data is quite remarkable. The wake of the VATT has been measured for first time according to the writer. Although flow measurements using ADV is a common practice in the research community, not many researcher have used tidal gauge to measure the water elevation of the wake any tidal turbine, neither horizontal nor vertical axis turbines. The analysis here presented could be extremely useful for future engineers if this type of turbine is finally designed for large scales. Also, the accuracy of the tidal gauges was better than expected firstly. Therefore, the tests have also proved that this technique could be used for further research. The quality of the data could be also used to calibrate numerical models that operate with free surface.

Finally, the intermediate scale testing corroborated several uncertainties of the design related to small scale. Thus, rotor and structure were proven to deliver great results, which is a milestone for continuing improving the technology. Also, the prototype was able to bear very turbulent flows, which is supposed to be a significant parameter for larger scales. The comparison between the corresponding performance curves for intermediate and small scale prototypes were very consistent, and the obvious drop on the performance can be observed. In hydrodynamic terms, further work that take into account length scale effects

would be necessary to improve the knowledge in the performance and behaviour for this technology when scaled up.

Part X

Conclusions

An extensive array of tests were carried out at Cardiff University in order to get a hydrodynamical optimisation of the rotor. Then, a new design for a cross-flow turbine was analysed in depth for small and intermediate scales. Processing the data and extracting information and conclusions from the results guided the optimisation of the rotor and has added knowledge to the scientific community. This technical solution for the rotor is a trade-off of parameters that control the behaviour and the performance of the turbine – rotational speed, torque, self-starting, etc., but aiming to maximise the turbine efficiency. The wake of this optimised VATT was fully measured as well and, to the author's best knowledge, utilised techniques that have never been used before for these purposes and delivered very accurate results.

1. Experimental tests have being carried out at Cardiff University to understand and quantify the different parameters and components that have an effect on the performance of a cross-flow turbine. Different turbine designs were compared in order to optimise the turbine efficiency. In addition to this, the data extracted from the tests confirmed that the facilities are suitable for these types of testing and provided reliable data.

    - The influence that the blade shape exerts on the rotor performance must always be analysed together with its pitch angle. The lift to drag ratios at different Reynolds number might help to optimise the best blade shape in terms of efficiency.
    - The influence of rotor solidity on the performance of the turbine is high, and is consistent with the existing knowledge. Low-solidity rotors reach higher rotational speeds when compared with their higher solidity counterparts. However, high-solidity rotors provide higher torque to the turbine system.

- The number of blades per turbine rotor plays a big role in their performance too. Two-bladed rotors perform best, probably due to lower wake-blade interaction than, for instance, four-bladed rotors. Generally, the fewer blades the faster the turbine spins, and the less significant the additional effect of blade roughness. On the other hand, the influence of the number of blades does not keep solidity constant, which could distort the outcome. In addition to this, two-bladed rotors will not self-start and their torque output per revolution is much more uneven than, for example, four-bladed rotors. Turbines with three and four blades have shown similar responses to self-starting processes.
- An angle of twist on the turbine blades might decrease the efficiency of the rotor, but provides interesting advantages. For instance, the larger the angle of twist, the lower are the load curves and the better self-starting behaviour was observed.
- If the connection between blades and shaft is carried out using spokes, these spokes must provide low drag coefficients. If the shape is not hydrodynamically smooth, the spokes will add losses to the power extraction
- Installing winglets at the end of the blades and placing obstacles upstream and downstream of the turbine increases the efficiency of the rotors; this might encourage further research in the near future. On the other hand, the inclusion of blades at different distances to the shaft or to increase the size of the shaft does not add any advantage to the turbine design.
- The effect that a constrained blockage provides to the rotor performance was assessed and evaluated at our facilities. High efficiencies were reached for higher blockage values, a fact that could be relevant if this tidal turbine is to be adapted to other purposes.

2. A series of experimental tests were carried out in the hydraulics laboratory

with the goal of assessing the influence of blade surface roughness on the performance of vertical axis turbines. Several conclusions can be drawn from the results.

- It has been shown that blade roughness negatively affects the turbine performance and, the rougher the blade, the poorer the performance of the turbine. This is irrespective of other important turbine parameters such as turbine solidity or the number of blades.
- The negative effect of blade roughness is much more significant at higher approach flow speeds. At low flow speeds rough-bladed turbines perform just as well as smooth-bladed turbines, however at these low Reynolds number, the turbine performance does not reach high efficiency values.
- The hypothesis that turbines with rough blades could benefit from a delay in the onset of stall or in a reduction of drag has not been confirmed; quite the contrary, and it should be discarded based on the findings presented herein.

3. The testing undertaken at the hydraulics facilities provided measurements of the main wake characteristics that a vertical axis tidal turbine generates when operating. Flow velocities were measured in downstream position, up to x/D = 10, and water elevation was tracked in the upstream and downstream regions.
    - Strong accelerations of the flow on the sides of the turbine were detected. Velocities up to 1.5 times faster than the approach flow speed were reached, a fact that could be attributed to a combination of the turbulence intensity, the blockage effect or the rectangle cross-section of vertical axis tidal turbines. The mean streamwise velocity experienced a critical decrease at close positions, undergoing a logarithmic recovery rate two diameters away from the centre of the turbine, within the range of values from other studies that analysed the wake form horizontal axis turbines. The upstream velocities were not

reached again at the furthest distance of the far-wake (10 diameters), as the streamwise velocity did not reach the same upstream velocity value and the flow at the channel sides was still slightly faster.

- The water surface measurements and its interpolation provided very useful data in order to complete the wake characterisation. Thus, 3- D figures enabled the visualisation of the V-shape of the wake and to obtain the difference on the water depth between upstream and downstream accurately. The rise on the water level upstream is 8% compared to the initial water depth at six diameters away from the turbine, and a trend that indicates the downwards evolution of the water level upstream cannot be figured out. On the contrary, the recovery rate of the water depth downstream is recognised, and the water elevation at six-diameters distance has almost reached the initial depth.
- These results aim to shed some light to the understanding of the hydrodynamics of the wake created by vertical axis tidal turbines. Further work should be focused on lower blockage ratios, in order to compare the impact of this effect and to apply the data and knowledge gathered from these experiments to natural environments and future arrays.

4. A new design for a cross-flow turbine was analysed in depth at both small and intermediate scales. This experiment presented the chance to test a tidal turbine in an environment very similar to that in the real world, but with the additional advantage of complete deployment control. These tests can therefore be considered unique, due to such unusual characteristics.

    - An obvious drop in the turbine performance emerged according to the degree of submergence of the turbine. Through our testing, the results have pointed to a clear trend: that the higher the approach flow speed is, the more immersed the rotor needs to be.
    - The power coefficients achieved from the intermediate scale testing

were lower than those for the small scale, but were slightly higher than the expected range. The blockage effect, electrical losses and the level of submergence were expected to detract more significantly from the turbine efficiency.

- These results provide initial data testifying to the structural limits of the turbine, in terms of explaining how some of the limitations will affect a future scale-up. The efficiency curves show a range for λ where the maximum power is extracted - this knowledge is important when working to optimise the power take off.

Part XI

Acknowledgments

Firstly, I would like to express my gratitude to my supervisor Prof. Thorsten Stoesser for the continuous support of my PhD work and related research, for his motivation and patience. He provided me the opportunity to join their team and his guidance was very useful to me throughout this three years. My sincere thanks also goes to Prof. Alan Kwan for supervising my work.

Besides my advisor, I would like to thank the rest of my research department, Sandeep, Ken, Stefan, McSherry, Mitrou, Yang, Guoxian, etc. They are the best officemates that anyone can have.

I would like to highlight the help provided by Bruño Fraga and Pablo Ouro. Not only for their insightful advices and guidance, but also because of their friendship that helped to make possible to conduct this research. Gracias amigos.

Last but not the least, I would like to thank my family: my parents Cipriana Molinos and Jose Luis Priegue and my sister Maria Priegue for supporting me on the distance spiritually and physically throughout writing this thesis and my life in general. And of course my amazing and beautiful girlfriend who put up with me all this time, as she is already a part of the family as well. A personal achievement also belongs to the family, so this success also belongs to all of you.

I would like to also pay homage to my beloved grandfather Mr. Juan Priegue Blanco, who sadly passed away this year. We will miss you Abuelo.

[1] T. Vlachogianni, A. Valavanidis, Energy and Environmental Impact on the Biosphere Energy Flow, Storage and Conversion in Human Civilization, American Journal of Educational Research. 1 (3) (2013) 68–78 doi:10.12691/education-1-3-2

[2] Encyclopedia.com http://www.encyclopedia.com/science-and-technology/technology/technology-terms-and-concepts/steam-engine

[3] Frankfurt School-UNEP Centre/BNEF. 2016. Global Trends in Renewable Energy Investment 2016, http://www.fs-unep-centre.org

[4] Deparment of Energy and Climate Change, Renewable sources of energy: Chapter 6, Digest of United Kingdom Energy Statistics (DUKES), 2015. https://www.gov.uk/government/uploads/system/uploads/attachment_data/file/540953/Chapter_6_web.pdf

[5] C. Klessmann, A. Held, M. Rathmann, M. Ragwitz, Status and perspectives of renewable energy policy and deployment in the European Union—What is needed to reach the 2020 targets? Energy Policy 39 (2011) 7637–7657, doi:10.1016/j.enpol.2011.08.038

[6] International Energy Agency, Joint Polcies and Measures database, 2016, http://www.iea.org/policiesandmeasures/renewableenergy

[7] http://gov.wales/funding/eu-funds/2014-2020/?lang=en

[8] C. Boehringer, The Kyoto Protocol: A Review and Perspectives, Oxford Review of Econonomy Policy 19 (3) (2003) 451–466 doi:10.1093/oxrep/19.3.451

[9] J. Rogelj, C. Chen, J. Nabel, K. Macey, W. Hare, M. Schaeffer, K. Markmann, N. Hohne, K.K. Andersen, M. Meinshausen, Analysis of the Copenhagen accord pledges and its global climatic impacts-a snapshot of dissonant ambitions. Environmental Research Letters 5 (3) (2010) 034013 (9pp), doi:10.1088/1748-9326/5/3/034013

[10] European Commission, The Paris Protocol – A blueprint for tackling global climate change beyond 2020, 2015 http://ec.europa.eu/clima/policies/international/paris_protocol/docs/com_2015_81_en.pdf

[11] European Commission, A policy framework for climate and energy in the period from 2020 to 2030, Brussels, 22/01/2014, http://eur-lex.europa.eu/legal-content/EN/TXT/PDF/?uri=CELEX:52014DC0015\&from=EN

[12] Global Energy Efficiency and Renewable Energy Fund (GEEREF), GEEREF IMPACT REPORT 2014, http://geeref.com/assets/documents/geeref-impact-report-2014-public.pdf

[13] Deparment of Energy and Climate Change, The UK Renewable Energy Strategy, 2009, http://www.gov.uk/government/uploads/system/uploads/attachment_data/file/228866/7686.pdf

[14] https://www.ofgem.gov.uk/

[15] Deparment of Communications, Energy and Natural Resources, Offshore Renewable Energy Development Plan, 2014 http://www.dccae.gov.ie/energy/SiteCollectionDocuments/Renewable-Energy/20140204\%20DCENR\%20-\%20Offshore\%20Renewable\%20Energy\%20Development\%20Plan.pdf.

[16] Deparment of Energy and Climate Change, UK Renewable Energy Roadmap, 2011, https://www.gov.uk/government/uploads/system/uploads/attachment_data/file/48128/2167-uk-renewable-energy-roadmap.pdf

[17] https://www.gov.uk/government/publications/contracts-for-difference/contract-for-difference

[18] United Nations Atlas of the Oceans (UNAO), http://www.oceansatlas.org.

[19] Energy Transformed and wealth from Ocean flagships, Ocean renewable energy: 2015-2050, An analysis of ocean energy in Australia, 2012 https://publications.csiro.au/rpr/download?pid=csiro:EP113441\&dsid=DS2

[20] B. Polagye, J. Epler, and J. Thomson, Limits to the predictability of tidal current energy, in Proc. MTS/IEEE OCEANS Conf., Seattle, WA, Sep. 2010 doi:10.1109/OCEANS.2010.5664588

[21] A. Uihlein, D. Magagna, Wave and tidal current energy – A review of the current state of research beyond technology, Renewable and Sustainable Energy Reviews 58 (2016) 1070–1081.

[22] F. Lefevre, F.H. Lyard, C. Le Provost, E.J.O. Schrama, FES99: a global tide finite element solution assimilating tide gauge and altimetric information, Journal of Atmospheric and Oceanic Technology, (2002) 1345–1356.

[23] J.J. McCarthy, O. F. Canziani, et al., Climate Change 2001: Impacts, Adaptation, and Vulnerability. Contribution of Working Group II to the Third Assessment Report of the Intergovernmental Panel on Climate Change (IPCC). Cambridge University Press, Cambridge, (2001).

[24] Aquatic Renewable Energy Technologies (Aqua-RET), www.aquaret.com

[25] The Crown State, UK Wave and Tidal Key Resource Areas Project, (2012) https://www.thecrownestate.co.uk/media/5476/uk-wave-and-tidal-key-resource-areas-project.pdf

[26] ABP Marine Environmental Research Ltd, Atlas of the UK marine renewable energy resources, (2008)

[27] N.N. Panicker, Power Resource Potential of Ocean Surface Waves, Proceedings of Wave and Salinity Gradient Workshop, Newark, Delaware, U.S.A. (1976) 1–48

[28] G. Mørk, S. Barstow, A. Kabuth, M. T. Pontes Lisboa, Portugal , Asessing the global wave energy potential, Proceedings of OMAE 2010 29th International Conference on Ocean, Offshore Mechanics and Arctic Engineering Shanghai, China, June 6-11, (2010). http://www.oceanor.no/related/59149/paper_OMAW_2010_20473_final.pdf

[29] A. M. Cornett, Global wave energy resource assessment. In: Proc of the eighteenth international offshore and polar eng. conference. Canada: Vancouver; July 6–11, 2008. https://www.onepetro.org/conference-paper/ISOPE-I-08-370

[30] Environment Energy Agency, Europe's onshore and offshore wind energy potential,Copenhagen, 2009 doi:10.2800/11373

[31] P. Dlugolecki, K. Nymeijer, S. Metz, M. Wessling, Current status of ion exchange membranes for power generation from salinity gradients, Journal of Membrane Science, 319, (1–2) (2008) 214–222 doi:10.1016/j.memsci.2008.03.037

[32] J.W. Post, J. Veerman, H.V.M. Hamelers, G.J.W. Euverink, S.J. Metz, K. Nymeijer, C.J.N. Buisman, Salinity-gradient power: evaluation of pressure-retarded osmosis and reverse electrodialysis Journal of Membrane Science, 288 (2007) 218–230 doi:10.1016/j.memsci.2006.11.018

[33] S. E. Skilhagen, Osmotic power – a new, renewable energy source. Desalin. Water Treat. 15, (2010) 271–278.

[34] M. Gautier, D.E. Lennard, Ocean Thermal Energy Conversion: an Opportunity for the Maritime Industry with Early Application to Islands, Euro-Caribbean Conference, May 2002, International Scientific Council for Island Development (INSULA), UNESCO, Paris, France

[35] D. Lennard, Ocean Thermal Energy Conversion, Survey of Energy Resources, World Energy Council, London, (2007) 565–581. ISBN 0-946121-26-5

[36] C. Gomis, E. Ferrandis, Potencial de la aplicación energética de las microalgas, La energía que viene del mar, Instituto Universitario de Estudios Marítimos (IUEM), Netbiblo, Oleiros, A Coruña, 93–98.ISBN 978-84-9745-265-6

[37] http://www.enalgae.eu/

[38] Y. Li, M. Horsman, N. Wu, C. Q. Lan, N. Dubois-Calero, Biofuels from Microalgae, Journal of Biotechnology Progress, 24 (4) (2008) 815–820

[39] D. J. Webb, Tides and the evolution of the Earth—Moon system, Geophysics Journal International 70 (1) (1982) 261–271. doi:10.1111/j.1365-246X.1982.tb06404.x

[40] S. D. Hicks, Understanding Tides (2006) https://tidesandcurrents.noaa.gov/publications/Understanding_Tides_by_Steacy_finalFINAL11_30.pdf

[41] M.L. Schwartz (Ed.), Encyclopedia of Coastal Science, Springer-Verlag, The Netherlands (2005) 1211pp.

[42] J. L. Davies, 1964, A morphogenic approach to world shore-lines, Zeitschrift fuar Geomorpholoige, NF, 8 (1964) 127–142.

[43] J.A.C. Orme, I. Masters, Analysis and comparison of support structure concepts for tidal stream turbines, Proceedings of World Maritime Techonlogy Conference (2006), https://www.researchgate.net/publication/237455420_Analysis_and_comparison_of_support_structure_concepts_for_tidal_stream_turbines

[44] A. Boisseau, P. Davies, F. Thiebaud, Fatigue Behaviour of Glass Fibre Reinforced Composites for Ocean Energy Conversion Systems, Applied Composite Materials, 20 (2013) 145–155 doi:10.1007/s10443-012-9260-0

[45] J. J. Coy, D. P. Townsend, E. V. Zaretsky, Gearing. NASA RP-1152; AVSCOM TR 84-C-15 (1985).

[46] K. Yuen, K. Thomas, M. Grabbe, P. Deglaire, M. Bouquerel, D. Österberg, M. Leijon, Matching a permanent magnet synchronous generator to a fixed pitch vertical axis turbine for marine current energy conversion. IEEE Journal of Oceanic Engineering, 34 (1) (2009), 24–31 doi:10.1109/JOE.2008.2010658

[47] M.N. Kotzalas, G.L. Doll, tribological advancements for reliable wind turbine performance. Philos Trans Roy Soc A (2010) 368 4829–4850.

[48] Z. Zhou, F. Scuiller, J.F. Charpentier, M.E.H. Benbouzid and T. Tang, An Up-to-Date Review of Large Marine Tidal Current Turbine Technologies, In IEEE Power Electronics and Application Conference (Shanghai), China, (November 2014)

[49] Alstom, 2013. urlhttps://www.gerenewableenergy.com/hydro-power.html

[50] http://www.hammerfeststrom.com/

[51] http://voith.com/en/products-services/hydro-power/ocean-energies/tidal-current-power-stations--591.html

[52] http://www.bbc.co.uk/news/uk-wales-south-west-wales-35087510

[53] https://www.atlantisresourcesltd.com/

[54] http://www.openhydro.com/

[55] P.L. Fraenkel, Power from marine turbines, Proc Inst Mech Eng A: J Power Energy 216 (A1) (2002) 1–14.

[56] F. O Rourke, F. Boyle, A. Reynolds, Tidal energy update 2009, Journal of Applied Energy 87 (2010) 398–409 doi:10.1016/j.apenergy.2009.08.014.

[57] http://www.sabella.fr/

[58] http://www.verdantpower.com/kinetic-hydropower-system.html

[59] http://www.straumgroup.com/hydratidal

[60] http://www.magallanesrenovables.com/en/proyecto

[61] http://www.all-energy.co.uk/_novadocuments/30345

[62] http://www.nautricity.com/

[63] http://tidalenergytoday.com/2015/06/01/clean-current-exits-hydrokinetic-industry/

[64] J. Hardisty, The Analysis of Tidal Stream Power, John Wiley & Sons, 2009, 342 pages ISBN 0470743123

[65] http://hgenergy.com/index.php/news_releases/hydro-green-energy-receives-50-year-license-from-the-ferc-for-5.25-mw-bradd

[66] http://www.tocardo.com/

[67] http://www.oceanflowenergy.com/

[68] B.K. Kirke, Tests on ducted and bare helical and straight blade Darrieus hydrokinetic turbines, Journal of Renewable Energy, 36 (2011) 3013–3022, doi:10.1016/j.renene.2011.03.036

[69] B.K. Kirke, L. Lazauskas, Limitations of fixed pitch Darrieus hydrokinetic turbines and the challenge of variable pitch, Renewable Energy 36 (2011) 893–897, doi:10.1016/j.renene.2010.08.027

[70] N. Batista, R. Melicio, J. Matias, J. Catalao, New blade profile for darrieus wind turbines capable to self-start, Renewable Power Generation CRPG, IET Conference (2011) 1–5 doi:10.1049/cp.2011.0219

[71] M. Shiono, K. Suzuki, S. Kiho, An experimental study of the characteristics of a Darrieus turbine for tidal power generation. Electrical Engineering in Japan, 132 (3) (2000) 38–47. doi:0.1002/1520-6416(200008)132:3

[72] G. Calcagno, A. Moroso, The Kobold marine turbine: from the testing model to the full scale prototype, Tidal Energy Summit, November 28-29,

2007, London, http://www.tidaltoday.com/tidal07/presentations/GuidoCalcagnoMoroso.pdf

[73] H. Eriksson, A. Moroso, A. Fiorentino, The vertical axis Kobold turbine in the Strait of Messina – a case study of a full scale marine current prototype, World maritime technology conference, London (2006)

[74] http://www.newenergycorp.ca/encurrent-125-series.html

[75] http://tidalenergy.com.au/

[76] M. Shiono, K. Suzuki, S. Kiho, Output Characteristics of Darrieus Water Turbine with Helical Blades for Tidal Current Generations, Proceedings of The 12th International Offshore and Polar Engineering Conference, Kitakyushu, Japan, (May 2002)

[77] A. M. Gorlov Helical Turbines for the Gulf Stream: Conceptual Approach to Design of a Large-Scale Power Farm, Journal of Marine Technology, 35 (3) (1998), (175–182).

[78] http://www.teknik.uu.se/electricity/research-areas/marine-currents/

[79] New Energy Corporation, Experience with EnCurrent Power Generation Systems, International Conference on Ocean Energy 2014, Halifax, Nova Scotia, November 6, 2014

[80] http://www.businessgreen.com/bg/news/2343696/decc-poised-to-remove-controversial-humber-tidal-device

[81] http://www.offshorewind.biz/2013/02/07/uk-neptune-renewable-energy-goes-into-liquidation/

[82] http://www.keplerenergy.co.uk/

[83] http://www.orpc.co/orpcpowersystem_tidgenpowersystem.aspx

[84] S. R. Waters, Analysing The Performance Of The Archimedes Screw Turbine Within Tidal Range Technologies, Lancaster University (2015), http://eprints.lancs.ac.uk/76794/1/2015ShaunWatersMSc.pdf

[85] http://minesto.com/

[86] http://atlantisresourcesltd.com/turbines/an-series.html

[87] http://pulsetidal.com/our-technology.html

[88] I. Ushiyama, H. Nagai, Optimum design configurations and performances of Savonius rotors. Wind Engineering 12 (1) 1988, 59–75.

[89] K.Sahim, D. Santoso, and A. Radentan Performance of Combined Water Turbine with Semielliptic Section of the Savonius Rotor, International Journal of Rotating Machinery Vol.2013 (2013) doi.org/10.1155/2013/985943

[90] T. Nakamura, K. Mizumukai, H. Akimoto, Y. Hara and T. Kawamura Floating Axis Wind and Water Turbine for High Utilization of Sea Surface Area: Design of Sub-Megawatt Prototype Turbine, ASME 2013 32nd International Conference on Ocean, Offshore and Arctic Engineering Ocean Renewable Energy Nantes, France, 8 (2013) doi:10.1115/OMAE2013-11287.

[91] G. G. Muscolo, R. Molfino, From Savonius to Bronzinus: a comparison among vertical wind turbines, The International Conference on Technologies and Materials for Renewable Energy, Environment and Sustainability, TMREES14

[92] http://www.bluewater.com/new-energy/texel-project/

[93] A. Owen, I. G. Bryden, Prototype support structure for seabed mounted tidal, current turbines, Proc. Institution of Mechanical Engineers, 219 Part M: J. Engineering for the Maritime Environment, 2005, doi:10.1243/14750902JEME28

[94] http://blogs.ei.columbia.edu/2010/05/19/limpet-land-installed-marine-powered-energy-transformer/

[95] https://uk.pinterest.com/pin/196539971214291734/

[96] http://www.pico-owc.net/

[97] http://www.power-technology.com/projects/mutriku-wave/

[98] M.T. Reis, R. Mestre, M.G. Neves, K. Hu, J. Dias, A. Mendonza, E. Didier1, C.J.E.M. Fortes1, A new application of the nonlinear shallow water numerical model amazon to study owc in vertical breakwaters, SCACR 2015, October 2015, https://www.researchgate.net/publication/305264751_A_NEW_APPLICATION_OF_THE_NONLINEAR_SHALLOW_WATER_NUMERICAL_MODEL_AMAZON_TO_STUDY_OWC_IN_VERTICAL_BREAKWATERS

[99] Atlantica Transnational Network, Desarrollo de las energías renovables marinas: condiciones de éxito en las regiones de la RTA del Arco Atlántico, 2010

[100] I. López, J. Andreu, S. Ceballos, I. Martínez de Alegría, I. Kortabarria, Review of wave energy technologies and the necessary power-equipment, Renewable and Sustainable Energy Reviews, (27) (2013) 413–434. doi.org/10.1016/j.rser.2013.07.009.

[101] Strategic Initiave for Ocean Engineering, Ocean Energy: State of the Art, (2012), http://si-ocean.eu/en/upload/docs/WP3/Technology\%20Status\%20Report_FV.pdf

[102] http://www.wavedragon.net

[103] http://www.aquamarinepower.com/technology/how-oyster-wave-power-works.aspx

[104] http://www.pelamiswave.com

[105] http://www.oceanpowertechnologies.com/powerbuoy/

[106] J. Cordonnier, F. Gorintin, A. De Cagny, A.H. Clément, A. Babarit, SEAREV: Case study of the development of a wave energy converter, Renewable Energy, 80, (2015), 40–52, doi.org/10.1016/j.renene.2015.01.061.

[107] Y. H. Baea, K. O. Kimb, B. H. Choi, Lake Sihwa tidal power plant project, Journal of Ocean Engineering 37 (5–6) (2010) 454–463.

[108] http://albanmariejoris-tpe.e-monsite.com/album-photos/do_xml/album/

[109] http://tidalenergytoday.com/2015/01/20/video-annapolis-tidal-power-station/

[110] http://www.tidallagoonswanseabay.com/the-project/proposal-overview-and-vision/51/

[111] R. Ahmadian, R. Falconer, B. Lin, Hydro-environmental modeling of proposed Severn barrage, UK, Proceedings of the Institution of Civil Engineers - Energy, 163 (3) (2010), 107–117

[112] K. Hulsbergen, D. Boer, R. Steijn, G. Banning, Dynamic Tidal Power for Korea, 1st Asian Wave and Tidal Conference Series (AWTEC), Korea, 29 November (2012), http://www.powerdtp.nl/Downloads/default.aspx

[113] J.K. Kaldellis, M. Kapsali, Shifting towards offshore wind energy—Recent activity and future development, Energy Policy, 53 (2013) 136–148 doi:10.1016/j.enpol.2012.10.032.

[114] G. Jackson , F. Stempinski, Concrete Gravity Foundations for Offshore Wind: New Guidelines for Design, Construction and Installation From Sea to Shore – Meeting the Challenges of the Sea, Institution of Civil Engineering (2015) doi:10.1680/fsts.59757.036.

[115] http://www.ramboll.co.uk/projects/re/150-monopiles-in-the-north-sea-push-offshore-wind-into-deeper-waters

[116] http://publications.arup.com/publications/g/gravitas_offshore

[117] http://www.sway.no/?page=206&news=761&title=Sway\%20successfully\%20deployed\%20prototype.

[118] European Wind Energy Association, The European offshore wind industry key 2011 trends and statistics, (2012). http://large.stanford.edu/courses/2012/ph240/pratt1/docs/EWEA_stats_offshore_2011_01.pdf

[119] Strategic Initiave for Ocean Engineering, Wave and Tidal Energy Market Deployment Strategy for Europe, (2014)

[120] http://www.emec.org.uk/standards/

[121] GL Renewables Certificagorlovtion (GL RC), List of Certifications (2015)

[122] DNV-GL , Standard DNVGL-ST-0164 Tidal turbines, October 2015 https://rules.dnvgl.com/docs/pdf/DNVGL/ST/2015-10/DNVGL-ST-0164.pdf

[123] European Wind Energy Association, Upwind Final Report 2011, http://www.ewea.org/fileadmin/ewea_documents/documents/upwind/21895_UpWind_Report_low_web.pdf

[124] C. Golightly, Offshore Wind Structures - Gambling With Grout: Worth the Risk?, 4th Durability and Fatigue Advances in Wind, Wave and Tidal Energy, 4th Durability and Fatigue Advances in Wind, Wave and Tidal Energy

[125] J. M. Harris, R. J. S. Whitehouse, J. Sutherland , Marine scour and offshore wind - lessons learnt and future challenges Proceedings of the ASME 2011 30th International Conference on Ocean, Offshore and Arctic Engineering, OMAE2011, June 19-24, (2011), Rotterdam, The Netherlands http://eprints.hrwallingford.co.uk/527/1/HRPP508_Marine_scour_offshore_wind.pdf

[126] R.J.S Whitehouse, J. M. Harris, J. Sutherland and J. Rees, The nature of scour development and scour protection at offshore windfarm foundations. Marine Pollution Bulletin, 62 (1) (2011) 73–88

[127] N. Tual, N. Carrerea, P. Davies, T. Bonnemains, E. Lolive, Characterization of sea water ageing effects on mechanical properties of carbon/epoxy composites for tidal turbine blades, Composites Part A: Applied Science and Manufacturing 78 (2015) 380–389 10.1016/j.compositesa.2015.08.035

[128] D.M. Grogan, S.B. Leen, C.R. Kennedy, C.M. O Bradaigh, Design of composite tidal turbine blades, Renewable Energy, 57 (2013) 151–162. doi:10.1016/j.renene.2013.01.021

[129] W. Li, H. Zhou, H. Liu, Y. Lin, Q. Xu, Review on the blade design technologies of tidal current turbine, Renewable and Sustainable Energy Reviews 63 (2016) 414–422, doi:10.1016/j.rser.2016.05.017

[130] `http://www.enerzine.com/7/17093sabella-implante`

[131] R.F. Nicholls-Lee, S.R. Turnock, S.W. Boyd, Simulation based optimisation of marine current turbine blades 7th international conference on computer and IT applications in the maritime industries (COMPIT'08), Liège, Belgium, April (2008), 314–328

[132] B. Polagye and J. Thomson, Screening for Biofouling and Corrosion of Tidal Energy Device Materials, Northwest National Marine Renewable Energy Center, Report number 1. April 8, (2010)

[133] J. Orme, I. Masters, R. Griffiths, Investigation of the effect of biofouling on marine current turbines. Proc. MAREC 2001, Institute of Marine Engineers, (2001) 91–99.

[134] H. T. Benbouzid, M. Benbouzid, Marine Renewable Energy Converters and Biofouling: A Review on Impacts and Prevention Conference: EWTEC, At Nantes (France), Paper 09P1-4-2, (2015), `https://hal.archives-ouvertes.fr/hal-01199624/document`

[135] Polagye B, Cleve B Van, Kirkendall K, Copping A. Environmental effects of tidal energy development. In: Proceedings of a scientific workshop. Seattle: National Oceanic and Atmospheric Administration (NOAA); 2011

[136] W. Shi, H.C. Park, J.H. Baek, C.W. Kim, Y.C. Kim, H.K. Shin Study on the marine growth effect on the dynamic response of offshore wind turbines International Journal Of Precision Engineering And Manufacturing 13 (7) (2012) 1167–1176, doi:10.1007/s12541-012-0155-7

[137] J. Wolfram, and A. Theophanatos, The Effects of Marine Fouling on the Fluid Loading of Cylinders: Some Experimental Results, Offshore Technology Conference, 1985

[138] http://www.international-pc.com/markets/infrastructure/Documents/iso-12944.pdf

[139] L. Chen, W. H. Lam, A review of survivability and remedial actions of tidal current turbines, Renewable and Sustainable Energy Reviews 43 (2015) 891–900. doi:10.1016/j.rser.2014.11.071.

[140] C. Powell and P. Webster, Copper Alloys for Marine Environments, Copper Development Association n.206 (2011). https://www.copper.org/applications/marine/cuni/pdf/pub206.pdf

[141] Offshore Standard, Composite Components, DNV-OS-C501 (2013), http://rules.dnvgl.com/docs/pdf/DNV/codes/docs/2013-11/OS-C501.pdf

[142] H. C. Buckland, I. Masters, J. A. C. Orme, T. Baker, Cavitation inception and simulation in blade element momentum theory for modelling tidal stream turbines, Proc IMechE Part A:J Power and Energy 227 (4) (2013) 479–485 doi:10.1177/0957650913477093.

[143] W. Shi, M. Atlar, R. Rosli, B. Aktas, R. Norman, Cavitation observations and noise measurements of horizontal axis tidal turbines with biomimetic blade leading-edge designs, Ocean Engineering 121 (2016) 143–155, doi:10.1016/j.oceaneng.2016.05.030.

[144] W.M.J. Batten, A.S. Bahaj, A.F. Molland, J.R. Chaplin, The prediction of the hydrodynamic performance of marine current turbines, Renewable Energy 33 (2008) 1085–1096, doi:10.1016/j.renene.2007.05.043.

[145] A.S.Bahaj, A.F.Molland, J.R. Chaplin, W.M.J. Batten, Power and thrust measurements of marine current turbines under various hydrodynamic flow conditions in a cavitation tunnel and a towing tank. Renewable Energy 32 (3) (2007) 407–426. doi:10.1016/j.renene.2006.01.012.

[146] C. Frid, E. Andonegi, J. Depestele, A. Judd, D. Rihan, S.I. Rogers et al. The environmental interactions of tidal and wave energy generation devices. Environ Impact Assess Rev (32) (2012) 133–139. doi:10.1016/j.eiar.2011.06.002.

[147] Electric Power Research Institute, Evaluation of Fish Injury and Mortality Associated with Hydrokinetic Turbines, Technical Report 2011. http://tethys.pnnl.gov/sites/default/files/publications/Evaluation_of_Fish_Injury_and_Mortality_Associated_with_Hydrokinetic_Turbines.pdf

[148] C. A. Douglas, G. P. Harrison, J. P. Chick, Life cycle assessment of the Seagen marine current turbine, Proceedings of the Institution of Mechanical Engineers, Part M: Journal of Engineering for the Maritime Environment March 1, 222 (1) (2008) 1–12 doi:10.1243/14750902JEME94.

[149] K.H. Betz, The Lanchester-Betz limit (energy conversion efficiency factor for windmills) Journal of Energy, 3 (6) (1979) 382–384 doi:10.2514/3.48013.

[150] M. Ragheb, A. M. Ragheb. Wind Turbines Theory - The Betz Equation and Optimal Rotor Tip Speed Ratio, Fundamental and Advanced Topics in Wind Power, Dr. Rupp Carriveau (Ed.), InTech, (2011) http://www.intechopen.com/books/fundamental-and-advanced-topics-in-wind-power/wind-turbines-theory-the-betz-equation-and-optimal-rotor-tip-speed-ratio doi:10.5772/21398.

[151] F. Ponta, G. S. Dutt, An improved vertical-axis water-current turbine incorporating a channelling device, Renewable Energy, 20 (2000) 223–241

[152] A. M. Roa, V. Aumelas, T. Maitre, C Pellone, Numerical and experimental analysis of a darrieus-type cross flow water turbine in bare and shrouded configurations, 25th IAHR Symposium on Hydraulic Machinery and Systems IOP Conf. Series: Earth and Environmental Science 12 (2010) doi:10.1088/1755-1315/12/1/012113.

[153] T. Setoguchi, N. Shiomi, K. Kaneko Development of two-way diffuser for fluid energy conversion system, Renewable Energy 29 (2004) 1757–1771

[154] A.R. Malipeddi, D. Chatterjee, Influence of duct geometry on the performance of Darrieus hydroturbine, Renewable Energy 43 (2012) 292–300

[155] E. Daniele, D. P. Coiro, Optimization of diffuser geometry for an horizontal axis shrouded hydro turbine, Clean Electrical Power (ICCEP), International Conference, 2013 doi:10.1109/ICCEP.2013.6586996.

[156] G. J. W. Van Bussel, An assessment of the performance of diffuser augmented wind turbines (DAWT's), 3rd ASME/JSME Fluid Engineering Conf. FEDSM99-7830, San Francisco, USA, 1999

[157] S. Khalid, Z. Liang, N. Shah, Harnessing tidal energy using vertical axis tidal turbine, Journal of Applied Sciences, Engineering and Technology 5 (1) (2012) 239–252. ISSN: 2040-7459.

[158] J. I. Whelan, T. J. Stallard, Arguments for modifying the geometry of a scale model rotor. In Proc. European Wave and Tidal Energy Conf., Southampton, UK, 5–9 September 2011

[159] T. Harries, A. Kwan, J. Brammer, R. Falconer, Physical testing of performance characteristics of a novel drag-driven vertical axis tidal stream turbine; with comparisons to a conventional Savonius, Journal of Marine Energy, Volume 14 (2016) 215–228.doi:10.1016/j.ijome.2016.01.008.

[160] T. Harries, Physical Testing and Numerical Modelling of a Novel Vertical-Axis Tidal Stream Turbine, PhD Thesis, Cardiff School of Engineering (March, 2014). `http://orca.cf.ac.uk/66145/`

[161] Futek advance sensor technology, inc, http://www.futek.com

[162] USB Multifunction DAQ, https://labjack.com/products/u6

[163] Hengstler RI32 Incremental Push Pull Rotary Encode, uk.rs-online.com/web/p/rotary-encoders/2603780/

[164] https://labjack.com/support/software/3rd-party-applications/daqfactoryurl

[165] http://www.dvetech.com

[166] D. C. Hanselman, Brushless Permanent Magnet Motor design, Mc Graw Hill Inc, 1994.

[167] urlhttp://en-us.fluke.com/products/portable-oscilloscopes/fluke-123-s-portable-oscilloscope.html#techspecs

[168] urlhttp://www.industrial-needs.com/technical-data/optical-tachometer-pce-dt62.html

[169] W. M. Haynes,Handbook of Chemistry and Physics, 96th Edition, 2015

[170] P. Ouro, T. Stoesser, R. McSherry, Large-Eddy Simulation of a Vertical Axis Tidal Turbine Using an Immersed Boundary Method, Chapter 5, CFD for Wind and Tidal Offshore Turbines, Springer (2015) 49–58 doi:10.1016/j.jfluidstructs.2013.12.014.

[171] C. Li, S. Zhua, Y.L. Xu, Y. Xiao, 2.5D large eddy simulation of vertical axis wind turbine in consideration of high angle of attack flow, Journal of Renewable Energy, 51 (2013) 317–330 doi:10.1016/j.renene.2012.09.011.

[172] J. McNaughton, F. Billard, A. Revell, Turbulence modelling of low Reynolds number flow effects around a vertical axis turbine at a range of tip-speed ratios, Journal of Fluids and Structures, 47 (2014) 124–138. 10.1016/j.jfluidstructs.2013.12.014.

[173] T. Maitre, E. Amet, C. Pellone, Y. Lee, S. Kim, Modeling of the flow in a Darrieus water turbine: Wall grid refinement analysis and comparison with experiments, Journal of Renewable Energy 57 (2013) 497–512 doi:10.1016/j.renene.2012.09.030.

[174] I. Hwang, S. Min, I. Jeong, Y. Lee, S. Kim, Efficiency improvement of a new vertical axis wind turbine by individual active control of blade motion, Proc. SPIE , Smart Structures and Integrated Systems 6172 (2006) 8 pages doi:10.1117/12.658935.

[175] I. Paraschivoiu, O. Trifu, F. Saeed, H-darrieus wind turbine with blade pitch control, International Journal of Rotating Machinery 2009 (2009) 1–7. doi:10.1155/2009/505343.

[176] K. Tsuji, K. Naoi, M. Shiono K. Suzuki, Study on the Gear Ratio for a Tidal Current Power Generation System Using the MPPT Control Method, Journal of Ocean and Wind Energy, 2 (2) (2015) 113–120 http://dx.doi.org/10.17736/jowe.2015.jcr26

[177] P. Bachant, M. Wosnik, Performance measurements of cylindrical- and spherical-helical cross-flow marine hydrokinetic turbines, with estimates of exergy efficiency, Journal of Renewable Energy, 74 (2015) 318–325

[178] P. Lissaman, Low-Reynolds-number airfoils, Ann. Rev. Fluid Mechanics, 15 (1) (1983) 223–239.

[179] B. Yang, X.W. Shu, Hydrofoil optimization and experimental validation in helical vertical axis turbine for power generation from marine current, Journal of Ocean Engineering 42 (2012) 35–46 doi:10.1016/j.oceaneng.2012.01.004

[180] Y. Kyozuka, K. Ogawa, Tidal Current Power Generation Making Use of a Bridge Pier, OCEANS 2006 - Asia Pacific 1–8, Singapore, Singapore (May 2007). doi:10.1109/OCEANSAP.2006.4393925

[181] A. J. Fiedler, S. Tullis, Blade offset and pitch effects on a high solidity vertical axis wind turbine, Wind Engineering 33 (3) (2009) 237–246. doi:10.1260/030952409789140955.

[182] S-C. Roh, S-H. Kang, Effects of a blade profile, the reynolds number, and the solidity on the performance of a straight bladed vertical axis wind turbine, Journal of Mechanical Science and Technology 27 (11) (2013) 3299–3307. doi:10.1007/s12206-013-0852-x.

[183] M. Islam, D. Ting, A. Fartaj, Aerodynamic models for darrieus-type straight-bladed vertical axis wind turbines, Renewable and Sustainable Energy Reviews 12 (4) (2008) 1087–1109. doi:10.1016/j.rser.2006.10.023.

[184] C. Soraghan, Influence of lift to drag ratio on optimal aerodynamic performance of straight blade vertical axis wind turbines. Europe's Premier Wind Energy Event. Vienna, Austria (February 2013).

[185] M. R. Ahmed, Blade sections for wind turbine and tidal current turbine applications—current status and future challenges, International journal of energy research 36 (2012) 829–844 doi:10.1002/er.2912

[186] M. Islam, D. Ting, A. Fartaj, Desirable airfoil features for smaller-capacity straight-bladed vawt, Wind Engineering 31 (3) (2007) 165–196. doi:10.1260/030952407781998800.

[187] Y. Takamatsu, A. Furukawa, K. Okuma, K. Takenouchi, Experimental Studies on a Preferable Blade Profile for High Efficiency and the Blade Characteristics of Darrieus-Type Cross-Flow Water Turbines, JSME international journal Ser. 2, Fluids engineering, heat transfer, power, combustion, thermophysical properties, 34–II(2) (1991) 149–156, ISSN: 09148817.

[188] `http://airfoiltools.com/airfoil/details?r=polar/index/\#xfoil`

[189] M. Drela, XFOIL: an analysis and design system for low Reynolds number airfoils. In: Conference on Low Reynolds Number Airfoil Aerodynamics, University of Notre Dame, 1989.

[190] `http://web.mit.edu/drela/Public/web/xfoil/`

[191] J.L. van Ingen, The eN method for transition prediction. Historical review of work at TU Delft, 138th Fluid Dynamics Conference and Exhibit, Seattle, Washington, 23 - 26 June 2008,

[192] D. H. Zeiner-Gundersen, A novel flexible foil vertical axis turbine for river, ocean, and tidal applications, Applied Energy 151 (2015) 60–66, doi:10.1016/j.apenergy.2015.04.005.

[193] T. Kinsey, G. Dumas, Parametric study of an oscillating airfoil in a power extraction regime. AIAA J 46 (6) (2008) 1318–1330 doi:10.2514/1.26253

[194] J.Young, J. C. S. Lai, M. F.Platzer, A review of progress and challenges in flapping foil power generation, Progress in Aerospace Sciences 67 (2014) 2–28 doi:10.1016/j.paerosci.2013.11.001

[195] I. Paraschivoiu, O. Trifu, F. Saeed, H-Darrieus Wind Turbine with Blade Pitch Control, International Journal of Rotating Machinery, 2009 (2009) 7 pages, doi:10.1155/2009/505343.

[196] G. Zhao, R. Yang, Y. Liu, P. Zhao, Hydrodynamic performance of a vertical-axis tidal-current turbine with different preset angles of attack, Journal of Hydrodynamics, 25 (2) (2013), 280–287, doi:10.1016/S1001-6058(13)60364-9.

[197] P. Klimas, C. Worstell Effects of blade preset pitch/offset on curved-blade Darrieus vertical axis wind turbine performance SAND-81–1762 Sandia National Laboratories (1981)

[198] J. Twidell, A. D. Weir, Renewable Energy Resources (3rd edition). London: Taylor and Francis (2015).

[199] Y.M.Dai, W. Lam, Numerical study of straight-bladed Darrieus-type tidal turbine. Proceedings of the Institution of Civil Engineers Energy, 162 (2) (2009) 67–76

[200] S. Antheaume, T. Maitre , J-L. Achard, Hydraulic Darrieus turbines efficiency for free fluid flow conditions versus power farms conditions, Journal of Renewable Energy, 33 (10) (2008) 2186–2198.

[201] M.J.Khan, M. Iqbal, J.E.Quaicoe, A technology review and simulation based performance analysis of river current turbine systems, Canadian Conference Electrical and Computer Engineering. Ottawa, Canada (May 2006) 2288–2293. doi:110.1109/CCECE.2006.277821.

[202] P. G. Migliore, W. P. Wolfe, and J. B. Fanucci, Flow Curvature Effects on Darrieus Turbine Blade Aerodynamics, Proceedings of the 24th International Conference on Offshore Mechanics and Arctic Engineering, Journal of Energy, 4 (2) (1980) 49–55. doi:10.2514/3.62459.

[203] D. Coiro, F. Nicolosi, A. De Marco, S. Melone, F. Montella, Flow curvature effects on dynamic behaviour of a novel vertical axis tidal current turbine: Numerical and experimental analysis, Proceedings of the 24th International Conference on Offshore Mechanics and Arctic Engineering,

[204] E. Amet, T. Maitre, C. Pellone, J.L. Achard, 2D Numerical Simulations of Blade-Vortex Interaction in a Darrieus Turbine, Journal of Fluids Engineering 131 (11) (2009) (15 pages) doi:10.1115/1.4000258.

[205] G. Brochier, P. Fraunie, C. Beguier, I. Paraschivoiu, Water Channel Experiments of Dynamic Stall on Darrieus Wind Turbine Blades, Journal of Propulsion 2(5) (1986) 445–449

[206] H. Beri, Y. Yao Effect of Camber airfoil on self starting of vertical axis wind turbine Journal of Environmental Science and Technology, 4 (3) (2011) 302–312

[207] N.C. Batista, R. Melício, J.C.O. Matias, J.P.S. Catala, Self-Start Performance Evaluation in Darrieus-Type Vertical Axis Wind Turbines: Methodology and Computational Tool Applied to Symmetrical Airfoils, Center for Innovation in Electrical and Energy Engineering, Instituto Superior Tecnico (2010).

[208] R. Dominy, P. Lunt, A. Bickerdyke, J. Dominy, Self-starting capability of a Darrieus turbine Proceedings of the Institution of Mechanical Engineers, Part A: Journal of Power and Energy, 221 (1) (2007) 111–120.

[209] A. Gorlov, Unidirectional helical reaction turbine, U.S. Patent No 5,451,137. U.S. Patent and Trademark Office (1994).

[210] A.H. Elbatran, O.B. Yaakob, Y. M. Ahmed, H.M. Shabara, Operation, performance and economic analysis of low head micro-hydropower turbines for rural and remote areas: A review, Renewable and Sustainable Energy Reviews 43 (2015) 40–50, doi:10.1016/j.rser.2014.11.045

[211] `https://www.grc.nasa.gov/www/k-12/airplane/shaped.html`

[212] S. Kassam, In-Situ Testing of a Darrieus Hydro Kinetic Turbine in Cold Climates, Master's thesis, University of Manitoba, Faculty of Engineering, Department of Mechanical and Manufacturing Engineering (2009).

[213] Y. Li, S. M. Calisal, Three-dimensional effects and arm effects on modeling a vertical axis tidal current turbine, Renewable Energy 35 (2010) 2325–2334, doi:10.1016/j.renene.2010.03.002

[214] W. Guo, H. G. Kang, B. Chen, Y. Xie, Y. Wang, Numerical and Experimental Study of the 3D Effect on Connecting Arm of Vertical Axis Tidal Current Turbine, China Ocean Engineering, 30 (1) (2015) 83–96 doi:10.1007/s13344-015-0080-5

[215] M. J. Smith, N. Komerath, R. Ames, O. Wong,, J. Pearson, Performance analysis of a wing with multiple winglets, American Institute of Aeronautics and Astronautics (2001) 10 pages

[216] F. Q. Chu, P. Chen,X. X. Shen, X. H. Yan, X.-H. Parameter selection of straight bladed vertical axis wind turbine. Alternative Energy Sources VI Volume 3 Wind/Ocean/Nuclear/Hydrogen: Proceedings of the Sixth Miami International Conference on Alternative Energy Sources, December 12-14, 1983, Miami Beach, Florida, USA 77–85.

[217] M.A. Singh, A. Biswas, R.D. Misra, Investigation of self-starting and high rotor solidity on the performance of a three S1210 blade H-type Darrieus rotor Renewable Energy, 76 (2015) 381–387 doi:10.1016/j.renene.2014.11.027

[218] T. Nishino, R. H.J. Willden, Effects of 3-D channel blockage and turbulent wake mixing on the limit of power extraction by tidal turbines, Journal of Heat and Fluid Flow, 37 (2012) 123–135. doi:10.1016/j.ijome.2015.09.002

[219] C.Garret and P.Cummins, The efficiency of a turbine in a tidal channel. Journal of Fluid Mechanics 588 (2007), 243–251 doi:10.1016/j.renene.2006.01.012.

[220] J. Whelan, J. Graham, J. Peiro, A free-surface and blockage correction for tidal turbines, J. Fluid Mech. 624 (2009) 281–291. doi:10.1017/S0022112009005916.

[221] T.Nishino, R.H.J. Willden, The efficiency of an array of tidal turbines partially blocking a wide channel, J. Fluid Mech 708 (2012) 596–606. doi:10.1017/jfm.2012.349.

[222] Polagye, B. Hydrodynamic effects of kinetic power extraction by in-stream tidal turbines University of Washington (2009).

[223] A. Pope, J.J Harper, Low-speed wind tunnel testing. John Wiley and Sons, New York (1966)

[224] K. Standish, P. Rimmington, J. Laursen, H. Paulsen, D. Nielsen, Computational predictions of airfoil roughness sensitivity, 48th AIAA Aerospace Sciences Meeting Including the New Horizons Forum and Aerospace Exposition. Orlando, USA (2010) doi:10.2514/6.2010-460.

[225] F. Hummel, M. Loetzerich, P. Cardamone, L. Fottner, Surface roughness effects on turbine blade aerodynamics, J. Turbomach. 127 (3) (2005) 453–461. doi:10.1115/1.1860377.

[226] R. Howell, , N. Qin, J. Edwards, N. Durrani, Wind tunnel and numerical study of a small vertical axis wind turbine. Journal of Renewable Energy, 35 (2) (2010) 412–422. doi:10.1016/j.renene.2009.07.025

[227] J. M. Walker, K. Flack, E. E. Lust, M. P. Schultz, L. Luznik, Experimental and numerical studies of blade roughness and fouling on marine current turbine performance. Journal of Renewable Energy, 66 (2014) 257–267. doi:10.1016/j.renene.2013.12.012

[228] E. Achenbach, The effects of surface roughness and tunnel blockage on the flow past spheres, J. Fluid Mech. 65 (1) (1974) 113–125. doi:10.1017/s0022112074001285.

[229] N. Fujisawa, S. Shibuya, Observations of dynamic stall on Darrieus wind turbine blades, Journal of Wind Engineering and Industrial Aerodynamics, 89 (2) (2001) 201–214. doi:10.1016/S0167-6105(00)00062-3.

[230] `http://www.taylor-hobson.com/products/12/107.html`

[231] J. Nikuradse, Gesetzmaessigkeiten der turbulenten stroemung in glatten rohren, Forschung auf dem Gebiete des Ingenieurwesens 4 (1) (1933) 44 pages. doi:10.1007/bf02716946.

[232] J. P. Bons, A review of surface roughness effects in gas turbines, J. Turbomach. 132 (2) (2010) 16 pages. doi:10.1115/1.3066315.

[233] S.C. Tatum, C.H. Frost, M. Allmark, D.M. O'Doherty, A. Mason-Jones, P.W. Prickett, R.I. Grosvenor, C.B. Byrne, T. O'Doherty, Wave–current interaction effects on tidal stream turbine performance and loading characteristics, Journal of Marine Energy, 14 (2016) 161–179 doi:10.1016/j.ijome.2015.09.002

[234] C-H. Jo, J-H. Lee, Y-H. Rho, K-H. Lee, Performance analysis of a HAT tidal current turbine and wake flow characteristics, Journal of Renewable Energy 65 (2014) 175–182 doi:10.1016/j.renene.2013.08.027

[235] T. Blackmore, W.M.J. Batten, A.S. Bahaj, Influence of turbulence on the wake of a marine current turbine simulator. Proc. R. Soc. A 470: 20140331 (2014) doi:10.1098/rspa.2014.0331.

[236] L. Vybulkova, M. Vezza, R. Brown, Simulating the Wake Downstream of a Horizontal Axis Tidal Turbine Using a Modified Vorticity Transport Model, IEEE Journal of Oceanic Engineering, 41 (2) (2016) doi:10.1109/JOE.2015.242923.

[237] A.S. Bahaj, L.E. Myers, M.D. Thomson, N. Jorge, Characterising the wake of horizontal axis marine current turbines, Proceedings of the 7th European Wave and Tidal Energy Conference, Porto, Portugal (2007)

[238] S.C. Tedds, I. Owen, R.J. Poole, Near-wake characteristics of a model horizontal axis tidal stream turbine, Journal of Renewable Energy, 63 (2014) 222–235

[239] T. Stallard, R. Collings, T. Feng, J. Whelan, Interactions between tidal turbine wakes: experimental study of a group of three-bladed rotors. Phil Trans R Soc A 371: 20120159 (2013) doi:10.1098/rsta.2012.0159

[240] B. Morandi, F. Di Felice, M. Costanzo, G.P. Romano, D. Dhomé, J.C. Allo, Experimental investigation of the near wake of a horizontal axis tidal current turbine, Journal of Marine Energy 14 (2016) 229–247, doi:10.1016/j.ijome.2016.02.004

[241] L. Myers, A.S. Bahaj, Wake studies of a 1/30th scale horizontal axis marine current turbine, Journal of Ocean Engineering 34 (2007) 758–762, doi:10.1016/j.oceaneng.2006.04.013.

[242] A.J. MacLeod, S. Barnes, K.G. Rados, I.G. Bryden, Wake effects in tidal current turbine farms, MAREC 2002 (2002).

[243] S. Turki, H. Abbassi, S.B. Nasrallah, Effect of the blockage ratio on the flow in a channel with a built-in square cylinder, Computational Mechanics 33 (2003) 22–29 doi:10.1007/s00466-003-0496-2.

[244] F. Maganga, G. Germain, J. King, G. Pinon, E. Rivoalen, Experimental characteri sation of flow effects on marine current turbine behaviour and on its wake properties. IET Renewable Power Generation 4 (6) (2010) 498–509.

[245] P. Mycek, B. Gaurier, G. Germain, G. Pinona, E. Rivoalen, Numerical and experimental study of the interaction between two marine current turbines Journal of Marine Energy, 1 (2013) 70–83

[246] T. Divett, R. Vennell, C. Stevens, Optimization of multiple turbine arrays in a channel with tidally reversing flow by numerical modelling with adaptive mesh. Phil Trans R Soc A 371:20120251. doi:10.1098/rsta.2012.0251.

[247] S.H. Han, J.S. Park, K.S Lee, W.S. Park, J.H. Yi. Evaluation of vertical axis turbine characteristics for tidal current power plant based on in situ experiment from marine current, Journal of Ocean Engineering 65 (2013) 83–89 doi:10.1016/j.oceaneng.2013.03.005

[248] K. Sahim, D. Santoso, A. Radentan, Performance of Combined Water Turbine with Semielliptic Section of the Savonius Rotor, International Journal of Rotating Machinery, 2013 (2013), 5 pages. doi:10.1155/2013/985943

[249] A. Gorban, A Gorlov, V. Silantyev, Limits of the Turbine Efficiency for Free Fluid Flow, Journal of Energy Resources Technology, 12 (2001) 311–317.

[250] I. Milne, R. Sharma, R. Flay, S. Bickerton, The role of onset turbulence on tidal turbine blade loads. In Proc. 17th Australasian Fluid Mechanics Conference, Auckland, New Zealand, 5–9, (December 2010)

[251] I. Milne, R. Sharma, R. Flay, S. Bickerton, Characteristics of the turbulence in the flow at a tidal stream power site, Philosophical Transactions of Royal Society A, 371:20120196 (2013); doi:10.1098/rsta.2012.0196.

Appendices

Experimental Apparatus

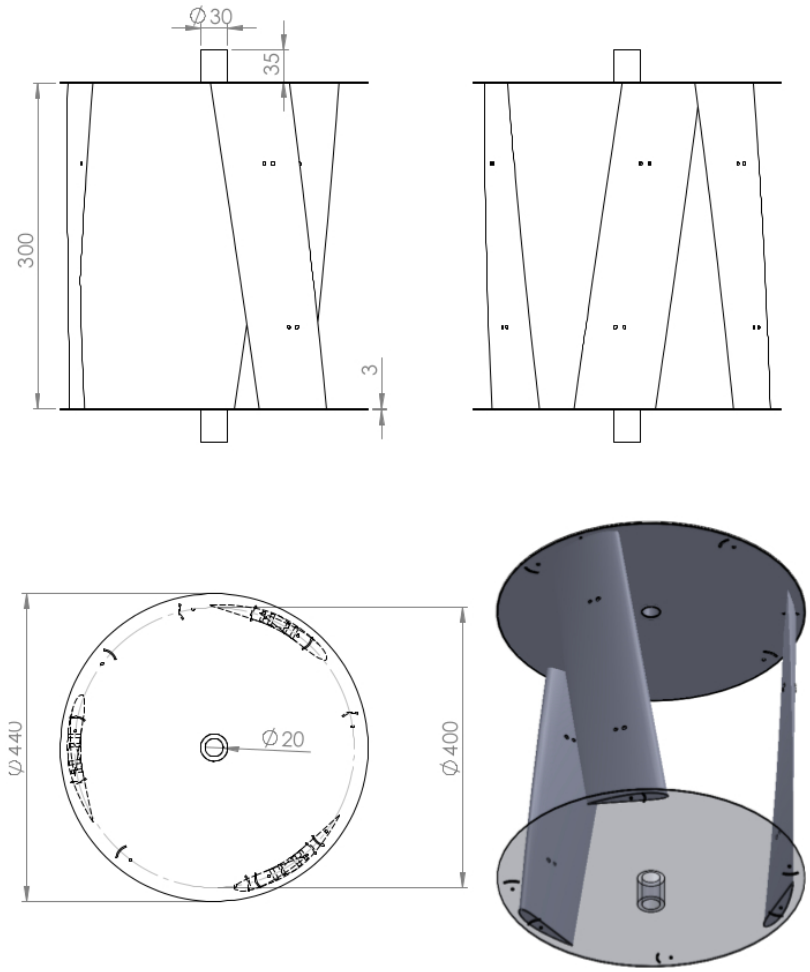

Figure 122: Example of the experimental set up used for part of the experiments. The set up is based on discs as the connection between blades and shaft.

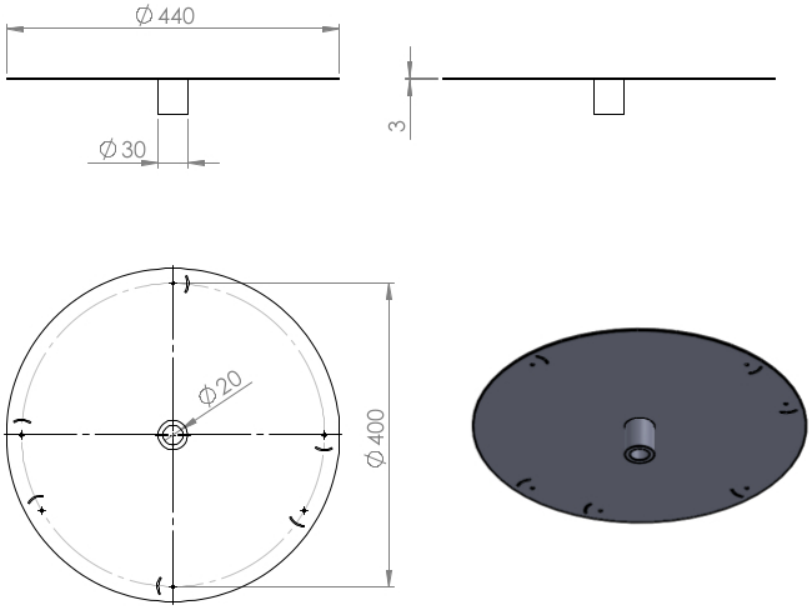

Figure 123: Detailed drawing of the discs used for part of the experiments.

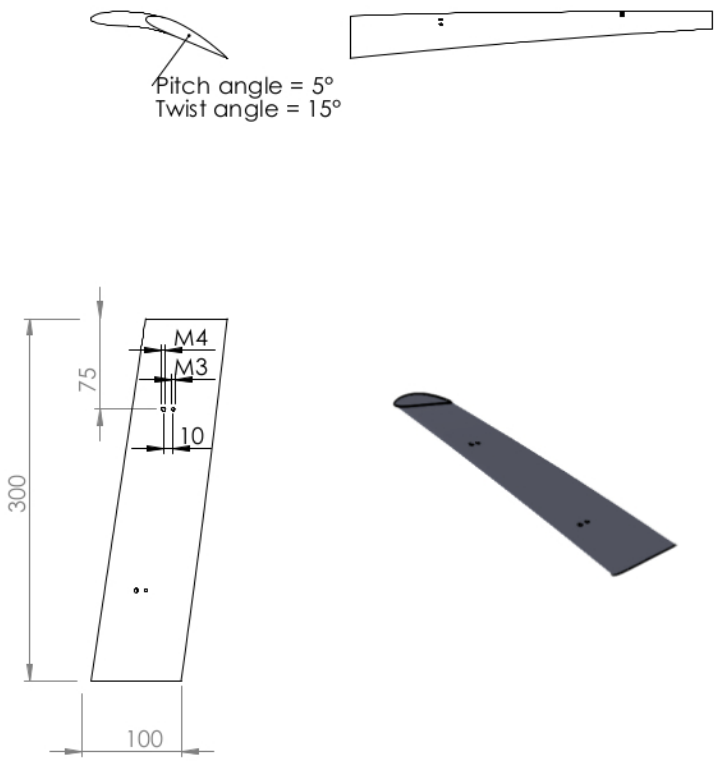

Figure 124: Detailed drawing of a twisted bladed used for part of the experiments. Straight blades had the same distribution of holes and distances

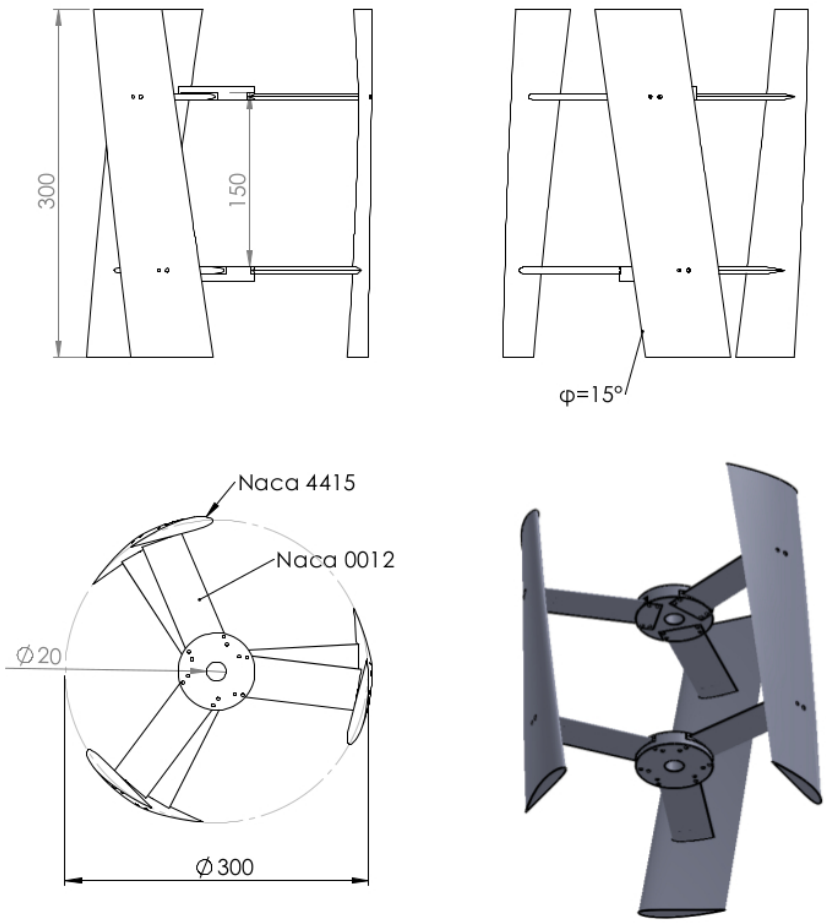

Figure 125: Example of the experimental set up used for part of the experiments. The set up is based on spokes as the connection between blades and shaft.

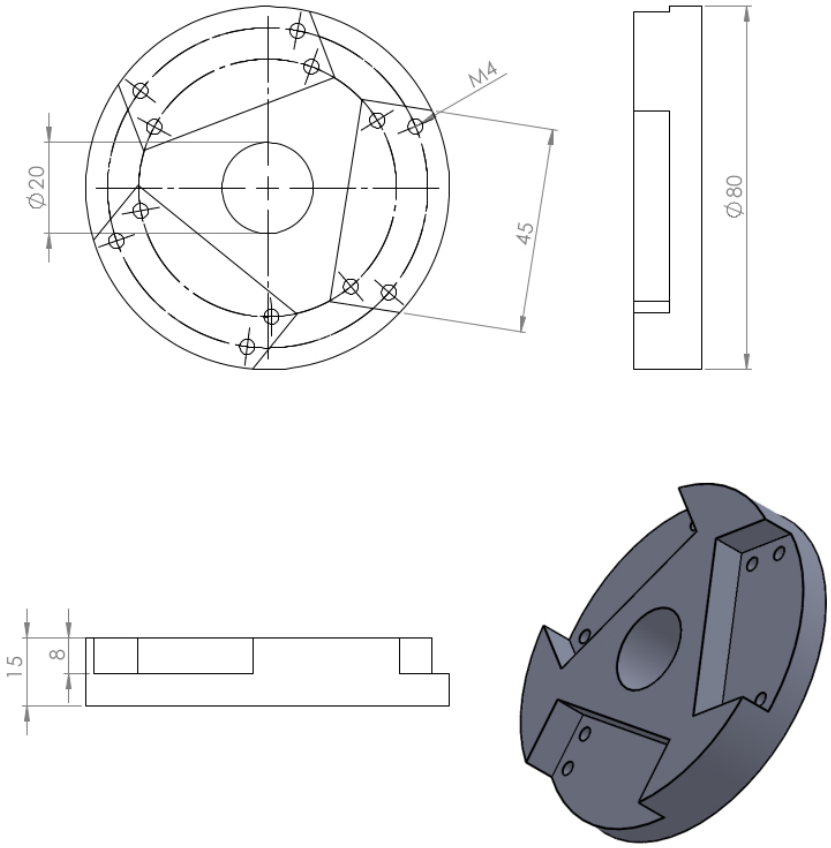

Figure 126: Detailed drawing of the piece that connected spokes and shaft, set up that was used for part of the experiments.

Spokes shape

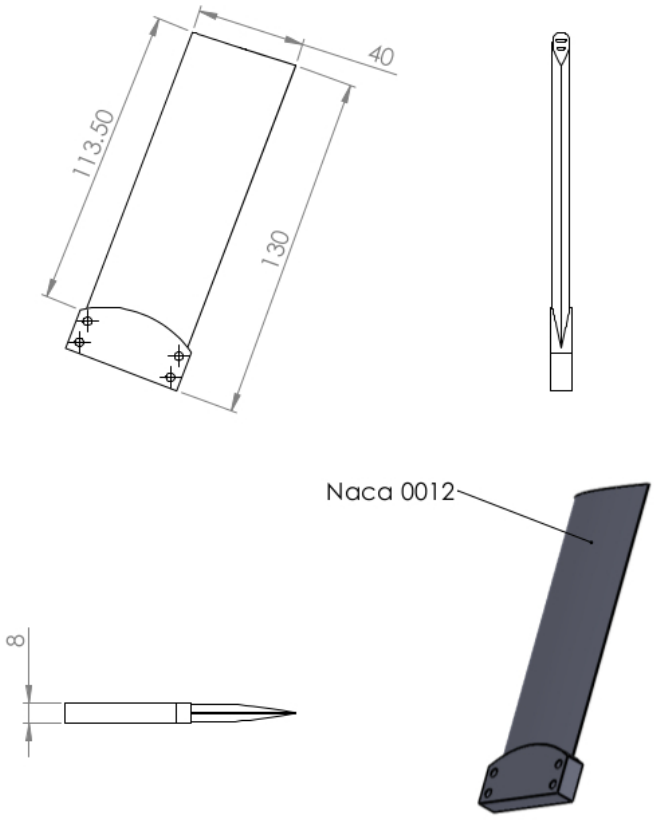

Figure 127: Detailed drawing of the spokes used for part of the experiments.

Winglets

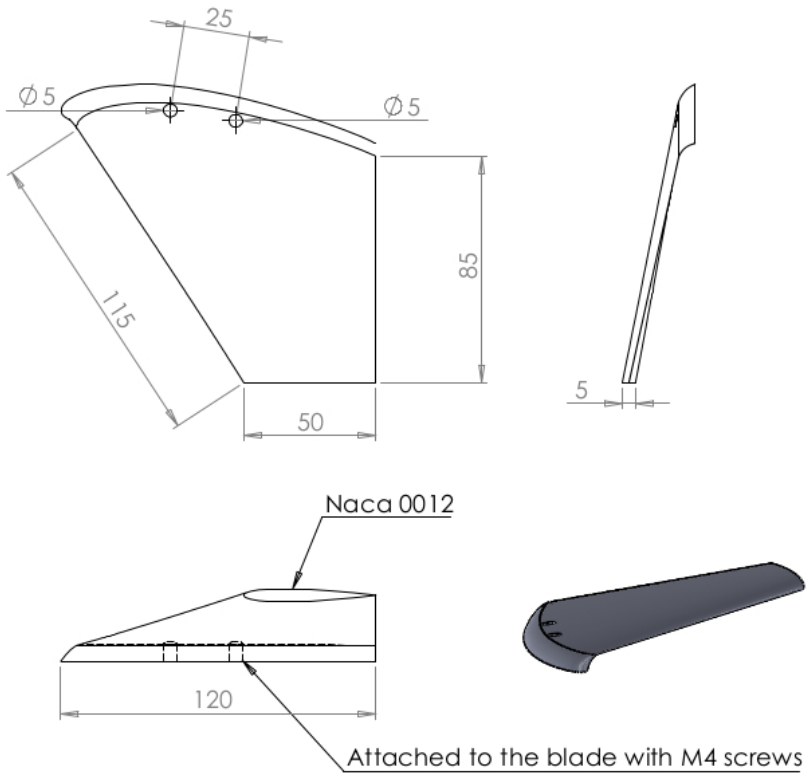

Figure 128: Detailed drawing of the winglets used for part of the experiments

Field testing

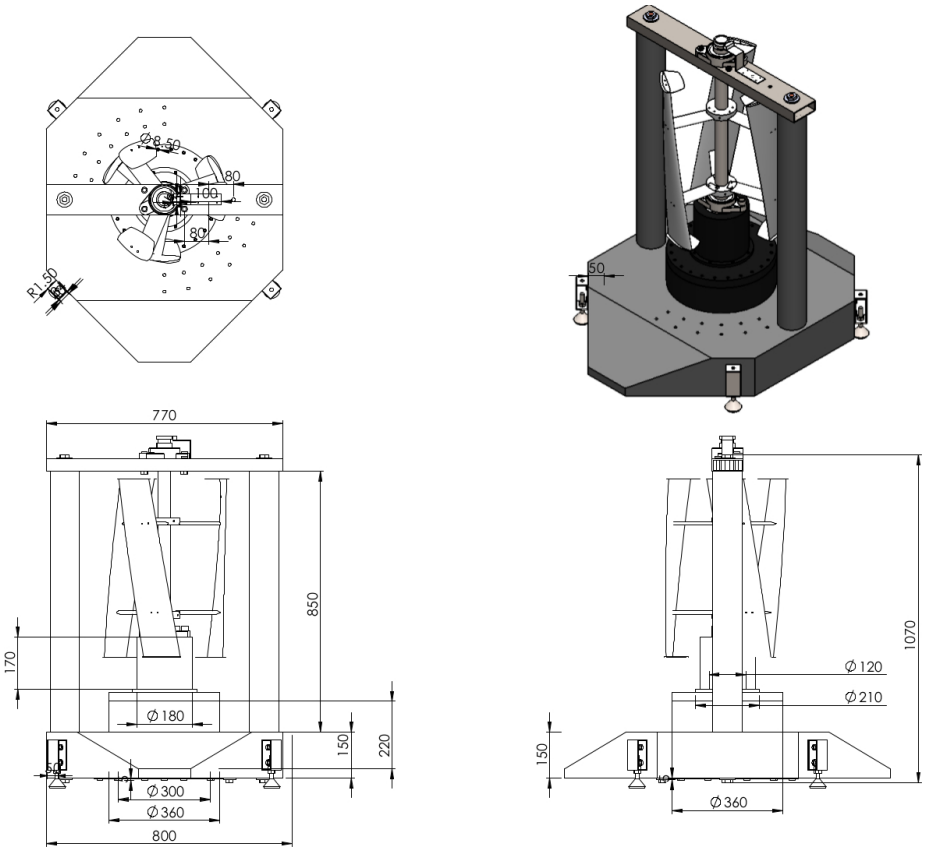

Figure 129: Drawings of the prototype tested at White Water Rafting Centre